

Faculty of Engineering

UNDERSTANDING THE INFLUENCE OF MINERALOGY AND MICROWAVE ENERGY INPUT ON THE MICROWAVE TREATMENT OF COPPER ORES

ALEXANDER URE, BSc (Hons)

Thesis submitted to the University of Nottingham for the degree of Doctor of Philosophy

March 2017

Abstract

Ore comminution is an energy intensive and inefficient process in which new innovative technologies could potentially deliver great benefits. Over the past two decades, the high power microwave treatment of ores has shown the potential of being a novel step-changing comminution technology. The ability of microwaves to rapidly and selectively heat certain minerals within an ore, and generate and propagate intergranular fractures at grain boundaries, has been shown to be an innovative process for reducing ore strength and enhancing mineral liberation. A review of the literature has identified that, while the understanding of the process has developed significantly over recent years, fundamental knowledge of how mineralogical characteristics of different ores influences their amenability to microwave treatment is still limited. Previous work in this field has also been primarily concerned with assessing the downstream mineral processing benefits achievable, rather than directly measuring the impact of the treatment on ore fracturing.

The aim of this experimental investigation has been to make an original and distinct contribution towards the current state of knowledge, through the application of innovative microwave treatment processes and conventional and novel analytical methods. Three copper ore samples, termed MZ, QZ and QX, were assessed following a series of microwave treatments at unprecedented conditions, for changes in Cu-sulphide mineral liberation using automated mineralogy, and changes in ore comminution using JK GeM Crushing Index and Bond Ball Mill Work Index testing methods. A novel fracture analysis and quantification method was also developed and applied for the first time to the assessment of microwave treated ores.

MZ and QZ ores achieved similar improvements in Cu-sulphide mineral liberation and comminution performance following microwave treatment, as it has been shown from coarse ore characterisation that both ores possess characteristics that render them highly amenable to

beneficial microwave treatment outcomes. This finding validates ore amenability characteristics proposed by previous researchers. Fracture analysis results have quantifiably shown for the first time that microwave treatments can induce additional beneficial fracturing in amenable ores. An additional original contribution to the field is that beneficial fracture outcomes were shown to correspond with benefits achieved in Cu-sulphide liberation, and ore comminution testing.

Investigations were also conducted to determine the minimum microwave energy input threshold at which measurable benefits in ore comminution and mineral liberation are achievable. Following an additional series of unprecedentedly low dose microwave treatments of MZ ore, it was observed that benefits in Cu-sulphide mineral liberation can be achieved from microwave treatment with a power density of $2.0x10^6 W/m^3$ and a total microwave energy input of 0.3kWh/t, at an applicator residence duration of ~0.25 seconds. Treatment conditions for total microwave energy input at which benefits have been shown to be achievable, are lower than conditions previously reported in the literature for any ore type. This outcome indicates that scale-up of the process to industrially relevant throughputs (i.e. >10,000 t/h) could potentially be achieved using existing microwave generator technology, eliminating the need for the development of higher power generators producing over 100kW of microwave power.

Conclusions from this experimental investigation have provided an original contribution to the fundamental knowledge of the microwave treatment of copper ores, and have advanced the understanding of the application of the process to enhancing mineral liberation and ore comminution. Further investigations of a range of amenable copper ores, or ores of different commodities, at low microwave treatment doses of 0.3-0.7kWh/t would allow for an assessment of whether this newly determined minimum energy threshold at which mineral processing benefits have been shown, also applies to ores with different mineralogical and textural characteristics.

Acknowledgements

Firstly, I would like to thank my supervisor, Professor Sam Kingman, for the opportunity to undertake this project, and for providing support, encouragement and motivation throughout the last three years. I would also like to thank my co-supervisor, Dr Andrew Batchelor, for his guidance and technical support throughout this project, and for his detailed reviews of my thesis chapters. In addition, I would like to acknowledge the support of Associate Professor Chris Dodds, and other current and former members of the Microwave Process Engineering (MPE) research group.

The support of the MPE group technicians during my research has been outstanding, and I am very appreciative of their expert assistance. I would like to thank Matt Rus, Matt Nicholls, Rachael Baines, Rich Meehan and Joe Meehan for their help and friendship during my time here, and for including me in the weekly Friday technician lunches. Getting to know you all and becoming good mates has been a highlight of my time in Nottingham.

I would like to acknowledge and thank Rio Tinto for financial support towards this project, and for the provision of ore samples. I would also like to thank former Rio Tinto T&I colleague Dr Grant Wellwood for helping to initiate this project, and for encouraging me to pursue the opportunity. The support and encouragement of former colleagues in the Rio Tinto T&I Process Mineralogy team has also been of great assistance both prior to and during this project.

My family and I have really enjoyed our time living in Nottingham while I have been completing this project. This has been primarily due to the great friends we have been fortunate to make while living in West Bridgford. Thank you to Tertia and Carl, and to Sarah and Matt, for letting us be part of your lives and for your friendship and support.

Finally, and most importantly, I want to thank my wife Lisa, and daughter Evelyn, for supporting me in pursuing this opportunity, and for accompanying me on the journey. Completing this PhD has been a team effort. It has been an exciting, and at times turbulent adventure, and we managed to get through it all together. Your love and support has made this experience possible for all of us, and I'm looking forward to whatever exciting adventures our future may hold.

Table of Contents

Abstract i

Acknowledgements iii

Table of Contents v

List of Figures xii

List of Tables xix

CHAPTER 1 – INTRODUCTION ..... - 1 -

1.1 Project Drivers ..... - 2 -

CHAPTER 2 – LITERATURE REVIEW ..... - 9 -

2.1 Mineral Processing ..... - 9 -

2.1.1 Introduction ..... - 9 -

2.1.2 Comminution ..... - 10 -

2.1.2.1 Introduction ..... - 10 -

2.1.2.2 Ore Fracture Mechanisms ..... - 12 -

2.1.2.3 The Energy-Size Reduction Relationship ..... - 17 -

2.1.2.4 Mineral Liberation ..... - 20 -

2.1.2.5 Flotation ..... - 24 -

2.2 Innovations in Comminution ..... - 25 -

2.2.1 Introduction ..... - 25 -

2.2.2 High Pressure Grinding Rolls ..... - 26 -

2.2.3 High Voltage Pulse Fragmentation ..... - 27 -

2.2.4 Summary ..... - 30 -

2.3 Microwave Treatment of Ores ..... - 31 -

2.3.1 Introduction ..... - 31 -

2.3.2 Background to Microwave Assisted Liberation and Comminution ..... - 31 -

2.3.3 The Influence of Power Density and Total Energy Input - 33 -

2.3.4 The Influence of Mineralogy ..... - 43 -

2.4 Summary.....- 53 -
2.5 Aims and Objectives.....- 57 -
CHAPTER 3 – FUNDAMENTALS OF MICROWAVES AND THE MICROWAVE HEATING OF MINERALS.....- 59 -
3.1 Introduction.....- 59 -
3.2 Electromagnetic Radiation.....- 60 -
3.2.1 The Electromagnetic Spectrum.....- 61 -
3.2.2 Electromagnetic Safety and Compliance.....- 62 -
3.3 Microwave Heating Mechanisms.....- 62 -
3.3.1 Dielectric Polarisation.....- 63 -
3.3.1.1 Electronic and Atomic Polarisation.....- 64 -
3.3.1.2 Dipolar Polarisation.....- 65 -
3.3.1.3 Interfacial Polarisation.....- 65 -
3.3.2 Ionic Conduction.....- 66 -
3.4 Dielectric Properties.....- 66 -
3.4.1 Permittivity and Permeability.....- 67 -
3.4.2 Complex Relative Permittivity and Loss Factor.....- 68 -
3.4.4 Factors Influencing Dielectric Properties.....- 69 -
3.4.5 Microwave Power Dissipation.....- 71 -
3.4.5.1 Dielectric Heating Equation.....- 71 -
3.4.5.2 Temperature Increase.....- 71 -
3.4.5.3 Penetration Depth.....- 72 -
3.4.5.4 Voltage Breakdown and Arcing.....- 73 -
3.4.5.5 Thermal Runaway.....- 73 -
3.5 Microwave Heating of Minerals.....- 74 -
3.6 Microwave Processing Systems.....- 79 -
3.6.1 Introduction.....- 79 -
3.6.2 Microwave Power Sources.....- 80 -
3.6.2.1 Magnetrons.....- 81 -
3.6.3 Microwave Transmission.....- 83 -

3.6.3.1 Coaxial Lines ..... - 83 -
3.6.3.2 Waveguides ..... - 83 -
3.6.3.3 Short Circuit Tuners ..... - 84 -
3.6.3.4 Stub Tuners ..... - 85 -
3.6.3.5 Reflected Power Dissipation ..... - 85 -
3.6.4 Microwave Applicators ..... - 86 -
3.6.4.1 Multimode Cavities ..... - 86 -
3.6.4.2 Single Mode Resonant Cavities ..... - 87 -
3.6.4.3 Microwave Choking in Continuous Flow Applicators - 88 -
3.6.5 Microwave Treatment Systems for Ore Comminution .... - 89 -
3.7 Summary ..... - 90 -
CHAPTER 4 - EXPERIMENTAL METHODS FOR MICROWAVE TREATMENTS AND ORE CHARACTERISATION ..... - 93 -
4.1 Introduction ..... - 93 -
4.2 Ore Sample Preparation ..... - 93 -
4.2.1 Sample Splitting ..... - 93 -
4.2.2 Crushing and Grinding ..... - 95 -
4.2.3 Size Classification ..... - 96 -
4.3 Microwave Treatment Systems ..... - 97 -
4.3.1 Microwave Treatment Pilot-Scale System ..... - 97 -
4.3.1.1 Introduction ..... - 97 -
4.3.1.2 Pilot System Treatment Process ..... - 104 -
4.3.2 Microwave Treatment Batch System ..... - 108 -
4.3.2.1 Introduction ..... - 108 -
4.3.2.2 Batch System Treatment Process ..... - 111 -
4.4 Mineralogical Characterisation ..... - 116 -
4.4.1 Introduction to Automated Mineralogy ..... - 116 -
4.4.2 Automated Mineralogy Systems ..... - 118 -
4.4.3 Principles of Operation ..... - 119 -

4.4.3.1 Principles of Scanning Electron Microscopy and Energy Dispersive Spectroscopy ..... - 121 -
4.4.3.2 Sample Preparation ..... - 124 -
4.4.3.3 Measurement and Analysis Procedure ..... - 125 -
4.4.3.4 Data Analysis ..... - 129 -
4.4.3.5 Mineral Groupings ..... - 131 -
4.4.3.6 Quality Control of Mineralogy Results ..... - 134 -
4.5 Comminution Testing ..... - 134 -
4.5.1 JK GeM Crushing Index Test ..... - 135 -
4.5.2 Bond Ball Mill Work Index Test ..... - 137 -
4.6 Fracture Analysis and Quantification ..... - 139 -
4.6.1 Introduction ..... - 139 -
4.6.2 Dye Penetration Method ..... - 140 -
4.6.2.1 Sample Preparation ..... - 140 -
4.6.2.2 Image Acquisition ..... - 142 -
4.6.2.3 Image Processing and Analysis ..... - 144 -
4.7 Summary ..... - 147 -
CHAPTER 5 – INVESTIGATING THE INFLUENCE OF MINERALOGY ON THE MICROWAVE TREATMENT OF COPPER ORES ..... - 149 -
5.1 Introduction ..... - 149 -
5.2 Ore Samples ..... - 150 -
5.2.1 Introduction ..... - 150 -
5.2.2 Geology of the Deposit ..... - 150 -
5.3 Coarse Ore Characterisation ..... - 152 -
5.3.1 Introduction ..... - 152 -
5.3.2 Sample Preparation and Analysis Procedure ..... - 153 -
5.3.3 MZ Ore ..... - 154 -
5.3.4 QZ Ore ..... - 156 -
5.3.5 QX Ore ..... - 159 -
5.3.6 Summary of Coarse Ore Characteristics ..... - 161 -

5.4 Microwave Treatments ..... - 165 -
5.4.1 Introduction ..... - 165 -
5.4.2 Microwave Treatment Conditions ..... - 166 -
5.5 Mineral Liberation Analysis ..... - 167 -
5.5.1 Introduction ..... - 167 -
5.5.2 Sample Preparation and Analysis Procedure ..... - 168 -
5.5.3 MZ Ore ..... - 169 -
5.5.4 QZ Ore ..... - 177 -
5.5.5 Summary of Liberation Results ..... - 183 -
5.6 Comminution Testing ..... - 185 -
5.6.1 Introduction ..... - 185 -
5.6.2 Sample Preparation and Testing Procedure ..... - 185 -
5.6.3 JK GeM Crushing Index Test Results ..... - 187 -
5.6.3.1 MZ Ore ..... - 187 -
5.6.3.2 QZ Ore ..... - 189 -
5.6.4 Bond Ball Mill Work Index Test Results ..... - 191 -
5.6.4.1 MZ Ore ..... - 191 -
5.6.4.2 QZ Ore ..... - 192 -
5.6.5 Summary of Comminution Test Results ..... - 192 -
5.7 Summary ..... - 195 -
CHAPTER 6 - ANALYSIS AND QUANTIFICATION OF FRACTURING IN MICROWAVE TREATED ORES ..... - 199 -
6.1 Introduction ..... - 199 -
6.1.1 Sample Preparation and Testing Procedure ..... - 200 -
6.2 Inherent Fracture Characteristics ..... - 201 -
6.2.1 MZ Ore ..... - 201 -
6.2.2 QZ Ore ..... - 202 -
6.2.3 QX Ore ..... - 203 -
6.3 Fracture Length ..... - 204 -
6.3.1 MZ Ore ..... - 205 -

6.3.2 QZ Ore ..... - 206 -
6.3.3 QX Ore ..... - 207 -
6.3.4 Statistical Analysis ..... - 208 -
6.4 Fracture Area ..... - 212 -
6.5 Fracture Density ..... - 216 -
6.6 Comparison to Mineral Liberation and Comminution Results - 221 -
6.7 Summary ..... - 225 -
CHAPTER 7 – INVESTIGATING THE INFLUENCE OF POWER DENSITY AND ENERGY INPUT ON THE MICROWAVE TREATMENT OF COPPER ORES ..... - 227 -
7.1 Introduction ..... - 227 -
7.2 Microwave Treatments ..... - 229 -
7.2.1 Introduction ..... - 229 -
7.2.2 Microwave Treatment Conditions ..... - 229 -
7.3 Mineral Liberation Analysis ..... - 231 -
7.3.1 Introduction ..... - 231 -
7.3.2 Sample Preparation and Analysis Procedure ..... - 231 -
7.3.3 Results ..... - 232 -
7.4 Comminution Testing ..... - 243 -
7.4.1 Introduction ..... - 243 -
7.4.2 Sample Preparation and Testing Procedure ..... - 243 -
7.4.3 JK GeM Crushing Index Test Results ..... - 245 -
7.4.4 Bond Ball Mill Work Index Test Results ..... - 246 -
7.5 Summary ..... - 248 -
CHAPTER 8 - CONCLUSIONS AND FURTHER WORK ..... - 251 -
8.1 Introduction ..... - 251 -
8.2 The Influence of Ore Mineralogy on Microwave Treatment Benefits ..... - 253 -
8.3 The Influence of Microwave Treatment on Ore Fracture .... - 255 -
8.4 The Influence of Microwave Energy Input and Power Density on Treatment Benefits ..... - 257 -

8.5 Recommendations for Further Work ..... - 258 -
REFERENCES ..... - 261 -
APPENDIX A - MINERALOGICAL DATA ..... - 281 -
A.1 Mineralogy Assay Reconciliation ..... - 281 -
A.2 Coarse Ore Mineral Grain Size Distribution Data ..... - 292 -
A.3 Mineral Abundance Data ..... - 295 -
A.4 Mineral Liberation and Locking Data ..... - 296 -
A.5 MZ Ore Grind Calibrations for Low Dose Treatments ..... - 299 -
APPENDIX B – COMMINUTION TEST DATA ..... - 309 -
B.1 Ci Test Data ..... - 309 -
B.2 BBMWi Test Data ..... - 318 -
APPENDIX C – FRACTURE ANALYSIS DATA ..... - 321 -
C.1 Fracture Length Distribution Data ..... - 321 -
C.2 Fracture Length K-S Test Tables ..... - 324 -

List of Figures

Figure 1.1 Global refined copper usage per capita 1950-2014. .... - 3 -

Figure 1.2 Historical copper ore grades to 2010 ..... - 4 -

Figure 1.3 Global copper production 1900-2013 ..... - 5 -

Figure 1.4 Forecast growth in copper demand and forecast copper production ..... - 5 -

Figure 2.1 Typical distribution of energy consumption to produce a copper concentrate .....- 11 -

Figure 2.2 Comminution energy consumption by commodity in the United States in 2000 .....- 11 -

Figure 2.3 A characteristic stress-strain curve .....- 15 -

Figure 2.4 Relationship between particle size reduction and the required comminution energy input .....- 18 -

Figure 2.5 Ore fracture characteristics .....- 22 -

Figure 2.6 Copper sulphide liberation versus grind size .....- 39 -

Figure 2.7 Cumulative copper sulphide liberation by composition profiles.....- 39 -

Figure 2.8 The effect of ore mineralogy on Bond Work Index following microwave treatments .....- 44 -

Figure 2.9: Comparison of the Modulus of Elasticity for common minerals .....- 48 -

Figure 2.10 Grain size distributions of grouped good microwave heating minerals for each ore. .....- 51 -

Figure 2.11 Summary of Point Load test results .....- 52 -

Figure 3.1 The Cosmic Microwave Background .....- 59 -

Figure 3.2 Diagram of an electromagnetic wave .....- 61 -

Figure 3.3 Electromagnetic spectrum .....- 61 -

Figure 3.4 The interaction of microwave energy with materials ....- 63 -

Figure 3.5 Characteristic frequencies of dielectric polarisation .....- 64 -

Figure 3.6 Dipolar polarisation mechanism .....- 65 -

Figure 3.7 Loss tangent vector diagram .....- 69 -

Figure 3.8 Dielectric loss tangent for selected minerals ..... - 77 -
Figure 3.9 Heating rates of selected copper ore minerals ..... - 78 -
Figure 3.10 Typical industrial microwave heating system ..... - 80 -
Figure 3.11 Diagram of a magnetron ..... - 82 -
Figure 3.12 Diagram of a coaxial cable ..... - 83 -
Figure 3.13 Example of the electric field pattern within a multimode cavity ..... - 87 -
Figure 4.1 Simulation of the regions of high electric field strength in each applicator ..... - 100 -
Figure 4.2 Photo of the dual applicator configuration of the pilot system..... - 101 -
Figure 4.3 Vertical flow configuration of the 150t/h and 2x100kW dual applicator pilot system. ..... - 102 -
Figure 4.4 Reactive and resistive choking structures..... - 103 -
Figure 4.5 Layout of the microwave treatment pilot system..... - 104 -
Figure 4.6 -50.8+25.4mm single size class ore feed ..... - 106 -
Figure 4.7 Example process log for an ore treated in the pilot system at 100kW and 130t/h..... - 107 -
Figure 4.8 Principle components of the batch system..... - 110 -
Figure 4.9 Batch system single applicator waveguide assembly.. - 111 -
Figure 4.10 Lower belt coupling assembly ..... - 113 -
Figure 4.11 Diagram of a typically loaded treatment tube of the batch system..... - 115 -
Figure 4.12 The recommended number of analysis points across an entire sample ..... - 119 -
Figure 4.13 FEI Quanta 600Mk1 MLA system ..... - 120 -
Figure 4.14 The region of the interaction volume from which the different signals originate. ..... - 122 -
Figure 4.15 Illustration of the relaxation of a higher-shell electrons into lower-shell vacancies ..... - 123 -
Figure 4.16 MLA measurement and analysis overview flowsheet - 127 -

Figure 4.17 Illustration comparing liberation by particle composition and free surface. .....- 130 -
Figure 4.18 Illustration of mineral locking.....- 130 -
Figure 4.19 The concept of mineral associations.....- 131 -
Figure 4.20 Mohs hardness and Microhardness (GPa).....- 133 -
Figure 4.21 Vacuum chamber used for epoxy impregnation of ore fragments.....- 141 -
Figure 4.22 Example of epoxy section produced for imaging. .....- 142 -
Figure 4.23 Leica M205FA stereomicroscope .....- 142 -
Figure 4.24 Example of a fragment image .....- 144 -
Figure 4.25 Fracture feature image analysis procedure .....- 146 -
Figure 4.26 Example of product of the total fragment surface area segmentation procedure.....- 147 -
Figure 5.1 MZ grain size distributions.....- 155 -
Figure 5.2 False colour mineral maps of MZ ore .....- 156 -
Figure 5.3 QZ grain size distributions.....- 157 -
Figure 5.4 False colour mineral maps of QZ ore.....- 158 -
Figure 5.5 QX grain size distributions.....- 159 -
Figure 5.6 False colour mineral maps of QX ore.....- 160 -
Figure 5.7 MZ ore Cu-sulphide distribution by liberation class. ...- 172 -
Figure 5.8: Cu-sulphide liberation (>98%) comparison for MZ untreated and treated samples .....- 173 -
Figure 5.9 Cu-sulphide liberation (>50%) comparison for MZ untreated and treated samples. .....- 174 -
Figure 5.10 MZ ore mineral locking data for Cu-sulphides occurring in binary particles with non-sulphide gangue. .....- 175 -
Figure 5.11 MZ ore mineral locking data for Cu-sulphides occurring in binary particles with pyrite. .....- 176 -
Figure 5.12 MZ ore mineral locking data for Cu-sulphides occurring in multiphase particles.....- 176 -
Figure 5.13 QZ ore Cu-sulphide distribution by liberation class...- 179 -

Figure 5.14: Cu-sulphide liberation (>98%) comparison for QZ untreated and treated samples ..... - 180 -

Figure 5.15 Cu-sulphide liberation (>50%) comparison for QZ untreated and treated samples ..... - 181 -

Figure 5.16 QZ ore mineral locking data for Cu-sulphides occurring in binary particles with non-sulphide gangue. ..... - 182 -

Figure 5.17 QZ ore mineral locking data for Cu-sulphides occurring in binary particles with pyrite. ..... - 182 -

Figure 5.18 QZ ore mineral locking data for Cu-sulphides occurring in multiphase particles. ..... - 183 -

Figure 5.19 Beneficial change in >98% liberated Cu-sulphides at varying microwave treatment doses. ..... - 184 -

Figure 5.20 Beneficial change in >98% liberated Cu-sulphides at varying microwave treatment power densities. ..... - 185 -

Figure 5.21 JK GeM Ci test -4.75mm product size distributions for MZ samples ..... - 188 -

Figure 5.22 JK GeM Ci test -4.75mm product size distributions for QZ samples ..... - 190 -

Figure 5.23 Beneficial change in comminution test results at varying microwave treatment doses for MZ ore. ..... - 193 -

Figure 5.24 Beneficial change in comminution test results at varying microwave treatment power densities for MZ ore. .... - 194 -

Figure 5.25 Beneficial change in comminution test results at varying microwave treatment doses for QZ ore. ..... - 194 -

Figure 5.26 Beneficial change in comminution test results at varying microwave treatment power densities for QZ ore. .... - 195 -

Figure 6.1 Example of pre-existing fractures in a highly mineralised untreated MZ fragment ..... - 202 -

Figure 6.2 Example of characteristic pre-existing fractures in an untreated QZ fragment ..... - 203 -

Figure 6.3 Example of pre-existing fractures in an untreated QX fragment ..... - 204 -

Figure 6.4 Fracture length distributions for untreated MZ, QZ and QX samples. .....- 205 -

Figure 6.5 Fracture length for MZ UT, T1 and T3. .....- 206 -

Figure 6.6 Fracture length for QZ UT, T1 and T3. .....- 207 -

Figure 6.7 Fracture length for QX UT, T1, T2 and T3 .....- 208 -

Figure 6.8 Beneficial change in fracture length D_{80} at varying microwave treatment doses. .....- 211 -

Figure 6.9 Beneficial change in fracture length D_{80} at varying microwave treatment power densities. .....- 212 -

Figure 6.10 Beneficial change in total fracture area at varying microwave treatment doses. .....- 215 -

Figure 6.11 Beneficial change in total fracture area at varying microwave treatment power densities. .....- 216 -

Figure 6.12 Percentage contribution of fracture length classes to total fracture density. .....- 218 -

Figure 6.13 Beneficial change in fracture density (1-5mm fractures) at varying microwave treatment doses. .....- 219 -

Figure 6.14 Beneficial change in fracture density (1-5mm fractures) at varying microwave treatment power densities. .....- 219 -

Figure 6.15 Beneficial change in fracture density (>5mm fractures) at varying microwave treatment doses. .....- 220 -

Figure 6.16 Beneficial change in fracture density (>5mm fractures) at varying microwave treatment power densities. .....- 221 -

Figure 6.17 Comparison of fracture analysis results with comminution test results .....- 222 -

Figure 6.18 Comparison of fracture analysis results with Cu-sulphide mineral liberation results. .....- 224 -

Figure 7.1 Particle size distribution of P_{80} 290μm target grinds for mineral liberation analysis. .....- 232 -

Figure 7.2 MZ ore Cu-sulphide distribution by liberation class. ...- 234 -

Figure 7.3 MZ ore Cu-sulphide distribution by 5% liberation classes for low dose treatments. .....- 235 -

Figure 7.4 Cu-Sulphide (Cu-S) mineral locking results for MZ ore low dose treatments. ..... - 236 -
Figure 7.5 Cu-Sulphide (Cu-S):Non-Sulphide Gangue (NSG) mineral locking results for MZ ore low dose treatments. ..... - 237 -
Figure 7.6 Beneficial change in >98% liberated Cu-sulphides for MZ ore at varying microwave treatment doses ..... - 240 -
Figure 7.7 Beneficial change in >98% liberated Cu-sulphides for MZ ore at varying microwave treatment power densities. - 241 -
Figure 7.8 Beneficial change in >98% liberated Cu-sulphides for MZ ore at varying microwave residence durations..... - 242 -
Figure A.1 MZ ore UT1 assay reconciliation. ..... - 282 -
Figure A.2 MZ ore T1 assay reconciliation..... - 282 -
Figure A.3 MZ ore T2 assay reconciliation..... - 283 -
Figure A.4 MZ ore T3 assay reconciliation..... - 283 -
Figure A.5 QZ ore UT assay reconciliation. ..... - 284 -
Figure A.6 QZ ore T1 assay reconciliation..... - 285 -
Figure A.7 QZ ore T2 assay reconciliation..... - 285 -
Figure A.8 QZ ore T3 assay reconciliation..... - 286 -
Figure A.9 MZ ore UT2 assay reconciliation. ..... - 287 -
Figure A.10 MZ ore T4 assay reconciliation..... - 288 -
Figure A.11 MZ ore T5 assay reconciliation..... - 289 -
Figure A.12 MZ ore T6 assay reconciliation..... - 290 -
Figure A.13 MZ ore T7 assay reconciliation..... - 291 -
Figure A.14 MZ UT2 target grind calibration ..... - 300 -
Figure A.15 MZ UT2 grind calibration particle size distributions. . - 300 -
Figure A.16 MZ T4 target grind calibration ..... - 302 -
Figure A.17 MZ T4 grind calibration particle size distributions. ... - 302 -
Figure A.18 MZ T5 target grind calibration ..... - 304 -
Figure A.19 MZ T5 grind calibration particle size distributions. ... - 304 -
Figure A.20 MZ T6 target grind calibration ..... - 306 -
Figure A.21 MZ T6 grind calibration particle size distributions. ... - 306 -

Figure A.22 MZ T7 target grind calibration ..... - 308 -
Figure A.23 MZ T7 grind calibration particle size distributions. ... - 308 -
Figure B.1 MZ UT1 Ci test data ..... - 309 -
Figure B.2 MZ T1 Ci test data..... - 309 -
Figure B.3 MZ T2 Ci test data..... - 310 -
Figure B.4 MZ T3 Ci test data..... - 310 -
Figure B.5 MZ UT2 Ci test data ..... - 311 -
Figure B.6 MZ T4 Ci test data..... - 312 -
Figure B.7 MZ T5 Ci test data..... - 313 -
Figure B.8 MZ T6 Ci test data..... - 314 -
Figure B.9 MZ T7 Ci test data..... - 315 -
Figure B.10 QZ UT Ci test data..... - 316 -
Figure B.11 QZ T1 Ci test data ..... - 316 -
Figure B.12 QZ T2 Ci test data ..... - 317 -
Figure B.13 QZ T3 Ci test data ..... - 317 -

List of Tables

Table 3.1 Dielectric constant (ε'), loss factor (ε") and loss tangent (tanδ) for sulphide and oxide minerals. ..... - 75 -

Table 3.2 Dielectric constant (ε'), loss factor (ε") and loss tangent (tanδ) for silicate, sheet silicate, carbonate, and other minerals. ..... - 76 -

Table 4.1 Sieve sizes. ..... - 97 -

Table 4.2 Number of sample mounts produced ..... - 125 -

Table 4.3 Mineral groupings ..... - 134 -

Table 5.1 Ungrouped modal mineralogy from coarse ore characterisation. ..... - 161 -

Table 5.2 Grouped mineral abundances from coarse ore characterisation ..... - 163 -

Table 5.3 Summary of MZ, QZ, and QX Ore microwave treatment amenability characteristics. ..... - 165 -

Table 5.4 Microwave treatment conditions s. ..... - 167 -

Table 5.5 MZ grouped mineral abundance for untreated and treated samples ..... - 170 -

Table 5.6 QZ grouped mineral abundance for untreated and treated samples ..... - 178 -

Table 5.7 JK GeM Ci test results ..... - 187 -

Table 5.8 BBMWi test results ..... - 191 -

Table 6.1 Samples selected for fracture analysis. ..... - 201 -

Table 6.2 K-S test outcomes for MZ samples ..... - 209 -

Table 6.3 K-S test outcomes for QZ samples ..... - 210 -

Table 6.4 K-S test outcomes for QX samples ..... - 210 -

Table 6.5 Total sample surface area and the total area of fractures measured in each sample. ..... - 213 -

Table 6.6 Total sample surface area and the total area of fractures >1mm in length measured in each sample. ..... - 214 -

Table 6.7 Fracture density results ..... - 217 -

Table 6.8 Summary of fracture analysis results .....- 221 -
Table 7.1 Microwave treatment conditions for MZ ore low dose treatments. .....- 230 -
Table 7.2 MZ ore grouped mineral abundance for untreated and low dose treated samples .....- 233 -
Table 7.3 MZ ore microwave treatment throughput, sample velocity and applicator residence duration. .....- 242 -
Table 7.4 JK GeM Ci test results. .....- 245 -
Table 7.5 BBMWi test results .....- 247 -
Table A.1 MZ ore UT1, T1, T2 and T3 XRF chemical assay data. .- 281 -
Table A.2 MZ ore UT1, T1, T2 and T3 QEMScan assay data. .....- 281 -
Table A.3 QZ ore UT1, T1, T2 and T3 XRF chemical assay data. .- 284 -
Table A.4 QZ ore UT1, T1, T2 and T3 QEMScan assay data. .....- 284 -
Table A.5 MZ ore UT2 XRF chemical assay data. .....- 287 -
Table A.6 MZ ore UT2 MLA calculated assay data. .....- 287 -
Table A.7 MZ ore T4 XRF chemical assay data. .....- 288 -
Table A.8 MZ ore T4 MLA calculated assay data. .....- 288 -
Table A.9 MZ ore T5 XRF chemical assay data. .....- 289 -
Table A.10 MZ ore T5 MLA calculated assay data. .....- 289 -
Table A.11 MZ ore T6 XRF chemical assay data. .....- 290 -
Table A.12 MZ ore T6 MLA calculated assay data. .....- 290 -
Table A.13 MZ ore T7 XRF chemical assay data. .....- 291 -
Table A.14 MZ ore T7 MLA calculated assay data. .....- 291 -
Table A.15 MZ coarse ore mineral grain size distribution .....- 292 -
Table A.16 QZ coarse ore mineral grain size distribution .....- 293 -
Table A.17 QX coarse ore mineral grain size distribution .....- 294 -
Table A.18 MZ Ore ungrouped mineral abundance. .....- 295 -
Table A.19 MZ Ore low dose microwave treatments ungrouped mineral abundance. .....- 295 -
Table A.20 QZ Ore ungrouped mineral abundance. .....- 296 -
Table A.21 MZ Ore liberation by free surface. .....- 296 -

Table A.22 QZ Ore liberation by free surface. ..... - 297 -
Table A.23 MZ Ore Cu-sulphide mineral liberation by free surface in 5% liberation classes ..... - 297 -
Table A.24 MZ Ore Cu-sulphide mineral locking ..... - 298 -
Table A.25 MZ Ore Cu-sulphide mineral locking with Non-Sulphide Gangue ..... - 298 -
Table A.26 QZ Ore Cu-sulphide mineral locking..... - 298 -
Table A.27 MZ Ore UT2 target liberation grind calibration data .. - 299 -
Table A.28 MZ Ore T4 target liberation grind calibration data .... - 301 -
Table A.29 MZ Ore T5 target liberation grind calibration data .... - 303 -
Table A.30 MZ Ore T6 target liberation grind calibration data .... - 305 -
Table A.31 MZ Ore T7 target liberation grind calibration data .... - 307 -
Table B.1 MZ Ore BBMWi test data summary ..... - 318 -
Table B.2 QZ Ore BBMWi test data summary ..... - 319 -
Table C.1 MZ Ore fracture length distribution data ..... - 321 -
Table C.2 QZ Ore fracture length distribution data ..... - 322 -
Table C.3 QX Ore fracture length distribution data ..... - 323 -
Table C.4: K-S test results for MZ Ore ..... - 324 -
Table C.5: K-S test results for QZ Ore ..... - 325 -
Table C.6: K-S test results for QX Ore ..... - 326 -
Table C.7: Values from K-S table used in calculating D crit for >95% and >99% confidence levels ..... - 327 -
Table C.8 K-S table of critical values for D_n ..... - 327 -

CHAPTER 1 – INTRODUCTION

Everything we use or consume in our daily lives ultimately originates from either farming or mining. As the demand for resources required for sustaining the global population increases, the development of more economically and environmentally sustainable methods and technologies to produce them has become an imperative for governments and corporations. This is no more evident than in the mining and minerals processing industry which provides many of the necessary raw materials for sustaining the development of modern civilisation. Many of these essential materials are produced through the mining of mineral ores from the Earth, and the extraction of useful and valuable non-metallic and metallic commodities.

Our global society is economically, socially and culturally dependent on minerals and metals that are extracted from the Earth's crust (Prior et al., 2012). The United Nations conservatively forecasts a global population of 9.6 billion in 2050, growing to 10.9 billion by 2100, which is an increase of ~50% on current population levels of 7.2 billion (United Nations, 2013). The increased demand for metals and minerals to support this growing population, the urbanisation and industrialisation of emerging economies, and continued advancement of developed economies, will necessitate an ongoing increase in the supply of these raw materials (Von Der Linden, 2006; Harmsen et al., 2013). This growth in demand is set against future conditions of increasingly constrained energy and water supplies, more complex ore bodies in challenging geographies, and stricter environmental legislative requirements. A necessary response to meet these future challenges is the development of step-change technological innovations in the field of mining and mineral processing. (Filippou and King, 2011).

1.1 PROJECT DRIVERS

In the context of the mining and minerals industry, the two main focusses for innovation are increasing the productivity of large-scale surface and underground mining processes, and improving the recovery and extraction of minerals and metals from increasingly complex and lower-grade ore bodies. Demand for copper (Cu) in particular, is growing throughout both emerging and developed economies (Gordon et al., 2006; Sverdrup et al., 2014). Usage of refined copper has increased by a compound annual growth rate of 3.4% per year since 1900 (ICSG, 2015), and demand is forecast to continue to grow (Sverdrup et al., 2014). As the global population increases and urbanisation progresses, continued increases in the per capita consumption of refined copper will accelerate the growth in demand, as is illustrated in Figure 1.1 (ICSG, 2015). In possessing properties of malleability, resistance to corrosion, and excellent conductivity of heat and electricity, copper is one of the most versatile and useful metals. It is used extensively throughout a range of applications, from computing and electronics to electrical and pipeline infrastructure (Northey et al., 2014).

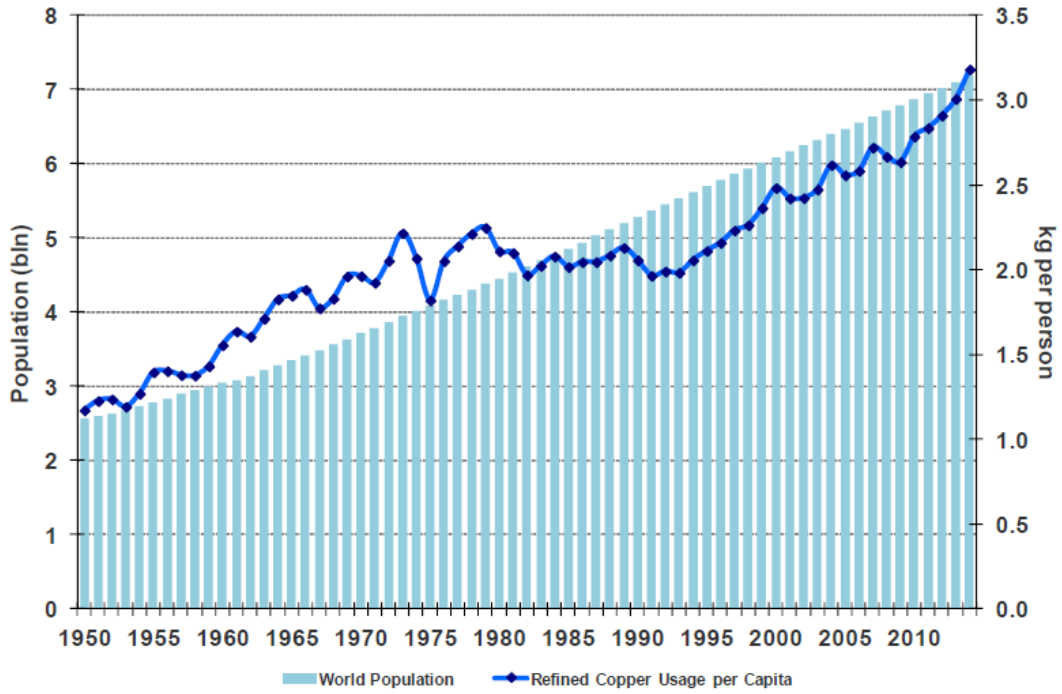


Figure 1.1 Global refined copper usage per capita 1950-2014. In this figure, per capita consumption of refined copper refers to the amount of copper consumed by global industry divided by the total global population. (ICSG, 2015)

Since industrial scale mining of copper began in the mid-19th century, a gradual long-term decline in ore grade has been well documented (Mudd, 2010; Crowson, 2012; Mudd et al., 2013; Northey et al., 2014). Since the early 20th century, average copper head grades of 1.5% to 4% Cu have declined significantly to a global average mined Cu ore grade of 0.62% in 2010, and average Cu ore deposit grades of 0.49% (Mudd et al., 2013; Northey et al., 2014). Ore grade models developed by Northey et al. (2014) project that the long term historical decline in copper grade will continue, as shown in Figure 1.2.

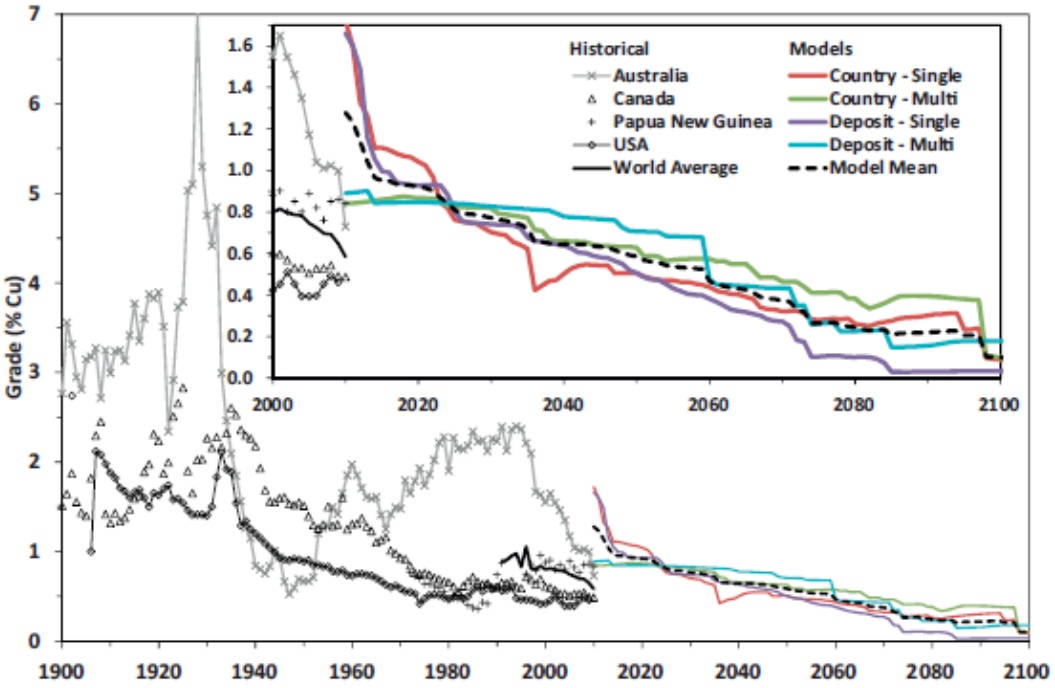


Figure 1.2 Historical copper ore grades to 2010 for selected countries, and projected global ore grades from 2010 to 2100 (Northey et al., 2014)

During this timeframe, global mined copper production has increased from <0.5Mt copper in 1900 to 18.1Mt in 2013, as shown in Figure 1.3 (ICSG, 2015). While copper supply is forecast to meet demand in the short-term, in the medium to long-term, demand for copper is projected to continue to grow. Figure 1.4 illustrates that current copper mining operations and probable future projects will be unable to provide the required production to meet the growing demand (Rio Tinto, 2014).

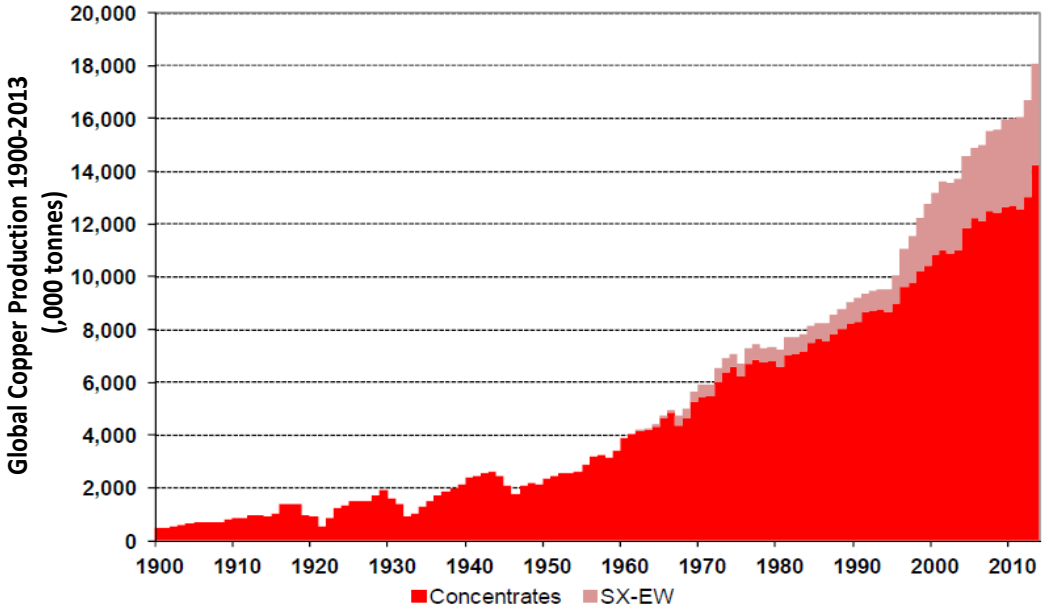


Figure 1.3 Global copper production 1900-2013 (ICSG, 2015)

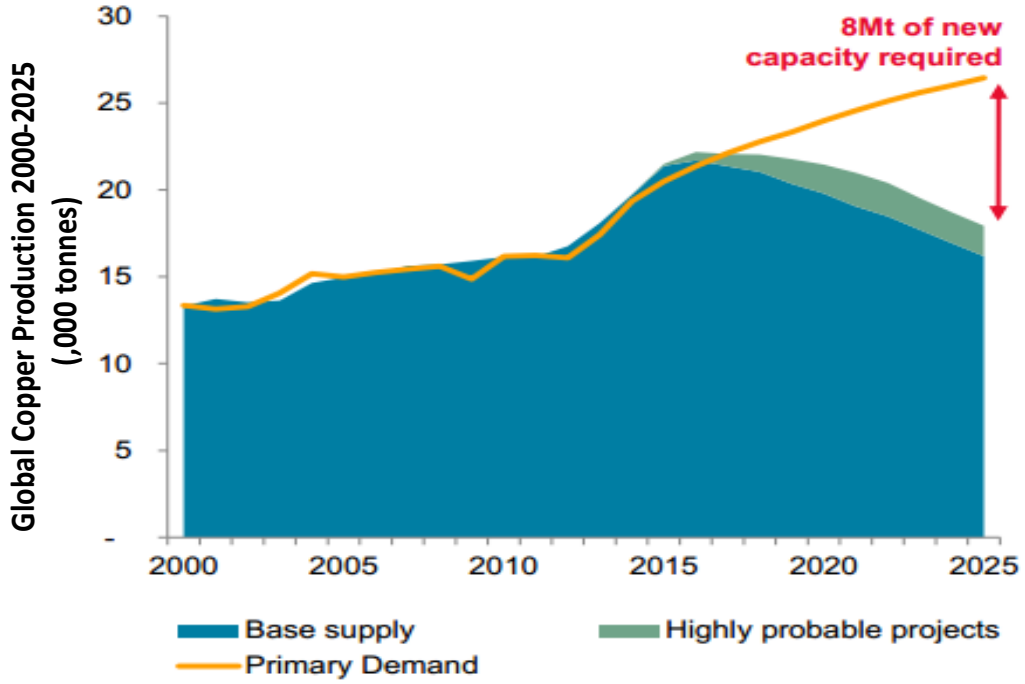


Figure 1.4 Forecast growth in copper demand and forecast copper production (Rio Tinto, 2014)

The idea of 'peak metals' in relation to copper is now being addressed, based on the fundamental concept that resources are finite and are being rapidly depleted, while replacing the supply is becoming increasingly expensive, and technically and geographically challenging

(May et al., 2012; Prior et al., 2012). As accessible resources of higher grade copper ore are being depleted, lower-grade and more complex porphyry style ore bodies must be mined and processed. The valuable minerals in these new lower-grade porphyry ore bodies tend to be finer grained and more disseminated throughout the host rock (Cooke et al., 2005; Sillitoe, 2010) . This makes recovery of the target minerals more difficult and less energy efficient, as finer grinding of the ore is required in order to achieve suitable levels of mineral liberation (Norgate and Jahanshahi, 2011). Lower grade ore will also necessitate that increased volumes of ore be processed in order to achieve the required levels of copper production (Prior et al., 2012). This in turn will lead to an increase in energy consumption in order to maintain required levels of global copper production (Harmsen et al., 2013). To overcome the future challenges in meeting the increasing global demand for copper and other minerals, new processes and technologies are required to efficiently and sustainably supply the required resources through the mining and processing of mineral ores.

A technique that has been shown to produce benefits for both comminution and mineral liberation, is through high power microwave treatment of mineral ores (Walkiewicz et al., 1988b; Walkiewicz et al., 1991; Kingman and Rowson, 1998; Bradshaw et al., 2007; Jones et al., 2007). The exposure of ores to microwave fields has been shown to induce a variable microwave response from different minerals, resulting in reduced ore strength and improved mineral liberation in ore fragments containing microwave heated mineralisation, through a process called thermally assisted liberation.

Microwave treatment technology exploits the properties of different mineral phases that cause only responsive or 'absorbent' minerals to be affected by incoming microwave radiation through rapid heating. Subsequent rapid thermal expansion due to heating within absorbent minerals causes physical stresses to be transferred to the surrounding non-absorbent or 'transparent' gangue minerals (Jones et al., 2005). The differential volumetric expansion of the microwave absorbent

minerals relative to the microwave transparent gangue is controlled by the differences in the heating rates of minerals in the ore (Rizmanoski, 2011). These stresses achieved can be high enough to exceed the strength of the material and cause cracking or micro-fracturing to occur along the grain boundaries between absorbent and transparent minerals. If sufficient microwave energy is applied to the ore, and the ore possesses suitable characteristics to effectively transfer the stresses throughout the ore matrix, then this network of micro-fractures can link together to create macro-fractures through fragments of treated ore.

The formation of micro-fractures around the grain boundaries of target minerals in the ore, would improve the ability to selectively liberate these minerals from the surrounding gangue minerals at a coarser grain size than is currently achievable with conventional comminution processes (Vizcarra et al., 2010). Limiting the degree of size reduction required to suitably liberate and separate the target minerals from the gangue would also limiting the amount of non-valuable material that is fed into the energy-intensive fine grinding (Vizcarra et al., 2010). This ability to liberate the value-bearing minerals from the ore at a coarser grind size would potentially deliver the step-change technology required to reduce the energy consumption, and improve the effectiveness and efficiency of comminution operations.

CHAPTER 2 – LITERATURE REVIEW

2.1 MINERAL PROCESSING

2.1.1 Introduction

A mineral ore is a mass of rock in which economically extractable minerals or metals have been deposited or concentrated in the Earth's crust through geological processes (Deer et al., 2013). Having been removed from the Earth through either open pit or underground mining, ores undergo subsequent downstream processing in order to extract the valuable minerals from the host rock.

Mineral processing is the initial stage in the process of extractive metallurgy, which is concerned with the economic extraction of valuable minerals from their host ores after mining (Wills and Napier-Munn, 2006). The two fundamental aims of mineral processing are the liberation of the valuable minerals from the host rock, and the separation of these minerals from this waste rock or gangue (Wills and Napier-Munn, 2006). The ultimate goal of mineral processing is to produce a concentrate of the valuable ore minerals by removing and discarding the gangue minerals, or waste rock with no economic value. This concentrate can then be submitted for further metallurgical processing to extract the target metal from the minerals to produce a saleable final product.

This section will provide a comprehensive background to the process of comminution as the initial stage of mineral processing, and describe some of the key innovative technologies that are being developed in this field. It will provide a background to microwave assisted comminution and liberation of ores, and present a review of previous experimental and theoretical work in this field. The chapter will conclude by summarising the current state of knowledge, identifying the current gaps existing in the understanding of the microwave treatment of ores, and will identify how the current investigation contributes to this field of study.

2.1.2 Comminution

2.1.2.1 Introduction

Liberation of valuable minerals is achieved through the process of comminution, which is the progressive mechanical size reduction of ore through in-pit blasting, crushing and grinding. This process will reduce an in-situ solid rock mass to a final target size where the valuable minerals are unlocked, or liberated, and able to be economically separated from the gangue (Wills and Napier-Munn, 2006). Crushing and grinding of the mined ore through a series of size reduction stages will reduce the ore to the particle size required for subsequent concentration or extractive processes.

The process of comminution is extremely energy intensive and inefficient, and typically represents 30-40% of the total energy used by mining and mineral processing operations to produce a mineral concentrate, as shown in Figure 2.1 (Tromans, 2008; Batterham, 2011; Curry et al., 2014; Nadolski et al., 2014). Crushing and grinding of mineral ores has been reported in several studies to consume between 1-4% of global electricity production (Daniel and Lewis-Gray, 2011; Norgate and Jahanshahi, 2011). Processing of copper ore has been shown to account for a disproportionate amount of this energy use, making up almost a quarter of all comminution energy consumption in the United States, as shown in Figure 2.2 (Herbst et al., 2003).

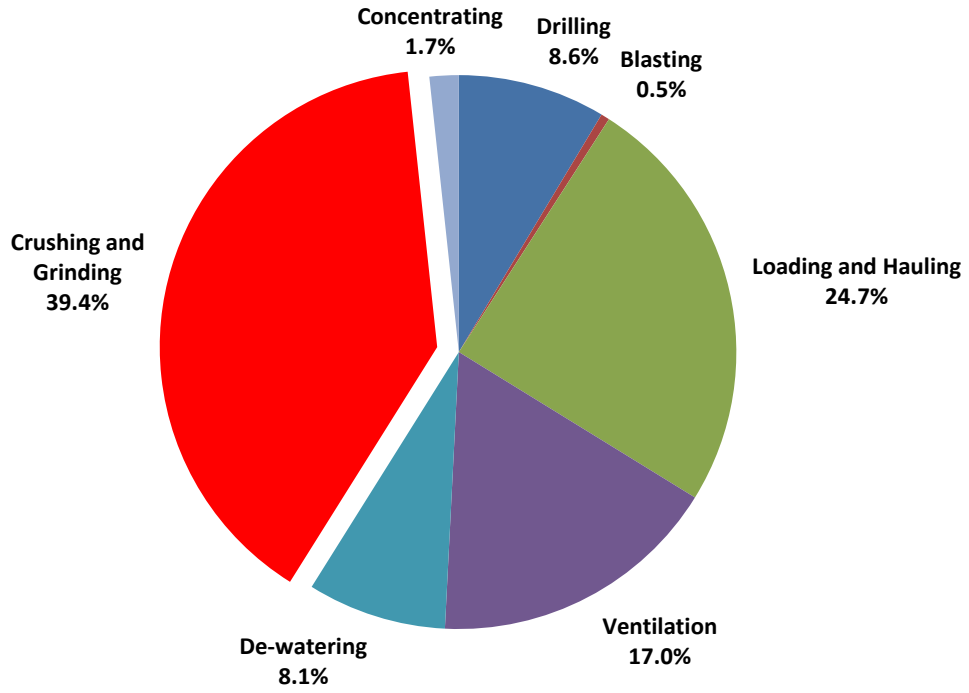


Figure 2.1 Typical distribution of energy consumption to produce a copper concentrate (Norgate and Haque, 2010)

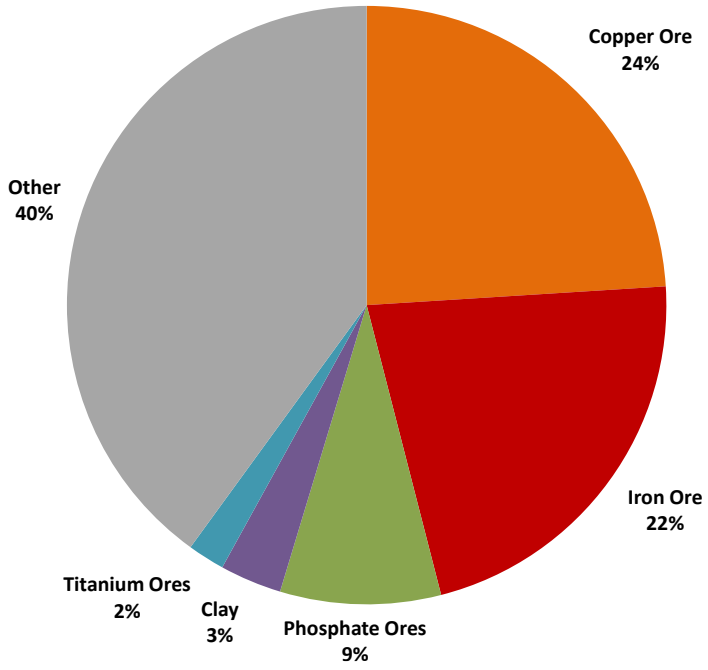


Figure 2.2 Comminution energy consumption by commodity in the United States in 2000 (Herbst et al., 2003)

Comminution has also been recognised as a fundamentally inefficient process, with only <1-2% of the energy consumed directly applied to the creation of new fracture surface area, with the rest of the input energy lost to the environment as heat and noise (Fuerstenau and

Abouzeid, 2002; Tromans, 2008; Djordjevic, 2010). The development of transformational or "step-change" mineral processing technologies is required to more efficiently liberate valuable minerals at a coarser grind size, through a more effective application of energy during the comminution of mineral ores (Batterham, 2011; Drinkwater et al., 2012b).

The ability to alter the properties of an ore in order to reduce strength and improve target mineral liberation is the most likely avenue by which significant improvements in the efficiency of comminution processes will be realised (Kingman et al., 2004b). Current comminution practices involve random mechanical and impact breakage, which focus on reducing the physical dimensions of the ore fragments, with liberation of target minerals occurring as a side-effect of this process (Wills and Napier-Munn, 2006). The only controllable factor is the final size distribution of the ore following comminution, with the aim of ensuring an acceptable amount of liberation of the target minerals for downstream separation processes. As an ore is progressively reduced in size, an increasing proportion of ultra-fine particles (<20μm) are also produced, which are difficult to extract during the subsequent separation process, and overall recovery of the target mineral can be reduced (Napier-Munn et al., 1999).

2.1.2.2 Ore Fracture Mechanisms

Rocks deform when an applied stress exceeds their strength (Hamblin and Christiansen, 2004). Where the magnitude of a stress is not the same in all directions a rock will experience differential stress. As a result, the rocks yield to the unequal stress and deform by changing shape, which is referred to as strain (Wills and Napier-Munn, 2006). Although strain in rocks proceeds by several complex phenomena, two end-member styles of deformation are recognised, with all gradations along a spectrum between them being possible. One end of the continuum is characterised by brittle deformation, where rocks accommodate strain through fracturing and non-recoverable loss of

cohesion within the rock mass. At the opposite end of the strain response spectrum, rocks accommodate strain through ductile deformation, where a rock mass deforms permanently without fracturing or loss of cohesion. It is the elastic properties of a material, rock or mineral that determines how it accommodates strain as the result of applied forces (Angel et al., 2009)

The term elasticity refers specifically to reversible and instantaneous changes, rather than the permanent and irreversible changes that occur during ductile deformation (Wills and Atkinson, 1993). If a material is said to be elastic, it implies that it can return to its initial state by itself when the applied stress is removed. If a material behaves in a ductile manner, it does not return to its original state, but remains in the final strain state achieved when the applied stress is removed. If a deforming force or stress is great enough, a material can undergo brittle deformation or fracture and is permanently damaged. Materials where the outcome of the relationship between stress and strain depends on time are termed viscoelastic. Commonly for viscoelastic materials, a slow strain rate will allow the material to recover to its original state once the stress has been removed, while a faster strain rate may overcome a materials resistance to strain, leading to permanent deformation occurring (Wang, 2015).

When a polycrystalline aggregate, such as a rock or an ore fragment, is subjected to an applied force, all of the individual grains making up the material are subjected to differential stresses determined not only by the applied force, but also by the varied interactions of grains with each other (Angel et al., 2009). In the context of ore comminution, the specific outcome of a deformation or breakage event is determined by the structure and composition of an ore, and how the ore material behaves under an applied load (Napier-Munn et al., 1999). When a crystalline material such as a mineral ore is placed under compression, tensile stresses are produced within the crystallographic lattice bonds in the ore. If a sufficient compressive load is applied, the lattice bonds joining together the constituent mineral grains in the ore will break

and a crack will be initiated (Napier-Munn et al., 1999). During the operation of a comminution circuit, stresses are applied to each particle with the goal of achieving a critical strain energy at which the particle breaks, and the energy is converted to surface energy (Martins, 2016)

Figure 2.3 shows an idealised stress-strain plot to illustrate the characteristic behaviour of a rock under an applied compressive load. The region from O to A is the elastic zone, and shows the ratio of stress to strain for a material. During this elastic deformation zone, any strain that occurs will be recoverable. Point A represents the yield point, or the elastic limit for the material where permanent strain begins to occur, with the applied stress at this point referred to as the yield stress. Prior to a material reaching its yield stress, the recoverable deformation occurs due to changes in the arrangement of atoms in the crystal lattice of the minerals comprising the rock (Wills and Atkinson, 1993). It is the accumulation of strain energy within the rock that is used to return it to its original shape and volume once the application of force has ceased. This relationship between stress and strain occurring in the region of elastic behaviour between points O and A is linear, and can be described by Hooke's Law:

$$\sigma = E \in \qquad \textbf{Equation 2.1}$$

Where σ is the applied stress (force per unit area), ∈ is strain, and E is Young's modulus of elasticity.

Young's modulus of elasticity describes tensile elasticity, or the tendency of an object to deform along an axis when opposing forces are applied along that axis, and is defined as the ratio of tensile stress to tensile strain and is often referred to as the elastic modulus. Essentially, the higher the value of Young's modulus for a material or mineral, the more resistance it is to elastic deformation.

Region A to B represents the ductile zone where non-recoverable deformation occurs, however the rock still retains its ability to resist the applied force. Deformation in this region is characterised by

micro-fracturing on the grain scale or smaller, commonly occurring through grain dilation and subsequent displacement or dislocations along grain boundaries or defects within the crystal lattice of constituent mineral grains (Atkinson, 1975; Wills and Atkinson, 1993).

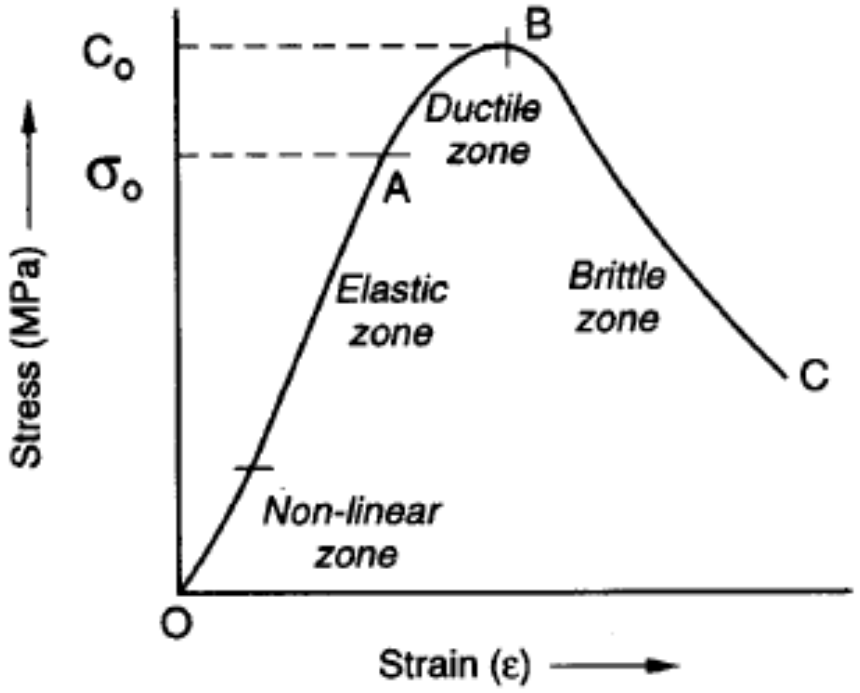


Figure 2.3 A characteristic stress-strain curve for a cylindrical rock sample under compression (Reproduced from Napier-Munn et al. (1999))

Once a rock undergoing deformation passes point B, brittle fracture occurs as the ability of the material to resist the force decreases. As a material is subjected to increased stress, the dislocations that occurred along grain boundaries during the ductile stage of deformation can join together to form continuous cracks. Point B indicates the transition between ductile and brittle deformation behaviour, and in the region from B to C, strain will take the form of a sudden and permanent loss of cohesion through brittle fracture, or macro-fracturing. Point C indicates the residual strength of the material.

In describing the mechanism of brittle fracture, Griffith (1921) showed that stresses which concentrate in regions around the tips of flaws in a material, lead to the initiation and propagation of brittle fractures at

these locations. The author further showed through energy balances on moving crack tips that the overall stress around the tip must reach a critical or threshold value at which a crack will begin to propagate. If the application of stress continues, unstable propagation of cracks will accelerate through the material to high velocities approaching 40% of the speed of sound in the solid material. The release of stored strain energy within the material during this process can exceed the energy associated with the new surface produced, and this surplus energy can also contribute to the initiation and propagation of fractures. The failure of a brittle solid such as a mineral ore can be deemed to be caused by the extension of Griffith cracks inherent within the material (Wills and Atkinson, 1993). The energy to drive this process is supplied by external forces applied during comminution, the release of stored strain energy in the solid, or by a combination of these two sources.

It is the microscale mineralogical and textural features of an ore that controls the mechanism by which the ore responds to an applied stress during comminution (Napier-Munn et al., 1999). A recent numerical modelling study by Wang (2015) investigated the influence of the elasticity of the minerals comprising an ore on complex heterogeneous rock breakage behaviour. The study demonstrated that heterogeneity of the mineral properties of a rock has a considerable effect on the breakage results, and that the occurrence of macro-fracturing is primarily dependent on the difference between the elastic properties of adjacent mineral grains. Where the elastic properties of the minerals and the strength of the bonds and ore matrix are similar, random breakage will tend to occur through the formation of transgranular, rather than intergranular fractures (Wills and Atkinson, 1993)

Fracture propagation during comminution is also influenced by the orientation of the cracks inside the particle with respect to the loading conditions. If the weaker grain boundaries can act as stress concentrators, then crack propagation will mainly follow grain boundaries as intergranular fractures. Intergranular fracture is

desirable from a mineral processing perspective as liberation can be achieved of the target minerals closer to their native grain size. Conventional comminution methods tend to promote transgranular fractures due to the random orientation of particles and complex loading conditions and particle interaction during comminution (Wills and Napier-Munn, 2006)

The nature and location of crack formation in an ore during comminution has been shown to be influenced by the elasticity of the constituent minerals, mineral grain size and texture, the associations between minerals with different elasticity, and the rate of strain (Djordjevic, 2014). As such, an understanding of these principles of fracture mechanisms in ores, and awareness of the influence of the elastic properties of the individual minerals comprising the ores, is important in achieving the aims of this investigation.

2.1.2.3 The Energy-Size Reduction Relationship

More energy is required to reduce the size of finer particles than coarser particles, as shown in Figure 2.4. This is due to finer particles having fewer remaining flaws to be exploited during comminution processes. As described in the previous section, weaker grain boundaries within particles can act as stress conduits, allowing for crack propagation and the creation and transmission of intergranular fractures. As particle size decreases and there are fewer internal flaws within the particles, the strength of the particles approaches the intrinsic strength of the individual mineral grains and increased energy is required to break them further (Hukki, 1961).

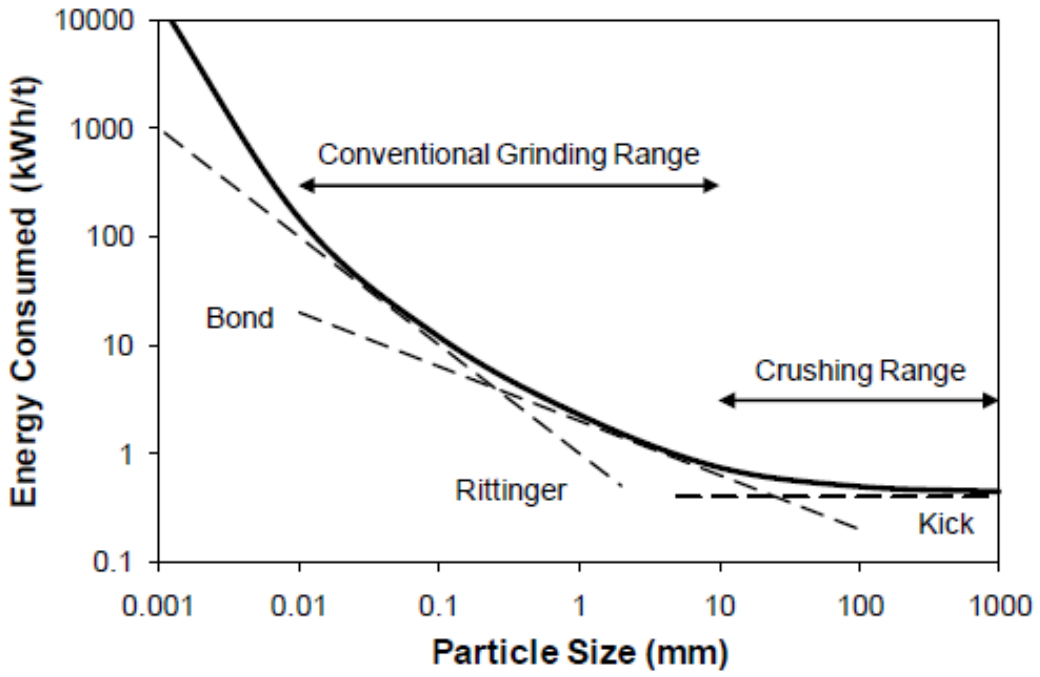


Figure 2.4 Relationship between particle size reduction and the required comminution energy input (After Hukki (1961))

While the fundamentals of this relationship have been investigated by several authors, none has provided an entirely satisfactory description (Wills and Atkinson, 1993). The proposed theories to describe the relationship do not take into account that the majority of the energy input to a comminution machine is turned into noise and heat, with only a small fraction being available for breaking the ore and the creation of new surface area (Tromans, 2008). The proposed theories also assume that all the material undergoes brittle fracture, and do not take into account energy that is consumed through elastic and ductile deformation processes that do not result in fracture (Wills and Napier-Munn, 2006).

The first author to attempt to describe the relationship was von Rittinger (1867) who stated that the energy consumed during size reduction is proportional to the area of new surface produced. Since the surface area of a known weight of particles of uniform diameter is inversely proportional to their diameter, Rittinger's law is expressed as:

$$E = K\left(\frac{1}{x_2} - \frac{1}{x_1}\right)$$

Equation 2.2

Where E is the breakage energy input, x_1 is the initial particle size, x_2 is the final particle size, and K is a constant.

Kick (1885) proposed a second theory on the energy requirements for comminution where he stated that the work required is proportional to the reduction in volume of the particles. This relationship is expressed as:

$$E = K.ln(x_1/x_2)$$

Equation 2.3

Where E is the breakage energy input, x_1 is the initial particle size, x_2 is the final particle size, and K is a constant.

A third theory describing comminution energy requirements was proposed by Bond (1952), and stated that the work input is proportional to the new crack tip length produced during particle breakage. In particles of similar shape, the surface area of unit volume is inversely proportional to the diameter. The crack length is considered to be proportional to one side of that area and therefore inversely proportional to the square root of the diameter (Wills and Napier-Munn, 2006). Bond's equation is expressed as:

$$E = K\left(\frac{1}{\sqrt{x_2}} - \frac{1}{\sqrt{x_1}}\right)$$

Equation 2.4

Where E = breakage energy per unit mass of feed, x_1 = initial particle size, x_2 = final particle size, K =is a constant.

This equation expressing Bond's theory is more commonly applied in a mineral processing context with the 80% passing size of the feed and product size distributions being used for the particle size terms (Napier-Munn et al., 1999). In this form the Work Index of an ore, which is material specific and dependent on the resistance of the material to crushing and grinding acts, as the constant. Work index can be defined as the energy requirement in kilowatt hours per ton (kWh/t) to reduce the particle size of a material from a known feed

size to 80% passing 100μm (Wills and Napier-Munn, 2006). The equation describes the work input required to reduce an ore from a particular feed size to a particular product size, and is expressed as:

$$W = WI\left(\frac{10}{\sqrt{P_{80}}} - \frac{10}{\sqrt{F_{80}}}\right)$$

Equation 2.5

Where W = work input, (kWh/t); WI = work index, (kWh/t); P80 = size at which 80% of the product passes, (μm); F80 = size at which 80% of the feed passes, (μm).

While none of these theories adequately describes the full range of the energy-size reduction relationship in mineral processing, each of the theories can be applied over the range of sizes for which they are most accurate (Hukki, 1961). As can be seen in Figure 2.4, Kick's theory applies to coarser crushing above a particle size of 10mm, Bond's theory describes grinding between ~10μm to 10mm, and fine grinding between ~1-100 μm is best described by Rittinger's theory (Hukki, 1961).

While several authors have attempted to unify or modify these theories into a universal model of comminution energy consumption (Hukki, 1961; Morrell, 2004; Martins, 2016), the theory of Bond has become the industry standard for use in comminution testing of ores (Morrell, 2004; Wills and Napier-Munn, 2006).

2.1.2.4 Mineral Liberation

The aim of ore comminution is to break ore delivered from a mine to a small enough particle size that the valuable or target minerals are liberated from the surrounding waste rock, or gangue (Napier-Munn et al., 1999). The degree of size reduction required for a given ore is determined by the mineralogy of the target minerals in the ore, in particular the target mineral grain size. Ores which possess target minerals with a fine grain size will require a greater degree of size reduction than ores possessing a coarser grain size. As was discussed in the introduction, the copper industry is experiencing a trend towards

finer grained ores which will require additional size reduction for concentration of the target minerals into a saleable product. As such, investigations into new technologies to enhance the process of comminution and mineral liberation are of paramount importance in the context of mining and mineral processing (Daniel and Lewis-Gray, 2011; Drinkwater et al., 2012a; Napier-Munn, 2015).

In theory, if the particle size of the comminution product of an ore could be reduced to below the size of the smallest constituent mineral grain, then 100% liberation would be achieved. Above this size, some target minerals will remain either partially or completely locked with gangue as composite multi-mineral particles. In practice it is difficult, and also not economically viable, to achieve 100% target mineral liberation of copper ores, as this would consume a vast amount of energy and time. In reality, comminution circuits produce a distribution of different particle compositions, and subsequently a distribution of recovery probabilities in the next stage of processing (Napier-Munn et al., 1999; Jameson, 2012). Comminution is therefore a compromise between achieving an acceptable degree of liberation for downstream separation processes, and the cost of crushing and grinding to the required particle size to achieve this degree of liberation. A high degree of liberation is required for processes such as froth flotation, where surface area exposure is required for optimal separation to occur (Wills and Atkinson, 1993). In this case the higher the degree of liberation, the higher the efficiency of the separation process. In other processes such as leaching where only a small surface of mineral may be sufficient for extraction, the required degree of liberation for efficient separation may be considerably lower (Al-Harahsheh et al., 2005).

The key to achieving successful liberation in mineral ores is the generation of intergranular, rather than transgranular fractures (Wills and Atkinson, 1993). Intergranular fracturing is an example of non-random breakage which involves selective fracture formation along grain boundaries (Mariano et al., 2016). Selective fracturing which

occurs more frequently along the boundaries of certain minerals can be termed preferential breakage (King and Schneider, 1998). In comminution processes where intergranular preferential breakage is observed, liberation by detachment can occur, which has the effect of loosening and liberating minerals exhibiting preferential breakage patterns closer to their 'native' or original grain size (Gaudin, 1939). It is through the preferential weakening of the interfaces and matrix between certain mineral grains that liberation by detachment can be achieved (Hsih and Wen, 1994).

In contrast, transgranular fracturing occurs as the result of random breakage, which has been summarised by Mariano et al. (2016) as the independence of breakage from both ore properties and mechanical properties during comminution, where grain boundary fracturing is not observed. Random breakage produces a fracture pattern which is spatially homogenous and isotropic, and is independent of ore texture or mineral properties (King, 1994). Where random transgranular breakage occurs, it is less likely for liberation of target mineral grains to be observed (Djordjevic, 2014). Random breakage has also been referred to as non-preferential breakage, where breakage occurs independent of mineral content (Gay, 1999; Wei and Gay, 1999; Gay, 2004). Figure 2.5 illustrates the different types of fracturing that can be observed in comminuted ore particles.

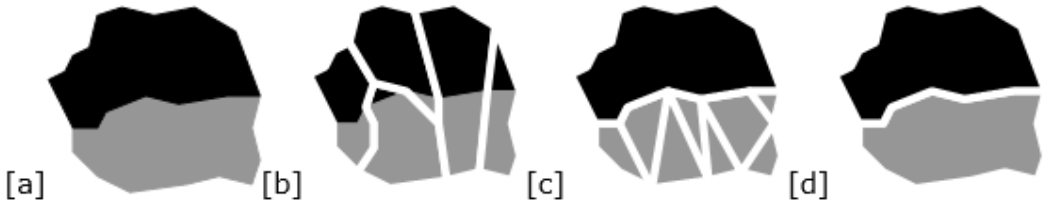


Figure 2.5 [a] Original particle; [b] shows random transgranular fracture across grain boundaries [c] shows preferential breakage [d] shows selective non-random intergranular fracture (reproduced from Batchelor (2013))

It has also been identified that the speed of crack propagation, which is related to the rate of strain, can influence whether random or non-random breakage takes place during comminution. It is suggested

that lower energy inputs, and a subsequently slower strain rate during comminution would promote stable crack propagation and exploit grain boundary weakness more effectively than high energy and fast-strain processes (Wills and Atkinson, 1993). Stable crack propagation along grain boundaries has been shown to be most effective at lower velocities, unlike in conventional comminution processes where high strain rates cause unstable crack propagation, leading to random transgranular fracturing (Meredith and Atkinson, 1983). Furthermore, it is suggested that comminution conducted through the slow application of pressure to an ore, rather than by rapid impact events, can create residual internal stresses which can cause cracking to occur during a subsequent relaxation phase in the material (Wills and Atkinson, 1993). Where comminution energy is transmitted rapidly to the ore, the material has little time to absorb the strain energy, and no material relaxation phase cracking will occur.

The ability to accurately measure mineral liberation in an ore comminution product is an essential pre-requisite for the provision of robust mineralogical data that is relevant for the optimisation of comminution processes (Gottlieb et al., 2000; Gu, 2003; Fandrich et al., 2007a; Sylvester, 2012a; Bradshaw, 2014). The development of quantitative automated mineralogy tools, and the advancement of the professional field of process mineralogy, which can be defined as the practical study of minerals associated with the processing and beneficiation of ores, have been instrumental in improving the understanding of mineral liberation and its importance in mineral processing operations (Fandrich et al., 2007a; Lotter, 2011; Bradshaw, 2014; Gu et al., 2014). A detailed background to automated mineralogy systems and their application will be provided in Chapter 4.

Comminution processes which can promote preferential intergranular fracturing to occur along grain boundaries of targeted valuable minerals, rather than random transgranular fracture, would be the optimal means through which to maximise the liberation potential of a mineral ore. The ability to selectively liberate minerals from the

surrounding gangue would be a significant advance in mineral processing technology (Vizcarra et al., 2010), and understanding the basic fundamentals of comminution, liberation and the mechanisms of ore fracture are essential aspects to the development and testing of new comminution technologies (Powell and Morrison, 2007).

2.1.2.5 Flotation

Mineral liberation is essential so that target minerals can be separated from the gangue via froth flotation, in order for a mineral concentrate to be produced for further metallurgical processing (Wills and Napier-Munn, 2006). Froth flotation is the most widely used method for concentrating metalliferous minerals, and has been the subject of a considerable body of research over the past century. As such, it is likely to be the final downstream process for producing mineral concentrate from ore particles produced using newly developed comminution technologies.

Flotation exploits differences in the surface chemistry of minerals by making them either hydrophobic or hydrophilic through the addition of chemicals, known as reagents. A slurry of ore and water is agitated and air is bubbled through the suspension. A reagent called a frother is added to the slurry, which makes a stable froth of bubbles so that the particles can be collected from the surface of the suspension into a concentrated stream. Without the frother, the bubbles would burst and the minerals would fall back into the slurry. Hydrophobic particles will become attracted to the bubbles, attach to them, and rise to the surface.

While there are several factors that influence flotation performance including air flow rate, bubble size, degree of agitation, pulp density, and reagent type and dosage (Jameson et al., 1977), successful recovery of a particle bearing the target mineral to the concentrate primarily depends on particle size, and the free surface of the hydrophobic mineral in the particle (Jameson, 2012). Coarser particles

can be too heavy and will not successfully attach to bubbles and remain in the suspension. Ultra-fine particles of low mass may readily oxidise or be coated in slimes, inhibiting bubble attachment. Therefore, an optimum particle size exists for maximum rate of flotation, and is usually in the range of 10-100μm (Wills, 2006). Additionally, particles with a larger proportion of free surface of hydrophobic mineral, or particles with a greater degree of liberation of the target minerals, will float more readily than particles with less exposed surface. This serves to highlight the importance of improving mineral liberation during the process of ore comminution.

2.2 Innovations in Comminution

2.2.1 Introduction

The present century has seen an ever growing emphasis on the need for more efficient use of energy in mineral processing, and progress is being seen in industry-academia research collaborations, optimisation of existing comminution circuits, and new technology innovations (CEEC, 2012b).

The development of novel comminution technologies has been identified as a key requirement for the mining and mineral processing industry, with a focus on achieving a more effective application of energy during the comminution of mineral ores (Pokrajcic et al., 2009; Batterham, 2011; Daniel and Lewis-Gray, 2011; Drinkwater et al., 2012b). The ability to alter the properties of an ore in order to reduce strength and improve target mineral liberation has been identified by several authors as the most likely avenue by which significant improvements in the efficiency of comminution processes will be realised (Veasey and Wills, 1991; Kingman et al., 2004b; Tavares, 2005; Andres, 2010; CEEC, 2012a; Batterham, 2013).

Despite considerable environmental and economic incentives, only a limited number of novel step-change innovations in ore comminution

methods have been investigated and developed (Napier-Munn, 2015), including electrical comminution using high-voltage pulses (Andres, 2010; Wang et al., 2011; Van Der Wielen et al., 2013; Zuo et al., 2015b), confined particle bed breakage by High Pressure Grinding Rolls (HPGR) (Schönert, 1988; Tavares, 2005; Baum and Ausburn, 2011; Kodali et al., 2011; Ghorbani et al., 2013; Liu and Powell, 2016), and thermally assisted liberation by high power microwave treatment (Kingman and Rowson, 1997; Vorster et al., 2001; Kingman et al., 2004a; Jones et al., 2005; Pickles, 2009; Rizmanoski, 2011; Batchelor et al., 2016; Marion et al., 2016).

2.2.2 High Pressure Grinding Rolls

High Pressure Grinding Rolls (HPGR) are a currently available technology with the potential for addressing the energy challenges facing the mineral processing industry (Schönert, 1988; Fuerstenau and Kapur, 1995).

The development of HPGR technology initially began with a fundamental study by Schönert (1979), which suggested that the most energy efficient method of comminuting particles is by compressing them between two plates. HPGR comminution was developed from this premise as a method for applying this principle in a continuous process, through compression of an ore particle bed which is choke-fed between two counter rotating rollers. Comminution occurs in the HPGR due to the high inter-particle stresses that are generated when a solid bed of ore particles is compressed as it moves through the gap between two pressurised rollers (Wills and Napier-Munn, 2006). The high inter-particle stresses that result during this process can result in a much greater production of finer material in comparison to conventional crushing methods (Tavares, 2005). It has also been observed that crushing ore in the HPGR produces a weakened product, particular in coarser particles which experience a longer exposure to the compressive forces between the rolls. This finding is consistent with the theory that slower strain rates during comminution promote

stable crack propagation and exploit grain boundary weakness more effectively, leading to a more pronounced weakening effect (Clarke and Wills, 1989; Wills and Atkinson, 1993).

Baum et al. (1997) identified key benefits of the use of HPGR as being reduced consumption of energy and steel grinding media, and improvements in mineral liberation in comminution processes following HPGR crushing, due to the introduction of micro-fractures in the ore. Baum et al. (1997) and Baum and Ausburn (2011) also suggested that induced micro-fractures can also be expected to improve heap and column leach extraction recoveries in ores crushed by HPGR, when compared to conventional comminution methods. HPGR have been accepted as an effective comminution technology in the kimberlite and lamproite diamond processing industry as a method of liberating the hard diamonds from the softer gangue material, with the advantage of not breaking any large diamonds in the process (von Michaelis, 2005).

Mineral processing benefits such as improved mineral liberation, a reduction in untreatable fines, reductions in grinding energy consumption and increases in mineral recovery have also been reported (Battersby et al., 1992; Norgate and Weller, 1994; Fuerstenau and Kapur, 1995; Aydoğan et al., 2006; Ghorbani et al., 2013). The application and advantages of HPGR in comminution circuits is becoming well established, and the technology has been accepted as a viable comminution option for appropriate ores (von Michaelis, 2005; Rosario and Drozdiak, 2015).

2.2.3 High Voltage Pulse Fragmentation

A novel comminution technology that is currently in the process of development and scale-up for commercialisation in mineral processing applications is the treatment and pre-weakening of ore particles by High Voltage Pulse (HVP) (Zuo et al., 2015b). HVP breakage is a comminution method that exploits the electrical properties of minerals and rocks, resulting in the electrical disintegration of ores by high

voltage electrical pulses (Andres, 2010). High voltage pulses initiate electrical breakdown inside ore particles that are immersed in water, which generates a strong tensile force resulting in disintegration of the particles. The explosive force resulting in electrical disintegration is provided by the rapid expansion of ionized gas, or plasma, from electrical pulses that causes the direct conversion of solids to gases at temperatures in the order of 10^4K. Electrical disintegration therefore occurs by a combination of plasma expansion exceeding the tensile strength of the material and reflection of pressure waves off inclusions (Andres, 1989).

Early investigations in this field focussed on the mechanisms of explosive electrical disintegration, and the effect of the associated ultrasonic pressure waves on mineral liberation (Yutkin, 1955; Andres, 1977; Parekh et al., 1984; Andres, 1989). This early work identified that reductions in ore competency and improved liberation of minerals was observable in HVP treated ores, and the method was recognised as a potential novel alternative to traditional mechanical comminution methods and warranted further investigation (Veasey and Wills, 1991).

As a new technology with the potential of addressing the challenges facing the mineral processing industry, HVP has attracted the attention of researchers and industry (Zuo et al., 2015b). It has been identified that HVP breakage presents an alternative to conventional mechanical comminution methods, as it has been shown to promote preferential intergranular breakage within treated ore particles (Parker et al., 2015).

Wang et al. (2011) found that particle strength of a number of ores can be reduced significantly by HVP treatment using a low specific energy, resulting in a reduction in energy consumption in downstream processing. Recent comparison studies between electrical comminution and laboratory rod mills at the same specific energy levels have also demonstrated the production of a coarser more liberated product with fewer fines (Wang et al., 2012).

The difference in breakage behaviour of HVP treated ores was investigated by Zuo et al. (2015a), who suggested that it is the content and location of minerals with high electrical conductivity that has the greatest effect on the breakage behaviour of ore particles. It is the concentration of breakage effects around these high conductivity minerals that promotes the fracturing of ore aggregates along the interfaces of the mineral constituents (Andres, 2010). Zuo et al. (2015b) also investigated the effects of energy input on the HVP breakage of ores. Energy input (kWh/t) was calculated from the total generator energy input and the total particle mass in the test. The results indicated that the majority of ore particles tested in the study can achieve body breakage, or macro-fracture, at a specific energy of between 2-4kWh/t. The study concluded that the energy input of HVP treatment is one of the most significant factors affecting breakage behaviour of an ore, with larger energy inputs producing a higher body breakage probability. The results also indicated that ore properties such as mineral composition, texture and particle size influence the effectiveness of HVP treatment outcomes.

A recent study by Parker et al. (2015) on HVP treatment of a porphyry copper ore, found that although an improvement in chalcopyrite liberation in coarse size fractions was observed, the HVP process led to oxidation and surface chemistry changes on the chalcopyrite. It was observed however, that the surface oxidation did not adversely affect mineral recovery in subsequent flotation tests, as it was proposed that rod mill grinding following the HVP treatment 'cleaned' the surface oxidation from the liberated mineral grains. The author does suggest however, that leaching directly after HVP treatment, without an intermediate grinding stage, may be inhibited by the passivating layer of surface oxidation.

HVP treatment effects have also been shown to be applicable in fields of research and industry beyond mineral processing (Van Der Wielen et al., 2014). Laboratory and pilot scale HVP treatment plants have been

applied to sample preparation and separation of mineral grains for geochronological studies (Giese et al., 2007; Reddy et al., 2015; Hertwig et al., 2016), low contamination crushing of high-purity silicon rods (Selfrag, 2014), and disaggregation of concrete and electronic scrap for recycling purposes(Bluhm et al., 2000; Diao et al., 2013).

It appears that there is considerable potential for the use of HVP treatment as a pre-treatment technology that could be incorporated into existing comminution circuits, or included in new circuit design. Research continues in this promising field to further develop the understanding of the fundamentals of the HVP treatment of ores, and how the technology can best be exploited in addressing the challenges faced in mineral processing.

2.2.4 Summary

To address the challenge of reducing energy use in comminution, new technologies are required that promote selective intergranular fracture to occur within ores, in order to liberate valuable minerals at their native grain size, at lower energy inputs than those used by conventional comminution processes. These technologies should promote preferential breakage at grain boundaries, rather than purely reducing the size of particles until all material is liberated. A key factor in improving the efficiency of future comminution operations, regardless of the technology, will be the understanding of the influence of ore mineralogy on the effectiveness of the process, and the design of comminution circuits that exploit the particular ore characteristics present in a deposit.

HPGR and HPV comminution technologies have both shown the potential to address the significant challenges facing the minerals industry in improving the performance of comminution processes. Another emergent comminution technology which has been researched extensively, and is currently under development, is the high power microwave treatment of ores.

2.3 Microwave Treatment of Ores

2.3.1 Introduction

A technique that has been shown to produce benefits in both comminution and liberation, is through the microwave treatment of mineral ores. The exposure of ores to microwave fields has been shown to induce a variable microwave response from different minerals, resulting in reduced ore strength and improved mineral liberation in ore fragments containing microwave heated mineralisation, through a process called thermally assisted liberation.

2.3.2 Background to Microwave Assisted Liberation and Comminution

The thermal treatment of ores in order to induce thermal fracturing and weaken the ore is not a new concept. Fire has been used for thousands of years as a method of heating rock in order to reduce its strength for mining and crushing purposes (Cowen, 2000; Eberhart, 2007). Thermally assisted liberation (TAL) is the process of heating and cooling an ore in order to induce fractures. Ores are typically composed of a range of different minerals possessing very different mechanical and thermal properties. Heating or cooling of an ore can lead to the formation of stresses of different magnitudes within the lattice. This is due to different minerals possessing significantly different thermal expansion coefficients, which describes how a material changes in size or shape in response to changes in temperature. The differential expansion of minerals within an ore during this process can lead to localised fracturing that can be either intergranular ore transgranular in nature (Kingman and Rowson, 1998).

This method of improving the process of comminution, which has been under investigation since the early 20th century, aims to introduce fractures into the material as an effect of thermal expansion. Fitzgibbon and Veasey (1990) reported that early applications of this

method were employed on Cornish tin ores (Yates, 1918) and quartzites (Holman, 1926). This early work showed that the thermal pre-treatment of ores before comminution resulted in a reduction of ore strength, and fewer fines being produced, and that the effectiveness of the heat treatment decreased with particle size. Another important aspect of this early work was the consistent finding that the degree of weakening of an ore is related to the rate of heating, with a more rapid application of heat producing a more effective treatment (Fitzgibbon and Veasey, 1990).

While heat treatment of ores had been shown to improve target mineral liberation and reduce ore competency, the high energy costs associated with the treatment resulted in the method being economically unviable. It was reported that heat treatment could cost up to six times more than conventional comminution methods, without achieving sufficient benefit to justify its application (Scheding et al., 1981).

Veasey and Wills (1991) also reviewed the application of TAL and suggested that the key area for further development was the optimisation of heat transfer to maximise the matrix weakening effect and induce intergranular fracture. The authors suggested that the use of microwave radiation could be a possible alternative to produce the desired heating effects. The benefit of using microwaves as the heating source is that they induce rapid volumetric heating throughout the ore of only selected minerals, which eliminates the need to rely on the inefficient process of conduction, and avoids wasting energy through the bulk heating of the surrounding rock (Jones et al., 2005; Batchelor et al., 2015).

The microwave treatment of ores is a method of thermally assisted liberation that uses microwaves to provide the energy input for heating, rather than conventional heating methods (Kingman and Rowson, 1998). The rate at which a mineral heats when subjected to an electromagnetic field is determined by its dielectric properties

(Metaxas and Meredith, 1983). The origin of heating is due to the ability of the electric field component of an electromagnetic wave to polarise the charges in a mineral. The heat is generated by molecular friction within the mineral lattice as the polarised charges oscillate in response to rapid reversals in the electric field (Metaxas and Meredith, 1983). When a heterogeneous material, such as a mineral ore, is subjected to an electromagnetic field, direct volumetric heating of the material causes dielectrically responsive minerals to heat instantaneously (Metaxas and Meredith, 1983). If the dielectric is an electrical conductor, or a poor conductor such as most metallic sulphide minerals including chalcopyrite, then the mineral will heat rapidly due to electrical resistance in a thin layer at the surface of a grain (Whittaker and Mingos, 1994). These selective heating methods cause only certain responsive phases in a mineral ore to heat rapidly, while non-responsive minerals are transparent to the electromagnetic field and do not heat. The fundamental theory of microwave heating, including the mechanisms by which minerals heat, and the factors that govern the rate of heating, will be examined in greater detail in Chapter 3.

2.3.3 The Influence of Power Density and Total Energy Input

Early research into the microwave treatment of ores was conducted by Walkiewicz et al. (1991) at the US Bureau of Mines. In this study, iron ore samples were subjected to microwave treatment at power inputs of 3kW at 2.45GHz in a multimode cavity for 3.5 minutes, resulting in a specific energy, or microwave 'dose' of ~500kWh/t, which raised the bulk temperature of the sample to between 840-940°C. While the treatment of the ore resulted in a reduction in the Work Index of between 10 and 24%, the energy input required to achieve this outweighed the benefits. The authors concluded that using higher power microwave treatments over a shorter duration may achieve a similar benefit at lower total energy inputs. Further work by Walkiewicz et al. (1993) using the same iron ore sample as their

previous study confirmed their hypothesis. Higher power microwave treatments performed at 6kW and 16kW achieved similar reductions in Work Index with bulk sample temperatures of <200°C. This study showed that achieving a higher microwave power density within the sample resulted in more rapid development of heat within the absorbent minerals, promoting a more effective ore weakening mechanism due to thermal expansion.

The findings of these early studies was supported by the work of Kingman and Rowson (1997). The effect of microwave treatment on a Norwegian Massive ilmenite ore was investigated through treatments conducted using microwave power inputs of 2.6kW at 2.45Ghz in a multimode cavity for varying durations. Samples treated for 10, 30 and 60 seconds resulted in microwave energy inputs of 36, 108 and 217kWh/t respectively. Work Index reductions of 50, 80 and 95% indicated that large reductions in ore competency could be achieved with short treatment durations, with diminishing returns seen with increases in the total microwave energy input.

Kingman et al. (2000a) and Vorster (2001) conducted microwave treatments of a carbonatite copper ore from Palabora mine. Treatments of 1kg samples were performed at 1.3kW and 2.6kW microwave power input in a 2.5kW multimode cavity operating at 2.45Ghz, for durations of 10, 30, 60, 90, 120, 180 and 240s. This resulted in a wide range of treatment energies between 4-170kWh/t. The findings from this study demonstrated that higher power density treatments resulted in larger reductions in ore strength. The study also showed that increases in the reduction in ore strength diminished with increased treatment duration, which indicated that energy inputs beyond a certain threshold level produce minimal further benefits. Short duration microwave treatments with energy inputs of 4-7kWh/t were shown to reduce ore strength through the propagation of intergranular fractures in the ore due to the differential heating and expansion of the constituent minerals. This was the first study to show beneficial ore weakening at energy inputs that had the potential to be

economically viable. Flotation tests were conducted for samples that received a 10s microwave treatment (~4-7kWh/t) after grinding them to a P_{80} of 300μm using a laboratory rod mill. The results showed a 1% improvement in flotation recovery for the microwave treated sample when compared to an untreated sample.

The use of microwave treatment to enhance the liberation of gold for subsequent gravity separation has been investigated by Amankwah et al. (2005). A gold ore, with the gold associated with hematite in a silicate matrix, was treated in a 1.5kW multimode cavity operating at 2.45Ghz for durations of 1min and 5min. These treatments resulted in total energy inputs of 200kWh/t and 1000kWh/t, and sample temperatures of 300°C and 735°C respectively. The microwave treatments resulted in a maximum of 18.5% reduction in Work Index. A 12% improvement in gold recovery in gravity separation tests was also observed, suggesting improved mineral liberation was also achieved by the treatments.

Generally, low power density studies have been conducted using microwave power of less than 3kW in a multimode cavity (Batchelor et al., 2015). Studies conducted by several researchers have shown that the microwave energy inputs used in these investigations, which are typically much greater than 10kWh/t, typically exceed the energy savings achievable in comminution processes. The long residence times required would also limit the ability to scale-up the technology to achieve the throughputs of potentially >1000t/h that would be relevant to the demands of the mining industry (Batchelor et al., 2015). This early research did show however, that reductions in ore strength, and enhanced liberation and separation performance, would still make microwave treatment of ores a possible solution to the comminution challenges facing the minerals industry. The outcomes of low power density studies justified further research at higher power densities and shorter exposure times to reduce overall energy input during the microwave treatment process.

After achieving promising results with low power density microwave treatments, Kingman et al. (2004a) investigated the effects of high power density treatments on a Swedish lead-zinc ore using a specially designed variable power 15kW single mode cavity at 2.45Ghz. Ten particles, with a mass of totalling ~1kg were treated in the single mode system at 10kW for 0.1, 0.5 and 1s, with resulting total treatment energies of 0.14 to 2.8kWh/t. Equivalent samples were also treated in a multimode cavity, in order to give comparative lower power density data. These tests were carried out at 5, 10 and 15kW, giving treatment energies of 1.4 to 41.7kWh/t. The high power density tests conducted in this investigation resulted in the largest strength reductions observed in microwave treated ores, at much reduced microwave exposure times and lower overall treatment energies.

Kingman et al. (2004b) also conducted a similar set of experiments using a Palabora copper carbonatite ore. 1kg samples of ore were treated in a single mode cavity operating at 2.45Ghz at 5, 10 and 15kW power for 0.1, 0.5 and 1s exposure times, resulting in treatment energies between approximately 0.14 and 4.2kWh/t. Despite the short exposure times and low treatment energies used in this study, significant reductions in ore strength were seen from point load tests. This study demonstrated that a microwave treated ore that had received just 0.83kWh/t of total microwave energy input, required less comminution energy to achieve the same product size distribution after breakage as the untreated ore. Liberation analysis conducted in this same treated ore also showed improvements in copper sulphide liberation, particularly in the coarser (+500μm) size fraction. This study showed that both improvements in target mineral liberation, and ore strength reductions, were achievable at economically feasible microwave energy inputs. The short microwave exposure times also suggested that the high throughputs required for scaling up the technology to industrial throughputs relevant for the mineral processing industry were possible.

Another study using Palabora copper carbonatite ore by Sahyoun et al. (2005) subjected 1kg samples of -22mm to microwave treatments in a single mode cavity at 5, 7.5, 10 and 12kW for 0.1 and 0.5s, resulting in microwave treatment energies between 0.14 and 1.7kWh/t. Flotation testing was conducted using the same conditions used by Kingman et al. (2000a) on the same ore in the previously mentioned low power density study. All treatment conditions showed higher copper recoveries compared to untreated ores, with up to 6.5% improvement for the 12kW treatments. Comparisons with the 1% improvements achieved by the low power density study suggest that the higher power density treatments improved the target mineral liberation to a greater extent, leading to improved recovery in flotation.

Scott et al. (2008) also studied the Palabora copper carbonatite ore, and conducted liberation analysis after microwave treatment and grinding in a laboratory rod mill to 80% passing 800µm. 1kg batches of ore were treated in a single mode cavity at 10.5kW and 0.5s, resulting in a microwave treatment energy of 1.46kWh/t. Liberation analysis was carried out over particle size ranges from 850µm to 25µm. Liberation of copper sulphides was improved in the -850+300µm size classes, but lower in the -300+25µm size classes, indicating a shift in the liberated material to coarser particle sizes fractions. It was suggested that, as a result of microwave treatment, intergranular fracture was induced between microwave heating and non-heating minerals, and the fracture pattern was changed, altering the size distribution of the gangue material. This study showed that microwave treatment of a copper ore had the potential to improve copper mineral liberation, leading to benefits for downstream separation processes in mineral recovery and comminution energy consumption.

In a recent study, Batchelor et al. (2016) investigated the changes to mineral liberation and flotation performance of a porphyry copper ore from Chile following high power microwave treatment. A different test

sample of the ore used in this study had been previously tested by Batchelor et al. (2015) for reductions in ore competency resulting from microwave treatment, and only achieved modest ~8% strength reductions, as measured by point load tests, from similar treatment conditions. The ore was subjected to high power density microwave treatments in a single mode cavity operating at 2.45Ghz at 15kW microwave power and ~2kWh/t total microwave energy input. Representative sub-samples of the untreated sample were milled to two different grind sizes necessary to approximate the host mine plant grind of P_{80} of 190µm, and a P_{80} of 290µm to investigate any change in liberation at 100µm coarser than the plant grind. The microwave-treated sample was then milled at the same grind times to achieve an equivalent amount of work on the ores, as opposed to targeting the same grind sizes. The resulting liberation sample grinds for the untreated sample were P_{80} 288µm and 182µm with corresponding microwave-treated sample P_{80}'s of 238µm and 162µm. The microwave-treated sample grinds were deemed to be finer after grinding, potentially due to microwave-induced fractures in the ore following treatments. Mineral liberation analysis of untreated and treated samples showed that equivalent copper sulphide liberation could be achieved at a grind size ~50–60µm coarser than the nominal plant grind due to the microwave treatment as shown in Figure 2.6.

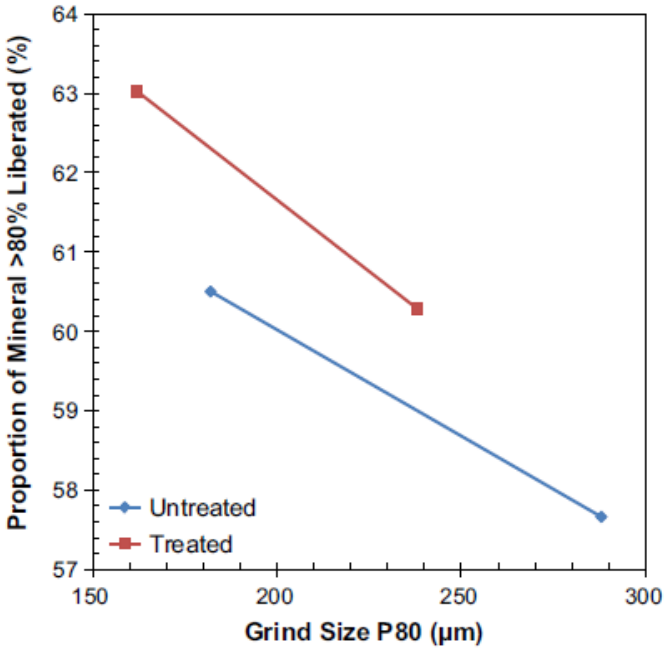


Figure 2.6 Copper sulphide liberation (proportion of mineral >80% liberated) versus grind size (reproduced from Batchelor et al. (2016))

Cumulative liberation profiles of the four grinds in this study are shown in Figure 2.7, and it can be seen that the microwave treated grinds have a higher degree of liberation than their corresponding untreated grinds.

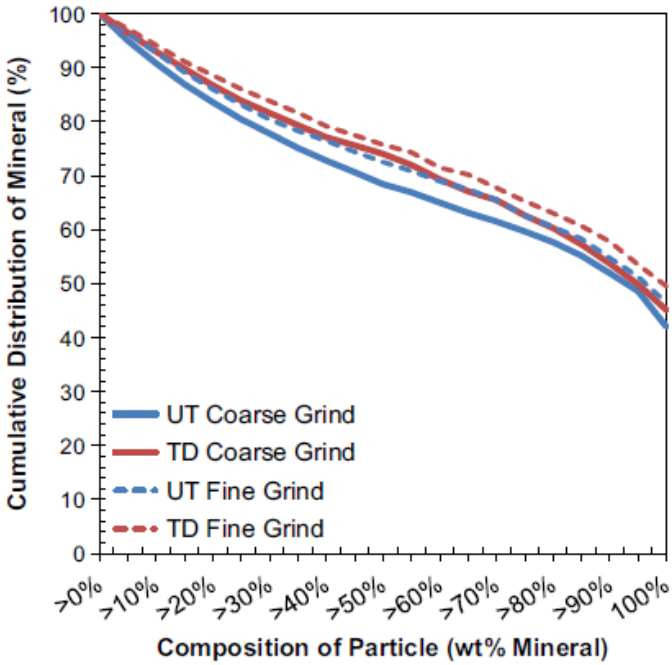


Figure 2.7 Cumulative copper sulphide liberation by composition profiles (reproduced from Batchelor et al. (2016))

It was suggested that the apparent increase in copper sulphide liberation in this study may be attributed to preferential breakage occurring around grain boundaries at the location of microwave induced fractures. Laboratory batch flotation testing also showed that copper recovery could be increased by up to ~1% at the nominal plant grind sizes, however statistical analysis demonstrated that it was difficult to attain confidence in such small increases in recovery, even when conducting batch flotation tests in triplicate. The key outcome from this work was that microwave treatments that do not result in substantial reductions in ore competency through inducing significant macro-fracturing, may still produce benefits in terms of mineral liberation through initiating preferential grain boundary micro-fractures.

The influence of microwave power density and total energy input on the effectiveness of the microwave treatment of mineral ores has also been considered by a number of researchers using theoretical modelling studies. These studies mainly used Fast Lagrangian Analysis of Continue (FLAC), a two dimensional finite difference program developed for the modelling of brittle failure in geotechnical applications (ITASCA, 2015). Distinct element modelling (DEM) has also been used to investigate different parameters for which this software is more suited. Jones (2004) and Ali (2010) provide detailed information on the application of these theoretical modelling methods to understanding the microwave treatment of ores.

In complex ores, it can be difficult to determine which combinations of minerals cause the most significant reductions in strength by experimental means. Modelling studies have been able to illustrate the mechanism of selective heating and fracture through differential thermal expansion by considering theoretical binary systems comprising two different minerals. A number of two dimensional numerical studies have been conducted on binary systems comprising circular pyrite grains in a microwave transparent calcite matrix (Salsman et al., 1996; Jones et al., 2005; Wang et al., 2008). These investigations found that increasing the power density in the heated phase, while maintaining constant energy input, resulted in more fracturing to occur in the calcite around the pyrite grain. Higher power density treatments for shorter exposure times resulted in larger thermal gradients and, therefore, larger thermal stress at the grain boundary as less was heat conducted from the heated phase to the matrix. Fractures occurring around the grain boundaries between the pyrite and calcite were determined to be due to shear stress, and fractures extending into the calcite matrix were due to radial tensile stresses. The pyrite grain experienced little to no damage as it has a higher modulus of elasticity than the calcite, and is subsequently more resistant to deformation, meaning that brittle failure occurred in the surrounding calcite matrix.

Further studies in the field of modelling the microwave treatment of ores have been conducted by several authors (Whittles et al., 2003; Jones et al., 2007; Ali and Bradshaw, 2009; Ali and Bradshaw, 2010; Ali and Bradshaw, 2011; Wang and Djordjevic, 2014). The consistent finding from these investigations was that the two most important factors for microwave-induced fracture to occur are microwave power density and microwave energy input. Modelling studies that applied higher power density always resulted in a higher degree of particle damage for a given total microwave energy input. Jones (2004) showed that as microwave exposure time is reduced for a given energy input, the velocity of the thermal expansion increases by the same order of magnitude, which means that the acceleration of the grain expansion also increases by two orders of magnitude. Larger accelerations lead to the formation of larger stresses that may contribute to weakening of the material. It was also consistently shown however, that for a given microwave power density, there is a minimum microwave energy input required to provide sufficient thermal expansion of the microwave absorbent minerals to initiate and propagate fractures. These studies suggested that achieving a microwave power density within the absorbent mineral grains greater than $\sim 1 \times 10^{10}$ W/m^3 would provide the most efficient fracture generating conditions.

A study by Ali (2010) also investigated the concept of selective breakage occurring at grain boundaries as a result of microwave treatment. The author simulated single particle breakage of a 2mm circular galena grain within a 10mm diameter calcite matrix for an untreated ore, and 1×10^9 W/m³ and 1×10^{11} W/m³ power density treatments to study the breakage patterns produced around the microwave-absorbent grains. The untreated ore showed random breakage occurring, while the low power density treatment demonstrated selective breakage of the microwave-absorbent phase with some preferential fracture of the microwave-absorbent grain, and the high power density treatment showed selective breakage of the

microwave-absorbent phase with the microwave-absorbent grain remaining intact.

A further study by Ali and Bradshaw (2011) simulated confined bed breakage of 1-2.5mm irregular shaped galena grains within a 12mm diameter calcite matrix for an untreated ore, and $1x10^{9}$ W/m³ and $1x10^{11}$ W/m³ power density treatments at equivalent energy inputs. Simulated confined bed breakage, which is similar in mechanism to HPGR crushing, was conducted at two different crusher closing rates of 0.1m/s and 0.05m/s. This investigation showed that an ore subjected to low power density microwave treatment resulted in a finer product size than the untreated ore. The high power density treatments were significantly finer than both the lower power density treatments and untreated ore for both crusher closing rates. The slower crushing rate produced a finer product size distributions and more liberated galena grains than the faster crushing velocity for both untreated and treated cases. This finding is consistent with the theory of Wills and Atkinson (1993) that slow, stable propagation of fractures in an ore is most effective for the formation of intergranular fractures and liberation of target minerals.

While theoretical modelling studies have proven to be a useful method for investigating the effects produced by the interaction of microwaves with simple composite mineral systems, there are limitations in the ability of the software to represent real ores. Mineral ores are infinitely complex and have an inherent natural variability which is very difficult to account for in models. Computing power restrictions and software limitations lead to reduced mesh sizes on grain size and shape, and the number of different minerals and physical properties that can be represented in an ore. Currently, software is also unable to represent natural flaws such as cracks, grain boundary weaknesses, or natural variability in mineral composition and physical properties. Despite these limitations, outcomes from theoretical studies have been validated by the findings of experimental studies, and have successfully highlighted the role that power density and total

microwave energy input play in achieving a beneficial microwave treatment outcome.

2.3.4 The Influence of Mineralogy

While the influence of microwave power density and energy input has been shown to be an important factor in the effectiveness of the microwave treatment of ores, it is also essential to understand the role that the mineralogy and texture of an ore plays in ensuring a beneficial outcome from the treatment. Despite the importance of understanding how the mineralogical and textural characteristics of different ores impacts their amenability to beneficial microwave treatment, previous studies in this field have been limited. The two main factors to consider when assessing the amenability of ore for microwave treatment are the characteristics of the microwave heating minerals, and the characteristics of the surrounding gangue.

In an important early study, Kingman et al. (2000b) conducted an experiment to investigate the influence of mineralogy on microwave assisted grinding using four different ores: the Palabora copper carbonatite ore, Neves Corvo massive copper ore, a Norwegian massive ilmenite ore, and a refractory gold ore from Lihir mine. Initial mineralogical and textural characterisation was conducted for each ore through evaluation under reflected light microscope. The Palabora copper carbonatite possessed coarse (>300μm) magnetite and copper sulphides in a gangue comprising predominantly calcite, quartz and dolerite, with minor dolomite, apatite, serpentine and K-feldspar. The Neves Corvo massive copper ore comprised mainly pyrite gangue with minor dolomite and quartz, and copper sulphides occurring as coarse grains with minor sphalerite, galena and arsenopyrite. The ilmenite ore possessed magnetite and ilmenite as the dominant microwave absorbent minerals, occurring as well-disseminated coarse grains (0.5-3mm) in a microwave transparent plagioclase and olivine gangue. The dominant microwave-absorbent mineral in the refractory gold ore was pyrite, which was finely disseminated throughout the ore with a grain

size typically less than 100µm or occasionally in pyrite veinlets with quartz. The microwave-transparent gangue matrix was mainly composed of quartz and K-feldspar.

The authors crushed all the ores to -22.5mm and 500g samples were treated in a 2.6kW multimode cavity operating at 2.45GHz for 10, 30, 60, 90 and 240s, resulting in treatment energies of 14, 43, 87, 130 and 347kWh/t. The Work Index for each microwave treated ore was calculated following grinding and the results are shown in Figure 2.8.

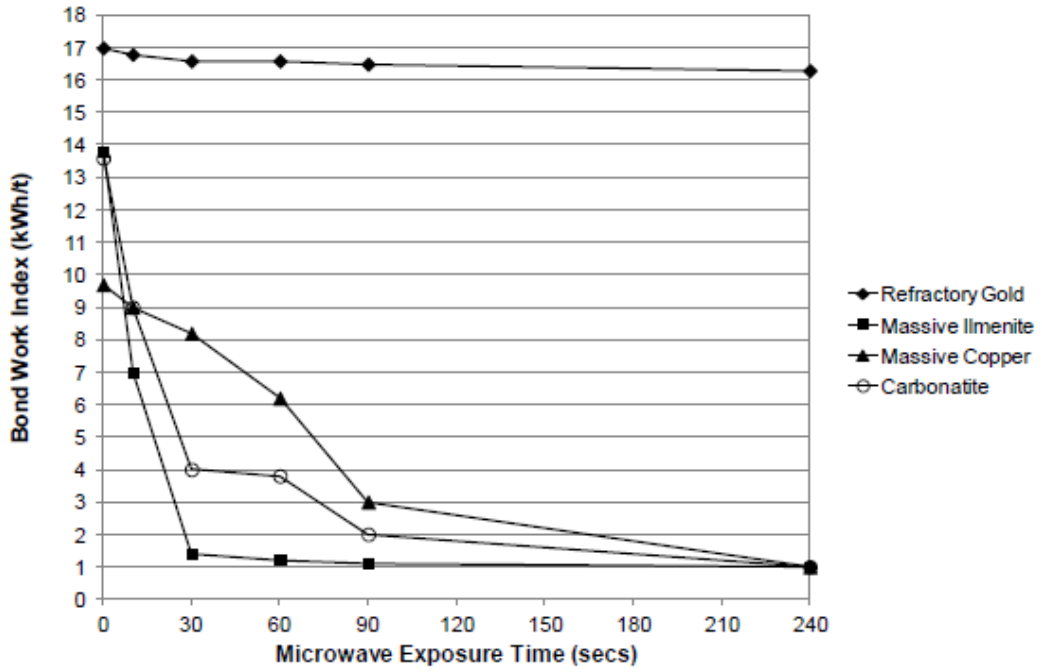


Figure 2.8 The effect of ore mineralogy on Bond Work Index following microwave treatments. The figure shows microwave exposure time v Work Index (kWh/t) (reproduced from Kingman et al. (2000b))

The results show that the microwave treatments of the carbonatite and ilmenite ores achieved the greatest reduction in Work Index, with the greatest benefit achieved in the 10-30s duration treatments. The authors suggested this was due to the coarse grain size and well disseminated nature of the microwave-absorbent minerals within a microwave-transparent matrix. Both ores showed minimal further reductions in strength after 30s, which is consistent with previous findings that beyond a maximum energy threshold, no extra microwave-induced fractures can be created as all amenable regions in

the ore have been exploited. The refractory gold ore showed only very minor reductions in strength due to the fine grain size and disseminated nature of the pyrite heating phase. The massive copper ore only showed strength reductions after 10s, which was believed to be due to the high content of microwave absorbing minerals. Greater microwave energy input over a longer duration was needed to raise the temperature of the ore to achieve the necessary thermal expansion to cause microwave fracture.

This study concluded that ores possessing consistent mineralogy, and containing a coarse microwave absorbent mineral contained within a transparent gangue were the most responsive to microwave treatment, while ores that contain small heating mineral grains that are finely disseminated respond poorly to microwave treatment in terms of reductions in Work Index. Another important conclusion identified in this research was that the development of purpose built microwave cavities may be essential in improving the effectiveness of the microwave treatment of ores, and would contribute to the economic viability of the technology.

A doctoral study by Batchelor (2013) reviewed literature published on experiments using high and low power density microwave treatments of metalliferous ores from the previous 20 years. Most of the studies reviewed only investigated single ore samples, and mineralogical descriptions tended to be limited to qualitative observations of mineral abundance, grain size, texture and mineral associations. Through collation of the findings for the wide range of ores tested, and taking into account the different microwave treatment conditions applied, and the findings of Kingman et al. (2000b), a qualitative guide for an amenable ore were established. It was suggested that the ores that typically performed best in terms of reduced ore strength following microwave treatment possessed a matrix comprised of 'hard' or brittle minerals such as quartz, feldspar, pyroxene and olivine, rather than 'softer' or more ductile minerals such as clays, micas or carbonates, containing a highly microwave absorbent phase such as magnetite.

A number of theoretical modelling studies have also addressed the influence that variations in mineralogy and mineral texture can have on microwave treatment (Salsman et al., 1996; Whittles et al., 2003; Jones et al., 2005; Jones et al., 2007; Ali and Bradshaw, 2009; Ali, 2010)). These studies demonstrated that minerals that heat better when subjected to microwave radiation, and that have a high thermal expansion coefficient, tend to generate fractures due to higher heating rates and more rapid volumetric expansion.

Finer microwave-absorbent grains (<100µm), have been shown to yield less fracturing than coarser grains (>500µm). This has been attributed to a rapid loss of heat through conduction to the matrix due to the greatly increased surface area to volume compared to coarser grains. The loss of heat reduces the thermal shock, and therefore requires a higher power density or microwave energy input to raise the stress enough to cause significant fracturing to occur. Coarse and granular heating minerals, rather than fine and disseminated absorbent minerals, have also been shown to be more effective at promoting micro and macro-fracturing in the surrounding gangue. A Finite Element Modelling (FEM) study by Wang and Djordjevic (2014) of a two-phase system with a pyrite heating grain in a calcite matrix found that peak stresses in the surrounding gangue matrix increased proportionally with increases to the pyrite grain size. Subsequently, the native grain size at which heating minerals occur within the ore is an important factor to be considered.

Pyrite in particular has been shown to be an important mineral in contributing to fracture propagation during microwave treatment. Pyrite abundance, texture and grain size, associations with hard gangue minerals and associations with copper (Cu) sulphide minerals have been shown to be dominant factors in ore fracture mechanisms. It can be seen in Figure 2.9 that pyrite has a modulus of elasticity that is much higher than Cu-sulphide minerals and typical gangue minerals such as quartz, feldspars, micas and carbonates. As has been

discussed previously, modulus of elasticity is related to mineral strength and hardness, and effectively describes how well a mineral will transfer mechanical stresses through the surrounding ore matrix (Djordjevic, 2014).

Where pyrite occurs in association with other high modulus of elasticity minerals such as magnetite, garnet or olivine, stress transfer throughout the ore matrix will be more effective, increasing the likelihood that macro-fracturing will occur. Where pyrite occurs in association with copper sulphide minerals such as chalcopyrite, improved liberation of the chalcopyrite mineral grains could be expected as thermal expansion of the pyrite causes disruption of the ore matrix and promotes both macro-fracturing through the ore fragment, and inter-granular micro-fracturing around the chalcopyrite grains (Djordjevic, 2014). If the pyrite in an ore is dominantly associated with 'soft' gangue minerals such as muscovite, biotite or carbonate minerals however, then the stresses produced during the thermal expansion of the pyrite will be absorbed by ductile deformation of the gangue, and the potential for macro-fracturing will be diminished. The dominant contribution of pyrite, rather than copper sulphide minerals, to an ore's potential to macro-fracturing is another important aspect in assessing the amenability of an ore to microwave treatment.

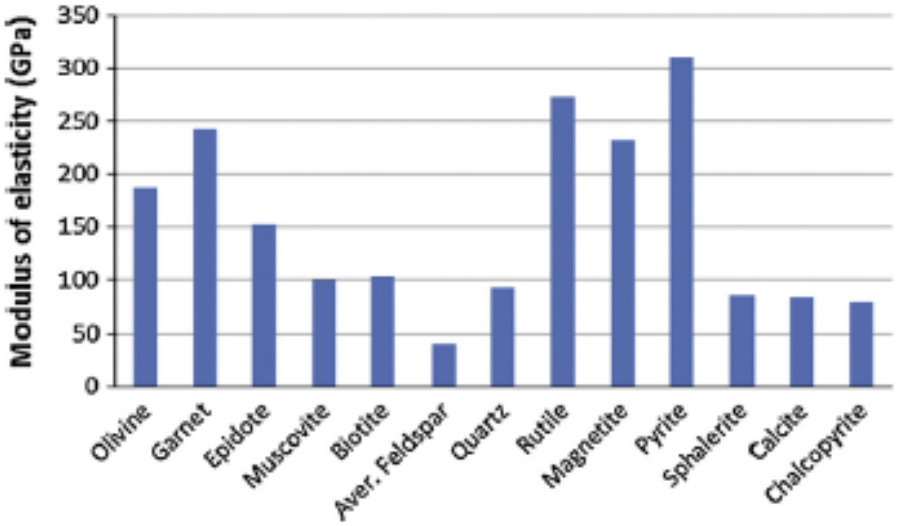


Figure 2.9: Comparison of the Modulus of Elasticity for common minerals (reproduced from Djordjevic (2014))

These studies also showed that gangue comprising a higher proportion of 'hard' or brittle minerals such as quartz, feldspar and pyrite, as opposed to softer micas and clays does not as readily undergo elastic or ductile deformation to absorb the thermal expansion, and is more likely to accommodate the strain through the formation and propagation of fractures. 'Hard' or brittle gangue minerals such as quartz, have been shown to distribute stresses from the expansion of the heating minerals through inter-granular cracking and fracturing (Jones, 2004; Jones et al., 2005). Ores that possess softer gangue, with higher proportions of clays or micas, are more likely to absorb the energy through ductile deformation within the ore fragment to absorb the expansion of the heating mineral. Therefore, ore samples possessing higher proportions of more brittle gangue minerals are likely to be more amenable to microwave treatment.

Hydrated phyllosilicate minerals, such as the clay mineral montmorillonite, which contain loosely-bound adsorbed interlayer water, have also been shown to contribute to fracturing within ores during microwave treatment (Kobusheshe, 2010). Water possesses properties which make it an excellent absorber of microwave energy, and it heats rapidly and yields steam when microwave energy is

applied (Metaxas and Meredith, 1983). While the microwave heating response of clay minerals is quite low compared to Cu-sulphide minerals, pyrite and magnetite, the interlayer water within the structure of certain clay minerals shows a rapid heating response and explosive dehydration of the contained water. This explosive dehydration mechanism can create an internal build-up of pressure within an ore fragment, causing it to fracture (Kobusheshe, 2010). The removal of this bound water from the mineral structure may also result in structural defects providing flaws or weakness in the matrix. While clay minerals with interlayer could be considered as strong microwave heaters that contribute to the overall breakage effect, the microwave energy inputs required to cause explosive dehydration of the water may negatively impact the economic viability of the treatment process.

Recent research by Batchelor et al. (2015) expanded upon this early work to study the influence of mineralogy on the microwave treatment of ores, and investigated a range of different ores for reductions in ore competency resulting from microwave treatment. The goal of the investigation was to derive the ideal ore texture for the microwave treatment of metalliferous ores, through evaluating the response of 13 different ores to high power density microwave treatments at different energy inputs.

Three nickel (Ni), six copper (Cu) and four lead-zinc (Pb/Zn) ores were selected from a variety of host mines throughout the world to represent a wide range of mineralogical characteristics likely to be encountered by microwave processing in the mining industry. Coarse ore mineralogical characterisation was conducted on polished sections of 15-30 fragments (~15-30mm in size) for each of the ores using a Mineral Liberation Analyser (MLA). This was performed to determine the modal mineralogy, mineral grain size and mineral association information that resulted in quantitative textural data of the natural mineral assemblage for each ore. Mineralogical characterisation revealed major microwave-heating minerals of varying abundance,

including nickel sulphides, copper sulphides, iron sulphides, galena, magnetite and hydrated clays, such as montmorillonite. Other poorly microwave-heating minerals included iron oxides such as haematite and sphalerite. The non-microwave-heating gangue minerals included varying proportions of more brittle minerals such as quartz, feldspars, amphiboles and pyroxenes, with 'softer' or more ductile micas, including biotite, muscovite and illite, other phyllosilicate and clay minerals, carbonates and serpentine-group minerals.

A wide variety of ore textures was also observed, with microwave heating minerals ranging from coarse and granular or veined sulphides and iron oxides, through to evenly disseminated fine-grained heating minerals. The grain size distributions of microwave heating minerals for each of the ores are shown in Figure 2.10 to illustrate the wide variety of heating mineral textures observed across the 13 different ores.

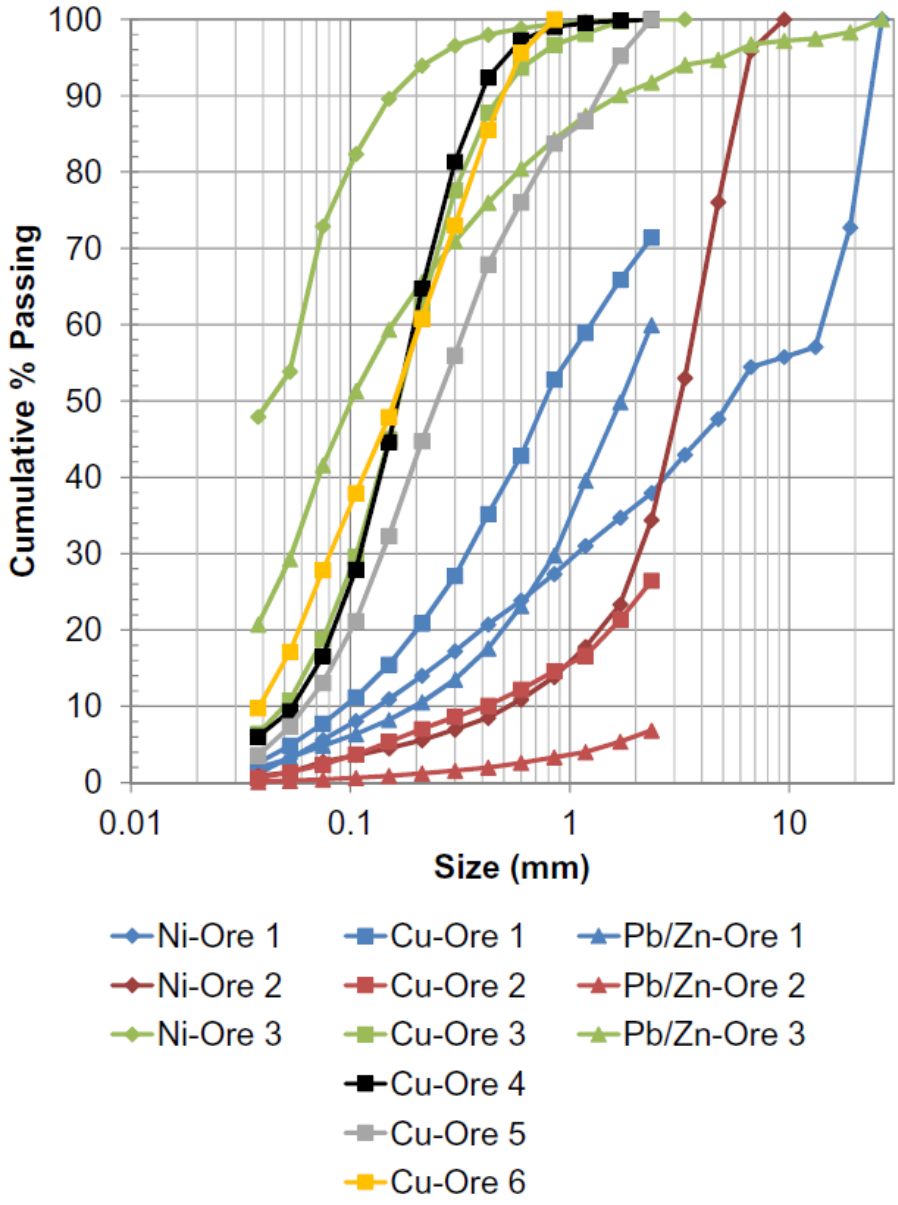


Figure 2.10 Grain size distributions of grouped good microwave heating minerals for each ore. The good microwave heating minerals group comprises galena, chalcopyrite, iron sulphides (pyrite, pyrrhotite, arsenopyrite) and magnetite (reproduced from Batchelor et al. (2015))

Each of the ores was subjected to high power density microwave treatments at up to 25 kW at 2.45GHz in a single mode cavity with microwave energy inputs ranging from ~0.5–15kWh/t, and subsequent reductions in ore strength were measured by the Point Load Test (Broch and Franklin, 1972). As expected from the findings of previous experimental and theoretical studies, the reduction in strength of each ore increases as the total microwave energy input increases. Figure 2.11 shows the corresponding reductions in the average Point Load

Index for each ore after microwave treatments, shown as the percentage of the original strength remaining.

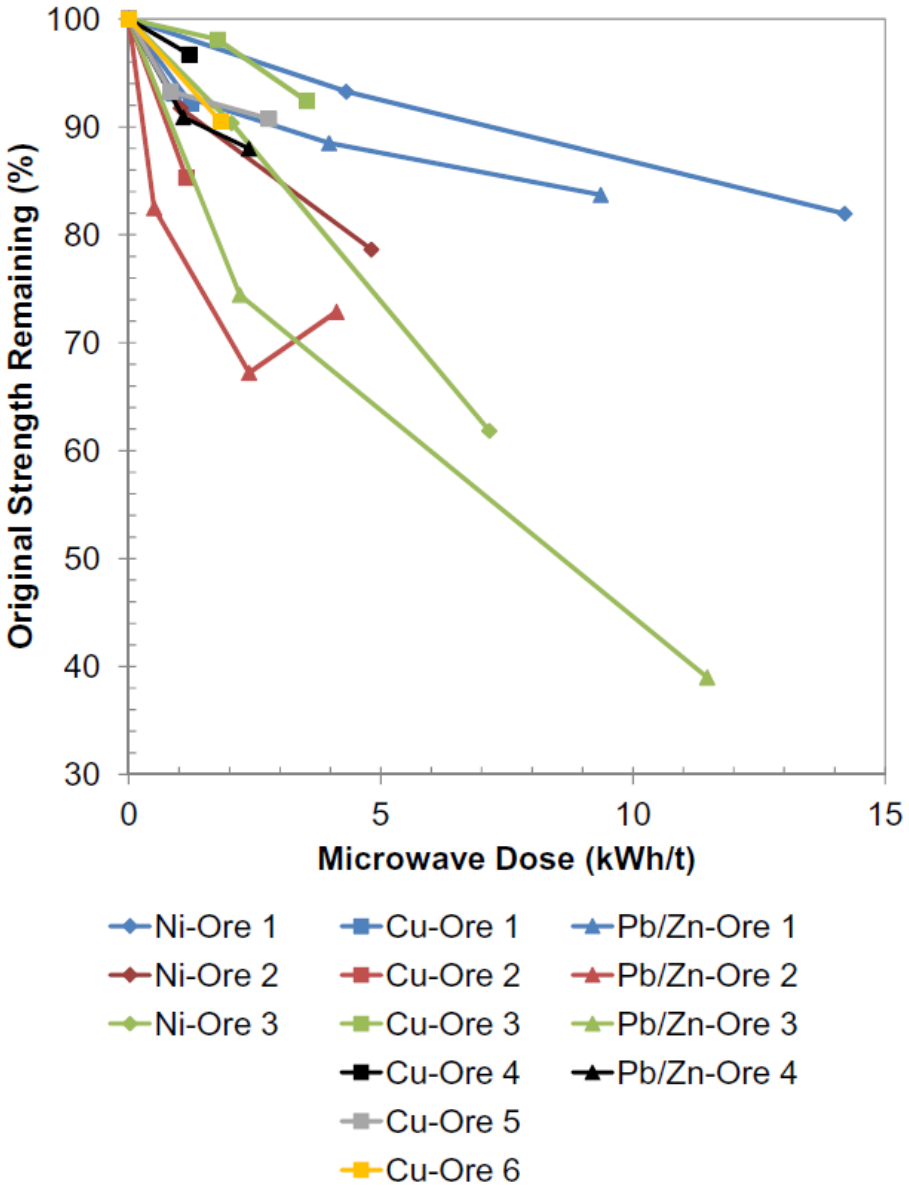


Figure 2.11 Summary of Point Load test results for each of the microwave treated ores (reproduced from Batchelor et al. (2015))

Through relating the coarse ore mineralogy and mineral texture, with the ore strength reduction benefits achieved from the microwave treatments, the authors derived a series of semi-quantitative mineralogical criteria through which to determine the ideal ore texture for beneficial microwave treatment. The ores that achieved the highest average reduction in Point Load Index at the lowest microwave energy inputs met the following criteria:

- The presence of good microwave heaters such as magnetite and lead, nickel, copper and iron sulphides.
- 2-20% abundance of good microwave heaters. Greater than 20% and the thermal expansion effect is diminished as the total energy must be distributed to a higher abundance of heating minerals.
- ~50% of the gangue constraining the microwave heating minerals comprised of 'hard' or brittle minerals such as quartz or feldspars. Softer gangue minerals may elastically absorb thermal expansion of the heating minerals, rather than effectively propagating fractures.
- An overall grain size distribution for the grouped microwave heating minerals with 50% of the grains coarser than 500μm.
- Well disseminated or veined microwave-heating phases within the individual fragments. These textures ensure that microwave induced fracture occurs throughout the fragment, rather than occurring near the surface or edges of the fragment.
- Texturally consistent with amenable ore textures present through the majority of ore fragments being treated. This ensures that a high proportion of the ore is affected by microwave treatment, and large average reductions in ore strength can be achieved.

The experimental findings from this investigation validated predictions made by previous theoretical modelling studies with heterogeneous real ores, and presented a semi-quantitative set of criteria for assessing the amenability of an ore to high power microwave treatment for strength reductions.

2.4 SUMMARY

This chapter has provided a comprehensive background to the process and fundamental mechanisms of ore comminution, as the initial stage of mineral processing. The copper mining industry in particular is

experiencing a trend towards more complex, finer-grained and lower-grade ores which will require additional size reduction, and subsequently an increase in comminution energy requirements, for concentration of the target minerals into a saleable product. As such, investigations into new technologies to enhance the process of comminution and mineral liberation are of paramount importance in the context of mining and mineral processing.

The development of new comminution technologies to physically alter the properties of an ore in order to reduce strength and improve target mineral liberation, has been identified as the most likely avenue by which significant improvements in the efficiency of comminution processes will be achieved. High Pressure Grinding Rolls, High Voltage Pulse treatment and Thermally Assisted Liberation have been identified has having the potential to address these challenges.

It is now widely recognised that high power microwave treatment of ores has the potential of being a novel and potentially step-changing comminution technology. The ability of microwave energy to rapidly and selectively heat certain minerals within an ore, and generate and propagate intergranular fractures at their grain boundaries, has demonstrated the potential of reducing ore strength and enhancing mineral liberation. Reviews of previous work conducted in this field have clearly shown that microwave energy inputs at low power density generally exceed the potential comminution energy savings due to the achievable reductions in ore strength. Higher power density treatments for short durations however, have shown the ability to achieved significant reductions in ore strength at economically viable energy inputs.

While the rapid thermal expansion of heating minerals and the generation of macro-fractures through fast strain rates has been shown to reduce ore strength, it was identified from the literature that the key to achieving successful liberation in mineral ores is the generation of non-random intergranular micro-fractures, rather than

random macro-fractures. It was also identified that the speed of crack propagation, which is related to the rate of strain, can influence whether random or non-random breakage takes place during comminution. It was suggested that lower energy inputs, and subsequently slower strain rates during comminution would promote stable crack propagation and exploit grain boundary weakness more effectively than high energy and fast-strain processes.

The studies reviewed in this chapter have shown that significant reductions in comminution energy due to a reduction in the bulk strength of ore fragments, and improvements in target mineral liberation, are achievable for mineral ores following short exposure to high power density microwaves (Kingman et al., 2004a; Amankwah et al., 2005; Jones et al., 2007; Rizmanoski, 2011; Batchelor et al., 2016). Results from both experimental and theoretical modelling studies have also shown that achieving a high power density (W/m^3) over a rapid heating interval is vital for the development of high thermal stresses and subsequent microwave-induced fracturing (Jones et al., 2005; Bradshaw et al., 2007; Wang et al., 2008; Ali and Bradshaw, 2009; Ali, 2010; Wang and Djordjevic, 2014). While theoretical simulations and modelling have proven to be useful tools for investigating the fundamental relationships between microwave energy delivery rate, stress formation and subsequent fracture formation, experimental investigations have been essential to elucidate the influence that microwave power density, total microwave energy input, and the complex range of mineralogical and textural ore variables has on the effectiveness of the technique. The outcomes achievable through the high power microwave treatment of ores could potentially lead to a range of downstream processing benefits including increased throughput, increased mineral recovery and reductions in comminution energy. These benefits also meet the economic requirements of the world's mineral producers by successfully being applied at economically feasible microwave energy inputs and with the potential for scale up to industrially relevant throughputs.

While the understanding of the fundamental process of microwave treatment of ores has developed significantly over recent years, knowledge of how the quantitative mineralogical and textural characteristics of different ores influences their amenability to microwave treatment is still limited (Kingman et al., 2000b; Ali and Bradshaw, 2009; Ali, 2010; Batchelor, 2013; Batchelor et al., 2015). This study will expand on this previous body of work in order to further improve the understanding of the influence that ore mineralogy has on the benefits achieved from high power microwave treatments.

Previous work in this field has tended to focus on the ore strength reductions achievable from high power microwave treatments through the generation of macro-fractures, rather than the mineral liberation benefits achieved through microwave induced intergranular micro-fractures. This may be due to the fact that automated mineralogy systems were not widely available for routine use prior to the mid-2000s, when the majority of this experimental research took place. Access to a Mineral Liberation Analyser at the University of Nottingham has enabled further studies into improvements in mineral liberation as a result of microwave treatment to be investigated.

In ores being subjected to microwave treatment, there appear to be two thresholds that exist which are determined by a complex range of factors involving mineralogy, microwave power density, and microwave energy input. The first threshold is where intergranular micro-fractures are generated and liberation enhancement is achieved. The second threshold occurs where the micro-fractures propagate and link together to form macro-fractures, and ore strength reductions are achieved. This study will investigate this process to develop the understanding of how microwave power density and energy input influence the potential outcomes of a microwave treatment.

Progress in the field of understanding the microwave treatment of ores has been primarily concerned with testing the downstream benefits achievable from the technology. While theoretical modelling studies

have investigated fracture mechanisms on simple binary mineral systems, the understanding of fractures induced by microwave treatment in complex multi-mineral ores was identified as a new field for study. Through experimental investigation, this study also intends to expand on this field of knowledge and develop the understanding of the generation and propagation of fractures in microwave treated ores.

2.5 Aims and Objectives

The overall aim of this project is to develop the understanding of the relationship between the mineralogical characteristics of a range of different copper ores from a single deposit, with the comminution and mineral liberation benefits achievable following high power microwave treatment. The experimental program and results presented in this thesis have been designed to address the following aims:

1. To improve the understanding of how mineralogical and textural characteristics of an ore influences the comminution and mineral liberation benefits achieved through microwave treatments.

2. To develop the understanding of the generation and propagation of fractures within microwave treated ores through characterisation and quantification of fractures produced during the microwave treatment process.

3. To develop the understanding of the optimal microwave treatment conditions for comminution or mineral liberation benefits to be achieved. This will be investigated in terms of both microwave power density (W/m^3), and the overall microwave energy input, or microwave 'dose' (kWh/t).

A series of specific objectives were developed in order to meet the aims of the project through analysis, testing and comparison of a range of untreated and microwave treated ores. The aims of the

research project were addressed through completing the following objectives:

1. Conduct an experimental program involving a series of high power microwave treatments, with varying total energy inputs, of two key sponsor ores representing different mineralogical amenability characteristics. The benefits achieved from the treatments, in terms of improved comminution behaviour and mineral liberation, will be assessed and compared between the ores, and related to ore mineralogy and microwave treatment conditions.

2. Develop a new experimental method for the analysis and quantification of fractures in ore fragments. This new method will be applied to the assessment of fragments from three microwave treated ores, and the results will be related to comminution and mineral liberation test results.

3. Conduct a series of low energy (<0.7kWh/t) microwave treatments of a single ore in order to expand the range of microwave treatment conditions to beyond those previously investigated and reported in the literature. Comminution testing and mineral liberation analysis will be conducted in order to measure the benefits achieved, and these results will be used to assess the influence of microwave power density (W/m^3) and total microwave power input (kWh/t) for a single ore.

CHAPTER 3 – FUNDAMENTALS OF MICROWAVES AND THE MICROWAVE HEATING OF MINERALS

3.1 INTRODUCTION

The Planck satellite, launched in 2009, captured the composite image shown in Figure 3.1. The image shows the anisotropies of the Cosmic Microwave Background (CMB), or the afterglow of the Big Bang (ESA, 2013). It represents the universe as it was 380,000 years following the initial hot, dense phase when atoms first began to form. Colour gradations in the image represent tiny temperature fluctuations, at the level of 1 part in 100,000, corresponding to minor density variations in the early universe. The red and slightly warmer regions represent regions with a greater density of matter, which ultimately seeded the formation of the galaxies (Cox, 2015). This variation in the properties of electromagnetic waves on a universal scale, was governed by similar principles that can be used to describe the interaction of microwaves with minerals on a much smaller scale

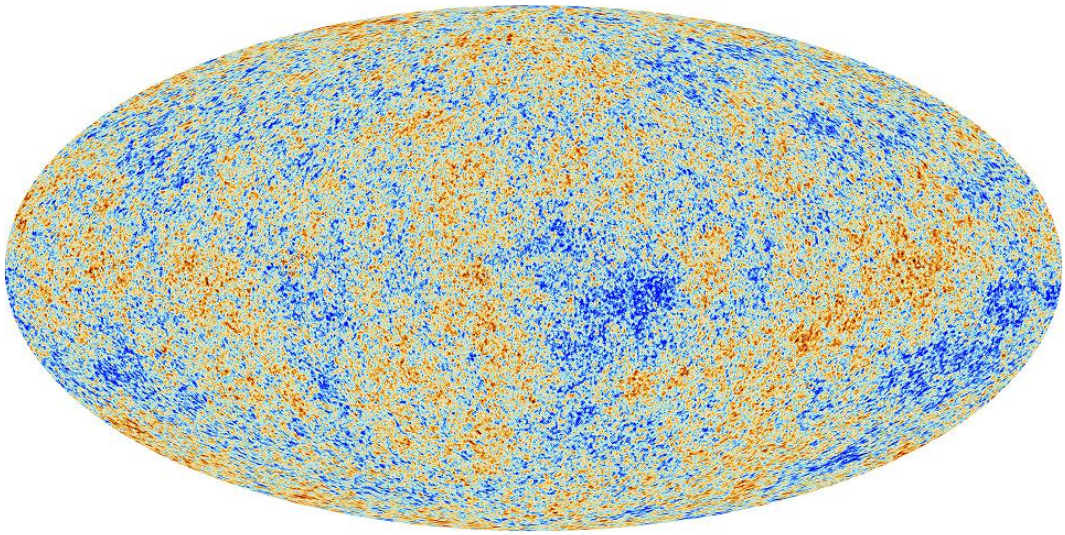


Figure 3.1 The anisotropies of the Cosmic Microwave Background as observed by the Planck satellite (ESA, 2013).

The use of microwaves has become ubiquitous throughout the world. Whether heating up food in a domestic microwave oven in our kitchen, transmitting signals from our mobile phones or over Wi-Fi, or

diagnosing and treating diseases in hospitals, the electromagnetic waves themselves, and the interaction of these waves with materials, are governed by the same fundamental principles.

Unlike conventional industrial heating methods which rely on radiation, conduction or convection to transfer heat into a material from the surface, electromagnetic heating is volumetric, and the energy is applied directly into the material. Heating occurs through the interaction of polar, ionic, electronic and magnetic features in the material with the applied electromagnetic waves. Subsequently, instantaneous heating of susceptible features within the material can be achieved, which can lead to significant reductions in heating times and improved uniformity of heating (Meredith, 1998). Another unique characteristic of electromagnetic heating is the ability to selectively heat different phases within a material based on differences in their electric and magnetic properties. Through application of electromagnetic heating to complex heterogeneous materials, such as ores, there is the potential to heat only susceptible minerals in the ore, rather than heating the entire mass.

This chapter will provide a background in the fundamental theory of microwaves, the interaction of microwaves with materials and the resulting effects, and more specifically on the interaction of microwaves with minerals and the subsequent heating mechanisms that result. This chapter will also introduce the principal components of industrial microwave processing systems.

3.2 Electromagnetic Radiation

Electromagnetic waves comprise electric (E, V/m) and magnetic (H, A/m) field components which occur as sinusoidal planar waves, transverse to each other and the direction of wave propagation, as shown in Figure 3.2.

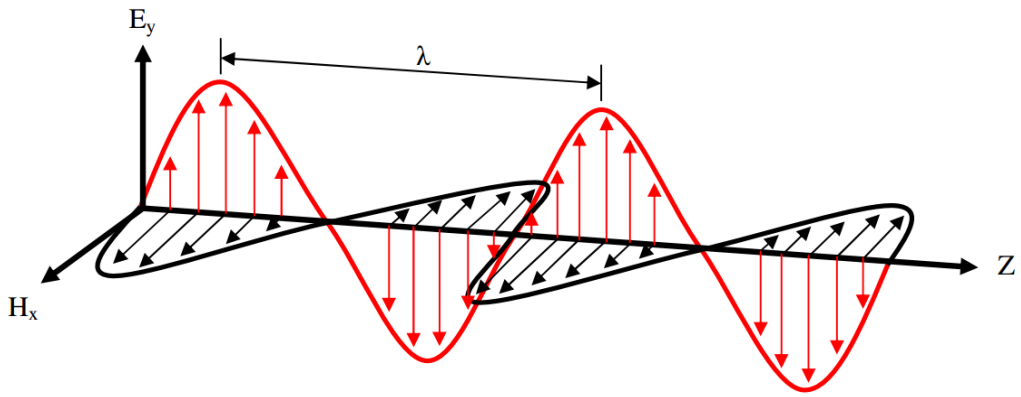


Figure 3.2 Diagram of an electromagnetic wave (reproduced from Hamilton (2009))

Electromagnetic waves propagate at the speed of light, or $3x10^8$ m/s in free space or a vacuum. The relationship between speed, frequency and wavelength of an electromagnetic wave is given by:

$$v = \lambda . f$$ **Equation 3.1**

Where v = wave propagation velocity, (m/s), λ = wavelength (m), f = frequency, (Hz)

3.2.1 The Electromagnetic Spectrum

Microwaves are a form of non-ionising electromagnetic radiation in the frequency range 300 MHz to 300 GHz, giving wavelengths between 1 m and 1 mm as shown in Figure 3.3.

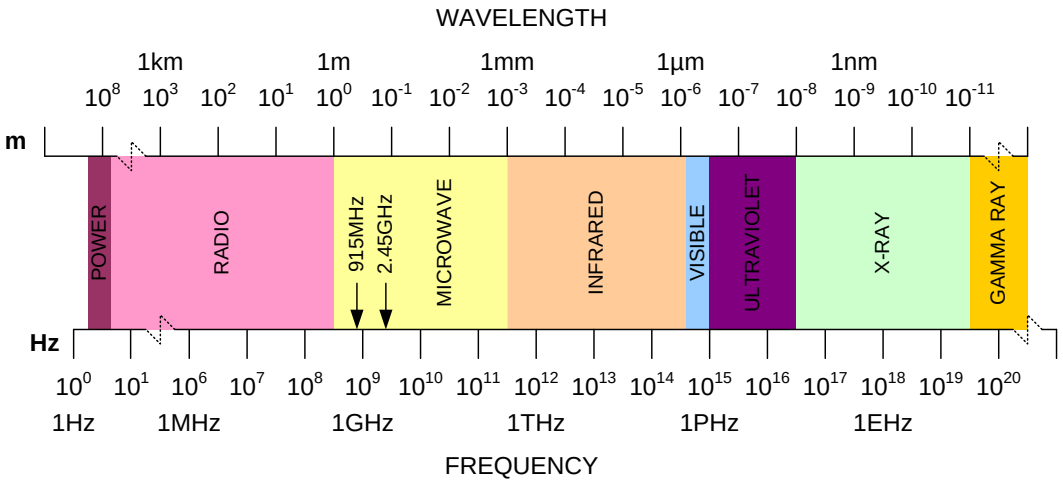


Figure 3.3 Electromagnetic spectrum (reproduced from Batchelor (2013))

There are restrictions upon the industrial use of certain frequencies of electromagnetic radiation in order to prevent interference between equipment and disruption of communications. Microwave frequencies used for heating applications in the UK are typically 433MHz, 896MHz and 2.45GHz, but these frequencies can vary for different countries. These frequencies have been reserved specifically for industrial, scientific and medical (ISM) applications.

3.2.2 Electromagnetic Safety and Compliance

Emissions of electromagnetic radiation are strictly governed by electromagnetic compatibility (EMC) regulations in order to limit personal exposure for health reasons, and also to minimise the potential for interference with other devices. Leakage standards address radiation escaping from equipment, while exposure standards account for safe limits for human exposure (Kitchen, 2001). The time averaged microwave leakage power density should not exceed 50 W/m^2 at a distance 0.05 m from equipment, with a maximum of up to 100 W/m^2 under abnormal conditions (British-Standards, 2011).

3.3 Microwave Heating Mechanisms

Materials can respond in one of three different ways when subjected to microwave treatment, which is to either insulate, conduct or absorb the energy (Church, 1988), as illustrated in Figure 3.4. Any material can be heated by electroheating unless it is a perfect conductor or insulator (Meredith and Metaxas, 1983). Insulators (such as quartz, PTFE or air) are effectively microwave-transparent, which means that electromagnetic waves pass through the material unaffected, whereas conductors (such as copper or aluminium) reflect the microwaves.

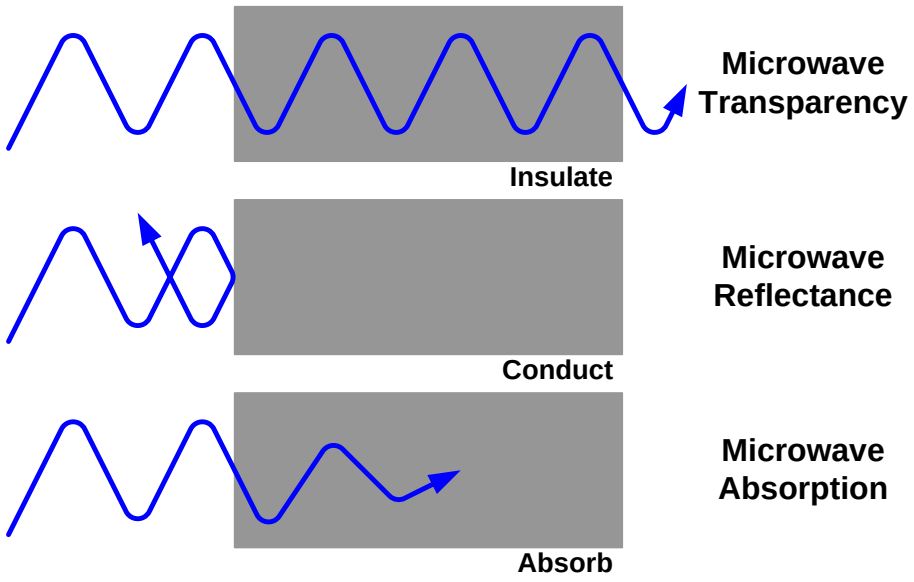


Figure 3.4 The interaction of microwave energy with materials (reproduced from Church et al. (1988))

Materials that absorb microwave energy are termed dielectrics, and respond to the application of microwaves by heating. The heating effect is due to the interaction of charged particles within the material with the electric field component of the electromagnetic wave, either by processes of dielectric polarisation or ionic conduction (Metaxas and Meredith, 1983).

3.3.1 Dielectric Polarisation

Dielectric polarisation occurs due to the induction and orientation of dipole moments. A dipole is essentially two equal and opposite charges separated by a finite distance (Harrop, 1972). The sum of four different polarisation mechanisms, electronic, atomic, dipolar and interfacial polarisation, contribute to the total dielectric polarisation effect and can be described as:

$$\alpha = \alpha_e + \alpha_a + \alpha_d + \alpha_i$$ **Equation 3.2**

Where α= total polarisability; α_e = electronic polarisation; α_a = atomic polarisation; α_d = dipolar polarisation; α_i = interfacial polarisation.

Each of these polarisation mechanisms has a characteristic frequency at which a maximum amount of electromagnetic energy can be

absorbed. Below their characteristic absorption frequencies, mechanisms do not contribute significantly to total polarisability, as polarisation is rapid enough to remain in phase with the incident alternating field (Harrop, 1972). This effect is illustrated in Figure 3.5. While dipole orientation and ionic conduction are dominant at microwave frequencies, atomic polarisation is most significant in the infrared range of the electromagnetic spectrum. Electronic polarisation occurs at visible and ultra-violet frequencies. Ionic polarisation at microwave frequencies is also demonstrated by the increased heating of dissolved salts or the accumulation of charge at material interfaces in crystalline solids.

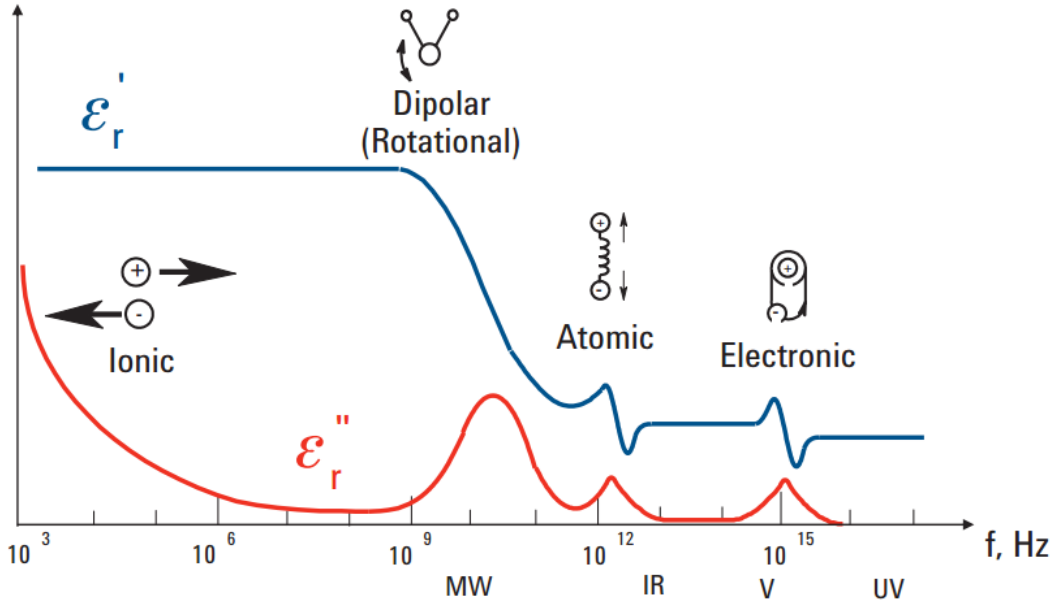


Figure 3.5 Characteristic frequencies of dielectric polarisation (Agilent, 2006)

3.3.1.1 Electronic and Atomic Polarisation

Atoms and molecules are made up of a positively charged nucleus with a negatively charged electron cloud. In the presence of an externally applied electric field, charges are displaced from their equilibrium positions by the distortion of the electron cloud resulting in an induced dipole moment (Anderson, 1964). While electronic polarisation results from the relative displacement of electron charges to the nucleus, atomic polarisation is the relative displacement of atomic nuclei in molecules with an uneven distribution of charge (Meredith, 1998). As

these mechanisms are rapid and alternate in phase with the applied electric field, they do not contribute to dielectric heating at microwave frequencies (Whittaker, 2007).

3.3.1.2 Dipolar Polarisation

Polar dielectrics containing permanent dipoles will attempt to orient themselves in phase with the direction of an applied electric field. As the field direction alternates the dipoles will attempt to reorient themselves in alignment with the field, however their movement will be restricted by the presence of other particles and energy will be lost as friction which generates heat (Whittaker, 2007). This mechanism is illustrated in Figure 3.6. At lower frequencies, full rotating is possible whereas at higher frequencies, no rotating occurs leading to little or no heating in both cases (Harrop, 1972).

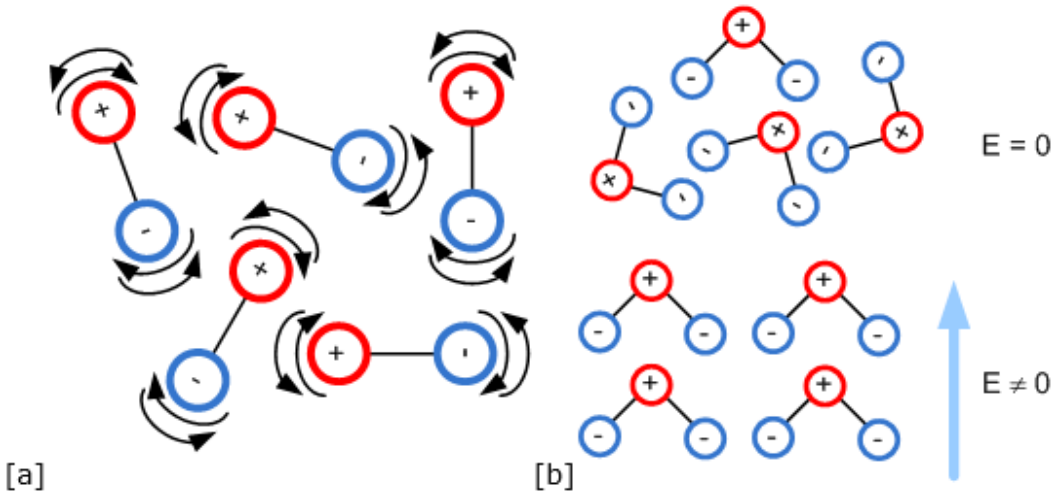


Figure 3.6 Dipolar polarisation mechanism. [a] Dipole reorientation with alternating electric field , [b] dipole alignment in the absence (above) and presence (below) of an electric field (reproduced fromBatchelor (2013))

3.3.1.3 Interfacial Polarisation

When subjected to an electric field, free charge carriers such as electrons and ions accumulate at defects or discontinuities in crystalline materials. In a mineral ore, these could be lattice vacancies, impurities, dislocations or interfaces between two minerals with varying dielectric properties. The accumulated charge induces a

corresponding opposite charge on the other side of the interface, forming a dipole moment. As the polarisation of the conducting phase is subject to the properties of the non-conducting phase, drag is induced in the polarisability with respect to the applied electric field and heating results (Anderson, 1964).

3.3.2 Ionic Conduction

When charged particles are free to travel through a material under an applied electric field, a current will be induced that will travel in phase with the field, resulting in heat that is generated due to electrical resistance within the material (Whittaker, 2007). This current is confined to the surface of the material in a thin skin composed of layers of current flowing in alternating directions, and rapidly diminishes with depth. This mechanism creates a skin heating effect in these types of dielectric materials (Meredith, 1998). If a material is an electrical conductor, such as metals, most of the microwave energy does not penetrate the surface and is reflected, resulting in the generation of very high surface voltages. These qualities make conducting metals, such as aluminium and stainless steel, suitable for use as waveguide materials as they will reflect microwave radiation. If a dielectric material has limited free charge carriers it will behave as a poor or semi-conductor, such as transition metal sulphide and oxide minerals (i.e. pyrite, chalcopyrite, and magnetite).

3.4 Dielectric Properties

The ability of materials to absorb, and subsequently heat, in response to the application of microwave energy, is dependent on their dielectric properties. The design of microwave cavities also requires detailed knowledge of a material's response to microwave energy. This section will describe the dielectric properties of materials and their effect on power dissipation and heating.

3.4.1 Permittivity and Permeability

The permittivity and permeability of a material are the two key factors which influence how a material will respond to microwave radiation. The permittivity of free space relates the mechanical forces existing between two electrostatic charges spaced apart in a vacuum. Similarly, the permeability of free space, relates the mechanical forces existing between two current loops spaced apart in a vacuum (Meredith, 1998). If the space contains an electric or magnetic medium, the forces will be altered by the relative permittivity, also known as the dielectric constant, or the relative permeability, respectively (Von-Hippel, 1954). These can be considered as the factor by which the medium's properties exceed that of free space and are described as:

$$\varepsilon^* = \varepsilon/\varepsilon_0 \qquad \textbf{Equation 3.3}$$

$$\mu^* = \mu/\mu_0 \qquad \textbf{Equation 3.4}$$

Where ε^* = relative permittivity, ε = permittivity, (F/m), ε_0 = permittivity of free space, (8.854×10^{-12} F/m), μ^* = relative permeability, μ = permeability, (H/m), μ_0 = permeability of free space, ($4\pi \times 10^{-7}$ H/m).

A related effect is the change in propagation velocity of a plane electromagnetic wave due to the characteristic impedance of a material (Meredith, 1998). Propagation velocity in free space can be defined as:

$$v = c = \sqrt{\frac{1}{\mu_0 \varepsilon_0}} \qquad \textbf{Equation 3.5}$$

Where v = wave velocity, (m/s); c = speed of light in vacuum, (m/s), μ_0 = permeability of free space, ($4\pi \times 10^{-7}$ H/m), ε_0 = permittivity of free space, (8.854×10^{-12} F/m).

If the medium is a dielectric material, the velocity of a plane electromagnetic wave will slow and the wavelength will shorten when it enters the material, while the frequency remains the same, owing to the changes in permittivity or permeability.

3.4.2 Complex Relative Permittivity and Loss Factor

The dielectric properties of a homogenous material are described by the complex relative permittivity, shown as:

$$\varepsilon^* = \varepsilon' - j.\varepsilon''$$ **Equation 3.6**

Where ε^* = complex relative permittivity or complex dielectric constant, ε' = relative permittivity or dielectric constant, ε'' = dielectric loss factor, $j = \sqrt{-1}$.

Under the influence of microwave energy the dielectric constant takes a complex form to account for losses as electromagnetic energy is converted to heat.

The real part of the complex dielectric constant, ε', represents the ability of a material to be polarised by an applied electric field, and is a measure of the ability of charges and dipoles in a material to store energy. The imaginary part, or the dielectric loss factor, is a measure of the ability of the material to dissipate this energy as heat (Whittaker, 2007). Since it can be difficult to separate the losses during measurement, they can be grouped together defining an effective loss factor, ε''_{eff}, shown as:

$$\varepsilon''_{eff} = \varepsilon''_e + \varepsilon''_a + \varepsilon''_d + \varepsilon''_i + \frac{\sigma}{\omega.\varepsilon_0}$$ **Equation 3.7**

Where $\omega = 2.\pi.f$

Where ε''_{eff}= effective dielectric loss factor, e, a, d and i denote electronic, atomic, dipolar and interfacial polarisation respectively; ε_0 = permittivity of free space, (8.854×10^{-12} F/m); σ = electrical conductivity, (S/m); f = frequency, (Hz); ω = angular frequency, (rad/s).

The loss tangent, tan δ, is the ratio of the energy dissipated as heat to the energy stored, when a material is subjected to an applied electric field. This is often termed 'lossiness' and is defined as:

$$\tan\delta = \frac{\varepsilon''}{\varepsilon'}$$ **Equation 3.8**

Where δ = loss angle, ε' = dielectric constant, ε'' = dielectric loss factor.

When the complex permittivity is drawn as a vector diagram, the real and imaginary components are 90° out of phase, and tanδ forms the angle with the real axis (ε'), as illustrated in Figure 3.7. The loss tangent can be thought of as the phase difference between the electric field and the polarisation of the material (Whittaker, 2007).

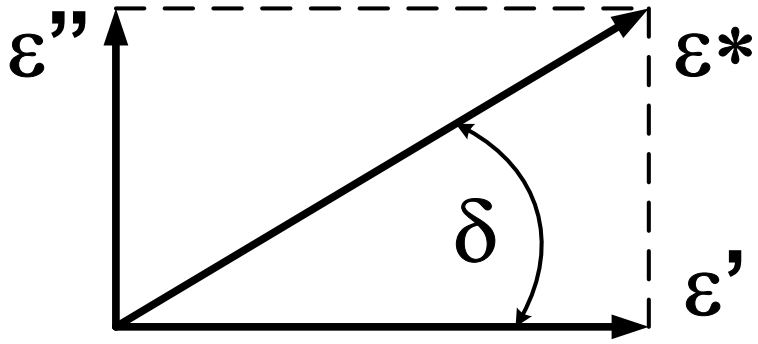


Figure 3.7 Loss tangent vector diagram (reproduced from Agilent (2006))

A high loss factor material, commonly referred to as being 'lossy', acts as a good heater when subjected to microwave radiation, while a low loss factor material is a poor heater.

3.4.4 Factors Influencing Dielectric Properties

The dielectric properties of materials vary extensively, and have been shown to vary in response to changes in both material temperature, and the frequency of the electromagnetic wave (Von Hippel, 1954; Meredith, 1998).

Frequency dependency is due to variations in the relative contribution of different heating mechanisms at different frequencies, as previously described in Section 3.3.1 and shown in Figure 3.5. As the frequency of the electromagnetic wave changes, the relative contributions of the different heating mechanisms also changes. At low frequencies, ionic conduction is the only mechanism contributing to the loss factor. The dielectric constant is high because all the different polarisation

mechanisms are contributing to full polarisation of the material. At these low frequencies the low rate of polarisation allows all forms of polarisation to occur in phase with the incident wave hence low contribution to the loss. At microwave and radio frequencies, electronic and atomic polarisations do not contribute to heating, and dipolar polarisation is the most significant heating mechanism (Meredith, 1998). Ionic conduction and conductive losses also contribute to heating at microwave frequencies. As frequency is increased into the microwave region of the spectrum, dipolar polarisation begins to lag behind the frequency of the oscillating electromagnetic wave. This lag causes the reduction in dielectric constant due to the reduced degree of polarisation occurring. The peak in loss is at the relaxation frequency for this mechanism. As frequency is further increased, both atomic and electronic polarisation reach their relaxation frequencies. Past this point, the rate of oscillation of the electromagnetic wave becomes so high that no polarisation occurs (Harrop, 1972).

The ability of a material to become polarised is determined by the way in which the molecule moves. Temperature has a direct effect upon this, and can either assist or impede the way in which the material is heated when subjected to microwaves. Variations in dielectric properties of materials with temperature is also dependent on the heating mechanism taking place in a particular material. In most materials, dielectric properties over the microwave range tend to increase with increasing temperature, due to a reduction in relaxation time. Dielectric relaxation is the time taken for dipoles to return to random orientation when the electric field is removed. The relaxation time decreases as dipoles have greater rotational freedom (Bőttcher, 1952). Some materials that are not microwave responsive at low temperature will demonstrate significant changes in loss factor, and subsequently their ability to heat as temperature increases.

In complex materials comprising multiple components, such as a mineral ore, the dielectric properties of the materials are of significant

importance, as they can have a profound effect upon the levels of heating achieved, and subsequently the effectiveness of the process.

3.4.5 Microwave Power Dissipation

3.4.5.1 Dielectric Heating Equation

The average power density (P_d) produced in a material, refers to the volumetric absorption of energy (W/m^3) of the material when subjected to electromagnetic radiation (Metaxas and Meredith, 1983). The calculation of power density in a material can be expressed as:

$$P_d = 2.\pi.f.E^2.\varepsilon_0.\varepsilon''$$ **Equation 3.9**

Where P_d = power dissipation density (W/m^3), f = frequency (Hz), E = electric field strength in the dielectric (V/m), ε'' = dielectric loss factor, ε_0 = permittivity of free space, ($8.854x10^{-12}$ F/m).

It can be seen in this equation that power dissipation density varies proportionally with the frequency of the electromagnetic waves, the loss factor of the material, as well as the internal electric field generated inside the material. Increases in the values of any of these factors can result in increases in the power dissipation density within a material, and subsequently increased rates of heating.

3.4.5.2 Temperature Increase

The temperature rise that results from power dissipation within a material during microwave heating can be expressed as:

$$\frac{dT}{dt} = \frac{P_d}{C.\rho}$$ **Equation 3.10**

Where dT = temperature change (°C), dt = time increment (s), P_d = power dissipation density (W/m^3), C = specific heat capacity, (J/kg.ºC), ρ = density of the material (kg/m^3).

P_d in this equation is calculated from Equation 3.9. In practice, the temperature rise experienced by a material as a result of microwave treatment is difficult to determine accurately, as it depends on

dielectric properties that, as has been previously discussed, can often vary with temperature.

3.4.5.3 Penetration Depth

As an electromagnetic wave enters a dielectric material, its amplitude diminishes due to power absorption in the material (Meredith, 1998). The electric field intensity and power density then fall exponentially with depth after entering the materials surface. The penetration depth, D_P, is defined as the depth into the material at which the power flux has fallen to 1/e of its surface value and is given as:

$$D_P = \frac{\lambda_0}{2\pi\sqrt{2\varepsilon'}} \frac{1}{\sqrt{\left[\left\{1+\left(\frac{\varepsilon''}{\varepsilon'}\right)^2\right\}^{0.5} - 1\right]}}$$

Equation 3.11

Where D_P = penetration depth (m), λ_0 = free space wavelength of incident radiation (m), ε' = dielectric constant, ε'' = dielectric loss factor.

When the material is a low loss dielectric, with $\varepsilon''/\varepsilon' \ll 1$, the penetration depth of electromagnetic waves into the material can be approximated to:

$$D_P = \frac{\lambda_0 \sqrt{\varepsilon'}}{2\pi.\varepsilon''}$$

Equation 3.12

Where D_P = penetration depth (m), λ_0 = free space wavelength of incident radiation (m), ε' = dielectric constant, ε'' = dielectric loss factor.

The penetration depth is an important factor to understand, as it provides an indication of the uniformity and distribution of heat within a material. It can be seen from Equation 3.11, that at higher electromagnetic wave frequencies and higher values for dielectric properties, surface heating occur, while at lower frequencies and smaller dielectric values, volumetric heating of the material will occur (Thostenson and Chou, 1999). It is important to note however, that heating will also occur beyond the calculated penetration depths.

3.4.5.4 Voltage Breakdown and Arcing

Arcing occurs when the electric field component of the incoming microwave energy exceeds the breakdown voltage of the air surrounding the material being treated (Metaxas and Meredith, 1983). Highly localised dissipations of power are characterised by intense light, and may result in burn damage to the material or equipment. This localised burning may create a region of high loss carbonised material which can potentially initiate thermal runaway, as discuss in the next section. While the critical electric field strength in air at ambient conditions is about 30kV/cm in a uniform field, this can vary significantly with changes in temperature and pressure, as the breakdown voltage of a gas is proportional to the molecular density of the gas. Since constant pressure density falls with rising temperature, as pressure decreases or temperature increases, the breakdown voltage at which arcs occur decreases (Meredith, 1998). The shape and heterogeneity of material being subjected to electromagnetic waves can also influence arc formation, with sharp edges or corners acting as locations for the concentration of electric fields. While arc formation can be difficult to predict or control if the material being treated is angular and heterogeneous, such as mineral ore fragments, minimising air gaps and material contacts, and the use of lower power densities are possible measures for addressing this issue.

3.4.5.5 Thermal Runaway

Thermal runaway is a phenomenon that can occur when the power dissipation into a material, exceeds the heat being transferred out of the material, leading to a temperature increase at an uncontrollable rate. Following initial electromagnetic energy absorption, the resultant rise in temperature will result in a corresponding increase in loss factor. This will initiate a positive feedback loop of increased power dissipation and loss factor in the material, and further temperature rises. This process can lead to thermal runaway and decomposition of the material and resultant arc formation (Metaxas and Meredith, 1983).

3.5 MICROWAVE HEATING OF MINERALS

Nature has been kind with regards to the application of microwaves to ore comminution process, in that many of the valuable mineral constituents of many ore deposits, and often the minerals with which they are associated, possess dielectric properties which make them amenable to microwave heating. An understanding of the fundamentals of the interactions of microwaves with minerals, and how different minerals respond to microwave radiation is of key importance when assessing the amenability of an ore to high power microwave treatment. This section will present the heating characteristics of minerals that are commonly found in copper sulphide ores, and will focus on heating that occurs at or near the ISM frequencies (433MHz, 896/915/922Mhz, 2.45GHz) that are relevant to the development of the microwave treatment of ores.

There have been several investigations into the heating rates of a variety of sulphide, oxide, carbonate, silicate and other minerals using microwaves. The majority of the literature reports testing conducted in multimode cavities at 2.45GHz and low powers of <2kW (Chen et al., 1984; Church et al., 1988; McGill et al., 1988a; Walkiewicz et al., 1988a; Harrison, 1997; Kingman et al., 2000b). These early studies showed that most silicates, carbonates and sulphates showed little heating, whereas most sulphides and metal oxides heated readily when exposed to microwave energy. It also demonstrated that higher microwave power levels resulted in faster heating rates of many minerals (McGill et al., 1988b). The findings from these early studies at 2.45Ghz allowed for the categorisation of different minerals into three groups, based on their dielectric response to microwave radiation. The high heating rate, or 'good' heating minerals group includes pyrite, pyrrhotite, chalcopyrite, bornite, galena and magnetite, the medium heating rate, or 'poor' heating minerals includes hematite, ilmenite, cassiterite and bauxite, and low heating rate, or the 'non-heaters' group includes quartz, calcite, feldspars and other silicate and carbonate minerals.

A compilation of the dielectric properties of minerals relevant to this investigation, measured at or near ISM frequencies, are shown Table 3.1 and Table 3.2. The values in this table come from the published work of Church et al. (1988), and from measurements conducted at the University of Nottingham and reported by Kobusheshe (2010) and Batchelor (2013).

	Mineral (Formula)	Dielectric Property	Frequency (MHz)			Reference
			400Mhz	910MHz	2450Mhz	
Sulphides	**Chalcopyrite** $CuFeS_2$	**ε'**	27.309	24.802	24.381	*Batchelor (2013)*
		ε"	6.329	4.093	3.046	
		tanδ	0.232	0.165	0.125	
	Chalcocite $Cu2_S$	**ε'**	106.163	107.784	120.107	*Batchelor (2013)*
		ε"	2.218	4.144	10.722	
		tanδ	0.021	0.038	0.089	
	Bornite Cu_5FeS_4	**ε'**	72.712	73.955	69.656	*Batchelor (2013)*
		ε"	3.809	7.723	15.414	
		tanδ	0.052	0.104	0.221	
	Molybdenite MoS_2	**ε'**	28.293	27.558	26.074	*Batchelor (2013)*
		ε"	3.980	4.187	4.702	
		tanδ	0.141	0.152	0.180	
	Pyrite FeS_2	**ε'**	23.138	21.675	21.497	*Batchelor (2013)*
		ε"	6.604	4.060	3.208	
		tanδ	0.285	0.187	0.149	
Oxides	**Magnetite** Fe_3O_4	**ε'**	21.918	21.660	22.462	*Batchelor (2013)*
		ε"	0.731	0.371	0.424	
		tanδ	0.033	0.017	0.019	
	Hematite Fe_2O_3	**ε'**	10.587	11.114	11.985	*Batchelor (2013)*
		ε"	1.690	0.843	0.495	
		tanδ	0.160	0.076	0.041	
	Goethite FeO(OH)	**ε'**	23.807	26.312	26.783	*Batchelor (2013)*
		ε"	0.676	0.237	0.169	
		tanδ	0.028	0.009	0.006	
	Ilmenite $FeTiO_3$	**ε'**	40.175	34.966	32.810	*Batchelor (2013)*
		ε"	2.072	2.318	2.597	
		tanδ	0.052	0.066	0.079	
	Rutile TiO_2	**ε'**	17.993	17.829	18.484	*Batchelor (2013)*
		ε"	0.692	0.090	0.074	
		tanδ	0.038	0.005	0.004	

Table 3.1 Dielectric constant (ε'), loss factor (ε") and loss tangent (tanδ) for sulphide and oxide minerals.

	Mineral (Formula)	Dielectric Property	Frequency (MHz)			Reference
			400Mhz	910Mhz	2450Mhz	
Silicates	**Quartz** SiO_2	**ε'**	3.782	3.708	3.813	*Kobusheshe (2010)*
		ε"	0.084	0.054	0.022	
		tanδ	0.022	0.015	0.006	
	Plagioclase $(Na,Ca)(Si,Al)_4O_8$	**ε'**	4.291	4.785	4.696	*Kobusheshe (2010)*
		ε"	0.001	0.001	0.001	
		tanδ	0.001	0.001	0.001	
	Orthoclase $KAlSi_3O_8$	**ε'**	5.250	4.767	4.772	*Kobusheshe (2010)*
		ε"	0.485	0.023	0.013	
		tanδ	0.092	0.005	0.003	
	Albite $NaAlSi_3O_8$	**ε'**	4.256	4.334	4.694	*Kobusheshe (2010)*
		ε"	0.000	0.026	0.023	
		tanδ	0.000	0.006	0.005	
Sheet Silicates	**Muscovite** $KAl_2(AlSi_3O_10)(F,OH)_2$	**ε'**	5.273	5.553	5.552	*Kobusheshe (2010)*
		ε"	1.146	0.250	0.110	
		tanδ	0.217	0.045	0.020	
	Biotite $K(Mg,Fe)_3AlSi_3O_{10}(F,OH)_2$	**ε'**	5.648	5.506	5.547	*Kobusheshe (2010)*
		ε"	0.414	0.413	0.241	
		tanδ	0.073	0.075	0.043	
	Na-Montmorillonite $(Na,Ca)_{0.33}(Al,Mg)_2(Si_4O_{10})(OH)_2.nH_2O$	**ε'**	7.112	6.654	6.387	*Kobusheshe (2010)*
		ε"	4.017	2.520	1.564	
		tanδ	0.565	0.379	0.245	
	Kaolinite $Al_2(Si_2O_5)(OH)_4$	**ε'**	6.478	6.105	6.018	*Kobusheshe (2010)*
		ε"	1.084	0.655	0.346	
		tanδ	0.167	0.107	0.057	
Carbonates	**Calcite** $CaCO_3$	**ε'**	8.890	8.840		*Church (1988)*
		ε"	0.077	0.500		
		tanδ	0.009	0.057		
	Dolomite $CaMg(CO_3)$	**ε'**	7.380	7.260		*Church (1988)*
		ε"	0.220	0.226		
		tanδ	0.030	0.031		
	Magnesite $MgCO_3$	**ε'**	6.710	6.610		*Church (1988)*
		ε"	0.122	0.104		
		tanδ	0.018	0.016		
	Siderite $FeCO_3$	**ε'**	7.160	7.100		*Church (1988)*
		ε"	0.193	0.190		
		tanδ	0.027	0.027		
Other	**Apatite** $Ca_5(PO_4)_3(OH,F,Cl)$	**ε'**	6.231	6.425	6.774	*Kobusheshe (2010)*
		ε"	0.226	0.045	0.012	
		tanδ	0.036	0.007	0.002	
	Zircon $ZrSiO_4$	**ε'**	6.165	6.915	7.064	*Kobusheshe (2010)*
		ε"	0.381	0.032	0.014	
		tanδ	0.062	0.005	0.002	

Table 3.2 Dielectric constant (ε'), loss factor (ε") and loss tangent (tanδ) for silicate, sheet silicate, carbonate, and other minerals.

It can be clearly seen in these tables that the sulphide and oxide minerals are generally more 'lossy' than the silicates, carbonates and other minerals, in that they exhibit a higher loss tangent (tan δ), or ratio of the energy dissipated as heat to the energy stored, when a mineral is subjected to microwave radiation. The exception is the

sheet silicate mineral montmorillonite, which heats readily due to the presence of interlayer water in its crystallographic structure (Kobusheshe, 2010).

The differences in the dielectric response of minerals is further illustrated in Figure 3.8, which compares the dielectric loss factor (ε") and the loss tangent (tan δ) at 910Mhz for minerals found in a typical copper ore. Minerals that plot towards the top-right of the chart are better heaters when subjected to microwaves than those to the bottom-left. This data provides the justification for the grouping of minerals into the good heating, poor heating and non-heating categories used in this investigation, and is designated by zoning in the figure.

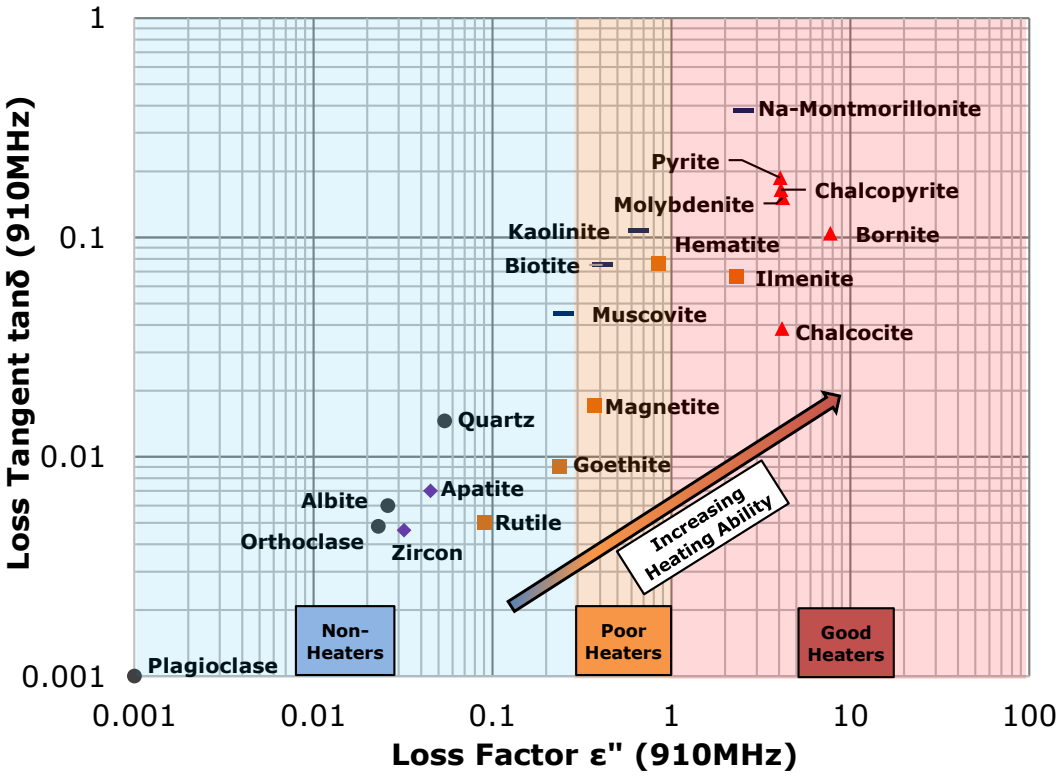


Figure 3.8 Dielectric loss tangent for selected minerals. Blue shaded region represents non-heating minerals, orange shaded region represents poor heating minerals, and red region represents good heating minerals.

In order to produce a selective differential heating effect in a mineral ore, it is a required that each mineral must also exhibit differences in

heating rates. A summary of the heating rate experiments of Kingman et al. (2000b), performed on a range of minerals found in copper sulphide ores at 2.6kW and 2.45Ghz, is shown in Figure 3.9. The results in this figure clearly show the differential heating effect between non-heating gangue minerals, such as quartz and feldspars, and the copper and iron sulphide heating minerals.

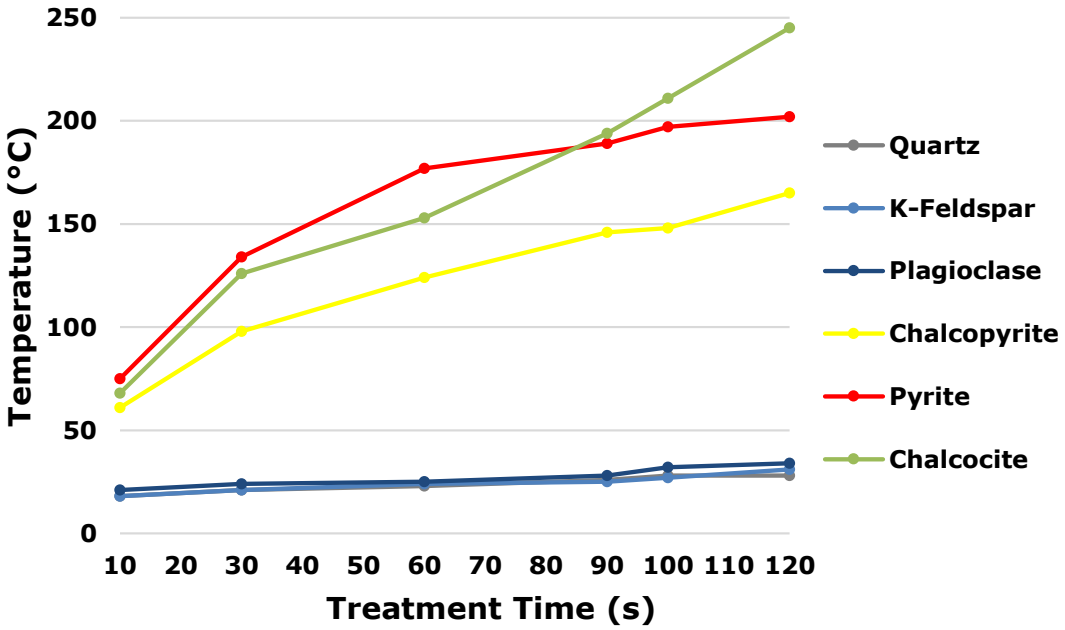


Figure 3.9 Heating rates of selected copper ore minerals (Kingman et al., 2000b)

It is this variation in heating rates of the constituent minerals in an ore, which produces the differential thermal expansion effect that is the driving mechanism behind enhanced comminution through high power microwave treatment.

In conventional heating processes, heat energy that is transferred to a material must pass through its surface, and across a temperature gradient through the material, by conduction, convection or radiation mechanisms. Therefore, the rate of heat transfer or flow within the material is limited by both the temperature at the surface interface, and the thermal diffusivity of the material. This can result in uneven temperature distributions, difficulty in controlling the level of heating, and slow heating rates (Meredith, 1998). Microwave energy has been

shown to selectively heat materials, as differences in material composition correspond with differences in dielectric properties, which leads to certain materials having the ability to heat more quickly than others. This is a significant advantage that dielectric heating has over conventional heating methods, in that no energy is wasted in heating the bulk sample throughout. Microwaves allow for the generation of high temperatures over very short time intervals in materials that are sufficiently absorbent, or 'lossy'. In large industrial microwave systems, the microwave efficiency can be defined as the percentage of the applied microwave energy which is dissipated as heat in the material being treated, and can be in the region of 95% (Meredith, 1998). It is the efficient, selective heating mechanism of microwaves that provides the advantage over conventional heating methods.

3.6 Microwave Processing Systems

3.6.1 Introduction

Industrial microwave processing systems typically consist of a power supply, a microwave generator, waveguide transmission lines, and an applicator. There are many possible configurations of these components depending on the requirements of the application. In microwave heating applications the aim of the process is to propagate microwave energy as standing waves, and contain the energy within a material treatment applicator, while also controlling emissions of fugitive microwaves to prevent interference with electrical devices and danger to people. The arrangement of the primary components of an industrial microwave heating system were outlined by Metaxas and Meredith (1983), and are shown in Figure 3.10.

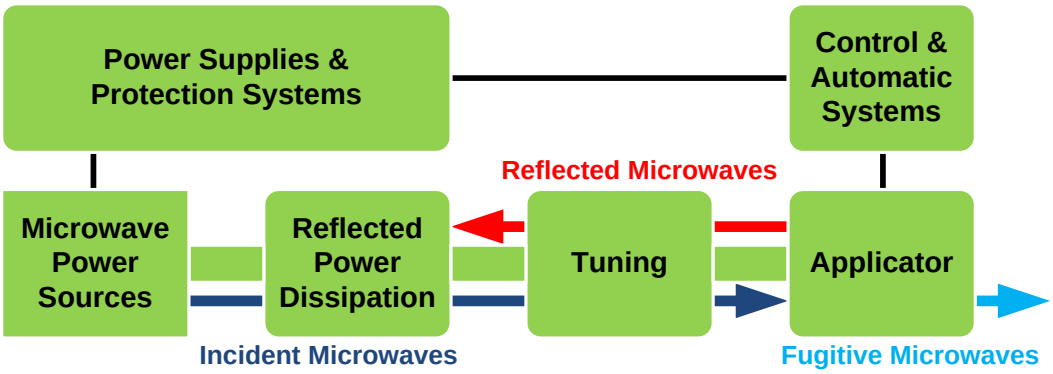


Figure 3.10 Diagram of a typical industrial microwave heating system (Batchelor, 2013).

There is a set of key criteria that are required to be met in order for a microwave processing system to be economically viable compared to conventional heating methods (Meredith, 1998). These requirements include:

- A high conversion efficiency of electrical power input to microwave power output.
- Stable operation within the regulated ISM frequency band.
- Low capital cost per kilowatt of power output, in order to offset the high cost of the microwave generators as a proportion of the total system.
- Low operating cost, including power consumption and replacement of consumables.
- The ability for reliable operation in challenging operating environments.
- Simple to use and easy to maintain, with comprehensive installation and operation manuals.

3.6.2 Microwave Power Sources

Industrial microwave heating processes typically require high power inputs of up to 30kW at 2.45GHz, and up to 100kW at 896/915/922MHz. There are several different types of microwave generators, however the three most relevant to industrial heating

applications are klystrons, solid state generators and magnetrons. Klystrons are a device that employs electromagnetic wave amplification. They tend to be used for high power applications (>50kW) where frequency stability is important, such as for communications, however they tend to be too expensive for industrial heating applications (Metaxas and Meredith, 1983). Solid state generators are more commonly used for low power applications (<200W), and are therefore unsuitable for high power microwave treatment processes (Sairem, 2012).

The most common type of generator used in microwave heating is the magnetron. The popularity of the magnetron is due to the simplicity and cheapness of manufacture, and its widespread use in domestic kitchen microwaves has led to large cost reductions. The extensive use of magnetrons in industrial processing systems is attributed to their high power conversion efficiencies of ~70% at 2450 MHz and ~90% at 900 MHz, high power outputs of up to 100kW continuous wave (CW) and 3MW pulsed power, and good frequency stability (Meredith, 1998). Currently the highest power L-Band (operating at 896/915/922Mhz) magnetrons commercially available can output up to 100kW of microwave power. There is a single reference in the literature to the development of a 500kW continuous wave L-band magnetron (Shibata et al., 1991), however this work does not yet appear to have come to fruition in terms of research or commercial applications.

3.6.2.1 Magnetrons

A magnetron comprises a hollow anode with an array of equal size cavities and vanes forming a resonant microwave structure which surrounds an electron emitting cathode, all of which is sealed under high vacuum. A diagram of the structure of a magnetron is shown in Figure 3.11. The cylindrical metal cathode (blue) is connected to a heater, and once it reaches operating temperature, electrons are released through thermionic emission. The anode (red) is supplied with

a high voltage positive DC potential relative to the cathode, so that thermionically emitted electrons will be attracted radially from the cathode to the anode.

A high strength magnetic field is aligned axially to the anode and cathode, and perpendicular to the electron path. The magnetic field forces the electrons to take a circular path around the cathode. When the electron cloud reaches the anode, it causes an alternating charge on the vane tips and current in the cavities. This induces a microwave field across the vane tips by transfer of energy from the DC field, and it is in this way that the dimensions of the cavities define the operating microwave frequency. The microwave field fringes into the space between the cathode and anode. Microwave power can then be extracted via the coupling strap through one of the cavities, and transmitted from the output antenna, or by means of a coaxial line or waveguide.

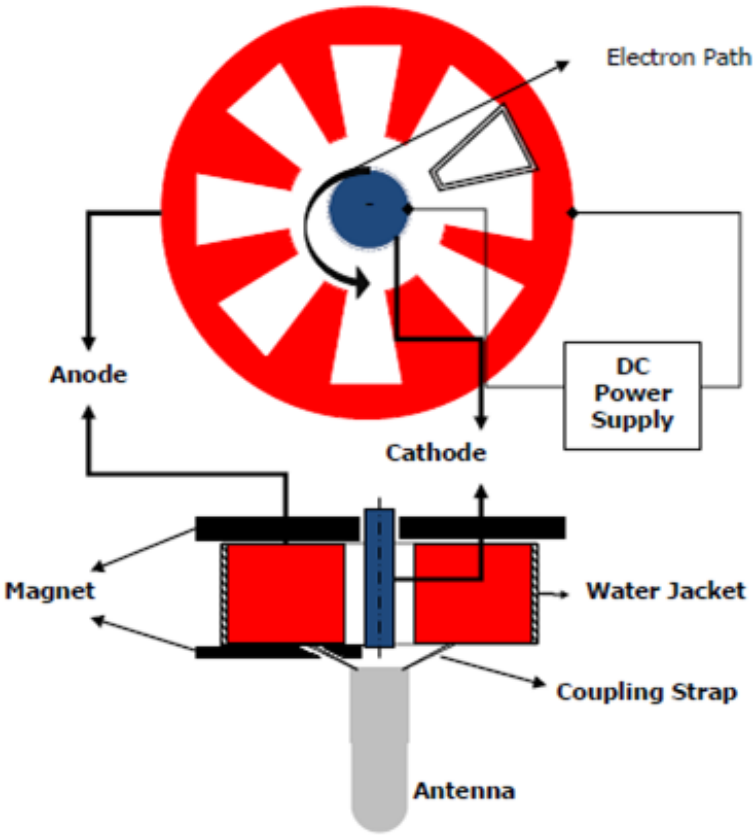


Figure 3.11 Diagram of a magnetron (Al Sayegh, 2012)

3.6.3 Microwave Transmission

Microwaves emitted from a magnetron can be transmitted through a number of different methods including via coaxial lines, waveguides, parallel plates or open wires (Meredith, 1998). The most commonly transmission method used in industrial microwave heating systems are coaxial lines and open waveguides.

3.6.3.1 Coaxial Lines

Coaxial lines are double metal cored cables used to transfer electromagnetic energy. As illustrated in Figure 3.12 they are constructed of a conductive metal core surrounded by a dielectric insulator, which is then surrounded by another metallic shield, and finally insulated with a plastic sheath. Coaxial lines are typically used with low power systems (<1kW) due to overheating that can occur from attenuation at high powers (Meredith and Atkinson, 1983).

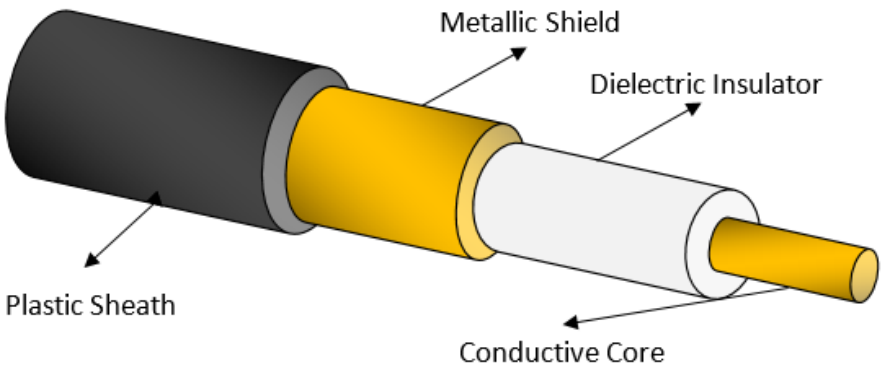


Figure 3.12 Diagram of a coaxial cable (Al Sayegh, 2012)

3.6.3.2 Waveguides

In industrial processes employing microwave power >1kW, it is more common for waveguides to be used to transmit the microwave energy. Waveguides are hollow metal tubes which allow for transmission of microwaves at high powers (>100kW) through air. Precise fabrication is required to minimise losses and prevent gaps at joins that may allow microwave leakage. The dimensions of the waveguide used are dependent upon the microwave frequency used, with increasingly

lower frequency waves requiring increasingly larger waveguides. Below microwave frequencies these sizes become prohibitively large and impractical, and coaxial cables are more commonly used (Metaxas and Meredith, 1983; Meredith, 1998).

In a rectangular waveguide, the electric field is perpendicular to the direction of propagation. For a given waveguide dimension there is a maximum cut-off wavelength, λC, above which the wave can't propagate. When microwave radiation is contained within a structure such as a waveguide or cavity, maxima and minima in the electric and magnetic fields form, due to constructive and destructive interference. These patterns are known as modes, of which are three main types:

- TM_{lmn} mode (transverse magnetic): no magnetic field in the direction of propagation.
- TE_{lmn} mode (transverse electric): no electric field in the direction of propagation.
- TEM_{lmn} (transverse electric and magnetic) mode: no electric or magnetic field in the direction of propagation.

The designations l, m and n are the number of half wavelengths of sinusoidal variation of the electric or magnetic field along the principle axes of transmission. Rectangular waveguides used for the 896Mhz microwave treatments in this study were designated WR975 with dimensions of 248x124mm, which transmitted microwaves with TE_{10n} mode.

3.6.3.3 Short Circuit Tuners

Short circuit tuners are common in microwave processing systems with single-mode resonant cavities, and this type of tuning was used by both microwave treatment systems used in this study. A short circuit tuner works by having a sliding plate positioned after the material within the cavity, and this plate can be adjusted forwards and backwards in relation to the incoming electromagnetic wave on a

threaded pin. The impedance of the material in the cavity will change the superposition and path of the incoming microwaves, and this must be corrected to ensure the electric field, and subsequently the power density, are maximised within the material being treated. The position of the short circuit tuner is required to be adjusted for different materials, due to differences in the impedance of the microwaves and changes to the incoming wavelength that are caused by variations in the dielectric properties of the material being treated (Meredith, 1998).

3.6.3.4 Stub Tuners

Two, three or four stub tuners are commonly used in systems that use waveguides for power transmission. Stub tuning devices are located in the waveguide between the generator and the cavity, and operation is by the insertion of metallic stubs at different lengths into the waveguide. This type of tuning works by changing the impedance of the load to match that of the generator. Stub tuners can be adjusted either manually or automatically, and then fixed in position. Alternatively, in systems comprising an automated 'HOMER' tuner, such as the microwave treatment systems used in this study, rapid dynamic matching of impedance can take place while a material is being processed to maximise energy transfer (S-Team, 2011). This device also allows the user to record a process log of incident and reflected microwave power on a millisecond basis.

3.6.3.5 Reflected Power Dissipation

A necessary component of high power microwave treatment systems is a terminating load to absorb residual power that is not absorbed by the material in the cavity, and is reflected back along the waveguide. This is required in order to minimise potential damage to system components associated with high levels of reflected power. Diversion of any reflected power into a circulating water load is the typical method used, due the abundance and high loss factor of water. Knowledge of the amounts of reflected power along with forward

power is also an important factor for impedance matching (Metaxas and Meredith, 1983).

3.6.4 Microwave Applicators

Once the transmission of microwaves has been achieved, the energy must be transferred into the material being treated as efficiently as possible, to maximise the effects of energy dissipation. A microwave applicator, also termed a cavity, is a structure designed to hold and deliver microwave energy into the material being treated. The type of applicator required will be dependent upon the both the properties of the material, and the desired process outcomes. The most common applicators employed in the microwave heating of ores are multimode cavities and single mode resonant cavities.

3.6.4.1 Multimode Cavities

Multimode cavities are the most common applicator types used in domestic, industrial and scientific applications. They are simple to construct, and are versatile in terms of being able to heat a wide range of different sized loads with varying properties. A multimode cavity is constructed of a metallic box with at least 2 wavelength dimensions in two axes, to allow for formation of multiple resonant modes within the applicator. The energy is conveyed to the cavity from the waveguide and subsequent reflections result in a relatively even distribution of energy. Multimode applicators can support a large number of resonant modes simultaneously (Metaxas and Meredith, 1983), which combined to give a resultant field pattern of high and low electric field strengths, as illustrated in Figure 3.13.

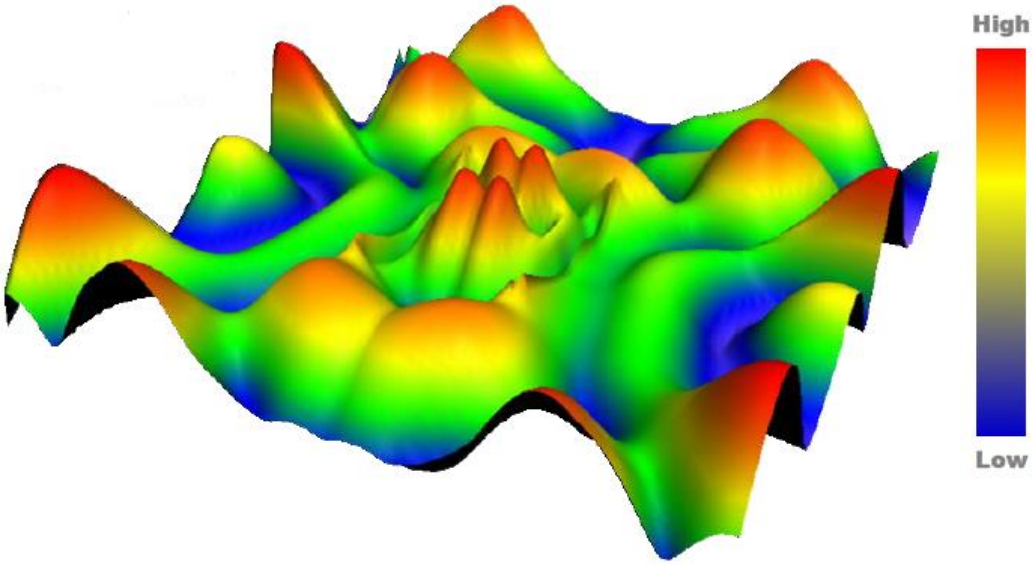


Figure 3.13 Example of the electric field pattern within a multimode cavity. Red areas indicate high electric field strength and blue areas indicate areas of lower electric field strength.

It is easier to achieve uniformity of heating when a large number of modes are present, and this is important in many heating applications. Many multimode cavities, such as domestic kitchen microwaves, incorporate turntables so that the load is rotated through the cavity, or mode stirrers to continuously change the field pattern. This subjects the material to areas of high and low electric field strength in order to minimise localised heating. Multimode cavities are not best suited however, to applications where high temperatures are required, as the energy is dissipated throughout a relatively large volume. Therefore, some low-loss materials do not heat sufficiently, or rapidly enough, in multimode cavities. It is for this reason that multimode cavities are not ideal for achieving the high power densities required for the microwave treatment of mineral ores for enhanced comminution.

3.6.4.2 Single Mode Resonant Cavities

As the name suggests, a single mode cavity, is designed in such a way that it can only support one mode of electromagnetic wave propagation. This produces a well-defined heating zone, and can be used to achieve very high power density and heating rates. A single mode cavity is said to be resonant when the stored electrical energy is

equal to that of the stored magnetic energy, and the resonance occurs at specific frequencies that are dependent on the cavity dimensions (Metaxas and Meredith, 1983). When a cavity is resonant, energy is dissipated in the walls, and when a material is inserted into the cavity, energy is also dissipated into it. The ratio of the energy stored to the energy dissipated is called the quality factor, Q, which is a measure of the lossiness of the empty or loaded cavity. Inserting a load changes the resonant frequency of the cavity according to the dielectric constant of the load, and there is a change in quality factor that is proportional to the dielectric loss of the load.

A simple single mode resonant cavity typically comprises a rectangular waveguide with an opening in either one or both broad faces of the cavity. This allows for the transfer of the material to be heated into the cavity, and ideally, through the position of maximum electric field strength, or the region of maximum power density. A sliding short device, which was previously described in Section 3.6.3.3, can be used to modify the position of the electric field maximum to optimise the transferal of microwave energy into the material. The single mode nature of this type of cavity means however, that there is an uneven electric field distribution within the cavity, with some regions of the material experiencing very low electric field strength, while other regions are subjected to the maximum electric field strength. This needs to be taken into consideration when designing industrial microwave treatment systems with single mode resonant cavities. The microwave treatments conducted for this investigation were performed in TE_{10n} single mode resonant cavities.

3.6.4.3 Microwave Choking in Continuous Flow Applicators

An important requirement for furthering the application of microwaves in industrial processing systems is the development of continuous flow microwave treatment applicators. A challenge to overcome in the development and operation of an 'open-ended' microwave processing

system, is limiting the emissions of fugitive microwaves from the system.

Choking structures are required to limit microwave leakage from open continuous flow applicators. The three commonly used techniques are reactive choking, resistive absorption by the load and resistive attenuation by a dielectrically absorbent choke liner. Reactive chokes use specifically shaped structures to prevent propagation of particular modes, essentially reflecting fugitive microwaves back into the applicator. The material being treated in the applicator will continue to absorb this power as it is reflected by choking structures, which has the effect of intensifying the microwave heating effect within the cavity. An additional precaution commonly added to a choking structure, is to line it with a highly dielectrically absorbent material such as carbon foam, with the aim of absorbing any remaining fugitive power that is not reflected back into the cavity.

3.6.5 Microwave Treatment Systems for Ore Comminution

The most effective method of treating ores at the high power densities required for microwave induced fracturing to take place, is through confining the electric field into a small volume within the material through the use of single mode resonant cavities. There are however processing system limitations determined by the waveguide and cavity dimensions required at different microwave frequencies. At the regulated ISM frequencies of 2.45GHz, 896/915/922MHz, and 433MHz, the required waveguide dimensions for transmission of microwaves at these frequencies, and subsequently the broad face dimensions of the applicators, limit the size of the aperture able to be used to transfer material into the cavity. Based on the region of high electric field strength able to be produced at each frequency in a single mode cavity, the practical area available for treatment is ~80mm diameter at 2.45GHz, ~200mm diameter at 896/915/922MHz and ~480mm at 433MHz for cylindrical flow apertures (Batchelor, 2013). To ensure

that material can undergo uninterrupted mass flow through a system, the width of the opening is required to be at least five particle diameters, based on established bulk solids handling theory (Jenike, 1964). This restricts the theoretical maximum for treatable particle size to ~16mm at 2.45GHz, ~40mm at 896/915/922MHz and ~96mm at 433MHz. This was a key factor in determining the particle sizes able to be treated in the microwave treatment systems used in this investigation.

All previously published works relating to the microwave treatment of ores for enhanced comminution have been conducted at 2.45Ghz. The microwave treatments conducted in this study were performed at 896MHz at up to the highest available power at this frequency, which is currently 100kW. Microwave treatments conducted at 896/915/922MHz ISM regulated frequencies was identified from previous research as a means to pilot microwave fracture of ores at increased microwave power and throughputs (Batchelor, 2013).

3.7 SUMMARY

This chapter has presented a detailed background to the fundamental aspects of the interaction of microwaves with materials, the dielectric properties of minerals, and the components of industrial microwave systems relevant to this investigation.

It has been identified from previous studies that sulphide minerals commonly associated with copper ore deposits, such as pyrite, chalcopyrite and bornite, heat more readily when subjected to microwave radiation than gangue minerals such as quartz, feldspars and micas. It is the rapid, selective and volumetric heating effect observed in these minerals that are common constituents of copper ores, which produces the 'thermal shock' mechanism and subsequent differential expansion of dielectrically absorbent minerals during microwave treatment. It is the ability of microwave energy to rapidly and selectively heat certain minerals within an ore, and generate and

propagate intergranular fractures at their grain boundaries, which has demonstrated the potential for reducing ore strength and enhancing mineral liberation through high power microwave treatment.

CHAPTER 4 - EXPERIMENTAL METHODS FOR MICROWAVE TREATMENTS AND ORE CHARACTERISATION

4.1 Introduction

The principle experimental components of this study involved mineralogical characterisation of coarse ore samples prior to treatment, high power microwave treatments conducted at varying conditions, and characterisation of ore samples after microwave treatment to assess the effects on ore strength, ore fracturing, and mineral liberation. A range of different experimental and analytical techniques were employed in achieving the aims of this investigation. This chapter will describe the methods and equipment used in this study, and provide justification for their selection.

4.2 Ore Sample Preparation

The three ore samples used throughout this study were all sourced from a major porphyry copper mine, owned and operated by the project sponsor. Details of each ore will be provided in the next chapter. Several tonnes of each bulk crushed ore were shipped from the mine as pre-screened samples, nominally sized to -50.8+25.4mm (-2+1”), and received at the University of Nottingham facility in a combination of bulk bags and drums. Sample preparation procedures including sample splitting, crushing and grinding, and size classification were required in order to prepare the individual ore sub-samples for microwave treatment, and for preparation of both untreated control and microwave treated samples for mineralogical and comminution testing.

4.2.1 Sample Splitting

Sampling is the means by which a small amount of material is taken from a bulk sample in a manner that it is representative of the larger

amount (Wills and Napier-Munn, 2006). Ensuring the accurate representivity of sub-sampling from a bulk sample is a key requirement for mineral processing and mineralogy investigations (Napier-Munn et al., 1999). Whether removing a 200kg sub-sample from a 2 tonne bulk sample for microwave treatment, 20kg out of 200kg for comminution testing, or 20gms out of 200gms for mineralogy sample preparation, strictly adhering to correct sampling techniques to ensure a high degree of confidence in the representivity of the sample is of paramount importance.

A number of sampling techniques are commonly used to split bulk material into representative sub-samples, including cone and quartering, fractional splitting, riffle splitting and rotary sample dividing. The most convenient and accurate method for splitting bulk bags and drums of ore is using a rotary sample divider (RSD), and this method was used during primary bulk sample division to produce samples for microwave treatment. In this study, ore in bulk bags was split into drums using an eight 200L drum RSD, and drums were split into smaller batches using a 60L RSD with either 3, 4 or 6 segments. Treated ore was either split by a smaller rotary sample divider or cone and quartering, to create sub-samples for comminution testing and fracture analysis respectively. Cone and quartering was used for fracture analysis samples to minimise the potential for affecting fracture properties through handling during sample splitting. A micro-RSD was used for splitting crushed, milled and screened size fractions of ore samples for mineralogical analysis.

One of the most important aspects of sampling is collecting the correct sub-sample mass in order to achieve a high level of confidence in the average composition or characteristics of the bulk ore. Representative sampling of ore fragments and particulate material was conducted using calculations based the equations of Gy (1976), which are given as:

$$M = \frac{C.d^3}{\sigma^2_{FE}} \text{ where} \qquad \textbf{Equation 4.1}$$

$$C = c.\beta.f.g \text{ and} \qquad \textbf{Equation 4.2}$$

$$c = \frac{\rho(1-\alpha)}{\alpha} \qquad \textbf{Equation 4.3}$$

$$\beta = \sqrt{d_{grain} - d} \qquad \textbf{Equation 4.4}$$

Where M = required sample mass, (g); d = nominal particle top size, (mm);σ^2_{FE}.= variance of the fundamental error; C = sampling constant, (g/cm³); c = constitution parameter, (g/cm³); ß= grain size parameter; f = shape factor; g = size range parameter; ρ = average density of the bulk sample, (g/cm³); α = expected average grade of component of interest; d_{grain} = grain size of component of interest, (mm).

When these equations are applied to the -50.8+25.4mm sized material used in this investigation, it can be determined that the sampling theory requires a sample of ~200kg for a high level of confidence in the mineral grade of the sub-sample for an ore. Throughout this study, appropriate sample splitting measures were applied to producing the largest and most representative sample possible for each stage of the investigation, within the feasible limits of the methods employed.

4.2.2 Crushing and Grinding

Crushing of ores in this study was conducted using a Retsch BB200 laboratory scale jaw crusher with a fixed pivot at the opening and a ~2mm throw at the discharge. The crusher has a maximum fragment feed size of ~90mm and can generate a product of ~1.5-30mm. The jaws are corrugated towards the top to increase forces applied to the material, but are smoothed at the discharge to allow closer control of product size. Product size was controlled by passing aluminium foil test lumps through the crusher to check the minimum jaw gap. Crushing of ore samples in this study was conducted in stages at closed size settings of 9.5mm, 4mm and 1mm, and starvation fed on a fragment by fragment basis to minimise production of fines. This

crusher was employed during comminution testing and to produce samples for further grinding.

Grinding of ores for mineralogical analysis was conducted using a laboratory scale rod mill. The mill is 203mm in diameter and 254mm long, with 4 internal pulp lifter bars and stainless steel grinding rods of three different sizes totalling ~10kg. The rod mill was rotated on heavy duty rollers at 70% critical speed (68rpm) with 60wt% solids (1kg sample to 665ml water).

Pulverising of milled ore samples for chemical assay was conducted using a TEMA ring and puck mill to a particle size nominally less than 75µm.

4.2.3 Size Classification

Classification of particulate ore samples was conducted in order to produce discreet size fractions for mineralogical analysis. Particle size distributions are determined using standardised sieving methods (ISO 2591-1:1988, ISO 3310-2:1999), including an initial stage of wet sieving to remove fines (-38µm material), before dry sieving with tapping or vibrating sieve shakers. A range of square aperture woven-wire or perforated plate sieves from the $\sqrt{2}$ geometric series, where the aperture area doubles with each interval, were used in this study. The range of sieve sizes used in this study are shown in Table 4.1.

Coarse Sieves Perforated Plates (mm)	Fine Sieves Wire Mesh (mm)
63.0	3.35
53.0	2.36
45.0	1.70
37.5	1.18
31.5	0.850
26.5	0.600
22.4	0.425
19.0	0.300
13.2	0.212
9.5	0.106
6.7	0.075
4.75	0.053
-	0.038

Table 4.1 Sieve sizes used in fragment and particle size classification.

4.3 Microwave Treatment Systems

Microwave treatments of ore samples in this investigation were conducted at the University of Nottingham using both a pilot-scale continuous throughput microwave treatment system, and a pilot-scale batch treatment system. This section will outline the design, capabilities and operation of these two systems.

4.3.1 Microwave Treatment Pilot-Scale System

4.3.1.1 Introduction

The microwave treatment pilot-scale system, hereafter referred to as the pilot system, was designed and developed to assess the feasibility, scalability and technical performance of continuous throughput high power microwave processing of mineral ores, and to allow for further development of the fundamental understanding of how mineral ores respond to high power microwave treatment. A comprehensive description of the background, basis of design, and all aspects of the technical development of the pilot system is presented by (Buttress et al., 2016).

The pilot system is a bespoke, laboratory-based 10-150t/h continuous throughput pilot plant, capable of treating mineral ores with between 60-200kW of microwave power at a frequency of 896MHz, and is the culmination of over fifteen years of research and development activity. It was designed, constructed and commissioned in order to understand the engineering challenges of microwave-induced fracture of ores at industrially relevant scales, and to generate large samples of material treated at between ~0.4-3kWh/t for comminution and mineral liberation testing. While the pilot plant is technically capable of treating ores at total energy inputs of ~0.4-20kWh/t (i.e. 60kw at 150t/h; 200kW at 10t/h), considerations of treatment stability and industrial relevance of the conditions mean that ~3kW/t is the practical maximum for the treatment of copper ores in the system. A critical aspect to the development of the pilot system is that it was designed to be scalable to throughputs of several thousand tonnes per hour. The pilot system was designed based on the concept of frequency scaling, with the system initially designed for 1000t/h throughputs at a microwave frequency of 433MHz with a correspondingly larger dimension vertical ore flow tube and applicator sections. The design was then scaled back to the next ISM frequency band at 896Mhz at lower throughputs to minimise technical risks and development costs, while also allowing the system to be located close to the University of Nottingham, rather than on a mine site. The design of the systems at both 433MHz and 896Mhz was essentially the same, comprising single mode applicators through which ore is continuously flowed downwards though an inner processing tube, in which the electric field confinement is achieved by circular choking structures. The development of circular corrugated choking structures was also a crucial component in the development of the open-ended and continuous throughput vertically-aligned applicator, and the design and testing of these choking structures has been considered in detail by (Katrib et al., 2016).

The requirements identified for the pilot system were identified by a set of key design criteria:

- The system must allow for high microwave power density in the heating minerals within a sample, and support rapid throughputs and subsequently short residence times in the applicator.
- The applicator must have a low ratio of stored energy to dissipated energy to assist with impedance matching, and must also allow for the formation of a uniform electric field.
- Large throughputs are required in order to assess the scalability of the system to industrially relevant throughputs.
- Most importantly, the system must be inherently safe, in terms of both the microwave and materials handling components.

The system was designed to run continuously to generate large samples, of up to several tonnes of microwave treated ore, for subsequent comminution and mineralogical testing, and to support the development of the value proposition for the technology. This ensured that not only were the samples representative, but that the system ran for sufficient time to the assess process stability and evaluate the wear and durability of system components. The system was also designed as a modular assembly which enabled the use of either one or two single mode resonant applicators in series, fed from two associated e2v 100kW generators operating at a frequency of 896MHz, with the capability of achieving electric field confinement to yield power densities of at least 6 $\times 10^6 W/m^3$ in the bulk ore.

The dual applicator configuration in series on the vertical ore flow tube was developed to improve the homogeneity of the overall electric field distribution achieved through the treatment process. Offsetting the maximum electric field strength between each of the applicators, through optimised positioning of the field using the sliding short tuner, allowed for the maximum area of power density to cover the majority of the cross sectional area of the ore treatment tube, as shown in Figure 4.1. The sliding short tuners and inline automatic stub tuner used for adjusting the position of the incident and reflected

microwaves, and optimising the regions of highest electric field strength in the applicator can be seen in Figure 4.2.

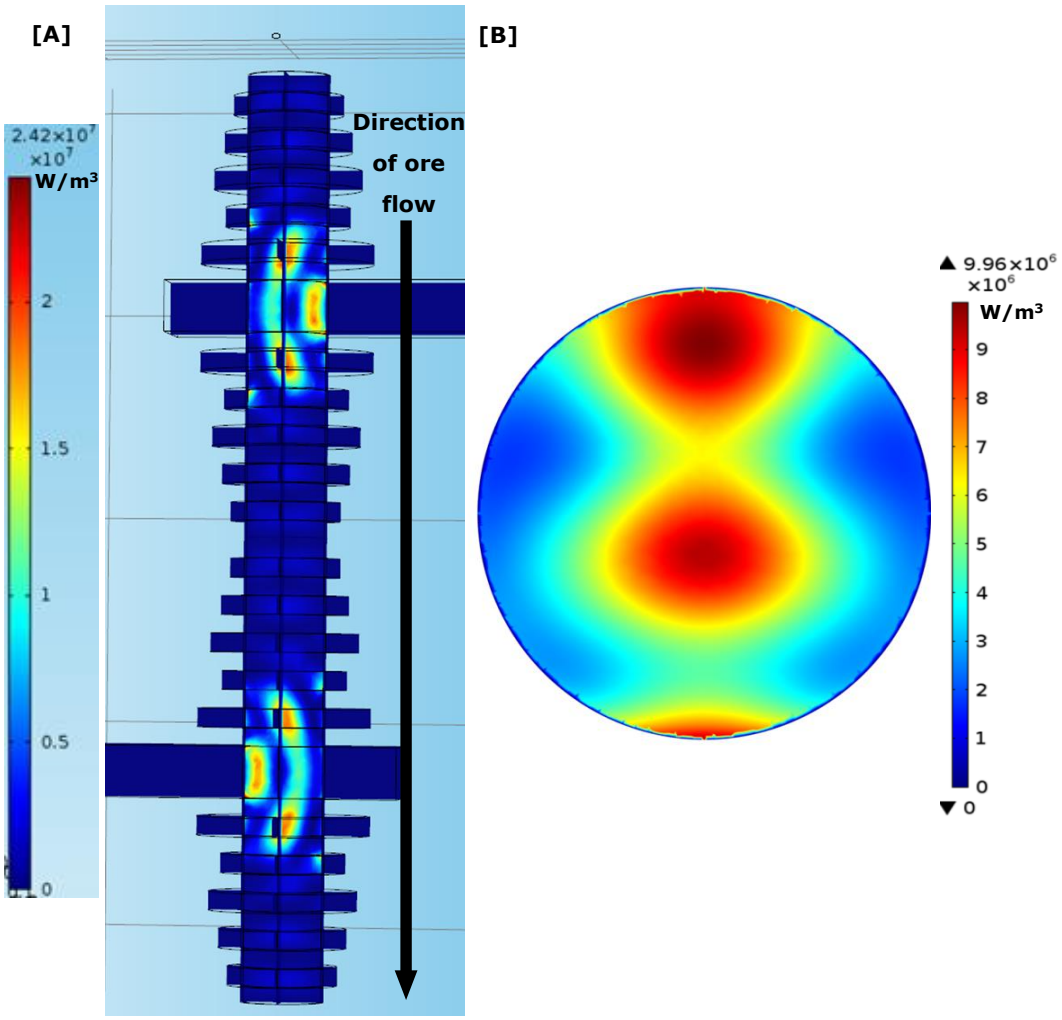


Figure 4.1 [A] Shows simulation of the regions of high electric field strength in each applicator. [B] Shows the cross sectional distribution of electric field strength for the dual applicator configuration looking down the treatment tube.

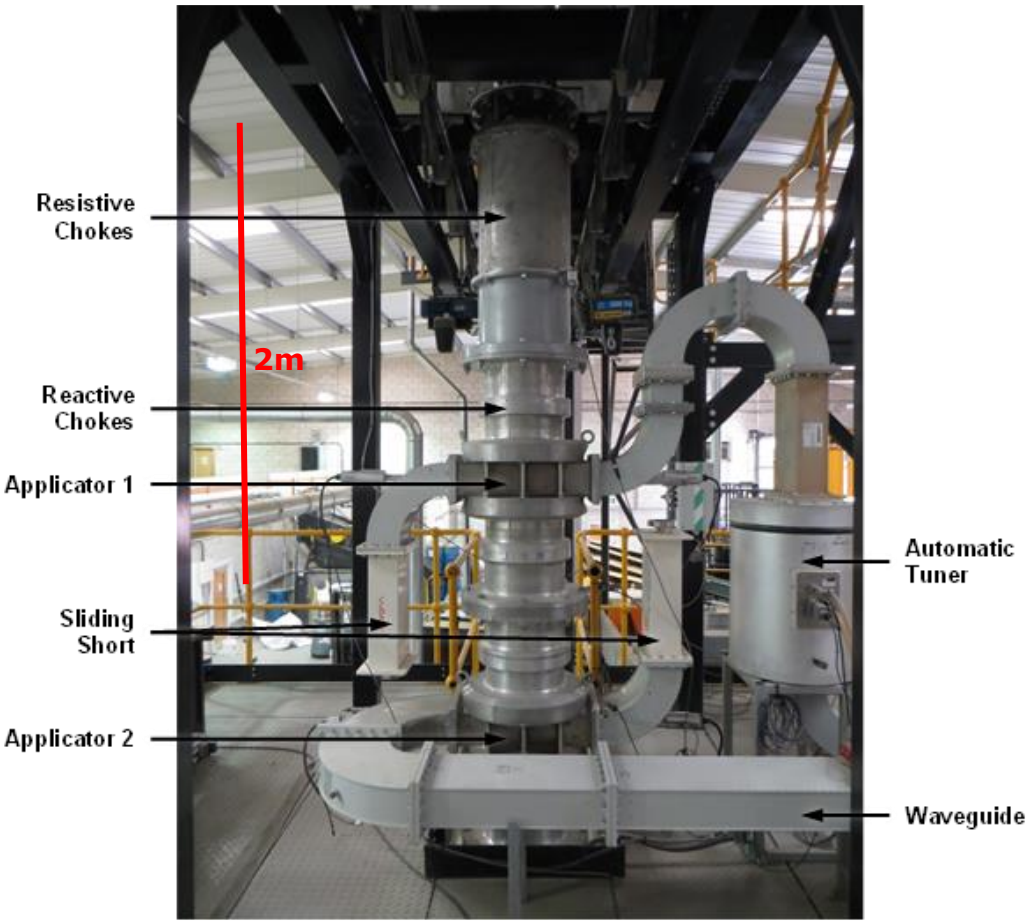


Figure 4.2 Photo of the dual applicator configuration of the pilot system.

Pilot system treated samples used in this study were all produced with the dual applicator configuration shown in the diagram in Figure 4.3. This diagram also clearly illustrates the relative positioning of the peak electric field strengths, or microwave 'hot spots' in each applicator, in the context of the treatment process.

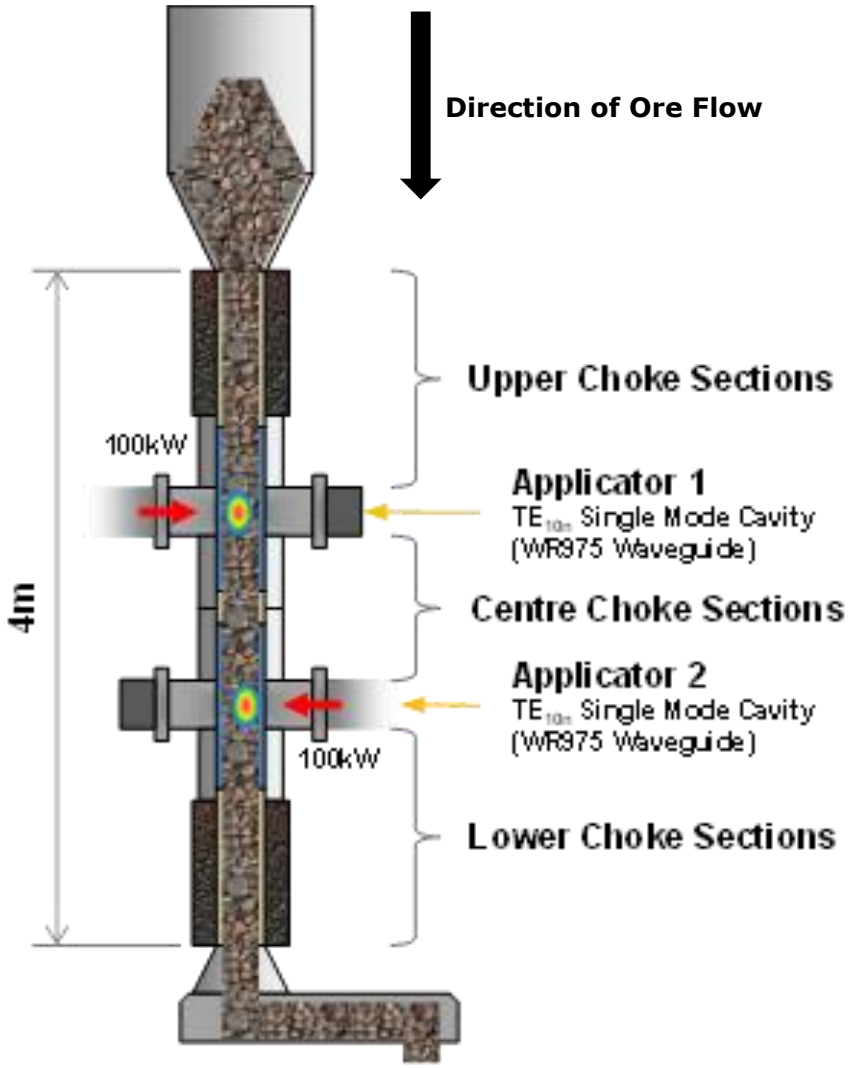


Figure 4.3 Vertical flow configuration of the 150t/h and 2x100kW dual applicator pilot system (Buttress et al., 2016).

The use of the corrugated circular chokes for electric field confinement was a critical development in the design of the pilot system, as it minimises the propagation of an electric field strength gradient outwards from the top or bottom of the applicator and along the process tube. This gradient would lead to incremental warming of the ore as it moves through the applicator and a corresponding reduction of microwave energy through transfer of the heat into the bulk rock. Through confinement of the field using the choking structures, the ore remains near ambient temperatures until it enters the applicator. It is the subsequent rapid heating of the microwave absorbent minerals in the ore, confined by the comparatively cold non-responsive gangue, which results in differential thermal expansion. As previously

discussed, it is this expansion that produces differential stresses around the mineral boundaries within the ore and leads to the generation and propagation of fractures. In addition to optimising the breakage process, the confining chokes, when coupled with resistive chokes filled with carbon foam, also serve to achieve compliance with both United Kingdom Environmental Health and Safety Legislation and Electromagnetic Compatibility Legislation. The configuration of the reflective and resistive chokes along the treatment tube is shown in Figure 4.4 for a single applicator configuration. This figure also illustrates the section of microwave transparent quartz tube which is used to allow the ore to flow through the applicators. An advantage of using the visually transparent quartz, is that it allowed for visual inspection of ore in the process tube to investigate flow and packing characteristics of the ore.

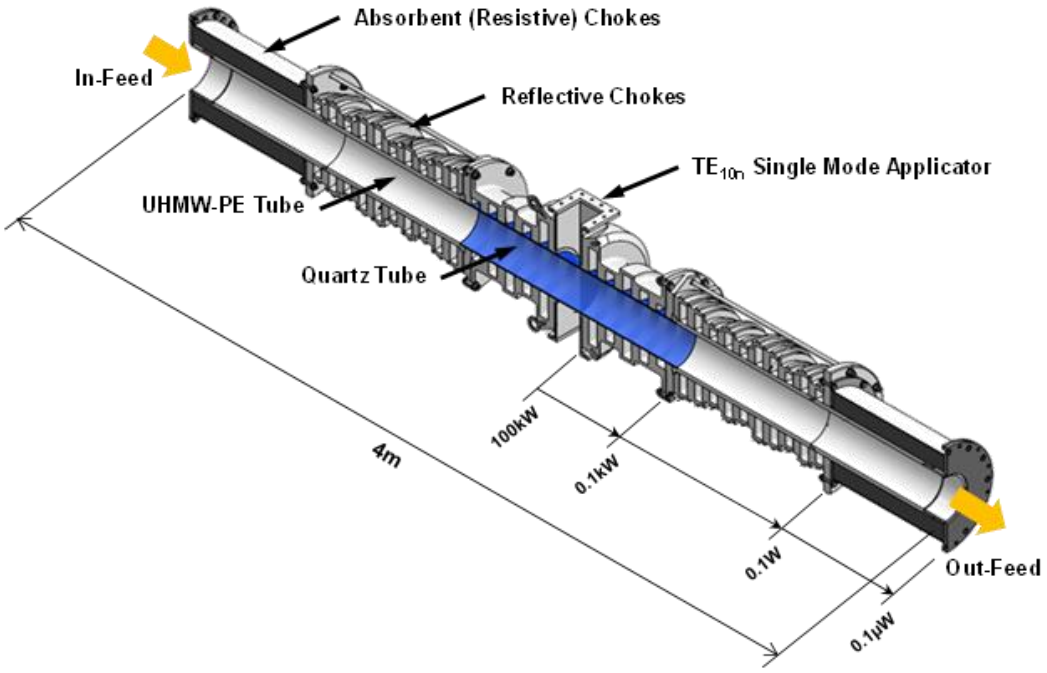


Figure 4.4 Reactive and resistive choking structures developed to confine the electric field in the single mode cavity while allowing ore to flow continuously (Buttress et al., 2016).

The pilot system is capable of treating up to ~50mm diameter ore fragments by controllably flowing a blend of ore fragment sizes downwards though a vertically aligned tube as a packed bed of material, and is currently understood to be one of the highest

throughput microwave processing plants in the world. Since its commissioning, the pilot system has completed ~200 recorded test runs on nine different ores, with a total of 900 tonnes of ore processed through the plant, with about 300 tonnes being under microwave power (Buttress et al., 2016).

4.3.1.2 Pilot System Treatment Process

As has been described, the pilot system was designed to expose batches of crushed ore material to high intensity microwave energy for a short duration. The layout of the pilot system is shown in Figure 4.5.

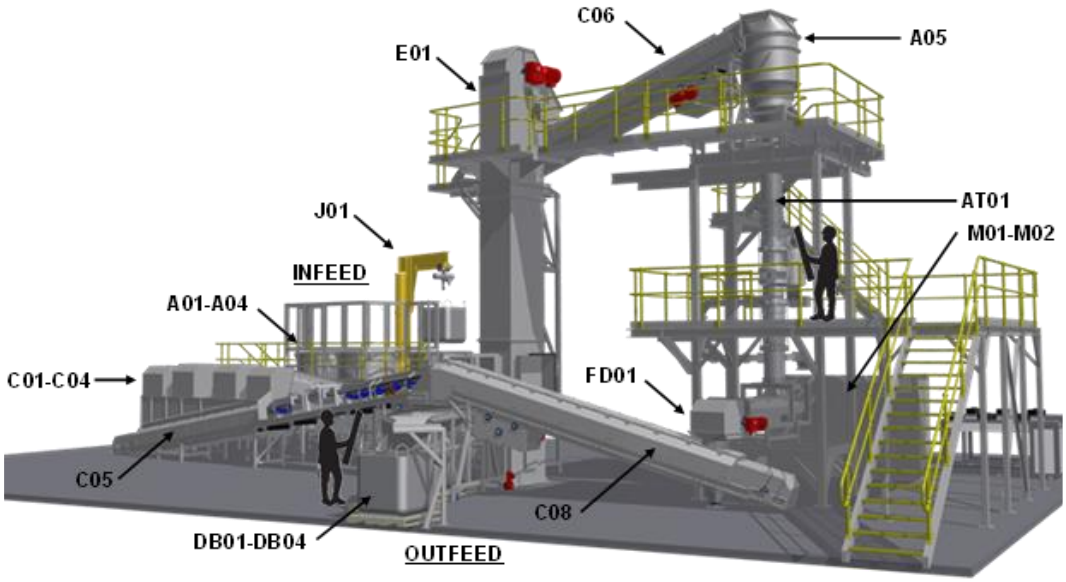


Figure 4.5 Layout of the microwave treatment pilot system. Note people for approximate scale.

Ore samples are loaded by jib crane (J01) from bulk sample bags into four separate feed hoppers (A01-A04). The hoppers are emptied via discharge conveyers (C01-C04), blended to a desired feed particle size distribution and transported via a series of conveyers (C05-C06) and a bucket elevator (E01) to a mass flow hopper (A05) at the top of the vertical treatment column (AT01). The ore flows downwards from the mass flow hopper under gravity, and through two single-mode microwave applicators where it is exposed to microwave energy provided by two 100kW generators (M01-M02). The ore throughput rate is controlled by the speed of the outtake conveyer (FD01) at the

bottom of the vertical treatment column. The outtake conveyor discharges onto a slewing conveyor (C08) which can swing between four discharge bulk bags (DB01-DB04).

While the pilot system is continuous in terms of the microwave treatment of ore samples, it does not have a recycle capability and has a maximum storage capacity in the discharge bulk bags of ~6 tonnes. Subsequently, total capacity, and therefore total system running time, is limited by the capacity of the discharge bags downstream of the applicator. This 'semi-batch' operation of the system necessitates that microwave start up is <1s. This is important as any continued ramping up of microwave power when the ore is already in transport through the applicator, will result in a blend of material which has received a variable dose of microwave energy. Through applying the full microwave power near instantaneously, the system can generate the maximum amount of microwave-treated material. Knowledge of the time, and therefore position in the sample, at which microwaves are at full power also provides a clear demarcation between untreated and microwave-treated material, which ensures that the ore has been treated in the applicator at the required power density and energy input. Each applicator comprises a 199mm internal diameter quartz tube which passes through a single mode resonant cavity through which microwave energy is transmitted. The hollow quartz tube is transparent to microwave energy, and allows the ore to flow through the applicator and be subjected to the microwave field, without the tube itself being affected.

A programmable logic controller (PLC) sequences all components of the pilot system to ensure that microwave energy of the specified power is present when the ore sample flows through each applicator. Once the treated ore has exited the applicator column, it is transported via the outtake conveyer and discharged into the bulk sample bags. Samples of the treated ore can then be collected for testing.

Ore samples treated in the pilot system for this investigation were treated as -50.8+25.4mm ore fragments. Early tests during the development of the pilot system showed that transient voiding occurred in the ore material when the system was run with a single size class of ore fragments. As a consequence of these voids, arcing was observed in the applicator during microwave treatment. Examples of voiding and subsequent arc formation during treatment are shown in Figure 4.6. To address this, coarse ore fragments (-50.8+25.4mm) were blended with fine ore material (<5mm) to enable the flow of the coarse fragments through the treatment column, and reduce the risk of blockages forming in the column by mechanical bridging of ore fragments. The use of fine material also served to fill in the air gaps between ore fragments, as air gaps can be a potential source of electrical arc formation within the applicator during the microwave treatment, potentially damaging the quartz liner.

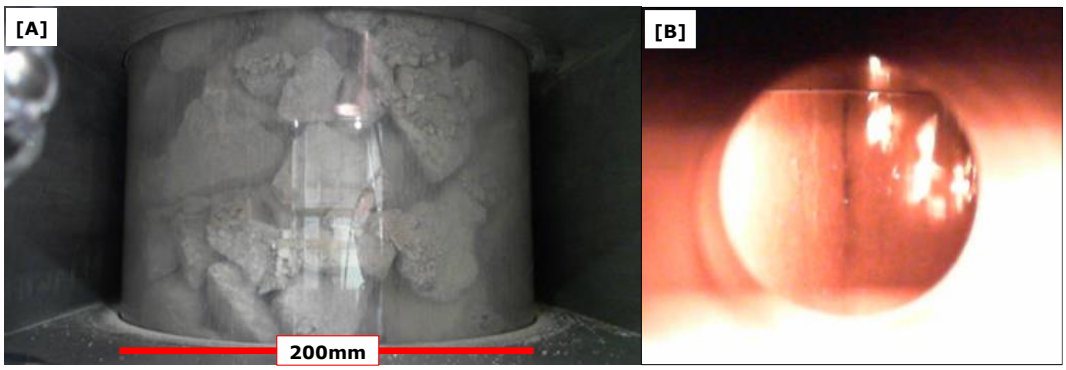


Figure 4.6 [A] -50.8+25.4mm single size class ore feed stationary in the quartz liner of the applicator. Note the voids between the fragments. [B] Process arcing during treatment of the same ore, taken from a digital camera positioned in the waveguide looking at the quartz tube.

The stability of microwave treatments in the pilot system is assessed from information provided by the plant data acquisition system. A typical treatment run is shown in Figure 4.7, which shows the mass of material flowing through the applicators, and the incident (or forward) and reflected microwave power during the run, as recorded by the automatic stub tuning device. This example treatment shows ore flowing at a throughput of 130t/h, with each microwave generator

producing 100kW of power. The figure shows that the microwave power is applied almost instantaneously to the ore once the treatment begins. The power takes ~5 seconds to stabilise, which is an artefact of the 'fast start' process inherent to the microwave generators. Once the generators have stabilised, the reflected microwave power is typically below 2-3 kW for the duration of the run. This treatment stability ensures that the power is efficiently and effectively transferred to the ore sample during the treatment process.

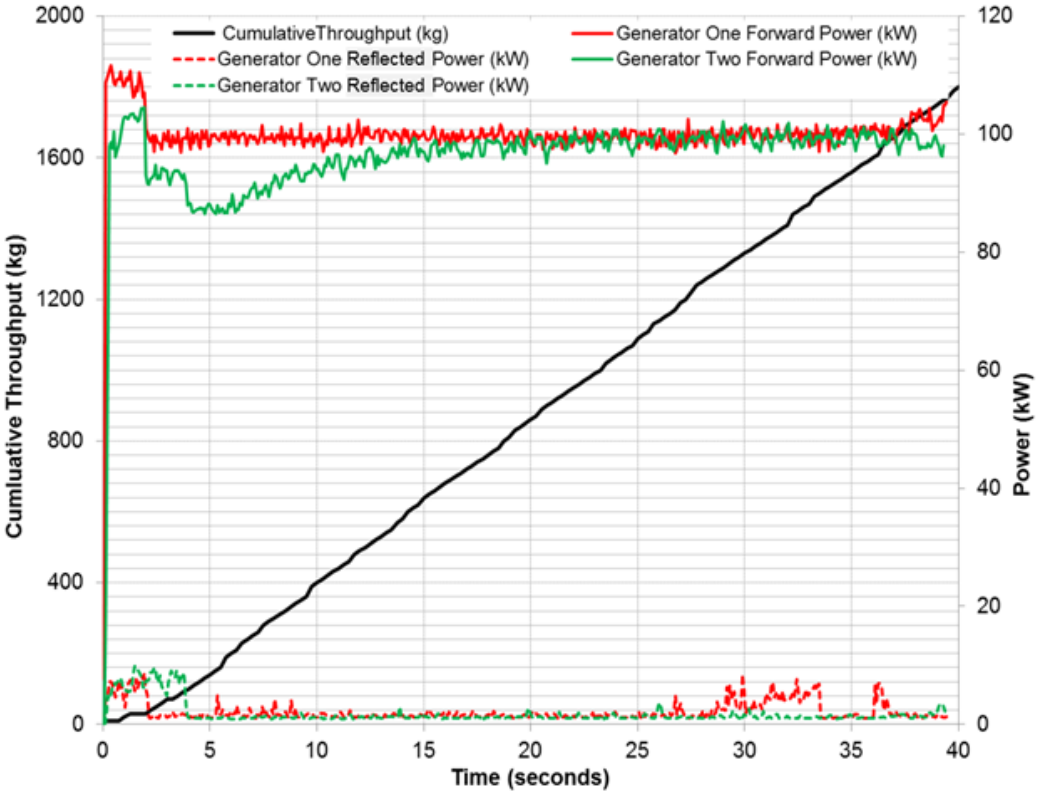


Figure 4.7 Example process log for an ore treated in the pilot system at 100kW and 130t/h.

New materials are under investigation for the production of the tubes used to flow ore through the applicator which possess suitable dielectric properties, and are more resistant to the damaging effects of arcing (Katrib et al., 2016). This development will help to enable the treatment of normal particle size distributions produced directly from an ore primary crusher, rather than the blended distributions currently used for treatments, and will assist the development and operation of an industrial scale microwave treatment system.

The pilot system is capable of operating at a maximum throughput of 150tph, and can treat ore samples with between 60-200kW of microwave power. The range of possible microwave treatment energies is controlled by the power output of each of the generators, which have a minimum output of 30kW in normal mode, and a maximum of 100kW. As the microwave treatment of ores has been shown by previous work to be most effective by achieving a high power density (W/m^3) over a rapid heating interval, the maximum throughput of the pilot system is the preferred treatment rate for all samples. A desired throughout of 150tph at possible microwave power inputs of 60-200kW, gives a range of possible microwave energy inputs, or 'doses', of between 0.4 - 1.3kWh/t. While higher microwave doses are possible by reducing the throughput of the MW pilot system, this would minimise the rapid formation of stresses inside the ore and reduce the effectiveness of the treatment.

At the optimal operating throughput of 150tph the pilot system treats ~44.4 kg/sec of sample, which necessitates that samples of over ~200kgs are required to ensure a successful treatment is achieved. This requirement for the treatment of large sample sizes in the pilot system, created the necessity for the development of a microwave treatment system that can perform batch treatments of smaller ore samples, at the same microwave power densities and energy input conditions achievable in the pilot system.

4.3.2 Microwave Treatment Batch System

4.3.2.1 Introduction

The microwave treatment batch system, hereafter referred to as the batch system, was developed to remove the continuous materials handling system, and the requirement for large (>200kg) samples, from the microwave treatment process. The batch system is a laboratory-based pilot plant, capable of treating ore samples of up to 60kg, at between 10-300t/h equivalent throughput, with between 60-

200kW of microwave power at a frequency of 896MHz. Total microwave treatment energies achievable by this system are between 0.2-20kWh/t (i.e. 60kW at 300t/h; 200kW at 10t/h), however, as for the pilot system, the system will be primarily used for treatments in the range of ~0.2-3kWh/t. The batch system was designed to replicate the pilot system treatment tube, applicator specifications and microwave treatment capabilities with a belt-driven ore tube transport system, rather than flowing ore through the applicators in a quartz tube. The Kevlar reinforced belt in this system is driven by a high-speed servo motor, capable of rapid acceleration and deceleration. The motor is capable of accelerating the 2950mm long, full ore treatment tube of up to ~150kg total mass (~60kg sample plus ~45kg sacrificial material at the top and bottom of the tube), to a treatment velocity of up to 1.5m/s, and then decelerating to a stop, within the length of the treatment tube. The high performance motor also enables higher treatment throughputs to be achieved, with a maximum throughput equivalent of 300t/h for a treatment tube of 150kg mass. This higher throughput feature of the batch system allows for lower total energy treatments to be conducted (as low as 0.2kWh/t), while still maintaining high microwave power input to the sample. This capability was essential in achieving the aims of this investigation, in terms of assessing the lowest total treatment energy input at which an ore still shows benefits in ore strength reductions or enhanced mineral liberation.

Due to facility height restrictions, construction cost considerations, and microwave generator accessibility, the batch system was designed with a single applicator configuration, rather than the dual applicator configuration of the pilot system. This means that the ore treatment tube is required to be passed through the applicator, rotated 180°, and then passed through the applicator again, in order for a sample to receive a microwave treatment to replicate a pilot system treatment. In all other aspects, such as applicator dimensions, sliding short and automatic stub tuning capabilities, positioning of the 'hot spot' or region of maximum electric field strength, and microwave choke

configuration, the batch system is identical to the pilot system. An image of the batch system showing the principle components is shown in Figure 4.8, and an image of the single applicator waveguide assembly is shown in Figure 4.9.

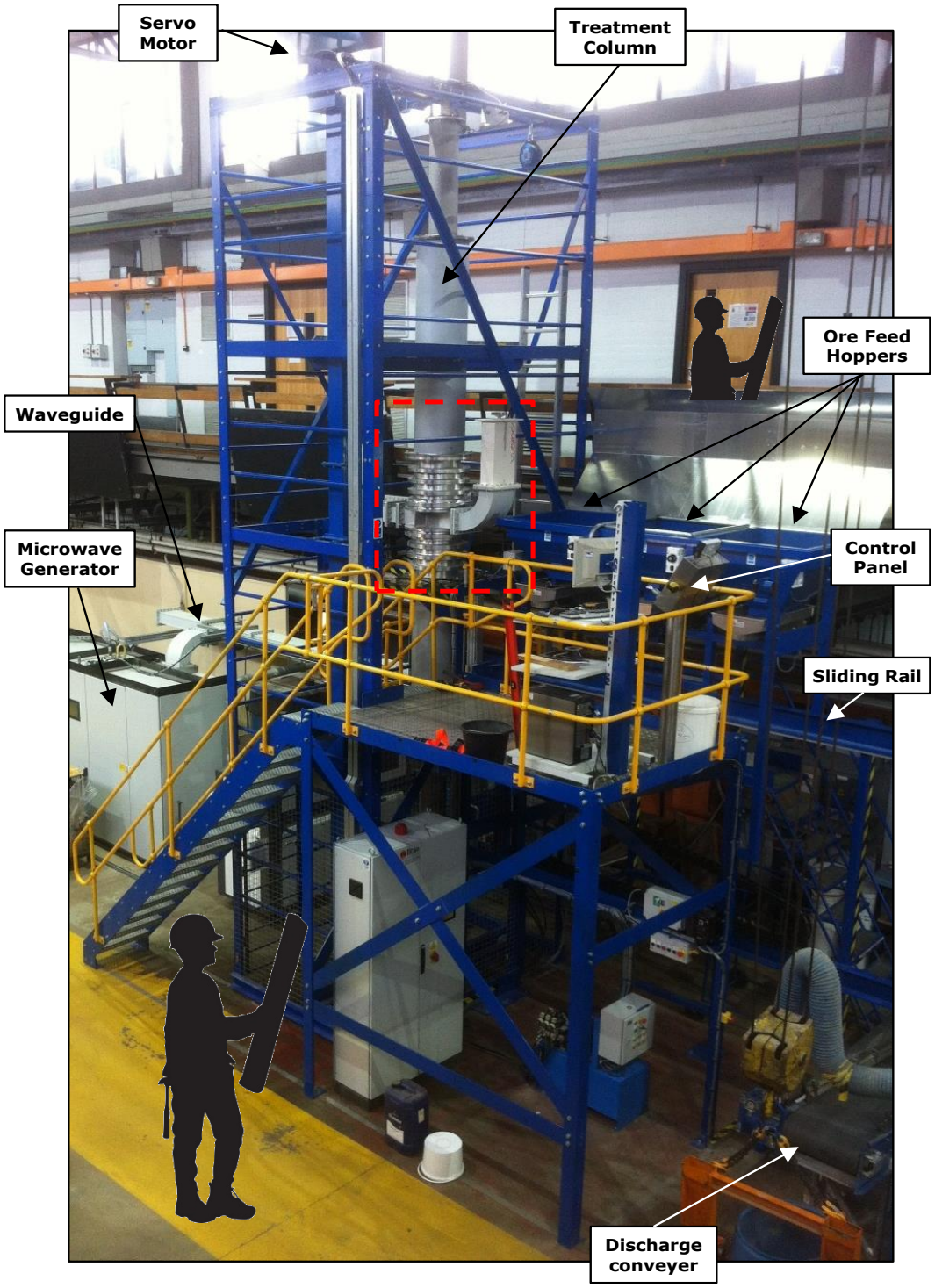


Figure 4.8 Principle components of the batch system. The waveguide assembly in the red dashed box is enlarged in the next figure. Note people for approximate scale.

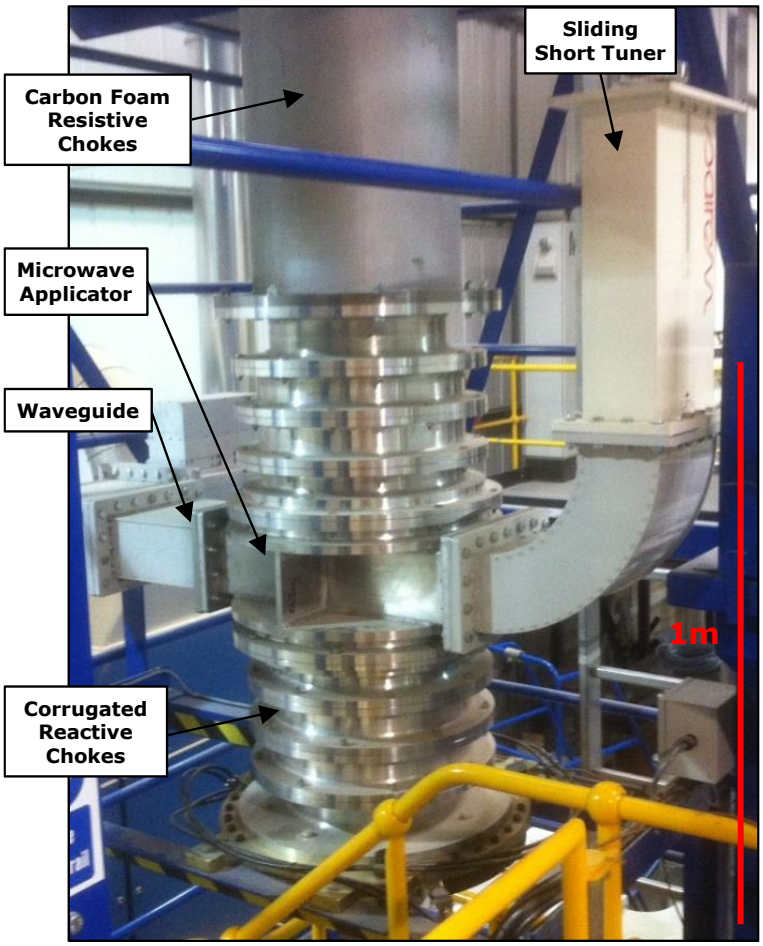


Figure 4.9 Batch system single applicator waveguide assembly.

In allowing for treatment of smaller samples, the batch system also provides the future opportunity for a greater range of different ore types to be treated, without the requirement of having tonnes of sample, as is the case with the pilot system. The system would also allow for evaluation of the influence of instantaneous sample composition and geometry on microwave applicator performance, which was not possible in the continuous throughput pilot system.

4.3.2.2 Batch System Treatment Process

Ore samples can be loaded from drums by a forklift drum-lifter, or alternatively by hand from buckets, into three separate ore feed hoppers. The ore is then fed into the 2950mm long and 200mm inner diameter Ultra High Density Polyethylene (UHDPE) treatment tube, and can be blended out of the different hoppers to a desired particle feed size distribution or bi-modal composition. Similar to the pilot system,

void filling fines (<5mm) are also included with the -50.8+25.4mm ore fragments being treated to minimise the risk of arc formation.

Sacrificial ore fines are also normally placed at the top and bottom of the treatment tube to allow for the microwave generator to ramp-up to steady state at the desired power, and ramp-down again outside of the ore sample being treated. While the e2v generators being used are equipped with 'fast-start' capabilities, the total treatment duration is so short, particularly at the maximum throughput velocity of 1.5m/s, where the total treatment time including acceleration and deceleration is ~2 seconds, that the sacrificial material is warranted. The microwave power ramping buffer ensures that the entire sample receives a microwave treatment at consistent power inputs.

The loaded treatment tube, which is inside the lower section of the application assembly, is then moved along a sliding rail into position below the upper section of the applicator assembly, and clamped into place. Bungs inserted in the ends of the treatment tube are connected to the system drive belt by aluminium coupling blocks, and the system is now ready for a microwave treatment to be conducted. The lower coupling assembly is shown in Figure 4.10.

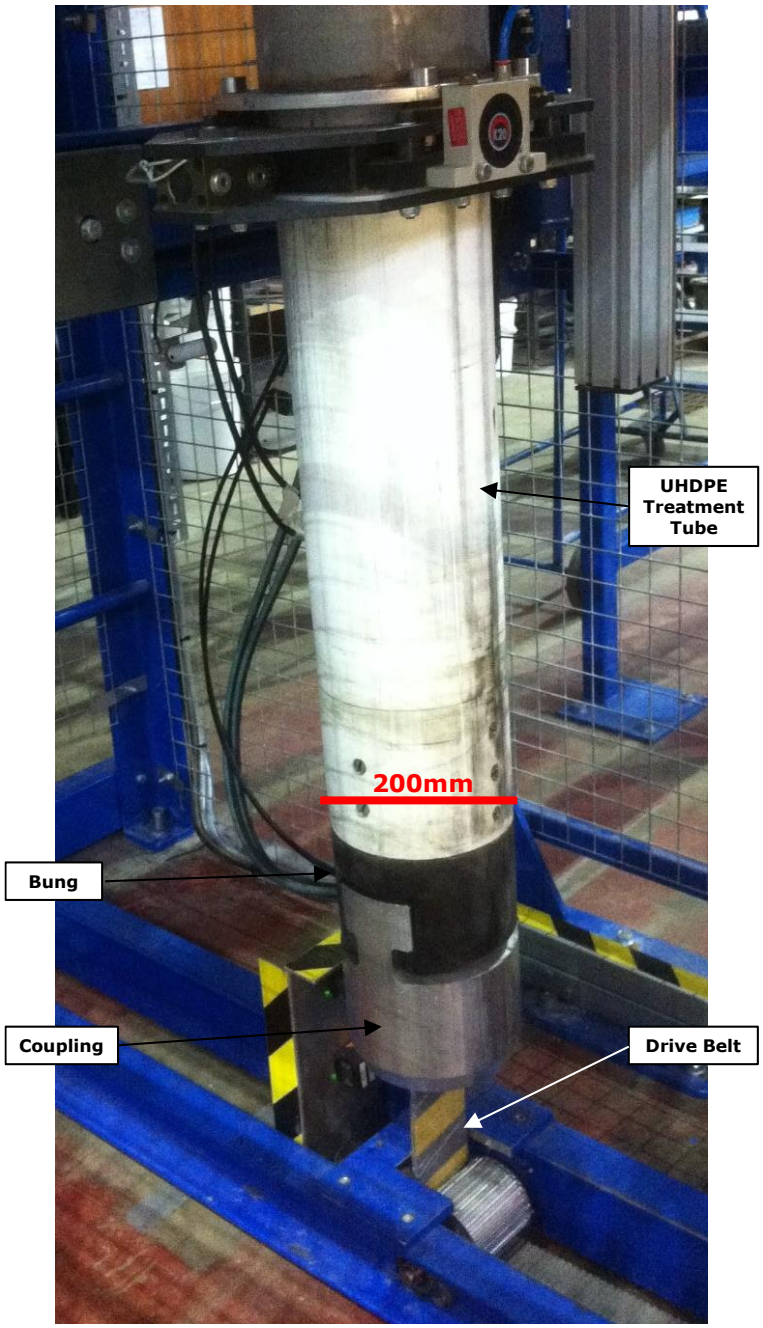


Figure 4.10 Lower belt coupling assembly at the bottom of the treatment tube. An identical assembly is present at the top of the tube.

Treatment conditions are controlled via a touchscreen panel, and once the desired conditions have been input and in-built safety checks have been satisfied, the treatment will be performed automatically at the input conditions. The treatment tube will be moved upwards through the applicator at the desired throughput while microwave power is entering the applicator. Once the first pass is complete, the treatment tube will be returned to its start point where it is rotated 180°, and the

same treatment is run again to ensure the entire ore sample receives a homogeneous treatment to replicate a pilot system treatment. Once the second pass has been completed, the treatment tube can be moved away from the applicator assembly on the sliding rail, the bottom bung removed, and the contents of the treatment tube discharged onto a conveyor. The material can then be screened at an appropriate size to separate the sacrificial fines and the void filling fines from the ore fragments. The microwave treated ore fragments are then ready to be subjected to appropriate testing.

Confirmation of a sample receiving a steady-state treatment at the desired power input can be determined through assessments of the process logs produced from the automatic stub tuner device. This process log provides a record of incident and reflected microwave power over the duration of a treatment run, so the total power absorbed during the treatment across the position of the ore sample in the tube can be assessed. Since the peak electric field position of the incident microwaves is optimised to transfer power most effectively into the sample rather than the sacrificial fines, the absorbed power in the sample will ideally be at the desired power input conditions for the treatment, while it will be lower when the power is going into the sacrificial fines at the top and bottom of the treatment tube. Through assessments of the tuner process logs, it is possible to ensure that stable microwave treatments are achieved for each sample at the desired microwave power input.

A diagram of a typically loaded full ore treatment tube, with a representative example of process log data from the automatic stub tuner used in assessing the stability of a microwave treatment, is shown in Figure 4.11. The example process log in this figure illustrates how the data for incident, reflected and absorbed microwave power can be used to assess the stability of a treatment conducted in the batch system. This is similar to the method used for assessing operational stability for the pilot system.

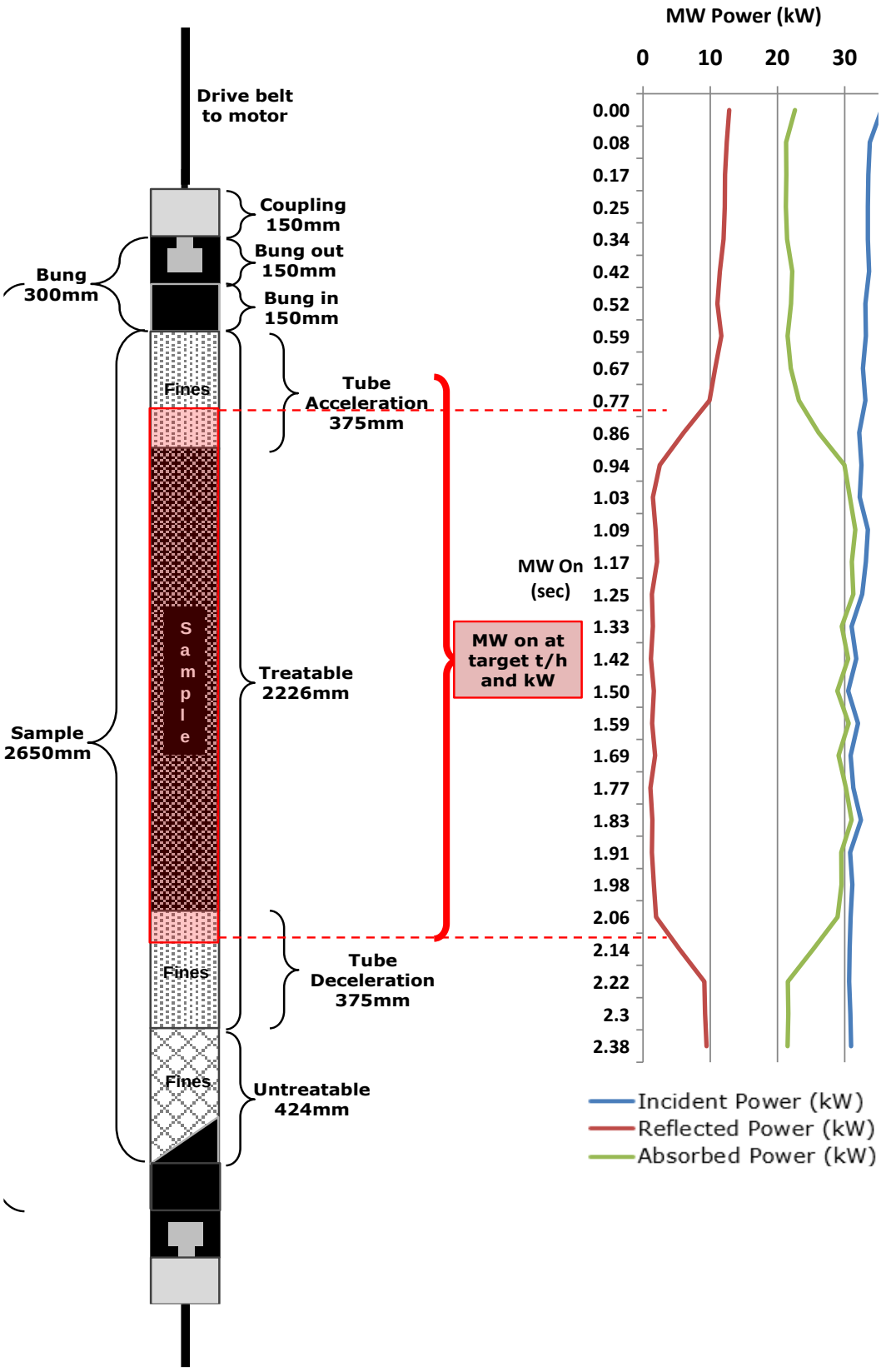


Figure 4.11 Diagram of a typically loaded treatment tube of the batch system, showing an ore sample loaded in between sacrificial ore fines, with an example process log showing incident, reflected and absorbed microwave power for a 30kW treatment.

4.4 MINERALOGICAL CHARACTERISATION

4.4.1 Introduction to Automated Mineralogy

Detailed mineralogical characterisation of ores has become an important aspect of both mining and mineral processing operations. Knowledge of the overall abundance of the valuable and gangue minerals in a ore, and textural characteristics such as grain size, mineral associations and mineral liberation, can be used to optimise the performance of mineral processing operations (Gu et al., 2014) These measurements were traditionally conducted with time-consuming manual measurement techniques using optical microscopy or semi-automated scanning electron microscopes (SEM), with analysis performed on small data-sets with insufficient observations made for the data to be deemed statistically valid (Fandrich et al., 2007a).

Rapid advances in electronics, computer technology and image analysis methods over the last two decades, have facilitated the accelerated development of modern automated SEM-based quantitative mineralogy tools. These systems allow for accurate, fast and user-friendly mineralogical analysis of ore samples. Mineral Liberation Analyser (MLA) and QEMScan (Quantitative Evaluation of Minerals by Scanning electron microscopy) represent the first generation of SEM-based automated mineralogy systems, and were both produced by FEI, a designer and manufacturer of high-performance microscopy hardware and software, and are widely used throughout the mining and minerals processing industry. System installations in both technology research laboratories and operational mineralogy support functions of major mining companies, are routinely applied to ore characterisation and process mineralogy applications (Gottlieb et al., 2000; Lastra, 2007; Evans et al., 2011; Hunt et al., 2011; Lotter et al., 2011; MacDonald et al., 2012; Leißner et al., 2013).

The development of quantitative automated mineralogy tools, and the advancement of the professional field of process mineralogy, have been instrumental in improving the understanding of mining and mineral processing operations. Automated mineralogy finds application in most parts of the life cycle of a mine, from the exploration stage through to production and mine closure (Lastra, 2007; Lotter, 2011; Rollinson et al., 2011; Sylvester, 2012b; Powell, 2013). In the exploration and pre-feasibility stage automated mineralogy techniques are routinely used to measure mineral characteristics such as mineral abundance, grain size, associations and liberation characteristics (Lastra, 2007; Hoal et al., 2009; Bushell, 2011; Hunt et al., 2011). During the mine production stage, automated mineralogy is used in mineral processing for tailings management and process plant optimisation (Gottlieb et al., 2000; Lotter et al., 2003; Fandrich et al., 2007b). Environmental applications include the assessment of tailings management strategies and environmental studies of acid rock drainage (Pirrie et al., 2009; Lottermoser, 2010; Brough et al., 2013; Becker et al., 2015).

Automated mineralogy can also be used to understand deleterious minerals that may be present in the ore, and this knowledge may be used to mitigate acid drainage and other environmental related hazards during the exploitation and production stages (Parbhakar-Fox et al., 2013; Parbhakar-Fox and Lottermoser, 2015). A number of systems also reside within research institutions and universities where they are used in developing the fundamental understanding of mineral processing operations, and to assist the development of innovative technologies and processes (Charikinya et al., 2015; Parker et al., 2015; Batchelor et al., 2016; Little et al., 2016). While a second generation of automated mineralogy systems are currently being produced and marketed by a range of other manufacturers, such as Zeiss Mineralogic, Oxford Instruments INCAMineral, and Tescan TIMA-X, the first generation MLA and QEMScan systems still dominate the market in terms of the number of global installations (Sandmann, 2015).

4.4.2 Automated Mineralogy Systems

In the mineral processing industry, individual point analysis of particulate ore samples is too time-consuming to produce the level of statistical reliability from which informed decisions can be made. If it is assumed that correct sampling of the material has been undertaken, then the analysis of the minerals in a sample should follow a binomial distribution. Under these conditions, the accepted confidence interval of 2 standard deviations can be expressed as:

$$95\% = \pm 2\sqrt{\frac{N(1-N)}{P}} \qquad \textbf{Equation 4.5}$$

where N is the area fraction of the phase of interest and P is the number of points of analysis. Rearranging and substituting the relative error of the phase (defined as the absolute error divided by the concentration of the phase) results in

$$P = \frac{4*(1-N)}{N*\Delta N^2} \qquad \textbf{Equation 4.6}$$

where P is the number of points, N is the area fraction of the phase of interest, and ΔN is the desired relative error.

Equation 4.6 describes the number of points of analysis recommended to accurately identify the presence of an unknown phase or mineral (Jones, 1987).

One of the key drivers for the development and application of automated mineralogy in minerals processing can be seen in Figure 4.12. Minerals of low concentration require such a large number of individual points of analysis that it is unrealistic for this to be done manually. As an example, a mineral of interest that accounts for only 1% of the total sample (as is commonly the case for Cu-sulphide minerals in a copper ore), requires ~10,000 individual points of analysis to be identified with 95% confidence and 20% relative error. The main advantage and justification for the use of MLA and QEMScan automated mineralogy systems, is the capability of being able to rapidly measure a sufficient number a points in order to obtain the statistical reliability required for meaningful analysis.

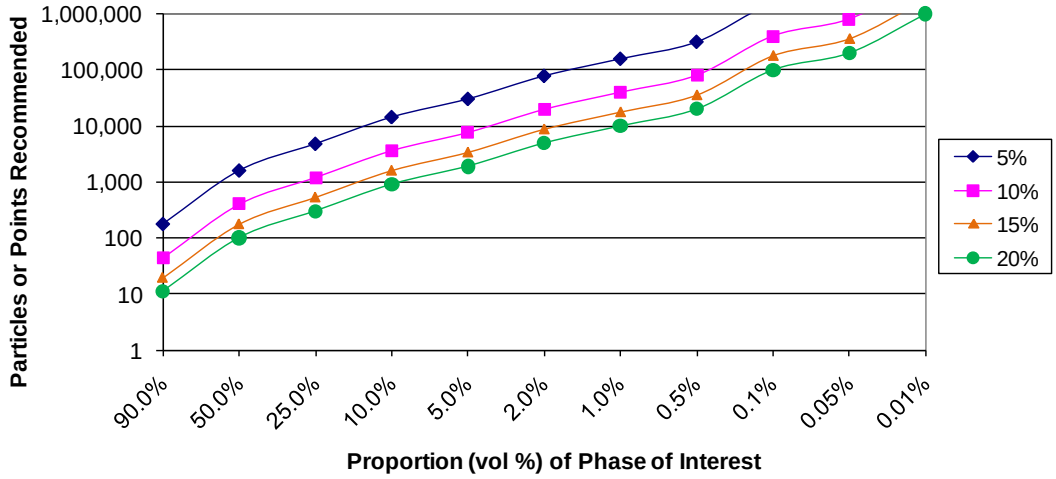


Figure 4.12 The recommended number of analysis points across an entire sample for accurate identification at a 95% confidence level for various mineral grades, at 5-20% relative error.

The Mineral Liberation Analyser (MLA) was developed at the Julius Kruttschnitt Mineral Research Centre (JKMRC), a specialised mineralogy and minerals processing focussed research group within the University of Queensland. When the MLA was first presented as a new development in automated mineralogy in 1997, it represented a unique analytical method through the combination of a number of different signals from the SEM in order to provide quantitative compositional and textural mineralogical characteristics for an ore sample (Gu and Napier-Munn, 1997). The QEMScan system was originally termed QEM*SEM, and was developed by the Australian Commonwealth Scientific and Industrial Research Organisation (CSIRO) from the late 1970s (Jackson et al., 1984). The technology has since developed into an instrument routinely used for characterisation of ores and investigating plant performance (Gottlieb et al., 2000).

4.4.3 Principles of Operation

The fundamental hardware design of both MLA and QEMScan systems is similar, involving a SEM platform with an electron beam source, in combination with backscattered electron (BSE) detection, secondary electron (SE) imaging and up to four energy dispersive x-ray (EDX) spectrometers. Proprietary MLA or QEMSCAN software modules

automate the operation of the SEM to collect raw data, construct digital images, and produce quantitative mineralogical data.

The automated mineralogy instrument at the University of Nottingham is a Quanta 600Mk1 SEM, manufactured by FEI, and equipped with a tungsten filament electron source, two Peltier-cooled Bruker XFlash® 5030 silicon drift detector (SDD) EDX spectrometers, a secondary electron detector and a backscatter electron (BSE) detector. The SEM is also equipped with a circular sample holder capable of holding 14 round sample mounts of 30mm in diameter, and operates MLA version 3.1 software (FEI, 2013). EDX characterisation capability is also available on this system using Bruker Esprit V1.9 software. The University of Nottingham MLA system is shown in Figure 4.13.

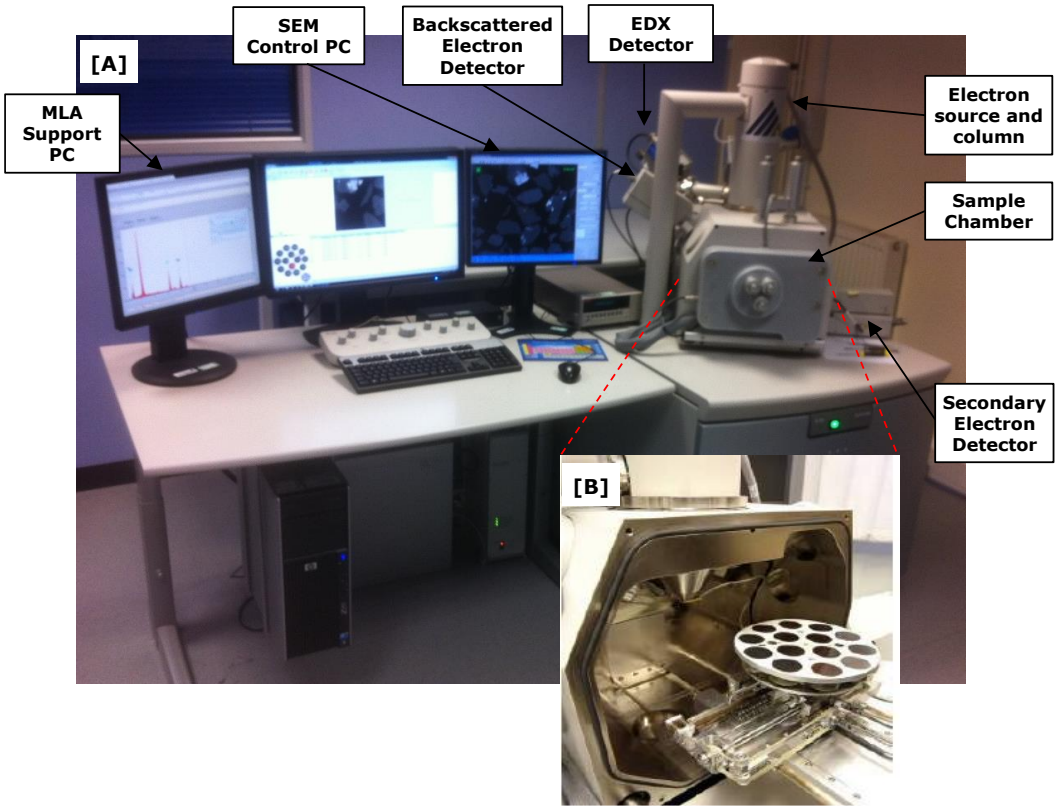


Figure 4.13 [A] FEI Quanta 600Mk1 MLA system [B] Sample chamber with 14 round sample holder with 30mm resin mounts

4.4.3.1 Principles of Scanning Electron Microscopy and Energy Dispersive Spectroscopy

All scanning electron microscopes operate under the same basic principles. An electron beam is extracted from a source by an accelerating potential, focussed into a small spatial area through a column of electromagnetic lenses, and rastered across the surface of a sample by deflection plates or coils. In early models of first generation systems, such as the FEI Quanta 600Mk1 MLA at the University of Nottingham, the electron beam is produced by a tungsten filament cathode through thermionic emission, accelerated by a potential difference of between 0-30keV. Later model first generation systems and second generation systems tend to use field emission gun (FEG) or lanthanum hexaboride (LaB_6) electron sources, due to their improved beam resolution, stability and lifespan (Johnson et al., 2015).

A large accelerating voltage is generated between the filament and the anode, stripping electrons from the filament and directing them down the column. The electrons pass through a series of electromagnetic lenses, being focussed into a narrow beam. Scanning plates or coils allow the electron beam to be rastered across the sample, with the signal from each point being captured and converted into a pixel of information. Standard detectors used to collect these signals are the backscatter electron detector and secondary electron detector, with EDX detectors becoming increasingly common. Typical SEM systems used for mineralogical applications operate in the high-vacuum regime ($\sim 10^{-6}$mbar), however some systems can also operate in 'environmental' (ESEM), or low-vacuum mode, which is primarily used for bioscience applications.

The electron beam penetrates into the surface of the sample, and the electrons undergo elastic and inelastic scattering as they propagate through the medium. The volume of the sample into which the electrons penetrate is known as the interaction volume, a region which extends approximately 100nm-5µm into the surface depending on the accelerating voltage and specimen mean atomic number. The

diameter of the interaction volume of the electron beam is generally around 1-3μm at the 20keV accelerating voltage and beam spot size used to measure samples in this investigation. The interaction of the electrons within the sample produces three primary effects: backscatter electrons, secondary electrons and characteristic X-rays (Vaughan, 1989). Figure 4.14 illustrates the approximate regions of the interaction volume from which each of these effects is detected. A constant background of X-ray 'noise' known as bremsstrahlung (braking radiation) is also produced.

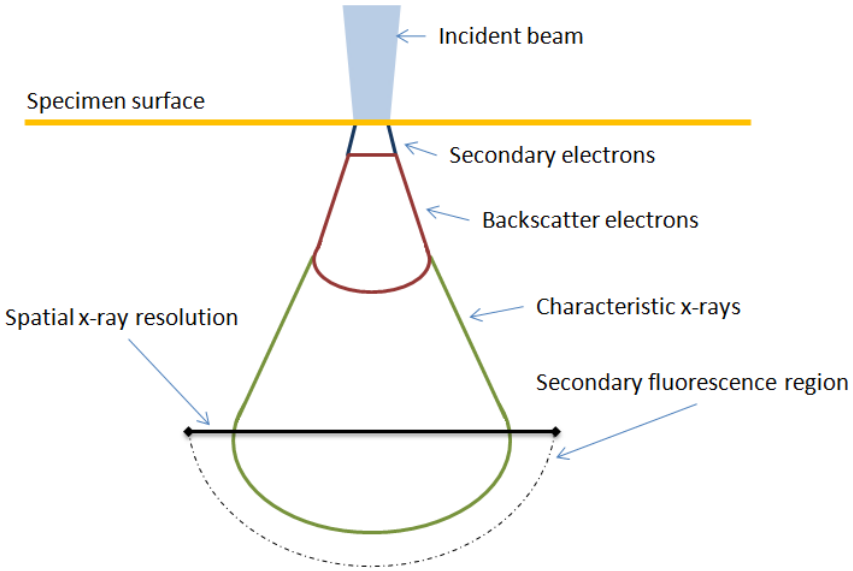


Figure 4.14 The region of the interaction volume from which the different signals originate (Adapted from Vaughan (1989)).

Backscatter electron images provide a greyscale image of the sample with the greyscale level at each pixel corresponding to the average atomic mass at each measured point, and generally have greater resolution than the other signals. Secondary electron images provide a greyscale image that conveys information on the topography of the surface of the sample with a similar resolution to the characteristic X-rays. Characteristic X-rays are created when an inner atomic electron is removed by the electron beam, and an electron of higher energy level moves from an outer electron shell to fill the vacancy. When this occurs, a photon of energy equal to the difference between the two electron bands is emitted in the form of an X-ray, which is

characteristic of the element from which it came, and is denoted by the degrees of movement of the electron into a particular electron shell, as illustrated in Figure 4.15. Since the electron structure of every element is unique, the X-rays emitted by this process are characteristic of the element responsible for the emission (Vaughan, 1989).

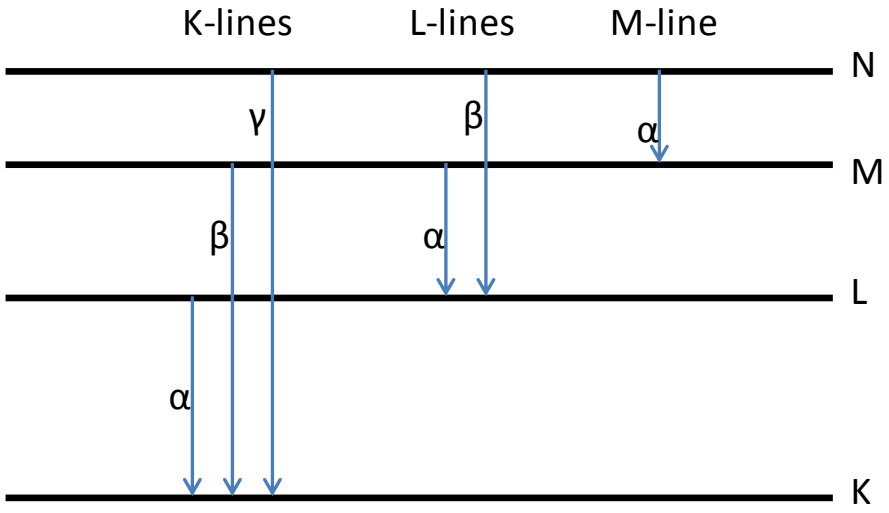


Figure 4.15 Illustration of the relaxation of a higher-shell electrons into lower-shell vacancies (Adapted from Vaughan (1989)).

In order to interpret a characteristic X-ray signal, the energy of the constituent X-rays must be known. These X-rays can be detected in scanning electron microscopy through energy-dispersive X-ray spectroscopy. All EDX detectors utilise a silicon crystal in which electron-hole pairs are formed by captured X-rays. The number of electron-hole pairs formed is equal to the energy of the incident X-ray divided by the bandgap of silicon, or around 3.8 eV. A potential across the silicon crystal causes the migration of the electrons to a detector, where the signal is converted by electronics into a single count in the spectrum at an energy determined by the number of electrons (Russ 1984). The constant background within an EDX spectrum is due to bremsstrahlung, or braking radiation, caused by the deceleration of electrons as they travel through the sample medium. Bremsstrahlung can be easily accounted in the analysis of EDX signals, as it forms a continuous, predictable background.

Since each element in a mineral emits its own set of x-ray signals, a composite energy spectrum of all the X-rays collected from a point can be produced which is characteristic of the mineral at the location of the electron beam. It is the automated collection and collation of these characteristic X-ray spectra, which is the foundation for the operation of automated mineralogy systems.

4.4.3.2 Sample Preparation

Automated mineralogy systems require ore fragments or particles to be presented as highly polished 2D sections for analysis. In this study, automated mineralogy measurements were conducted on ~25mm ore fragments for the purposes of coarse ore characterisation, and on milled ore particles for mineral liberation analysis.

Ore fragments are first cut on a diamond saw to create a flat surface for analysis, and then trimmed to fit into 30mm round mounting cups. Ore particles are first classified into discrete size fractions determined by the √2 sieve series, in order to minimise the influence of stereological error on the results. Particle samples are then split using a micro-rotary riffle into ~1-3gm sub-samples, depending on the size fraction, and are then placed in 30mm mounting cups. The number of individual mounts required for each size fraction is determined by the number of particles required to be measured in order to achieve statistical representivity for the mineral of interest in the sample. This is determined by applying the principles previously discussed in Equations 4.5 and 4.6. The number of sample mounts produced for coarse ore characterisation and mineral liberation analysis of particle samples in this study is shown in Table 4.2. While it is understood that the measurement of only 20 fragments of each sample for coarse ore characterisation does not meet requirements for statistical representivity, it is a sufficient number, within limitations of instrument availability and measurement time, to provide a reliable representation of ores with a reasonably homogeneous texture.

Size Fraction (µm)	30mm Mounts	Particles Measured per size fraction
Coarse Fragment ~25mm	20	20 fragments
+425	8	~20000
-425+300	6	~20000
-300+212	4	~30000
-212+150	2	~30000
-150+106	1	~20000
-106+75	1	~30000
-75+53	1	~40000
-53+38	1	~40000
-38	1	~40000

Table 4.2 Number of sample mounts produced for automated mineralogy.

Sample preparation is then essentially consistent for both types of sample. Struers 'Epofix' resin is prepared and added to the mounting cups to the desired level, and particle samples are stirred using a 'figure of 8' motion for ~2-3mins each to minimise agglomeration and segregation effects, and homogenise the sample. Mounts are then placed in a Struers 'Epovac' chamber and subjected to a controlled vacuum for 15mins to remove unwanted air bubbles from the resin. Mounts are then placed in a Technomat pressure vessel to further facilitate the extraction of air bubbles, and left to cure under pressure overnight. The hard resin mounts can then be removed from the mounting cups and subjected to progressive grinding with diamond impregnated abrasive discs, and polished on cloth discs with a diamond-suspension media to a 1µm finish on a Struers Tegrapol system. Polished surfaces for analysis are then carbon coated to a thickness of ~25-30nm using a Quorum Q150R carbon coater, to make the sample surface conductive, and prevent 'charging' of the sample by the SEM electron beam.

4.4.3.3 Measurement and Analysis Procedure

There are two key definitions for automated mineralogy systems that are important to clarify. A particle is defined as any complete, discrete area on a polished surface. A grain is defined as any region of

continuous backscatter greyscale, either within a complex multi-phase particle, or as a particle which comprises just a single mineral grain.

Automated mineralogy systems, such as the MLA, perform automated collection of image frames and energy dispersive X-rays from a user-defined measurement area of the prepared sample surface, according to a range of different software controlled measurement protocols. A sample holder of up to 14 mounts is placed in a specimen chamber under vacuum where an electron beam is scanned across the sample surface along a pre-defined raster scan pattern. The interaction of the beam at each image pixel generates backscattered electrons and characteristic x-rays.

The BSE image is used to determine particle and grain boundaries in order to provide locations for the acquisition of x-ray spectra from many thousands of individual points of analysis across the sample surface. These spectra are then matched against a mineral library of known characteristic X-ray spectra, and each point is classified as the mineral which best matches the library entry (Gu, 2003). If no match is found with a suitable probability for a given point, then it is assigned as an 'unknown', which will require further analysis for identification. Standard settings in the MLA software require a minimum of 2000 X-ray counts in a spectrum at each collection point for it to be matched. If this condition is not met, then the grain connected to that spectra is classed as invalid. The typical MLA measurement and analysis process is summarised in the flowchart shown in Figure 4.16.

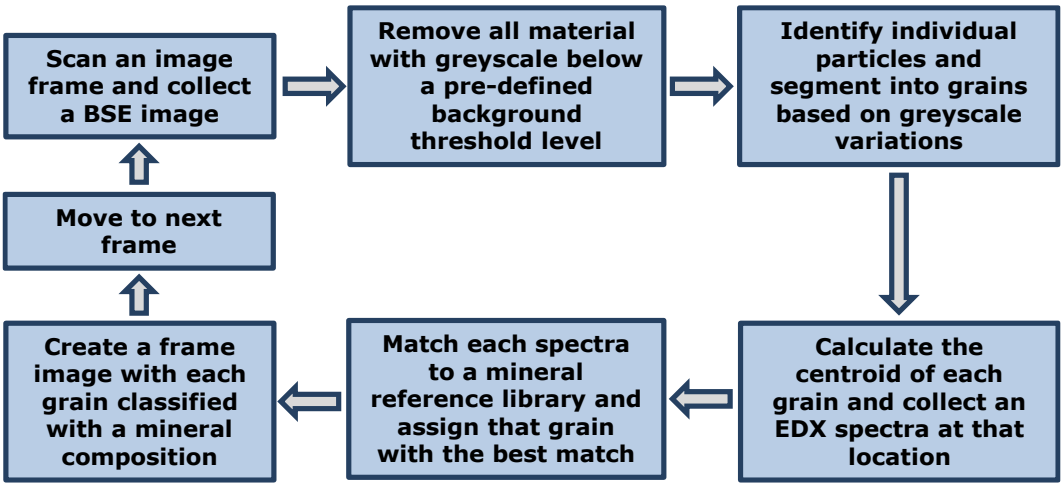


Figure 4.16 MLA measurement and analysis overview flowsheet

While the measurement and mineral identification procedures for the MLA and QEMSCAN are not identical, they are similar in that they use backscattered electron image analysis and x-ray mineral identification to provide quantitative mineral identification. Both systems use a combination of point x-ray, linear x-ray and full-x-ray mapping to produce accurate and comparable quantitative mineralogical data including modal or bulk mineralogy, mineral grain size distributions and mineral association and liberation.

The MLA system uses the SEM control software and the MLA Measurement software module to set the operating conditions for each measurement run. The standard operating conditions for the FEI Quanta 600Mk1 SEM used in this study were a 20kV accelerating voltage, 40nA of beam current, and spot size of ~7 units. SEM brightness and contrast settings were used to define the BSE greyscale range (0-256), with an in-built Cu standard representing the 'brightest' value set at 255, and the resin mount background set to ~20. The MLA Measurement module was used to set specific parameters for each measurement. Comprehensive descriptions of the different MLA measurement types have been conducted by several authors (Gu, 2003; Fandrich et al., 2007a; Sylvester, 2012a). Three different MLA measurement modes were used to produce the mineralogical data for this study.

Coarse ore characterisation was conducted using a combination of XMOD (X-ray Modal) and SPL_Lt (Sparse Phase Liberation_Lite) measurement modes. The XMOD method is a comprehensive X-ray point count of the entire sample using an evenly spaced grid of points. At each grid point, one X-ray spectrum is collected, saved and compared to a user-defined mineral reference library to enable mineral identification. This method produces modal mineralogy information as an area or mineral weight percent. The XMOD method also produces a BSE image of the entire sample. The SPL_Lt method of MLA analysis searches the BSE image for any minerals of interest that occur within a specified BSE greyscale range, for example the grey scale range of pyrite and chalcopyrite (>~160 BSE value). The software draws virtual boxes around the minerals of interest, and collects X-ray spectra from all mineral grains within these boxes. This method produces maps of the 'bright' minerals and their immediate associations only, and avoids time consuming measurements of large areas of sulphide-free gangue. The SPL_Lt method can provide data on sulphide grain size and associations in a more efficient manner than methods that map the entire sample.

XBSE (Extended Backscattered Electron) measurement mode was used for analysis of ore particle samples to assess mineral liberation. This measurement mode collects a BSE image for each frame, and then collects a single X-ray spectrum from the centroid of each individual segmented grain within the frame. This mode produces mineral abundance and dimensional data for all mineral grains in a sample, and is the standard measurement mode applied to the routine analysis of ore particles in the context of mineral processing of copper ores (Fandrich et al., 2007a; Sylvester, 2012a).

Once MLA measurements have been classified against a mineral library, they can be processed to join image frames, check and correct unknowns, and clean up any unwanted 'noise' or contamination from the measurement. The measurement results can then be extracted to

a database where they can be interrogated using the MLA Dataview module.

QEMScan data used in this investigation was produced by a commercial mineralogy laboratory using the Particle Mineralogical Analysis (PMA) measurement mode. This type of measurement is similar to the MLA XBSE measurement, except that rather than collecting just a single X-ray from a grain centroid, it conducts X-ray mapping of each segmented grain at a user-defined pixel spacing (Gottlieb et al., 2000). The data produced using this measurement is comparable to the data produced using the MLA XBSE measurement mode.

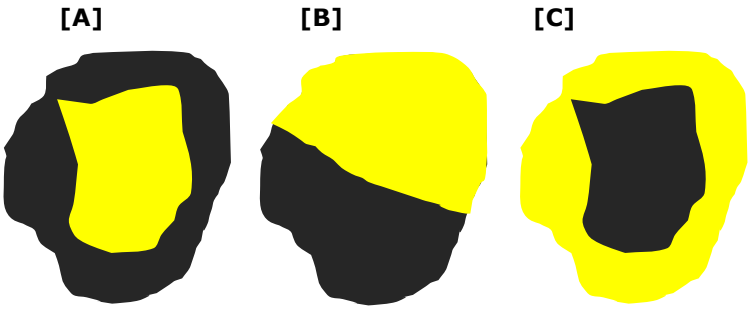
4.4.3.4 Data Analysis

A range of mineralogical characteristics relevant to meeting the aims of this investigation are able to be extracted from the MLA measurements.

Modal mineralogy and calculated elemental assays are determined from the measured mineral area by a volume calculation, taking a unit depth across the measured mineral surface. The volume can then take into account the specific density of each mineral in the mineral library to give a weight percentage. Elemental calculations are then performed based on the chemical composition for each mineral in the sample.

Liberation data can describe the proportions of a particular mineral in a particle by composition, either by weight or area, or represents the percentage of a mineral that is exposed on a particle surface. Free surface is the boundary of a mineral grain that is not in contact with another grain, but is in contact with the background. Figure 4.17 illustrates the concepts of liberation by particle composition and free surface, with the yellow mineral representing the mineral to which the liberation data refers. In all cases, the yellow mineral makes up 50%

of the composition of the particle by area, however the free or exposed surface of the mineral varies.



Liberation by particle composition	50%	50%	50%
Liberation by free surface	0%	50%	100%

Figure 4.17 Illustration comparing liberation by particle composition and free surface.

Mineral locking determines what proportion of a mineral is combined in a particle with one or more other minerals. If a mineral grain is not completely liberated, or 'unlocked', from all other minerals, then it remains locked as a binary or multiphase particle. The concept of locking is illustrated using chalcopyrite as an example in Figure 4.18. In this figure, Image A shows chalcopyrite occurring in a binary particle with gangue, Image B show chalcopyrite as a binary with pyrite, and Image C shows chalcopyrite as a grain within a multiphase particle (i.e. containing three or more mineral grains).

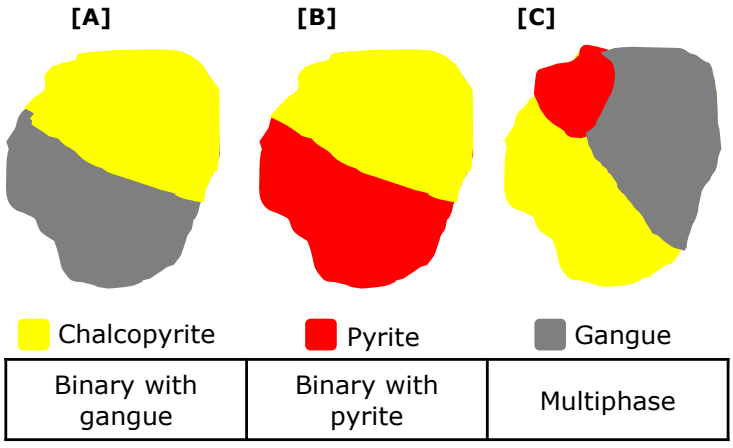


Figure 4.18 Illustration of mineral locking.

Mineral association refers to minerals being in contact with each other within the ore, and is reported as the percentage of the grain perimeters of a selected mineral that is in contact with the grain perimeters of other minerals. In the example shown in Figure 4.19, the individual pyrite grain is associated 25% with chalcopyrite and 75% with quartz. This association is measured for every individual grain in the sample, which is then able to be averaged to provide an indication of the overall tendency for certain minerals in an ore to be associated preferentially with other minerals.

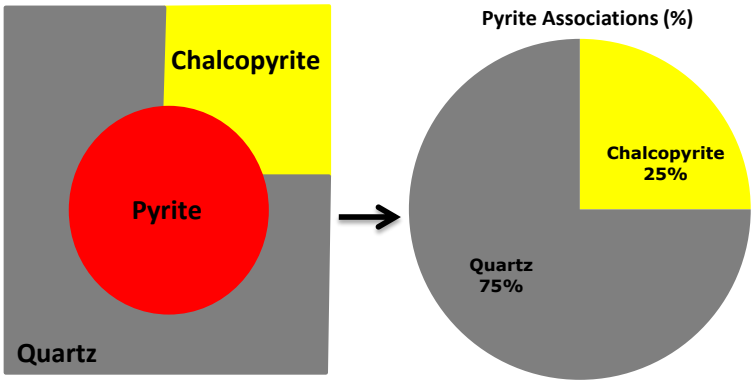


Figure 4.19 Diagram illustrating the concept of mineral associations

Particle and grain sizes used in this study are calculated from the area of each particle or mineral grain converted to an equivalent area circle, and can be reported as either weight or area percent. The size fraction that a particle or grain reports to is dependent on the diameter of the equivalent circle.

4.4.3.5 Mineral Groupings

In reporting the mineralogical and textural characteristics of the ores used for this investigation, minerals were grouped according to their heating response when subjected to high power microwave radiation, and by their 'hardness', or the physical resistance of constituent minerals to an applied mechanical stress. In terms of their heating response, minerals were grouped as being good heaters, poor heaters,

or non-heaters, as determined by the variations in their dielectric response described in Section 3.5.

While mineral 'hardness' can be described using many different values, such as modulus of elasticity, fracture toughness, and tensile or compressive strength, for ease of classification, Mohs hardness scale was used for grouping minerals in this study. Mohs hardness scale is a relative measure of a mineral's resistance to mechanical damage, and in effect, is a measure of the strength of the atomic bonds within the crystallographic structure of a mineral (Hamblin and Christiansen, 2004). Mohs hardness scale assigns numbers to different minerals between 1 and 10, with 1 being 'soft' minerals such as talc, and 10 being the 'hard' mineral diamond. Minerals are assigned values along this spectrum base on their 'hardness' relative to the other minerals on the scale, or their ability to damage minerals of a lower Mohs value, and be damaged by minerals that are higher on the scale. While Mohs scale may not be as precise as other absolute measures of hardness such as Vickers or Knoop hardness, it provides a suitably accurate reference by which to group minerals as either 'hard' (Mohs ≥6) or 'soft' (Mohs <6), when assessing the influence of associations between heating minerals with different gangue minerals on microwave treatment outcomes (Batchelor et al., 2015). A study by Broz et al. (2006) found that micro-hardness values (GPa) for the common Mohs minerals, as measured using a Vickers type micro-indentation tester, showed a step-wise increase in hardness along the Mohs scale. This relationship is shown in Figure 4.20, where it can also be seen that increases in micro-hardness values appear to be greater at higher Mohs values. This relationship serves to justify the use of Mohs values for the grouping of minerals by hardness in the context of this study.

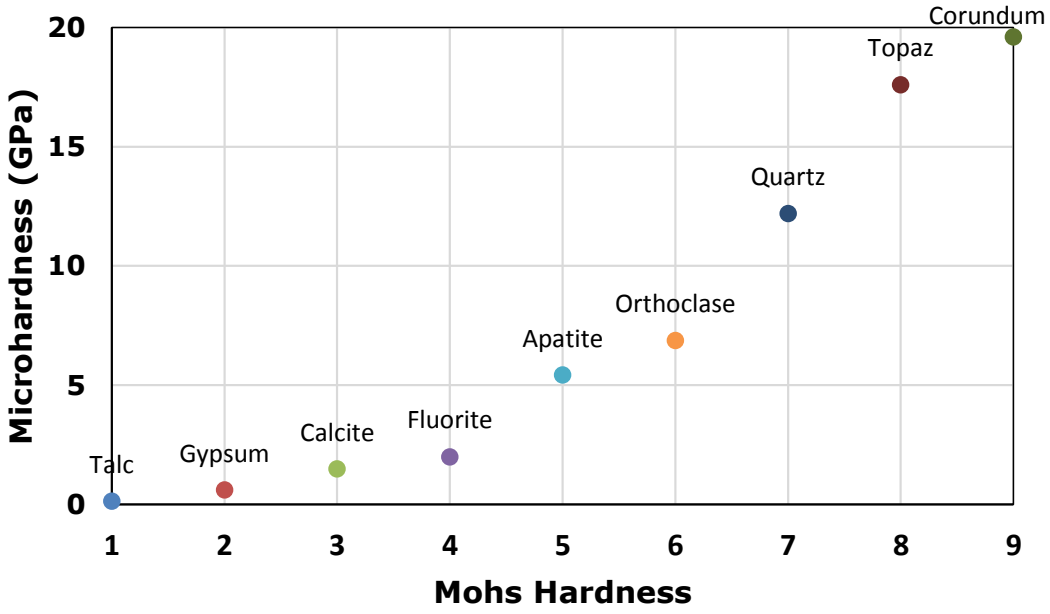


Figure 4.20 Mohs hardness and Microhardness (GPa) for the standard Mohs minerals (Adapted from Broz et al. (2006)).

The microwave heating and gangue mineral hardness groupings used for this investigation are shown in Table 4.3. These groupings were used during mineralogical analysis of both coarse ore fragments, and particulate samples, in order to assess the influence of mineralogical characteristics of an ore on the benefits achieved from microwave treatment. The groupings were also used for the production of false colour mineral maps of fragments during coarse ore characterisation studies.

Mineral Groupings		
Good Heaters	Copper Sulphides	Chalcopyrite
		Bornite
		Chalcocite
		Covellite
	Other Sulphides	Pyrite
		Molybdenite
		Sphalerite
	Non-sulphide	Montmorillonite
Other Heaters	Non-Sulphides	Fe-Oxides
		Ilmenite
		Rutile
Non-Heating Gangue	'Hard' Gangue (Mohs ≥6)	Quartz
		Plagioclase Feldspar
		Orthoclase Feldspar
		Pyroxene/Amphibole
		Zircon
	'Soft' Gangue (Mohs <6)	Muscovite
		Phlogopite
		Biotite
		Calcite

Table 4.3 Mineral groupings based on microwave heating characteristics and Mohs hardness.

4.4.3.6 Quality Control of Mineralogy Results

In order the assess the accuracy of the mineralogy data used in this study, calculated elemental assays from samples run on both MLA and QEMScan automated mineralogy systems were reconciled against elemental chemical assays conducted on the same samples using XRF. The assay reconciliations for all samples measured show excellent agreement between the calculated and chemical assays, indicating that the mineral classification lists used in the analysis accurately identified minerals in the samples in the correct proportions. Assay reconciliations of untreated and microwave treated samples are included in APPENDIX A.

4.5 Comminution Testing

Reliably testing the comminution response of an ore is an essential component in assessing and quantifying the benefits of new

comminution technologies, such as the high power microwave treatment of ores. There are two main categories of comminution tests, those that measure the strength or fracture toughness of an ore, and those that measure the energy-size reduction relationship of an ore (Napier-Munn et al., 1999). Tests of ore strength focus on assessing the resistance of a material to catastrophic failure under an applied stress, while energy-size relationship tests attempt to determine the energy required by a particular breakage mechanism to reduce ore fragments or particles from a certain feed size ,to a certain product size (Wills and Napier-Munn, 2006). Since one of the aims of high powered microwave treatment of ores is to reduce ore strength and comminution energy consumption, testing the potential benefits achievable in a microwave treated ore sample compared to an untreated sample of the same ore, is an appropriate method for assessing the effectiveness of a treatment. This section will present the details and justification for the use of the comminution testing methods employed in this investigation.

4.5.1 JK GeM Crushing Index Test

The JK GeM Crushing Index (Ci) Test is a proprietary test that was developed during the AMIRA P843 Geometallurgy project as a rapid and robust testing method for assessing the strength or breakage behaviour of different ores as part of a geometallurgical domaining process (AMIRA, 2009). The JK GeM Ci test has been designed to provide information on comparative size reduction characteristics through the use of a standard jaw crusher, and is described in Michaux (2013) and Kojovic et al. (2010). The test was originally developed for the assessment of segmented drill core for geometallurgical domaining purposes, but is equally applicable to natural rock fragments (Kojovic et al., 2010).

The test is performed by starvation crushing of a narrow size class (e.g. -31.5+26.5mm) of ore at a fixed size reduction ratio of 2.5, representing the geometric mean particle size to crusher closed side

setting. The test produces three key values; two indices that are defined as CRU and GRD, and the percentage of material passing a 4.75mm sieve after crushing. GRD and CRU indices represent changes in the particle size distribution of an ore crushing product. The CRU index represents a mass ratio of coarse to fine material generated during crushing, which tends to correlate with the impact resistance of the material. Differences in CRU index between ores reflect differences in impact breakage behaviour or 'crushability' characteristics. Typically, a higher CRU index represents a beneficial change in ore impact resistance. The GRD index represents the normalised slope of the product size distribution on a log-log scale, and changes in GRD reflect changes in the ore matrix breakage response during crushing. Typically, a lower GRD index indicates a beneficial change in the response of the ore matrix to crushing. JK GeM P843 project studies have shown a high level of correlation between this slope and the 'grindability' of an ore, making the GRD index a useful measure for the comparison of changes in ore breakage properties (Kojovic et al., 2010).

Both CRU and GRD index values are produced using an unpublished proprietary algorithm (AMIRA, 2009). In order to apply this testing methodology in this investigation, a secure JK GeM Ci testing spreadsheet was provided which allowed for in-house testing to be performed. The Ci test algorithm is derived from the particle size distribution of the crushed material. Analysis of the slope and intercept of the particle size distribution on a log-log scale is conducted, and certain characteristics of the size distribution are assessed to calculate the numerical CRU and GRD index values that provide an indication of ore breakage parameters (Michaux, 2013).

In the context of this study, increases or decreases in CRU or GRD indices do not necessarily indicate that a positive or negative change has occurred, or that the comminution response of a microwave treated ore has improved or declined relative to the untreated sample. While Ci test outcomes will be referred to as being beneficial or

detrimental based on the typical responses of CRU and GRD indices to changes in ore breakage behaviour, this does not mean that a beneficial or detrimental outcome from a microwave treatment has occurred in comparison to an untreated sample. Ci testing does, however, indicate whether a change in the breakage behaviour or characteristics of an ore has occurred due to the alteration of the physical properties of the ore through microwave treatment.

The JK GeM Ci test methodology also has the advantage of producing a crushed product that can be used for subsequent testing, meaning the test can be included into an ore characterisation testwork flowsheet as a prerequisite to later tests. This test was selected as a rapid coarse particle evaluation tool to replace the laborious Point Load Index test, which has been used extensively in earlier published literature on the microwave treatments of ore (Kingman et al., 2004a; Kingman et al., 2004b; Batchelor et al., 2015).

4.5.2 Bond Ball Mill Work Index Test

The Bond Ball Mill Work Index (BBMWi) test measures the specific energy required to reduce ore material from a theoretically infinite feed size to 80% passing a given product size, which in the case of this study is ~160µm. When combined with Bond's 'third theory' equation, previously discussed in Section 2.1.2.3, it predicts the work input required to reduce a given F_{80} to desired P_{80} for a 2.44m diameter wet overflow ball mill operating at 250% circulating load. Mill dimensions for an industrial unit may then be scaled using ball mill size-power correlations (Napier-Munn et al, 1999).

The test is conducted by stage crushing ore to a nominal top size of 3.35mm, and determining the feed size distribution by dry sieving. 700cm^3 of the crushed ore is placed in a standard Bond batch ball mill (305mm diameter x 305mm length) and operated at 70rpm with standard ball charge. The standard charge consists of 285 steel balls weighing a total of 20.125kg and consisting of exactly 25x38.1mm

balls, 39x31.75mm balls, 60x25.4mm balls, 68x22.23mm balls and 93x19.1mm balls. After 100 revolutions, the mill is emptied and all material finer than the closing sieve is removed and fresh crushed material is added to the oversize to make up the initial weight. The material is ground for the number of revolutions calculated to produce a 250% circulating load. The material is again removed, screened and the undersize replaced by fresh feed. This cycle is repeated until the oversize material produced per cycle reaches a steady state, and is consistently 2.5 times greater than the undersize. The average of the net mass per revolution from the last three cycles is taken as the ball mill grindability (Gbp) and the product size distribution is determined (Napier-Munn et al., 1999). The work index can then be calculated using:

$$WI = \frac{49.1}{P_1^{0.23} \times Gbp^{0.82} \times \left(\frac{10}{\sqrt{P_{80}}} - \frac{10}{\sqrt{F_{80}}} \right)}$$ **Equation 4.7**

Where WI = Ball Mill Work Index, (kWh/t), P_1 = closing sieve size, (µm), Gbp = ball mill grindability, (g/rev), P_{80} = size at which 80% of the product passes, (µm), F_{80} = size at which 80% of the feed passes, (µm).

Despite being quite a complex procedure, requiring several grinding stages to reach the steady state, the test has proven to be reliable and repeatable if the procedure and mill comply with the standard process (Mwanga et al., 2015). While there are limitations to the applicability of Bond's method for specifying industrial mills, the Work Index is a suitable measure of rock hardness (Napier-Munn et al., 1999), and may be used to compare untreated and microwave treated material to determine changes in comminution energy requirements for grinding of an ore following microwave treatment. As a general rule, Bond Work Index values of 7-9kWh/t indicate a soft ore, 9-14kWh/t indicate a medium ore, 14-20kWh/t a hard ore, and >20kWh/t can be deemed as very hard ores in terms of their response to comminution (Napier-Munn et al., 1999).

4.6 Fracture Analysis and Quantification

4.6.1 Introduction

Previous studies conducted to investigate the benefits of the microwave treatment of ores, have focussed on assessing improvements in mineral liberation or reductions in ore strength, rather than directly measuring and quantifying ore fracturing that results from the treatment. The aim of the fracture analysis component of this study was to directly measure and quantify the fractures produced in ore fragments from the microwave treatments, and determine whether comminution benefits can be related to a quantifiable increase in fracturing in treated ore samples, compared to untreated samples.

An experimental method previously applied to qualitative and quantitative investigations of cracking in concrete materials (Knab et al., 1984; Hornain et al., 1996; Ringot and Bascoul, 2001; Soroushian et al., 2003; Litorowicz, 2006), the analysis of leach fluid pathways through ore materials (Lane et al., 2006), and the assessment of HPGR fracture properties (Baum et al., 1997), was adapted and applied to the assessment of microwave treated ores.

The method involves the vacuum impregnation of ore fragments with low-viscosity epoxy resin containing a fluorescent dye to produce resin mounts from which large-area 2D sections can be cut and polished (DS, 2002; Laugesen, 2003). The sample preparation is followed by high-resolution fluorescent microscopy imaging of the sectioned surfaces, and image analysis through segmentation of fluorescent features in the images. The artificially introduced fluorescent fracture features appear as a new 'phase' within the images of the ore fragments, and appear similar to mineral phases mapped using automated mineralogy techniques. As such, similar image collection, image processing, and feature and data analysis techniques have been applied to the study of the fracture features within the images as those

used in the assessment of grains or particles produced by automated mineralogy systems.

X-ray micro-tomography (XMT) was also considered as a potential method for the assessment of fracturing in microwave treated ore fragments. A sample comprising 84 individual QZ ore fragments was submitted for imaging by XMT before microwave treatment, and again after being treated in the batch system at a microwave energy input of 1.3kWh/t. Whole rock scans were conducted at a voxel resolution of 33µm, and region of interest (ROI) scan were conducted at a voxel resolution of 16µm. There was no change in fractures observable between the untreated and treated scans at the resolutions utilised. It was suggested that scans conducted at a voxel resolution of <10µm would be required in order to image and quantify fractures using XMT. This was impractical for this investigations due to the size of fragments being measured, and the costs and timescales involved in conducting the analysis. As such, XMT was deemed an inappropriate tool for this study, and the dye penetration method was used to address the aims of the investigation. Further work conducted in this field could investigate the combination of vacuum impregnation of ore fragments with a medium that presents as a high contrast phase within an XMT image. This may allow for enhanced highlighting and imaging of fractures within 3D XMT images.

4.6.2 Dye Penetration Method

4.6.2.1 Sample Preparation

Fifty ore fragments from both untreated and microwave treated samples were selected for preparation and analysis. Sample preparation involved the production of large area epoxy-resin mounts for imaging. -50.8+25.4mm ore fragments were placed in large (180mm x 90mm x 60mm (LxWxD)) aluminium moulds. The moulds were then placed in a bespoke laboratory vacuum chamber, which was then evacuated to -1bar for 20 mins to allow for outgassing of fractures in the ore fragments. A low-viscosity epoxy, comprising

Resiblend RB-158 resin and Aradur-21 hardener with a fluorescent dye powder additive (Struers Epodye/CI Solvent Yellow 43), was then fed into the moulds in the vacuum chamber through feed ports in the chamber wall. Figure 4.21 shows an image of the sample moulds filled with fluorescent resin inside the vacuum chamber.

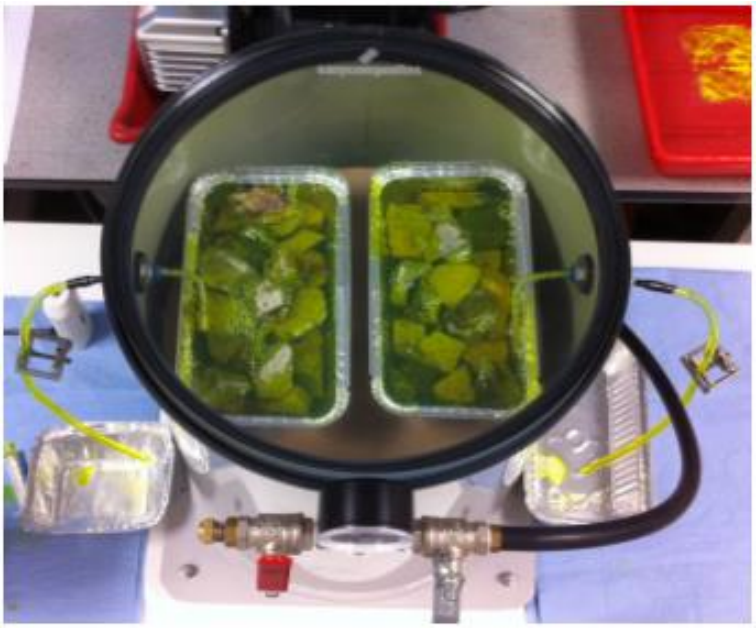


Figure 4.21 Vacuum chamber used for epoxy impregnation of ore fragments

Once full, the moulds were left for 15mins under vacuum to allow the resin to infiltrate into fractures in the ore fragments. The moulds were then removed from the vacuum chamber and placed in a water bath to keep them from overheating during the thermogenic resin hardening reaction, and left overnight to cure. After curing, the hardened epoxy blocks were removed from their moulds and each block sectioned into six slices (~90mm x 90mm x 15mm (LxWxD)) using a heavy-duty diamond-blade rotating saw. Slices were then progressively ground and polished on a Struers Tegrapol rotating disc polisher, with MD-Piano 220 grit, 500 grit and 1200 grit diamond impregnated abrasive discs, to remove any fluorescent surface contamination and produce a high-quality plane polished surface for image acquisition. An example of a completed sample mount is shown in Figure 4.22.

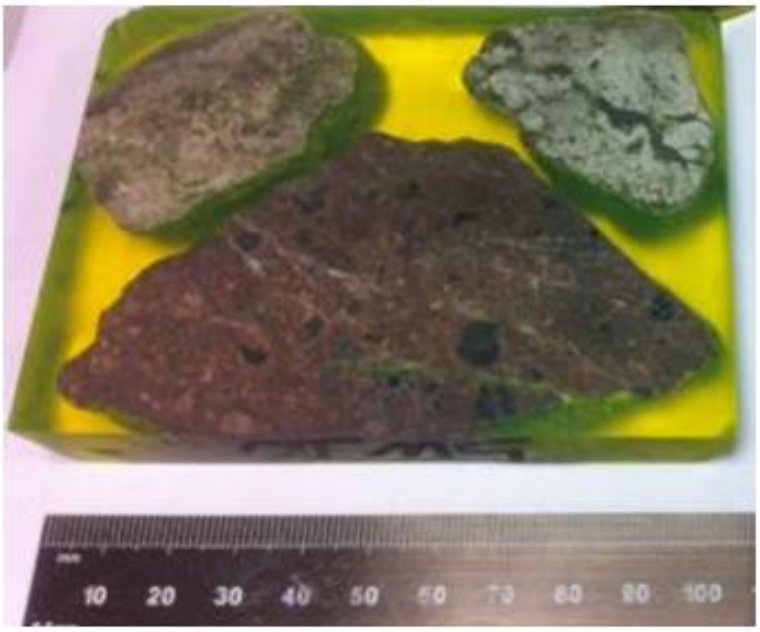


Figure 4.22 Example of epoxy section produced for imaging.

4.6.2.2 Image Acquisition

Image acquisition was conducted using a Leica M205FA stereomicroscope with fluorescent light source and a motorised X-Y stage, as can be seen in Figure 4.23.

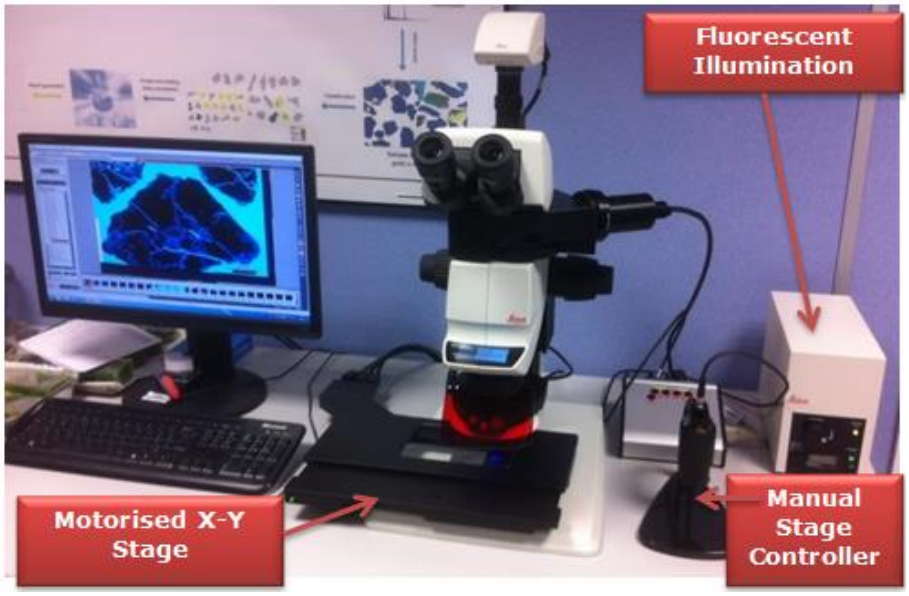


Figure 4.23 Leica M205FA stereomicroscope used for image acquisition.

This semi-automated software controlled microscope allowed for accurate, consistent and repeatable collection of high quality fracture

images. Considerable initial development time and testing was required to optimise the image collection procedure and settings prior to beginning the analysis of the samples. Ensuring consistency in image collection settings for magnification, fluorescent illumination and image stitching was essential to the production of reliable and comparable images of fracturing in the multiple sections analysed for each sample. Image acquisition settings were chosen to meet a balance of sample throughput, and a sufficient resolution to enable accurate and effective image processing. Images were acquired at 15x magnification with ~3μm per pixel original image resolution, and maximum fluorescent illumination was employed to ensure optimal fluorescence of the epoxy in the fracture features. Images were acquired in grey-scale to remove the colour conversion step from the image processing stage, and reduce the influence of potential variability in the RGB to grey-scale conversion. Manual focussing was required for sample mount, and automated image collection and stitching was performed using the Leica LAS Multistep module to control the X-Y motorised stage and image acquisition. Acquired and stitched images required compression from their original file size (>2GB) to allow for further processing and analysis. An example of an acquired image is shown in Figure 4.24.

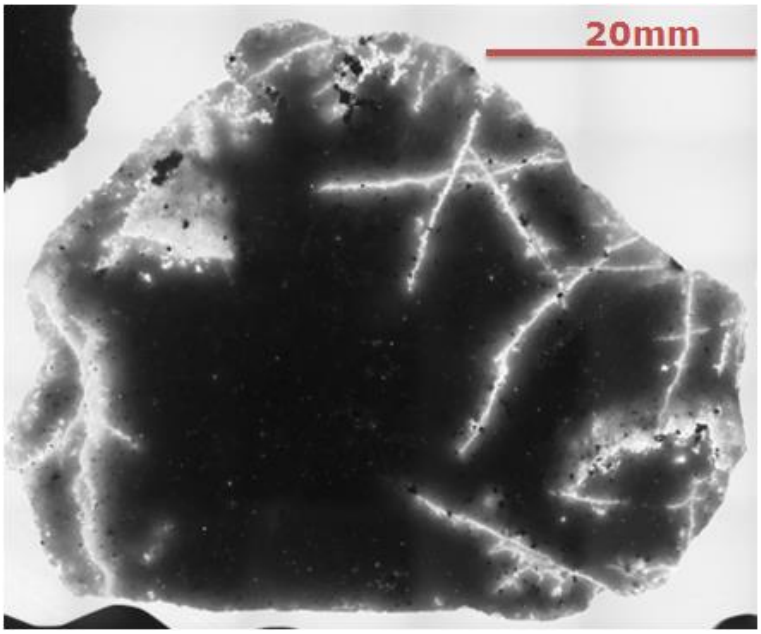


Figure 4.24 Example of a fragment image collected using this method showing fractures in a microwave treated MZ fragment.

4.6.2.3 Image Processing and Analysis

Due to the optimised image acquisition procedures developed in initial testing, minimal post-processing of the final images was required. Additional processing or manipulation of the acquired images prior to analysis was also undesirable, due to the need to maintain consistency in the conditions used in producing the final image for analysis. Image processing was limited to cropping of extraneous regions of the image to reduce image size and simplify the analysis of the final images.

Two stages of image analysis were performed to produce the required data for this study. An initial stage to segment the fracture features from the ore fragment area, and an additional stage to segment the total measured fragment surface area from the background.

Image analysis to segment the fracture features involved following a multi-step procedure. Initially, a white detail top-hat filter was applied to extract the 'bright' fracture feature details from the background. The settings controlling the dimensions of the filtered region, through defining a threshold around a peak grey-scale value, were selected through interactive trials across multiple images. The optimised filter

settings were applied consistently throughout the image analysis process, and ongoing assessments of the filtered outputs was conducted to ensure an accurate representation of the fracture features was achieved.

Segmentation of the filtered fracture features was conducted based on grey-scale values. The values used for segmentation were assessed and optimised for each image to account for any slight variations or inconsistencies in image brightness ranges. A white-detail binary processing clean-up filter was applied to remove noise or potential remnant contamination features (<~200µm). This filter was applied interactively for each image to ensure consistent removal of unwanted features from the image, without influencing the structure or dimensions of the remaining fracture features. Manual binary image editing was conducted for each image to remove any unwanted artefacts from the final images.

Measurement was completed through labelling of individual fracture features in the image, and the extraction of selected dimensional attributes of the labelled features. A report was created for each image, containing data for the individual features, and compiled data for the entire image frame. The feature data from these reports was compiled in MS Excel to create the final data set for each sample. A diagram outlining the image analysis process is shown in Figure 4.25.

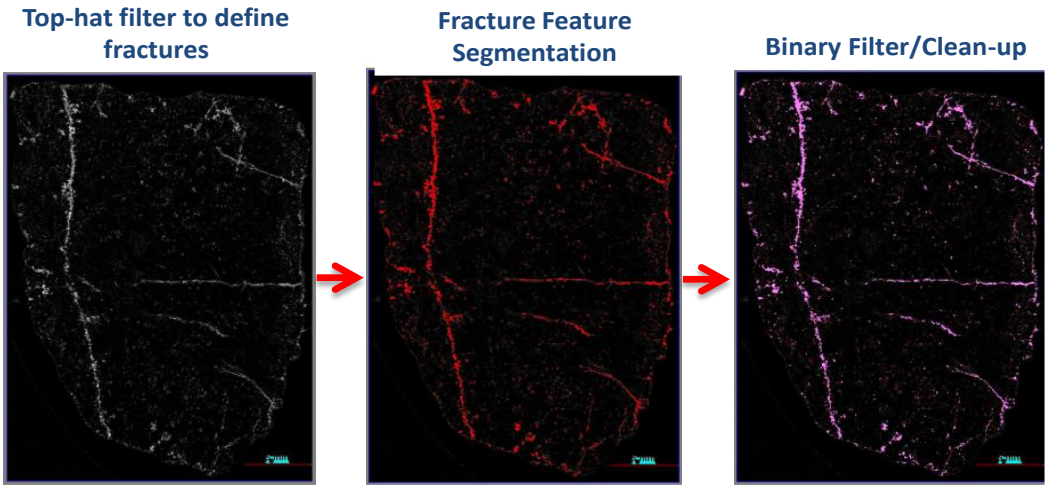


Figure 4.25 Diagram of fracture feature image analysis procedure

Fracture length measurements reported in this study refer to the maximum Feret diameter, which can be defined as the maximum possible length of the feature measured between two parallel lines drawn tangential to the boundary of the shape. Area measurements are calculated from the total pixel count of a feature, taking into account the pixel resolution of the image.

An additional stage of image analysis was conducted to segment the total surface area of the ore fragments in the images. Grey-scale segmentation was performed for the darker 'rock' fragment phase from the brighter background and fracture features, to create a binary image. A dilation-erosion binary processing filter was applied to close and fill the fracture features within the fragment surface area. Manual binary image editing was conducted to fill any remnant fracture features and remove unwanted artefacts from the images. An example of the input and output images in this process are shown in Figure 4.26. This measurement was used to provide the total fragment surface area measured for each sample.

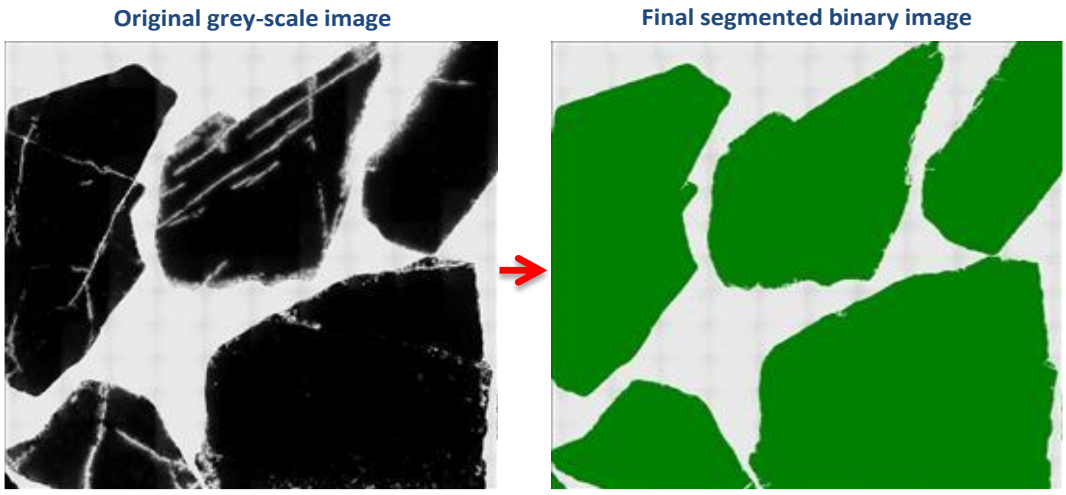


Figure 4.26 Example of product of the total fragment surface area segmentation procedure

4.7 SUMMARY

This chapter has presented a comprehensive background to the design, development and operation of both of the microwave treatment systems used in producing the microwave treated samples for this study. It has also provided a detailed background and description of the sample preparation methods, automated mineralogy systems, fracture analysis procedures, and comminution tests used in order to achieve the aims of this investigation, and provided justification for their selection.

CHAPTER 5 – INVESTIGATING THE INFLUENCE OF MINERALOGY ON THE MICROWAVE TREATMENT OF COPPER ORES

5.1 INTRODUCTION

A number of key mineralogical criteria have been identified by previous researchers as contributing to the amenability of an ore to achieving beneficial outcomes from high power microwave treatment (Kingman et al., 2000b; Ali and Bradshaw, 2009; Batchelor et al., 2015). The initial aim identified for this study is to expand on these previous findings, in order to further improve the understanding of the influence that copper ore mineralogy has on the comminution and mineral liberation benefits achieved from high power microwave treatments.

This chapter will present the experimental work conducted to address the initial aim for the study, through conducting a series of high power microwave treatments of copper ores known to possess differences in relevant mineralogical and textural characteristics. The benefits achieved from the treatments, in terms of improved comminution behaviour and mineral liberation, will be assessed and compared between the ores, and related to both ore mineralogy, and microwave treatment conditions. Unlike previous studies, which have employed <30kW microwave power, predominantly in multimode cavities, the samples for this investigation will be treated with up to 200kW total microwave power in a single mode resonant applicator. The capability of the pilot system in achieving high sample throughputs of up to 150t/h, also allows for testing the comminution and mineral liberation benefits achieved from total microwave energy inputs, or doses, of between 0.7-1.3kWh/t, which is lower than for previous studies reported in the literature.

5.2 Ore Samples

5.2.1 Introduction

The copper ores investigated in this study were supplied by the sponsoring company, and originated from the Rio Tinto Kennecott operation at the Bingham Canyon Mine in the Oquirrh Mountains of Utah, USA. A total of three different ores have been used throughout this investigation, and were chosen to represent variations in mineralogical and textural characteristics of microwave heating minerals such as copper and iron sulphides, and varying gangue compositions.

A porphyritic monzonite ore, hereafter referred to as MZ ore, and two quartzite ores, hereafter referred to as QZ ore and QX ore, were used in this study. The MZ and QZ ores are currently economically mined and processed at the operation, whereas the QX ore is designated as 'waste' material, having a copper grade below that which can be economically exploited with current processes and technology.

Each of the ore samples were mined from different zones of the pit at Bingham Canyon, crushed and screened to a nominal fragment size of -50.8+25.4mm, and several tonnes of each ore was transported to the University of Nottingham in a combination of ~200kg drums and ~1-2 tonne bulk bags. Sub-samples for each of these ores were subsequently produced, using appropriate representative sample methods, for the microwave treatments conducted to meet the aims of this investigation.

5.2.2 Geology of the Deposit

The economic mineralisation of large, low-grade porphyry copper deposits consists predominantly of disseminated veinlets of chalcopyrite, deposited through hydrothermal processes within the body of an igneous quartz monzonite intrusion, or distributed throughout the country rocks already in place around the intrusion

(White, 1999). The term 'porphyry' relates to the porphyritic texture common in the igneous quartz monzonite emplacements. A porphyritic texture is one in which phenocrysts, or large euhedral grains commonly of feldspathic composition, occur within a fine-grained matrix (Sillitoe, 2010). This type of texture represents the occurrence of an initial slow period of cooling following the emplacement of the intrusion, allowing for larger crystals to grow, before more rapid cooling gives rise to a finer-grained matrix of different composition.

The Bingham Canyon deposit consists of a porphyry copper ore, in which metal-bearing minerals are disseminated throughout a monzonitic igneous intrusive stock and adjacent sedimentary country rocks that consist of quartzite, shale altered to hornfels, and limestone altered to skarn (Sillitoe, 2010). These sedimentary and igneous zones of mineralisation comprise a world-class low-grade disseminated copper ore deposit (Phillips et al., 1998). Recovered metals include copper, silver and gold. In addition, molybdenite (MoS_2) is recovered, from which molybdenum and rare-earth elements including rhenium can be extracted.

The monzonite comprising the core of the Bingham Canyon deposit was emplaced as an igneous intrusion into quartzite and limestone of the Bingham Mine Formation. The monzonite of various compositions was initially not mineralized as it was emplaced before the main mineralizing event. During the mineralizing event that coincided with the intrusive emplacement of quartz monzonite porphyries, hydro-thermal mineral-bearing fluids were injected along fractures in the earlier monzonitic and sedimentary rocks (Cooke et al., 2005). Subsequent cooling resulted in the precipitation of metal-bearing minerals including chalcopyrite, pyrite, bornite and molybdenite, concentrated along fractures in the rock. These metalliferous minerals become sparser internally in the rock, away from the fractures, where they become finer-grained and more disseminated (Sillitoe, 2002).

The MZ ore sample used in this study was collected from an intrusive porphyritic monzonite body known as the Ohio Copper Dike, which is a lateral offshoot from the main body of the Bingham intrusion (Cooke et al., 2005). The QZ sample was collected from the quartzitic country rock, adjacent to the Ohio Copper Dike intrusion, where mineralisation occurred through precipitation of sulphide minerals from hydrothermal fluids derived from the igneous intrusion event. The host quartzite is a metamorphosed quartz-rich sandstone comprising an interlocking mosaic of quartz crystals (Ross, 2010). The QX sample is of similar composition and origin to the QZ sample, however with insufficient copper sulphide mineralisation for it to be economic to mine and process.

The MZ ore represents typical characteristics of a quartz monzonite porphyry ore, comprising a range of microwave heating sulphide minerals, within a gangue comprising both 'softer', more ductile micas, and 'harder', or more brittle quartz and feldspars (White, 1999). The QZ and QX ores have a very similar gangue composition of predominantly quartz, with only minor micas and feldspar, however they exhibit differences in both the abundance and textural characteristics of sulphide heating minerals. As such, the three ores represent a suitable range of microwave treatment amenability characteristics to address the aims of this investigation. In order to be able to relate the mineralogical and textural characteristics for each ore to the outcomes achieved from microwave treatments, a detailed mineralogical study of the characteristics of coarse ore fragments was required for each ore.

5.3 Coarse Ore Characterisation

5.3.1 Introduction

Measurements of 20 coarse ore fragments (~25mm) for each ore was conducted by MLA, in order to assess the mineralogical and textural characteristics of the different ores. It was identified by Napier-Munn

et al. (1999) that it is the microscale mineralogical and textural features of an ore that controls the mechanism by which the ore responds to an applied stress during comminution. The same relationship between ore mineralogy and comminution response exists in relation to the microwave treatment of ores, necessitating the coarse ore mineralogical investigation. The coarse ore characterisation study was not designed to be statistically representative, as insufficient material is analysed and large variability in the abundance of heating minerals between individual fragments can be observed. Analysis of a statistically significant sample of ~25mm ore fragments is impractical, as it would involve the preparation and measurement of hundreds of MLA sample mounts for each ore. The coarse ore characterisation serves to investigate and quantify the mineralogical and textural characteristics of each sample, and provide data for each ore on modal mineralogy, heating mineral abundance, mineral grain size, and associations between microwave heating minerals and gangue minerals.

5.3.2 Sample Preparation and Analysis Procedure

Twenty fragments for each of the ores were prepared as 30mm epoxy resin mounts, according to the process described in Section 4.4.3.2, and submitted for MLA measurement. Two different MLA measurements were conducted on each of the twenty mounts for the three ores. The SPL_Lt measurement mode was used to characterise the microwave heating minerals of interest, which are identifiable based on their BSE brightness, and to produce images detailing the textural characteristics of the microwave heating minerals for each of the ores. Modal mineralogy data was collected using the XMOD measurement mode. Both MLA measurements were performed at 200x magnification and 1000x1000 pixel frame resolution, using SEM setup parameters details in Section 4.4.3.3. The BSE search range for the SPL_Lt measurement was set between greyscale levels of 150-255, in order to conduct X-ray mapping of all 'bright' heating minerals in the samples. The XMOD measurement was performed with an x-y step

size of 32x32 pixels, resulting in the collection of ~30000-40000 individual x-rays across the surface of each fragment, with the range being due to variations in fragment total surface area.

5.3.3 MZ Ore

The microwave heating minerals within the MZ ore are chalcopyrite (0.72 wt%), pyrite (2.91 wt%), Fe-oxides (0.17 wt%) and montmorillonite (3.45 wt%). Gangue mineralogy is comprised predominantly of orthoclase feldspar (32.0 wt%), quartz (21.6 wt%), phlogopite (11.5 wt%) and biotite (9.7 wt%), with smaller amounts of muscovite (6.3 wt%), plagioclase feldspar (4.9 wt%) and chlorite (3.1 wt%). The gangue comprises ~70% hard minerals, with the remainder being softer micaceous minerals such as phlogopite, biotite and muscovite.

MZ ore possesses a copper sulphide native grain size D_{80} ~240µm, and a D_{80} ~350µm for other sulphides, with pyrite making up the majority of the group. Grain size distributions for grouped copper sulphides, other sulphides (predominantly pyrite), and other heaters, are shown in Figure 5.1. Microwave heating minerals in the ore have a ~53.5% association with hard gangue minerals, ~30.6% association with soft gangue minerals, and ~10% association with free surface, which means it is occurring in contact with background at the edge of the fragment image.

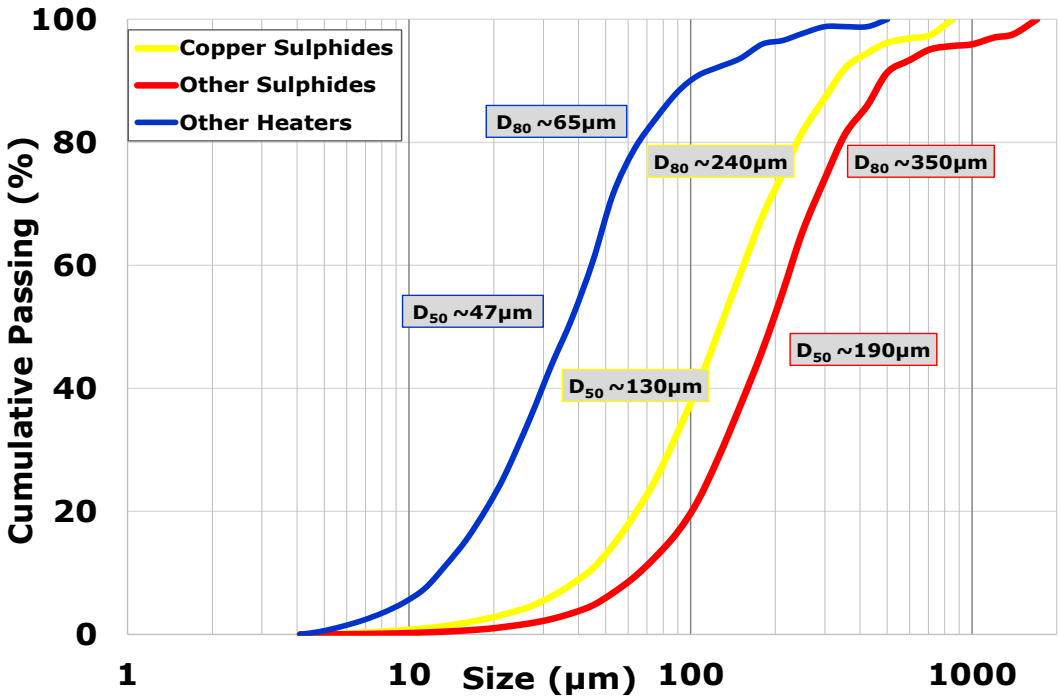


Figure 5.1 MZ grain size distributions for grouped microwave heating minerals.

False colour mineral maps shown in Figure 5.2 serve to illustrate the typical mineral textures encountered in MZ ore. Copper sulphides occur as either disseminated finer grains, or as micro-veins running across the fragments, as can be clearly seen in images G and H. Pyrite is the other dominant sulphide and has a similar texture to the copper sulphides in the ore, however it also occurs as coarser, discrete grains of >1mm. The other heaters group is predominantly Fe-oxides, and they are disseminated throughout the fragments as very fine (<50µm) grains.

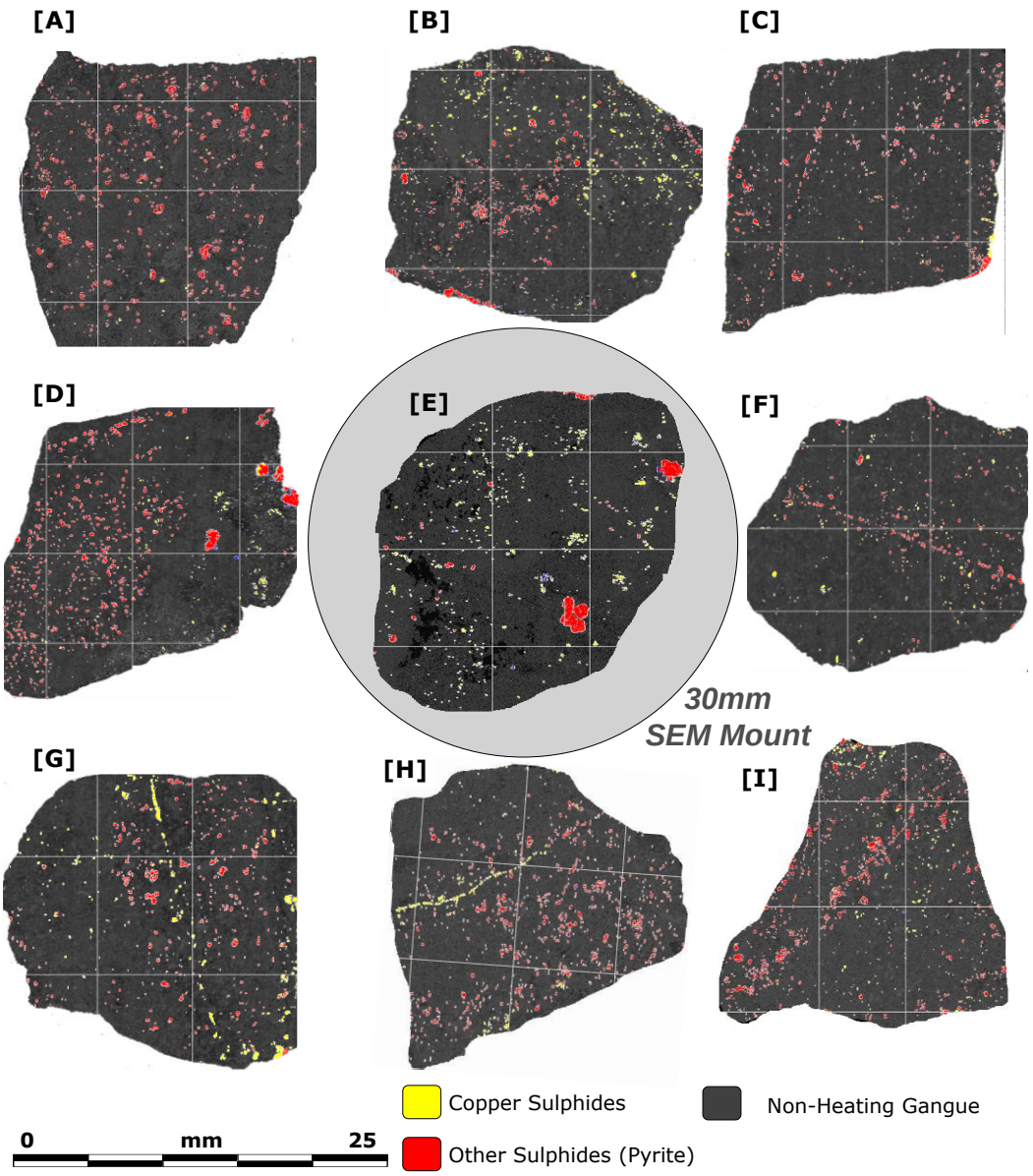


Figure 5.2 False colour mineral maps of MZ ore from coarse ore MLA measurement.

5.3.4 QZ Ore

The microwave heating minerals within the QZ ore are chalcopyrite (0.82 wt%), pyrite (0.56 wt%), bornite (0.27 wt%) and the hydrous clay montmorillonite (0.30 wt%). Gangue mineralogy is dominated by quartz (90.8 wt%), with smaller amounts of phlogopite (3.1 wt%), orthoclase feldspar (1.6 wt%), muscovite (1.2 wt%) and biotite (1.2 wt%). As QZ ore is a mineralised quartzite, unsurprisingly >92% of the gangue comprises minerals classified as being hard, with quartz being the main constituent.

Textural characteristics of sulphide heating minerals within the sample are predominantly disseminated and granular, possessing a native grain size D_{80} of ~260µm for copper sulphides and ~265µm for other sulphides. Grain size distributions for grouped heating minerals in the QZ ore are shown in Figure 5.3.

Microwave heating minerals in the ore have a ~65.5% association with hard gangue minerals, and only ~8% association with soft gangue minerals. Interestingly, microwave heaters in the QZ ore have a ~19% association with free surface, suggesting that the ore tends to preferentially break along sulphide mineralised fracture planes during crushing, exposing sulphides on the surfaces of the fragments. This is not ideal from a microwave treatment perspective, as the differential thermal expansion breakage mechanism requires that the heating minerals be enclosed by the transparent gangue in order for the transfer of stresses and propagation of fractures.

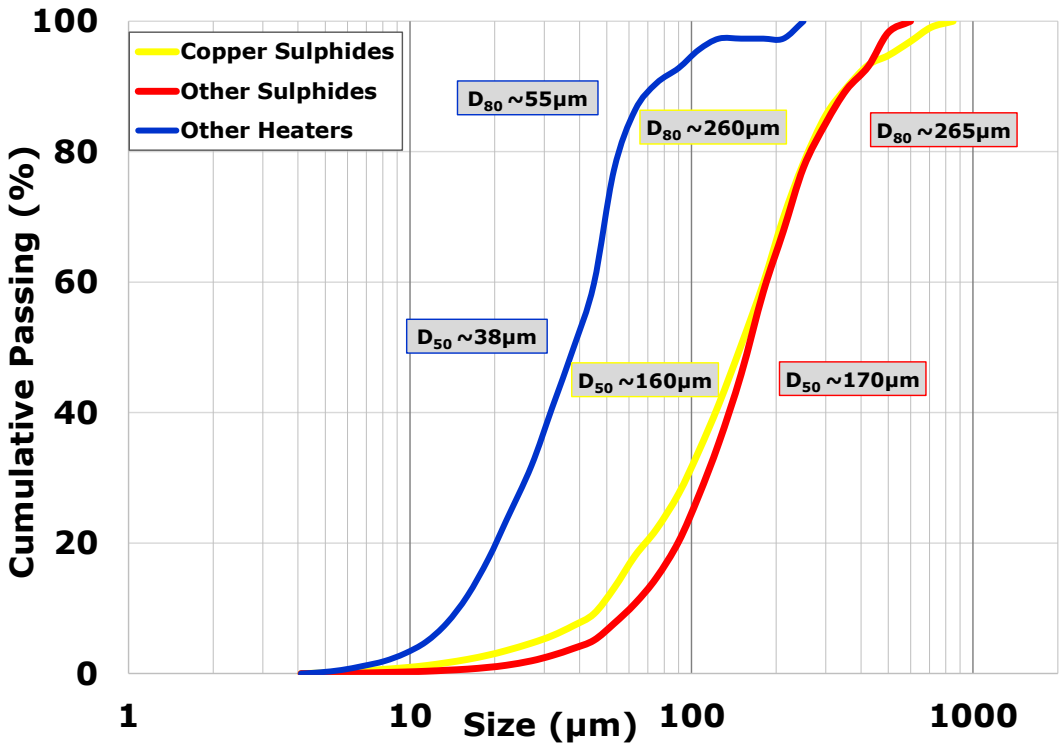


Figure 5.3 QZ grain size distributions for grouped microwave heating minerals.

Sulphide mineralisation in QZ ore tends to be either well disseminated throughout the ore as discrete grains, or deposited along pre-existing fracture planes within the fragments, as can be seen in the mineral maps in Figure 5.4. There does appear to be some heterogeneity in the distribution of the different sulphide minerals, with some fragments having a higher abundance of copper sulphides, while some fragments have more pyrite.

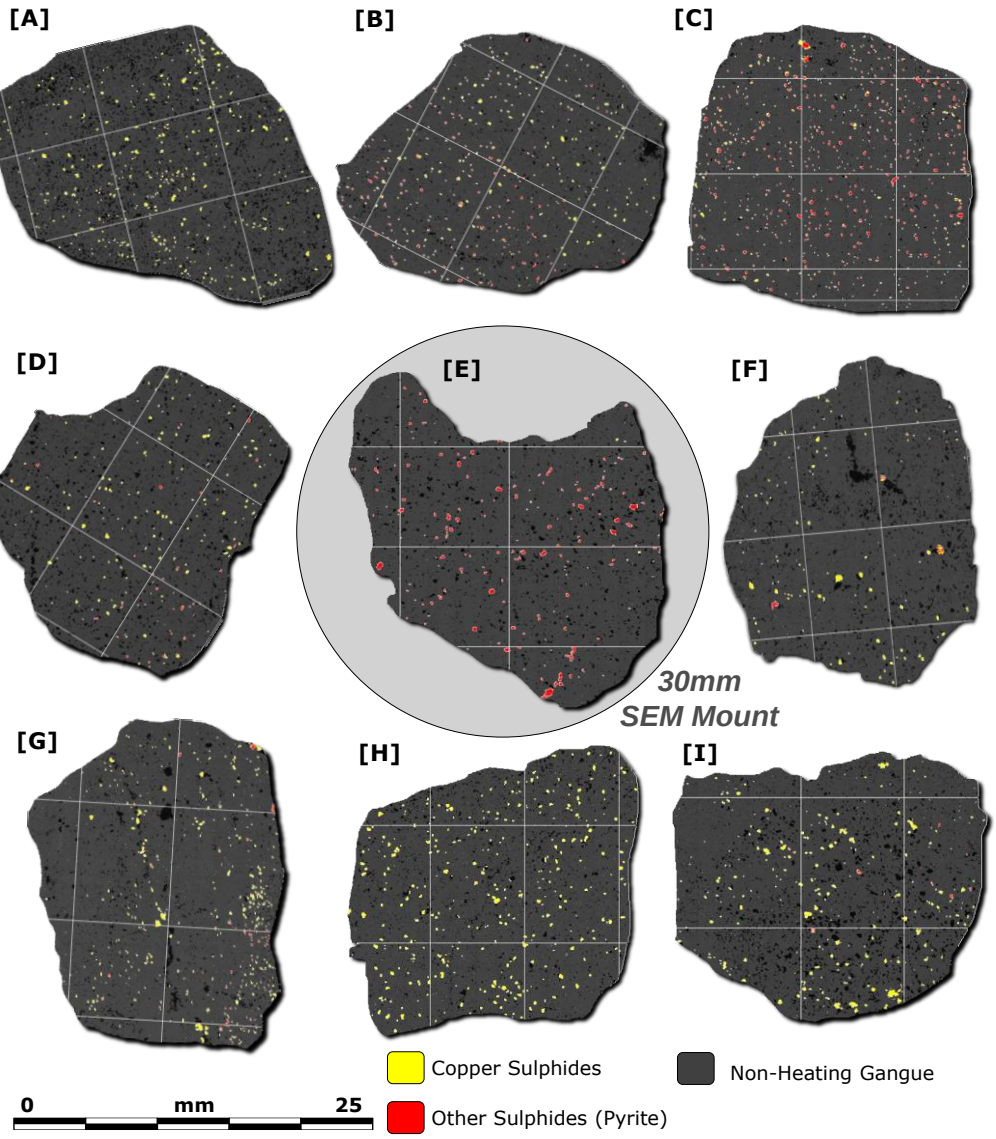


Figure 5.4 False colour mineral maps of QZ ore from coarse ore MLA measurement.

5.3.5 QX Ore

The microwave heating minerals within the QX ore are chalcopyrite (0.12 wt%), pyrite (2.55 wt%), and the hydrous clay, montmorillonite (0.35 wt%). Gangue mineralogy is dominated by quartz (88.5 wt%), with smaller amounts of orthoclase feldspar (1.5 wt%), muscovite (1.8 wt%) and biotite (4.7 wt%). Similar to the QZ ore, since the mineralogy of the QX ore is also dominated by quartz, ~90% of the gangue comprises hard minerals. As QX ore is 'waste' material with very low copper sulphide content, other sulphides make up the majority of the heating minerals in the ore, with pyrite being dominant.

Textural characteristics of other sulphide group minerals within the ore are predominantly coarse and granular, possessing a native grain size D_{80} of ~320µm. The low abundance of copper sulphides in the ore tend to be finer grained than in the QZ ore, with a grain size D_{80} of ~145µm.

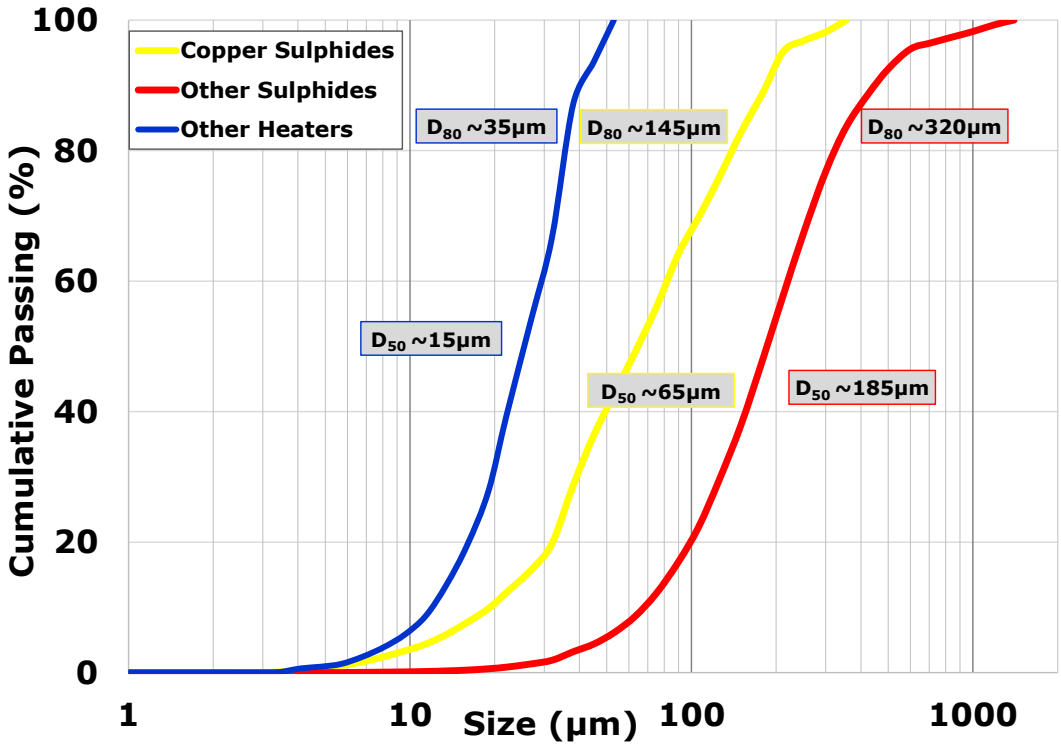


Figure 5.5 QX grain size distributions for grouped microwave heating minerals.

Microwave heating minerals in the ore have a ~69.8% association with hard gangue minerals, and only ~12.2% association with soft gangue minerals. Associations of heating minerals with free surface is ~6.6%, which is considerably lower than for the QZ ore, suggesting that the breakage along mineralised fracture planes seen in the QZ ore, is not as prevalent in the QX ore. The predominantly coarse and granular nature of the heating minerals within the QX ore can be seen in Figure 5.6.

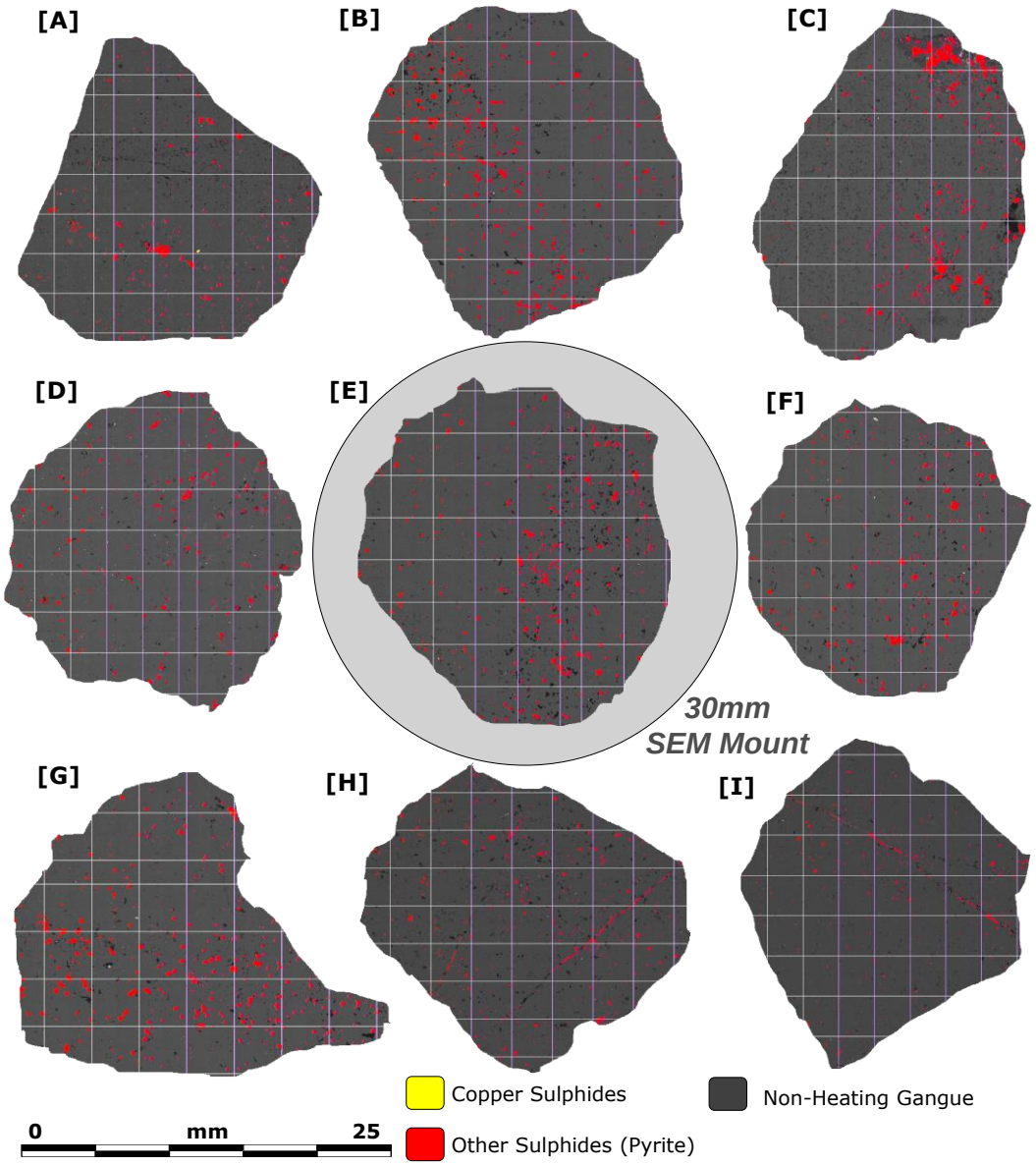


Figure 5.6 False colour mineral maps of QX ore from coarse ore MLA measurement.

5.3.6 Summary of Coarse Ore Characteristics

Understanding the mineralogy and mineral textures of the three ores used in this study was a key requirement in achieving the aims of the investigation. Comparing the differences in the three ores is essential in developing the understanding of how variations in mineralogy and mineral texture influence the comminution benefits achieved through microwave treatments of the ores.

The modal mineralogy of the three ores from the coarse ore characterisation is shown in Table 5.1.

Coarse Ore Modal Mineralogy (wt %)					
Grouped Minerals		**Mineral**	**MZ**	**QZ**	**QX**
Good Heaters	**Copper Sulphides**	**Chalcopyrite**	0.71	0.82	0.12
		Bornite	0.02	0.27	0.15
	Other Sulphides	**Pyrite**	2.78	0.56	2.55
		Molybdenite	0.00	0.01	0.00
		Other Sulphides	0.01	0.04	0.10
	Non-sulphide	**Montmorillonite**	2.64	0.30	0.35
Other Heaters		**Fe Oxide**	0.17	0.00	0.00
Non-heating Gangue	**Hard Gangue Mohs ≥6**	**Quartz**	37.01	90.76	88.51
		Plagioclase	3.71	0.00	0.00
		Orthoclase	24.32	1.61	1.48
		Albite	1.43	0.00	0.00
	Soft Gangue Mohs <6	**Phlogopite**	11.08	3.14	0.01
		Muscovite	4.75	1.15	1.80
		Biotite	7.64	1.16	4.71
		Chlorite	2.46	0.07	0.02
		Carbonates	0.04	0.00	0.00
	Others	**Apatite**	0.66	0.04	0.00
		Zircon	0.04	0.03	0.03
		Other	0.53	0.04	0.17
		Total	**100**	**100**	**100**

Table 5.1 Ungrouped modal mineralogy from coarse ore characterisation.

Table 5.2 shows the grouped mineral abundances for key microwave treatment amenability characteristics for each of the ores. The differences between the ores in terms of both microwave heating mineral abundances, and gangue mineral composition are clearly seen

in this table. MZ ore has the highest abundance of both sulphide and non-sulphide heating minerals, and the lowest abundance of hard gangue minerals. QZ ore has the lowest abundance of heating minerals, and the highest proportion of hard gangue minerals, which more effectively accommodate strain through brittle fracture and the propagation of cracks.

While QZ and QX ores have very similar gangue composition, it is the difference in their heating mineral content that is of greatest interest for this investigation. QX ore has a greater abundance of pyrite (2.55 wt%), compared to the QZ ore (0.56 wt%), and they possess very similar abundances of non-sulphide heaters of 0.30wt% and 0.35wt% respectively. This difference in pyrite content between the two very similar ores, will allow for testing of the influence of pyrite on the outcomes from high power microwave treatments. As was previously discussed in Section 2.3.4, pyrite has been shown to effectively transfer stresses through an ore during comminution processes due to its high modulus of elasticity. The comparison of QZ and QX ores in this study will allow for the testing of this theory in the context of the microwave treatment of ores, and will assess the influence of pyrite on the generation of fractures during microwave treatment. The differences in the total abundance of heaters and gangue compositions between the MZ and QZ ores, will allow for these amenability characteristics to be tested in terms of the benefits achieved in ore strength reductions and improved mineral liberation.

Coarse Ore Grouped Mineral Abundance (wt %)					
Grouped Minerals			MZ	QZ	QX
Good Heaters	Copper Sulphides	Chalcopyrite	0.71	0.82	0.12
		Other Cu Sulphides	0.02	0.27	0.15
	Other Sulphides	Pyrite	2.78	0.56	2.55
		Other Sulphides	0.01	0.05	0.10
	Non-sulphide	Montmorillonite	2.64	0.30	0.35
Other Heaters		Iron Oxides	0.17	0.00	0.00
Non-heating Gangue	Hard Gangue Mohs ≥6	Quartz	37.01	90.76	88.51
		Feldspar	29.46	1.61	1.48
	Soft Gangue Mohs <6	Micas	25.93	5.52	6.53
		Carbonates	0.04	0.00	0.00
	Others		1.23	0.11	0.20
	Total		**100**	**100**	**100**
	All Sulphide Heaters		3.52	1.70	2.91
	Good Heaters		6.16	2.00	3.27
	All Heaters		6.33	2.00	3.27
	Hard Gangue Minerals		66.47	92.37	89.99
	Soft Gangue Minerals		25.97	5.52	6.53

Table 5.2 Grouped mineral abundances from coarse ore characterisation. [Other Cu-Sulphides comprises bornite, chalcocite, covellite; Other Sulphides comprises molybdenite, sphalerite; Iron Oxides comprises magnetite, hematite; Other Hard comprises zircon, pyroxenes/amphiboles, apatite; Other Soft comprises talc, gypsum fluorite; Micas comprises muscovite, phlogopite, biotite, chlorite; Carbonates comprises calcite, dolomite, siderite.]

A summary of the key microwave treatment amenability characteristics for each of the ores used in this study is shown in Table 5.3. Assessing each of the ores against the semi-quantitative criteria proposed by Batchelor et al. (2015) as describing the ideal ore characteristics for beneficial microwave treatment outcomes, shows that all three ores could be expected to show benefits from microwave treatments. Each ore has between 2-20% abundance of good microwave heating minerals, with the QZ ore being at the lowest end of this scale, and the MZ ore having the highest abundance. Microwave heating minerals in all three ores are constrained >50% by hard gangue minerals. While this factor may be important for reductions in ore strength through macro-fracturing, associations of heating minerals with soft gangue may be more beneficial for mineral liberation improvements. As could be expected, associations between microwave heating minerals and either hard or soft gangue vary in

accordance with changes in gangue composition for each of the ores tested. As QZ and QX ores possess a gangue composition dominated by 'hard' quartz, microwave heating minerals show a higher association with hard gangue due to there being a higher abundance in these ores. Conversely, as MZ ore possesses a higher proportion of 'soft' micaceous minerals in its gangue, microwave heating minerals show a higher association with soft gangue than in the QZ and QX occurs. Essentially, the mineral associations observed in the ore are controlled by the proportions of hard and soft minerals in the gangue.

None of the ores are ideal in terms of the grain size of the microwave heating minerals, as they do not meet the 50% of grains >500μm criteria, however previous work has shown that heating grains >100μm are sufficient for the breakage mechanism to have an effect (Jones et al., 2005). The ores possess a combination of amenable textures, exhibiting both disseminated and granular, or veined textures, which occur throughout the majority of ore fragments in each sample. The amenable characteristics of each of the ores suggests that ore strength reductions, improvements in mineral liberation, or potentially both, will be achieved through high power microwave treatments. While MZ ore possesses more amenable heating mineral characteristics, having both a higher abundance and coarser pyrite grain size, QZ ore has more amenable gangue characteristics, with a higher proportion of hard and brittle minerals. The relative contributions of these amenability characteristics will be considered when assessing the outcomes of the microwave treatments conducted in this investigation.

Ore Amenability Characteristics		Ore		
		MZ	QZ	QX
Heating Mineral Abundance (wt%)	Sulphide Heaters	3.52	1.70	2.91
	All Good Heaters (inc. montmorillonite)	6.16	2.00	3.27
	Pyrite	2.78	0.56	2.55
Heating Mineral Grain Size (μm)	Copper Sulphide Grain Size D_{80}	240	260	145
	Other Sulphide (Pyrite) Grain Size D_{80}	350	265	320
Gangue Composition (wt%)	Hard Gangue (Mohs≥6)	66.47	92.37	89.99
	Soft Gangue (Mohs<6)	25.97	5.52	6.53
Mineral Associations (%)	Heating Minerals to Hard Gangue	54	66	70
	Heating Minerals to Soft Gangue	31	8	12
	Heating Minerals to Free Surface	10	19	7
	Copper Sulphide to Pyrite	7	2	17

Table 5.3 Summary of MZ, QZ, and QX Ore microwave treatment amenability characteristics.

5.4 Microwave Treatments

5.4.1 Introduction

High power microwave treatments of MZ, QZ and QX ores, to meet the first two aims of this investigation, were conducted using the dual-applicator microwave treatment pilot system described in detail in Section 4.3.1. The aim of these treatments was to fix the throughput of the pilot system to the maximum 150t/h, and vary the microwave power input (kW), and subsequently the microwave dose (kWh/t) received by the ore. Treatment stability considerations meant that the targeted higher total dose treatments for the MZ and QX ores required lower throughputs and lower power, in order to minimise arcing in the applicator. The microwave treatment conditions were selected to allow for the assessment of the influence of microwave power density and total energy input, on ores with different mineralogical characteristics. Microwave treatments were conducted on MZ, QZ and QX ores, with the MZ and QZ ores assessed in this chapter for benefits in mineral liberation and reductions in ore strength, and all three ores assessed in the next chapter for changes in the fracture properties of the ores resulting from varying microwave treatment conditions.

5.4.2 Microwave Treatment Conditions

Three 750kg representative sub-samples of -50.8+25.4mm ore fragments were split, using a large rotary sample divider, from the bulk sample stock of each ore for each microwave treatment. Additional representative sub-samples were spilt from the bulk stock for each ore to act as an untreated control sample for comparison. Ore fines (<5mm) for each of the ore types were also screened from the bulk ore stock to act as void filling material. The use of fines of the same composition as the ore fragments being treated ensured that the dielectric properties of the material in the applicator would be more homogeneous than if fines of a different composition, such as builder's sand, was used. Ore and fines were blended out of the pilot system feed hoppers to produce a 40:60 ore to fines ratio. The use of fines for filling voids to aid material flow through the applicator and minimise arcing was discussed in detail in Section 4.3.1.2. After accounting for partially treated ore during microwave ramp up, and ore remaining in the treatment tube once microwave power had turned off, ~500kg of treated sample was produced at a steady state to the desired microwave conditions.

A program of three microwave treatments was performed using the pilot system on the three sub-samples for each of the MZ, QZ and QX ores. The three treatments for each of the ores were designated T1, T2, and T3, with the untreated control sample for each ore designated as UT. In the case of the MZ ore, a second untreated control sample and four further samples for treatment were also spilt from the original bulk sample for additional treatments conducted on that ore, as such, the two MZ untreated ores are designated UT1 and UT2. The microwave treatment conditions used in producing the treated MZ, QZ and QX ore samples are detailed in Table 5.4.

Ore	Sample	Microwave Treatment System	Throughput (t/h)	Total Microwave Power (kW)	Treatment Energy 'Dose' (kWh/t)	Power Density in Applicator (W/m^3)
MZ	**T1**	Pilot	150	2 x 50	**0.7**	$3.3x10^6$
	T2	Pilot	150	2 x 75	**1.0**	$5.0x10^6$
	T3	Pilot	120	2 x 80	**1.3**	$5.3x10^6$
QZ	**T1**	Pilot	150	2 x 50	**0.7**	$3.3x10^6$
	T2	Pilot	150	2 x 75	**1.0**	$5.0x10^6$
	T3	Pilot	150	2 x 100	**1.3**	$6.6x10^6$
QX	**T1**	Pilot	150	2 x 50	**0.7**	$3.3x10^6$
	T2	Pilot	100	2 x 75	**1.5**	$5.0x10^6$
	T3	Pilot	60	2 x 65	**2.2**	$4.3x10^6$

Table 5.4 Microwave treatment conditions for MZ, QZ and QX ores.

It should be noted that only a single sample has been produced for MZ, QZ and QX ores at each microwave treatment condition. While it would have been advantageous to be able to assess the reproducibility of the benefits achieved at each microwave treatment condition employed in this study by conducting multiple treatments at each condition, limitations regarding the timescales required for the analysis and quantification of the benefits achieved made this impractical for this investigation. Future work could be conducted to assess this issue through a comparison of the benefits achieved for a single ore across a series of treatments conducted for a number of different sample batches at identical microwave treatment conditions. This would allow for an investigation into the variability of microwave treatment outcomes, and an assessment of the reproducibility of results.

5.5 Mineral Liberation Analysis

5.5.1 Introduction

In order to assess the benefits of the microwave treatments on liberation of copper sulphide minerals in the MZ and QZ ores, both the untreated and microwave treated samples were subjected to analysis by QEMScan automated mineralogy.

5.5.2 Sample Preparation and Analysis Procedure

Representative 50kg sub-samples of the untreated and each of the microwave treated samples, for both the MZ and QZ ores, were prepared for analysis. Both untreated and microwave-treated samples were stage crushed to 3.35mm in a laboratory jaw crusher at the same closed side settings (CSS) to ensure consistent breakage conditions across all the samples. The crusher products were split by rotary sample divider into representative 1kg sub-samples for batch grinding. The laboratory rod mill was operated at 65%wt solids and 63% critical speed. A series of rod mill calibration grinds were conducted at varying durations on the untreated and treated samples to find the grind time necessary to achieve target grind P_{80} of 150µm for both untreated and treated samples, and a target grind P_{80} of 370µm for untreated and 425µm for treated samples, to investigate any benefits in liberation at a coarser grind size. The milled samples were then wet and dry sieved into the $\sqrt{2}$ series, and prepared for mineralogical analysis by QEMScan using the PMA measurement mode, as described in Section 4.4.3.3.

One of the primary aims of the microwave treatment of copper ores is to enhance the liberation of the valuable Cu-sulphide minerals in the ore, and in doing so, enhance their ability to be recovered during subsequent separation by froth flotation or other processes. In the MZ and QZ ores, the Cu-sulphide group is predominantly made up of chalcopyrite, with minor bornite and chalcocite. While other minerals in the ore, such as pyrite or iron oxides, may also experience enhanced liberation in microwave treated ores, this study will focus on the liberation of the economically relevant Cu-sulphide minerals when assessing the benefits achieved by from the microwave treatment process.

In order to assess the liberation of Cu-sulphide minerals in the ore, particles are grouped into one of four liberation groups or 'classes'. Liberated Cu-sulphides are those which comprise >98% of a particle,

high-grade middlings particles comprising 50-98% Cu-sulphide, low-grade middlings comprising 10-50% Cu-sulphides, and particles with <10% are referred to as being locked. The conventional mineral processing operational understanding, or 'rule of thumb', is that particles in the >50% Cu-sulphide liberation classes are recoverable by froth flotation (Welsby et al., 2010; Michaud, 2015; Smith, 2015). Subsequently, the analysis of liberation results in this investigation will focus on the proportions of Cu-sulphide minerals that report to the high-grade middlings and the liberated classes. In order for a change in the liberation characteristics of Cu-sulphide minerals to be deemed an enhancement, an increase in the proportions of Cu-sulphides reporting to the liberated and high-grade middlings classes would need to be achieved. As such, the >98% liberated Cu-sulphide class and >50% liberated Cu-sulphides, which could be termed the 'recoverable' material, will be analysed to assess the liberation benefits achieved through the microwave treatments.

5.5.3 MZ Ore

The grouped modal mineralogy, or 'bulk' mineral abundance, for the untreated and treated MZ ore samples is shown in Table 5.5. It can be seen in this figure that the modal mineralogy for the MZ ore is reasonably consistent across the four sub-samples. All samples have an abundance of sulphide heaters of between 5.17-5.65 wt%, and a total microwave heating mineral abundance of between 6.50-7.34 wt%. There is minor variation between the gangue composition of the UT1 sample and the microwave treated samples, with the UT1 sample having slightly less quartz and slightly more feldspars and micas. This variation produces a slight disparity in the proportions of hard and soft gangue minerals when comparing between the untreated and treated samples. It appears that the source of this variation in gangue minerals may potentially be related to the microwave treatment or materials handling process, as a similar effect is also observed in the QZ ore. The variation in composition is limited to between the

untreated and treated samples. Between the three different treated samples, the gangue composition is reasonably consistent.

It is also interesting to note that there are minor differences between the modal mineralogy of the coarse ore fragments and the results for the particulates, with the coarse ore showing lower abundances of sulphide minerals. As previously mentioned, the coarse ore fragment study was primarily conducted to investigate ore textures and mineral associations in their native state, rather than provide representative modal mineralogy data. As such, the modal mineralogy produced in the particulate analysis study could be deemed to be more reliable than the coarse ore results, for assessing the influence of mineral abundances and gangue composition on the benefits derived from the microwave treatments.

MZ Ore Grouped Mineral Abundance (wt %)									
Grouped Minerals			UT1	T1	T2	T3	AVE	Std Dev.	CoV %
Good Heaters	Copper Sulphides	Chalcopyrite	1.09	1.02	0.98	1.06	1.03	0.05	5
		Other Cu Sulphides	0.02	0.07	0.06	0.06	0.05	0.02	40
	Other Sulphides	Pyrite	4.21	4.43	4.13	4.53	4.32	0.19	4
		Other Sulphides	0.02	0.01	0.01	0.01	0.01	0.01	71
Other Heaters	Non-sulphide	Montmorillonite	0.93	1.27	1.11	1.18	1.12	0.14	13
		Iron Oxides	0.24	0.44	0.35	0.52	0.38	0.12	31
Non-heating Gangue	Hard Gangue Mohs ≥6	Quartz	35.40	38.00	39.10	38.85	37.84	1.69	4
		Feldspar	32.55	29.10	30.15	28.50	30.08	1.79	6
		Other Hard	1.58	3.68	3.40	4.45	3.28	1.22	37
	Soft Gangue Mohs <6	Micas	23.20	20.55	19.50	19.85	20.78	1.67	8
		Carbonates	0.21	0.43	0.50	0.45	0.40	0.13	33
		Other Soft	0.00	0.00	0.00	0.00	0.00	0.00	0
	Others		0.60	0.95	0.74	0.60	0.72	0.17	23
	Total		100	100	100	100	100		
	All Sulphide Heaters		5.34	5.52	5.17	5.65	5.42	0.21	4
	Good Heaters		6.26	6.78	6.27	6.82	6.53	0.31	5
	All Heaters		6.50	7.22	6.62	7.34	6.92	0.42	6
	Hard Gangue Minerals		69.53	70.78	72.65	71.80	71.19	1.35	2
	Soft Gangue Minerals		23.41	20.98	20.00	20.30	21.17	1.55	7

Table 5.5 MZ grouped mineral abundance for untreated and treated samples. [Other Cu-Sulphides comprises bornite, chalcocite, covellite; Other Sulphides comprises molybdenite, sphalerite; Iron Oxides comprises magnetite, hematite; Other Hard comprises zircon, pyroxenes/amphiboles, apatite; Other Soft comprises talc, gypsum fluorite; Micas comprises muscovite, phlogopite, biotite, chlorite; Carbonates comprises calcite, dolomite, siderite.]

The distribution of Cu-sulphide minerals by liberation class for the fine grind and coarse grind MZ samples are shown in Figure 5.7. At the finer P_{80} 150µm grinds, increases of Cu-sulphide reporting to the >98% liberation class of between ~7-12% are observed for the microwave treated samples when compare to the untreated control. All treated samples at the grind P_{80} of 425µm show ~4% greater total Cu-sulphide liberation than for the untreated sample at a grind P_{80} of 370µm. While the liberation improvement may not appear as great at the coarse grind sizes, it is important to highlight that the microwave treated samples were milled to a final grind size with a P_{80} 55µm coarser than the untreated sample, and still resulted in considerable improvements in Cu-sulphide liberation.

Observations of the 50-98% liberation classes generally show a decrease in the proportion of Cu-sulphides in this class in both the fine and coarse grind microwave treated samples compared to the untreated. These results suggest that Cu-sulphides occurring in the high-grade middlings class are being 'split', or separated from the other minerals comprising these binary or multiphase particles, and are moving into the >98% liberated class. This indicates that the microwave treatment has successfully altered the properties of the MZ ore, and promoted the preferential liberation of Cu-sulphide minerals through the generation of intergranular micro-fractures, according to the mechanisms presented in detail in Section 2.3.2. The 'splitting' of the middlings particles is also observed in the low-grade middlings, with these Cu-sulphide grains also moving into a higher liberation class. It is the re-distribution of previously locked Cu-Sulphide minerals from the middlings classes that accounts for the increases observed in the >98% liberated class.

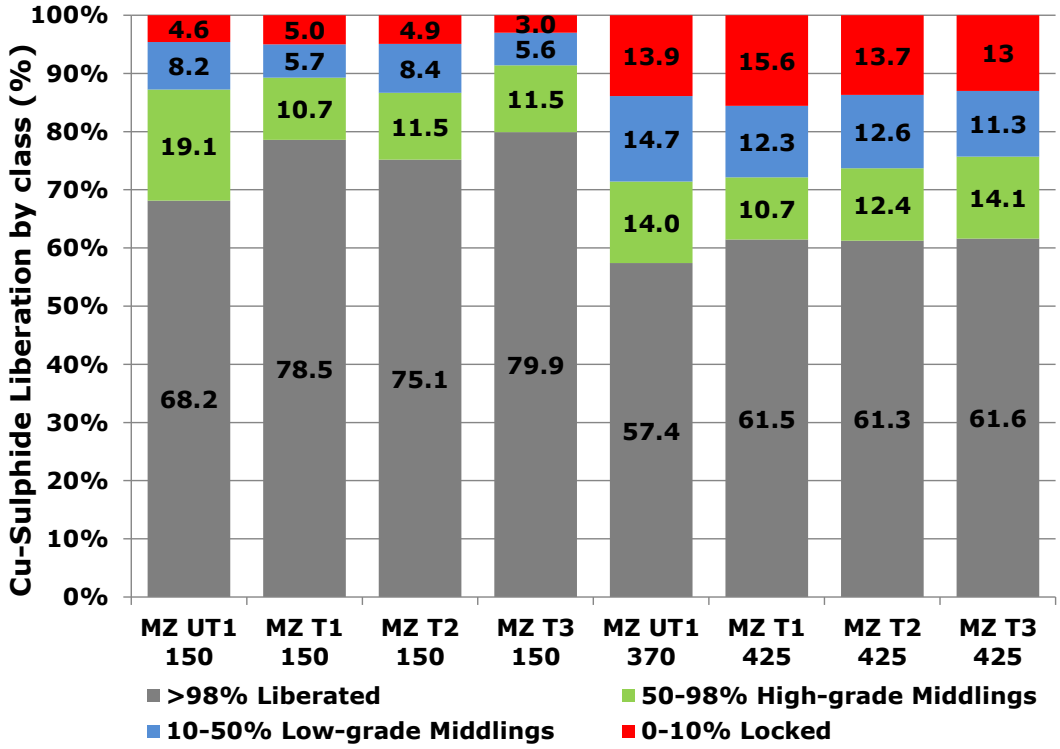


Figure 5.7 MZ ore Cu-sulphide distribution by liberation class.

The overall increase in the proportion of Cu-sulphides reporting to the >98% liberation class in both fine and coarse grinds for the MZ ore, are illustrated in Figure 5.8. As would be expected, the coarser grinds show a lower proportion of liberated Cu-Sulphides than the finer grinds. If a linear relationship is assumed between the liberation results for the fine and coarse grinds, it would indicate that equivalent Cu-sulphide liberation could be achieved in a microwave treated MZ ore at a grind P_{80} of ~300µm as for the untreated ore at a grind P_{80} of ~150µm.

An important aspect to highlight in these results is that there is no clearly observable difference between the liberation results for samples treated at different microwave energy inputs. The results for the T1, T2 and T3 samples are all relatively consistent in terms of the liberation improvements seen following the microwave treatments. This important finding suggests that the microwave treatment power density and energy input 'threshold', or the minimum conditions required for liberation improvements to be achieved in MZ ore, is equal to or less than $3.3x10^6 W/m^3$ and 0.7kWh/t. Additional microwave

power or energy input beyond these levels up to $5.3x10^6 W/m^3$ and 1.3kWh/t appears to have no further measurable beneficial effect on liberation of Cu-sulphide minerals in MZ ore. This microwave treatment threshold effect has been previously observed by several researchers (Kingman et al., 2004a; Jones et al., 2007; Ali and Bradshaw, 2010; Batchelor et al., 2015), and indicates that an optimum relationship exists between the microwave treatment conditions and the liberation benefits achieved for an ore of a given mineralogy.

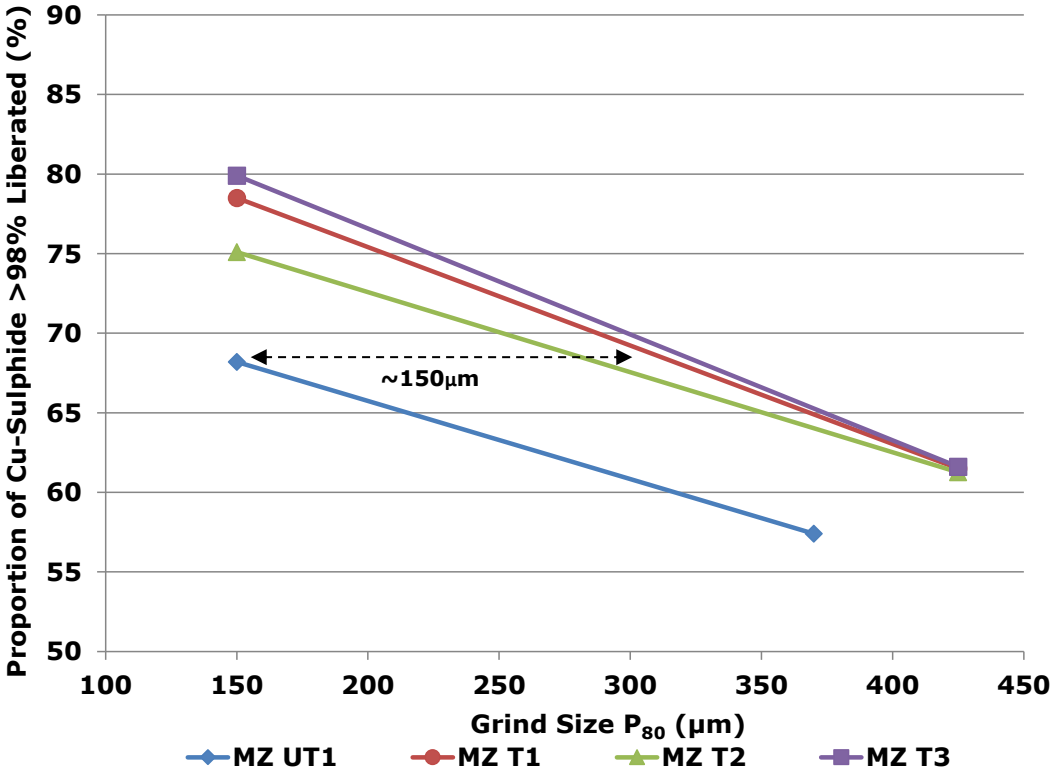


Figure 5.8: Cu-sulphide liberation (>98%) comparison for MZ untreated and treated samples at 150, 370 and 425 µm grind sizes. The dashed line highlights equivalent liberation occurring at ~150µm coarser in the microwave treated ores.

In comparison to the improvements seen in the >98% liberated Cu-Sulphide class, the liberation improvements in the >50% liberation class are less pronounced. While there appears to be an overall trend towards improvements in the >50% liberated or recoverable Cu-sulphides in the treated samples, it appears that the considerable improvements seen in the >98% liberation class resulted primarily from the splitting of middlings particles, rather than upgrading of

locked particles. The magnitude of the increases seen in the >50% liberated Cu-sulphide class are similar to the decreases seen in the 10-50% low-grade middlings class. This finding suggests that overall improvements in recoverable Cu-sulphide minerals can be attributed to the unlocking and redistribution of Cu-sulphides from low-grade middlings particles to more liberated classes. This enhanced ability to unlock Cu-sulphides from gangue minerals in binary or multiphase particles is one of the primary aims of the high power microwave treatment of copper ores.

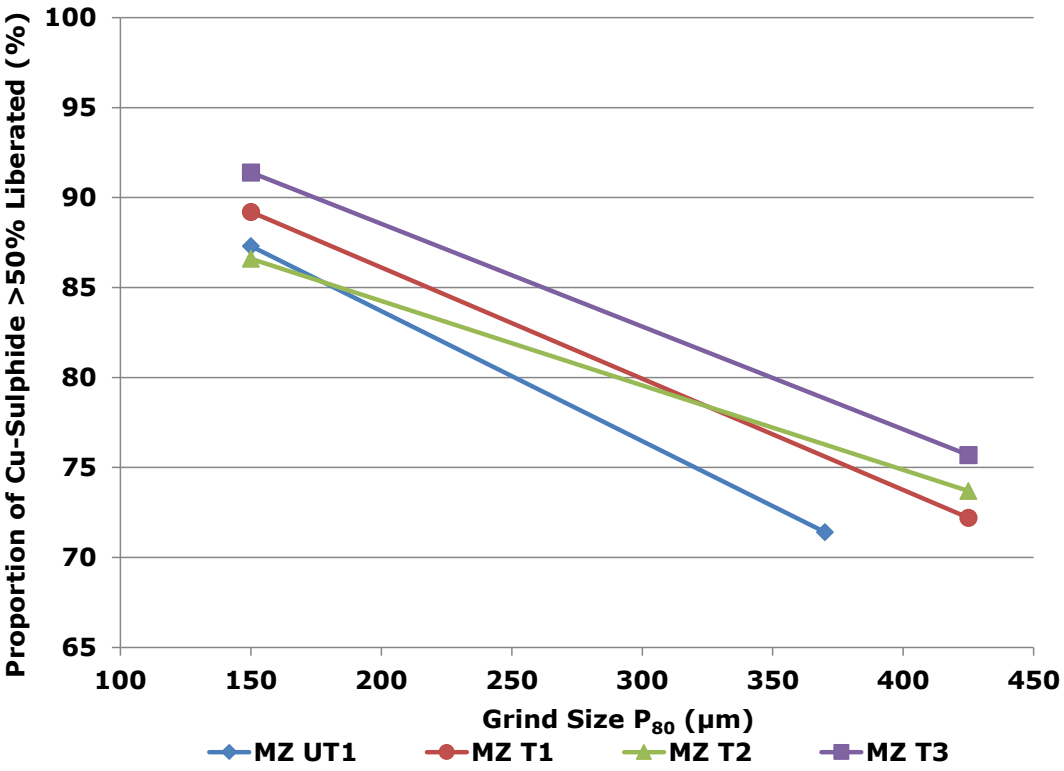


Figure 5.9 Cu-sulphide liberation (>50%) comparison for MZ untreated and treated samples at 150, 370 and 425 µm grind sizes.

The degree of unlocking of Cu-sulphides from gangue minerals can be determined from automated mineralogy measurements, as described in Section 4.4.3.4. Mineral locking data for Cu-sulphides occurring as binary particles with non-sulphide gangue (NSG) minerals (i.e. quartz, feldspars, micas) is shown in Figure 5.10. This figure clearly shows the reductions in the proportion of Cu-sulphide:NSG binary particles between the untreated and microwave treated samples. A ~6-11% reduction is seen in these binary particles, attributable to intergranular

fracturing and preferential breakage occurring in the microwave treated samples. This reduction in Cu-sulphide:NSG binary particles would account for the decreases seen in the proportions of the low-grade and high-grade middlings particles, due to the splitting and liberation of the Cu-sulphides from the gangue.

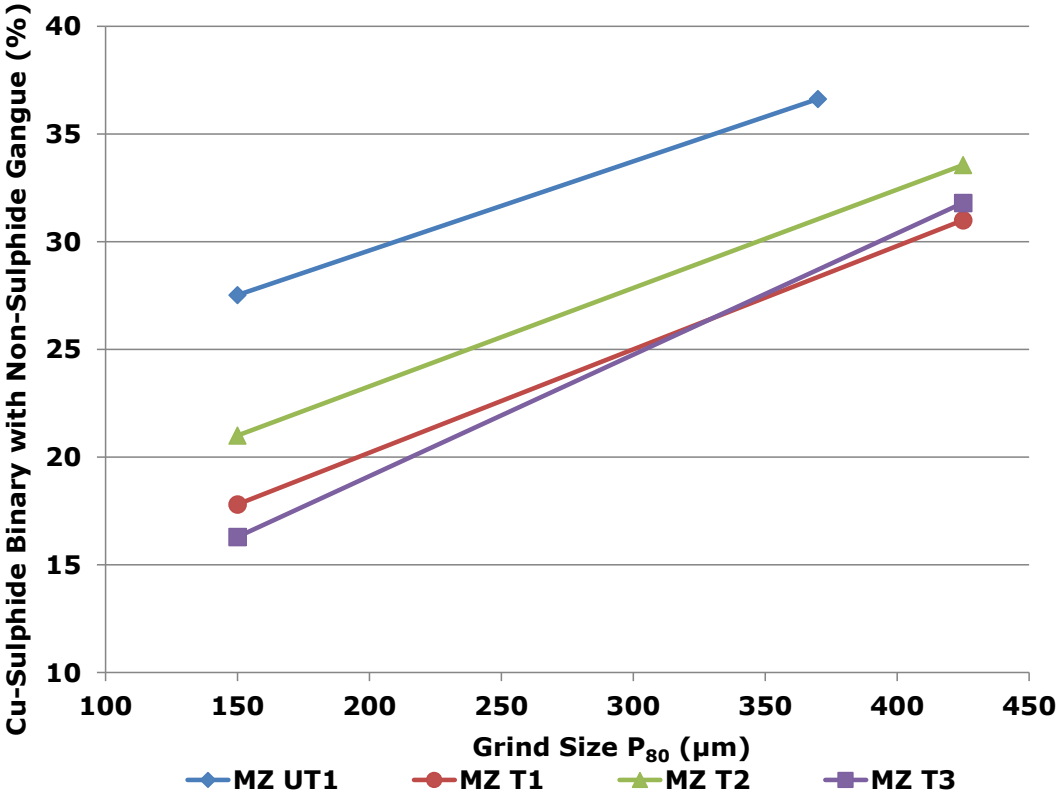


Figure 5.10 MZ ore mineral locking data for Cu-sulphides occurring in binary particles with non-sulphide gangue.

The behaviour of Cu-sulphide:pyrite binary particles was also investigated, and is shown in Figure 5.11. The changes observed between untreated and treated samples are typically within ±1%, and no consistent trends are observable. This observation is most likely due to the relatively low Cu-sulphide to pyrite mineral associations of only ~7% in the MZ ore. As the minerals are not strongly associated in the ore to begin with, there is only a low abundance of Cu-sulphide:pyrite binary particles able to be spilt. The locking of Cu-sulphides in multiphase particles is shown in Figure 5.12. While the fine grind appears to show a minor reduction in multiphase particles in the microwave treated ores, the difference is within 1%, and could not be deemed to be conclusive.

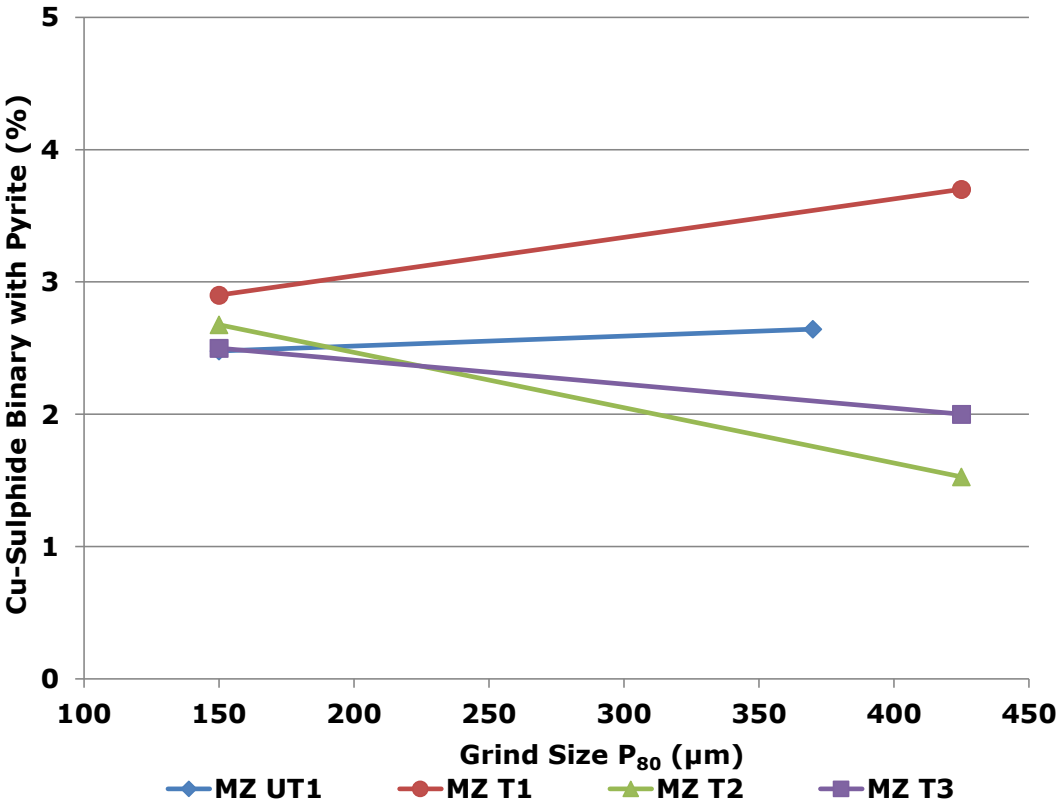


Figure 5.11 MZ ore mineral locking data for Cu-sulphides occurring in binary particles with pyrite.

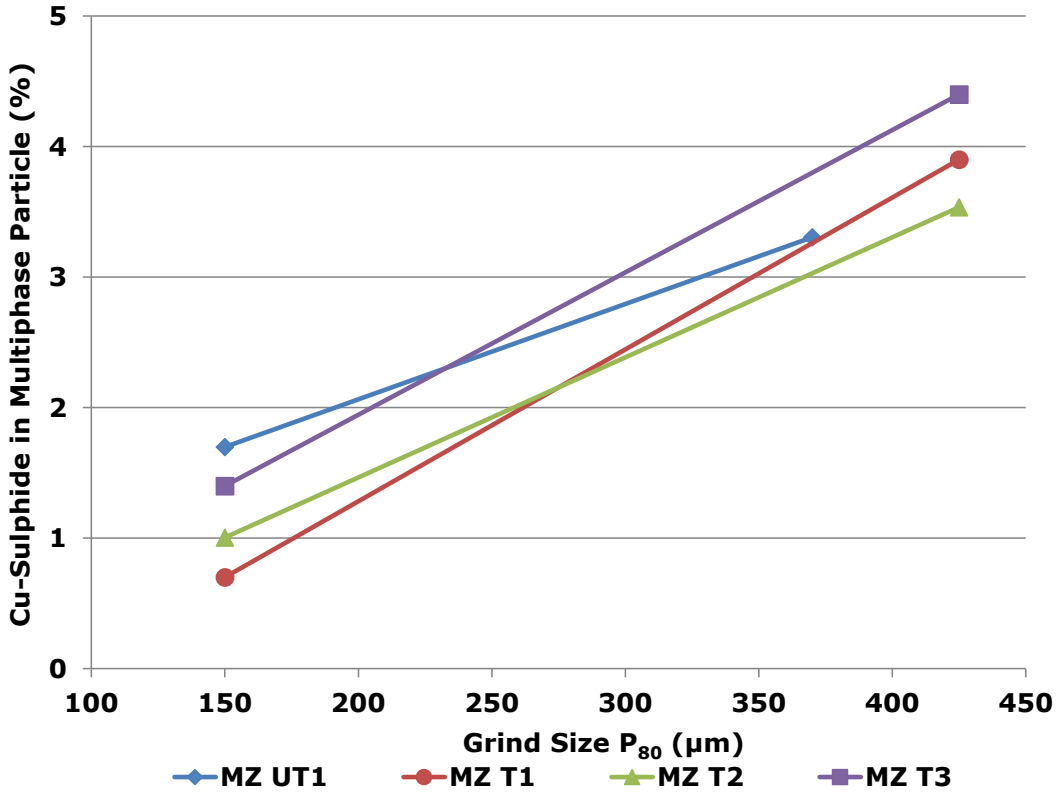


Figure 5.12 MZ ore mineral locking data for Cu-sulphides occurring in multiphase particles.

Analysis of the liberation and locking of Cu-sulphide minerals following the microwave treatment of MZ ore has shown an enhancement of liberation in the treated samples compared to the untreated. This improved Cu-sulphide liberation is attributed to intergranular micro-fractures produced during microwave treatment, and through subsequent preferential breakage leading to liberation of Cu-sulphide grains by detachment. As was previously described, it is through the preferential weakening of the interfaces and matrix between certain mineral grains that liberation by detachment can be achieved (Hsih and Wen, 1994). This preferential breakage mechanism and liberation by detachment is further evidenced by the reduction in Cu-sulphide:NSG binary particles, and the splitting of the middlings liberation classes.

5.5.4 QZ Ore

The grouped modal mineralogy for the untreated and treated QZ ore samples are shown in Table 5.6. As for the MZ ore, it can be seen that the modal mineralogy for the QZ ore is reasonably consistent across the four sub-samples. All samples have an abundance of sulphide heaters of between 2.14-2.19 wt%, and a total microwave heating mineral abundance of between 2.44-2.50 wt%. Similar to the MZ ore, there is minor variation between the gangue composition of the UT sample and the microwave treated samples, with the UT sample having slightly less quartz and slightly more feldspars and micas. Again, this variation produces a slight disparity in the proportions of hard and soft gangue minerals when comparing between the untreated and treated samples.

The QZ ore differs from the MZ ore in terms of its microwave treatment amenability characteristics, having a lower abundance of microwave heating minerals of ~2.50%, compare to ~6.50-7% for the MZ ore. The QZ ore does however have a higher proportion of hard gangue than the MZ ore (~90% and ~70% respectively), and subsequently a higher association between heating minerals and the

hard gangue. While the QZ ore has a lower abundance of microwave heating minerals, the presence of a gangue dominated by hard and brittle quartz could be expected to more effectively transfer stresses through the ore fragments than in the MZ ore.

QZ Ore Grouped Mineral Abundance (wt %)									
Grouped Minerals			UT	T1	T2	T3	AVE	Std Dev.	CoV %
Good Heaters	Copper Sulphides	Chalcopyrite	1.00	1.12	1.04	1.00	1.04	0.06	5
		Other Cu Sulphides	0.47	0.42	0.45	0.45	0.45	0.02	4
	Other Sulphides	Pyrite	0.71	0.62	0.64	0.68	0.66	0.04	6
		Other Sulphides	0.01	0.03	0.02	0.02	0.02	0.01	37
	Non-sulphide	Montmorillonite	0.04	0.03	0.04	0.03	0.03	0.00	14
Other Heaters		Iron Oxides	0.23	0.29	0.27	0.26	0.26	0.03	10
Non-heating Gangue	Hard Gangue Mohs ≥6	Quartz	87.80	89.50	89.55	89.55	89.10	0.87	1
		Feldspar	2.19	1.76	1.72	1.68	1.84	0.24	13
		Other Hard	0.10	0.10	0.13	0.09	0.11	0.02	16
	Soft Gangue Mohs <6	Micas	7.22	6.03	5.99	5.98	6.30	0.61	10
		Carbonates	0.12	0.03	0.05	0.08	0.07	0.04	58
		Other Soft	0.00	0.00	0.00	0.00	0.00	0.00	0
	Others		0.11	0.12	0.17	0.14	0.13	0.02	18
	Total		100	100	100	100	100		
	All Sulphide Heaters		2.19	2.18	2.14	2.15	2.16	0.02	1
	Good Heaters		2.23	2.21	2.17	2.18	2.20	0.03	1
	All Heaters		2.45	2.50	2.44	2.44	2.46	0.03	1
	Hard Gangue Minerals		90.09	91.36	91.40	91.32	91.04	0.64	1
	Soft Gangue Minerals		7.34	6.05	6.04	6.06	6.37	0.64	10

Table 5.6 QZ grouped mineral abundance for untreated and treated samples. [Other Cu-Sulphides comprises bornite, chalcocite, covellite; Other Sulphides comprises molybdenite, sphalerite; Iron Oxides comprises magnetite, hematite; Other Hard comprises zircon, pyroxenes/amphiboles, apatite; Other Soft comprises talc, gypsum fluorite; Micas comprises muscovite, phlogopite, biotite, chlorite; Carbonates comprises calcite, dolomite, siderite.]

The distribution of Cu-sulphide minerals by liberation class for the fine grind and coarse grind QZ samples are shown in Figure 5.13. The finer P_{80} 150µm grinds show increases of Cu-sulphides reporting to the >98% liberation class of between ~6-10% for the microwave treated samples, when compare to the untreated control. QZ T1 and T3 treated samples at the grind P_{80} of 425µm show ~6% greater total Cu-sulphide liberation than for the untreated sample at a grind P_{80} of 370µm. The T2 sample however, shows essentially no change from the untreated at the coarse grind. As for the MZ ore, it is again important to note that the microwave treated samples were milled to a final grind size with a P_{80} 55µm coarser than the untreated sample. A challenge in using the QZ ore for assessing benefits in liberation from

microwave treatment is that even in the untreated ore, Cu-sulphide minerals are already very highly liberated during grinding. This means that the window for enhancing Cu-sulphide liberation in this particular ore is very small. .This is clearly shown in the Cu-sulphide liberation distributions, where the untreated ore has over ~92% of Cu-sulphides already in the high-grade middlings and >98% liberated groups for the P_{80} 150µm grind, and ~81% for the P_{80} 370µm grind.

As was seen for the MZ ore, there is no observable difference in liberation benefits achieved in the QZ ores treated at different microwave conditions. This again suggests that the threshold at which liberation enhancements occur in QZ ore is equal to or less than $3.3x10^6 W/m^3$ and 0.7kWh/t.

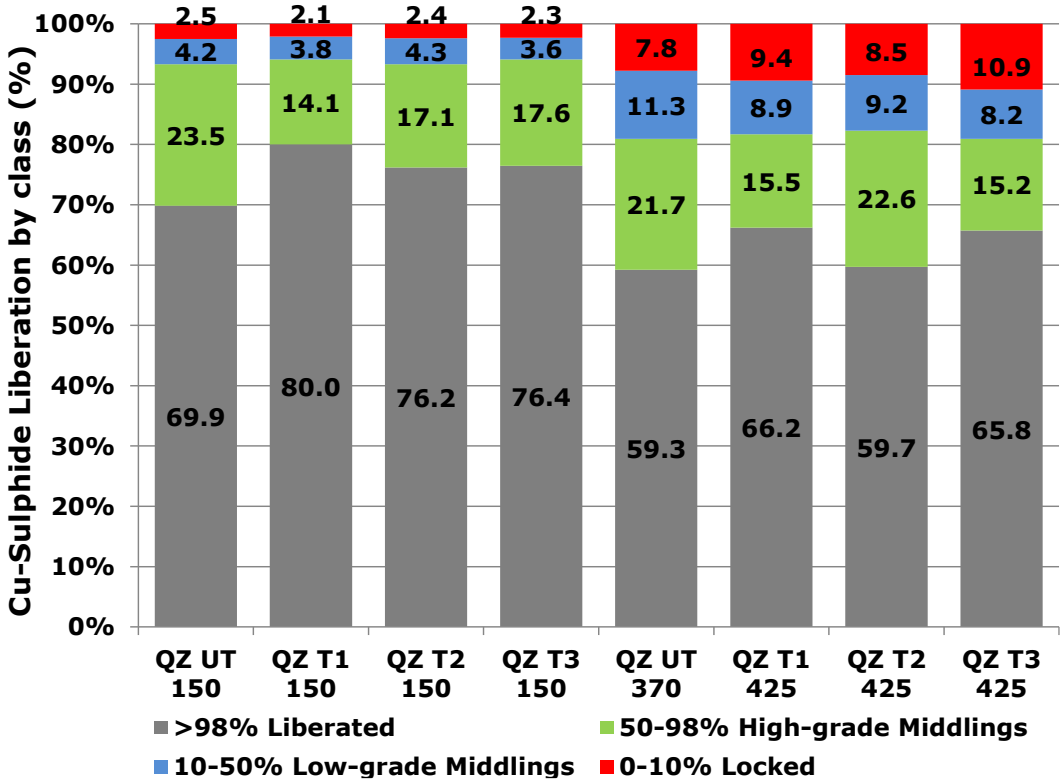


Figure 5.13 QZ ore Cu-sulphide distribution by liberation class.

It can be seen in Figure 5.14 that improvements have been achieved in terms of Cu-sulphides reporting to the >98% liberation class due to upgrading of high-grade middlings particles. There is very little change however in the proportion of Cu-sulphides reporting to the

>50% liberation class, as shown in Figure 5.15. It appears from these results that the microwave treatment is enabling the splitting of the high-grade middlings particles, and re-distributing the Cu-sulphides into the >98% liberated class, while not having a significant effect on upgrading the low-grade middlings or locked particles. There does appear to be an improvement in the >50% Cu-sulphide liberation results for the coarse grind due to the difference in grind size P_{80} between the untreated and microwave treated samples, assuming that a linear relationship exists between the Cu-sulphide liberation results at the different grind sizes. Testing the relationship between changes in Cu-sulphide liberation at a greater number of different grind sizes of untreated and microwave treated ores would be a potential avenue for future work in this field.

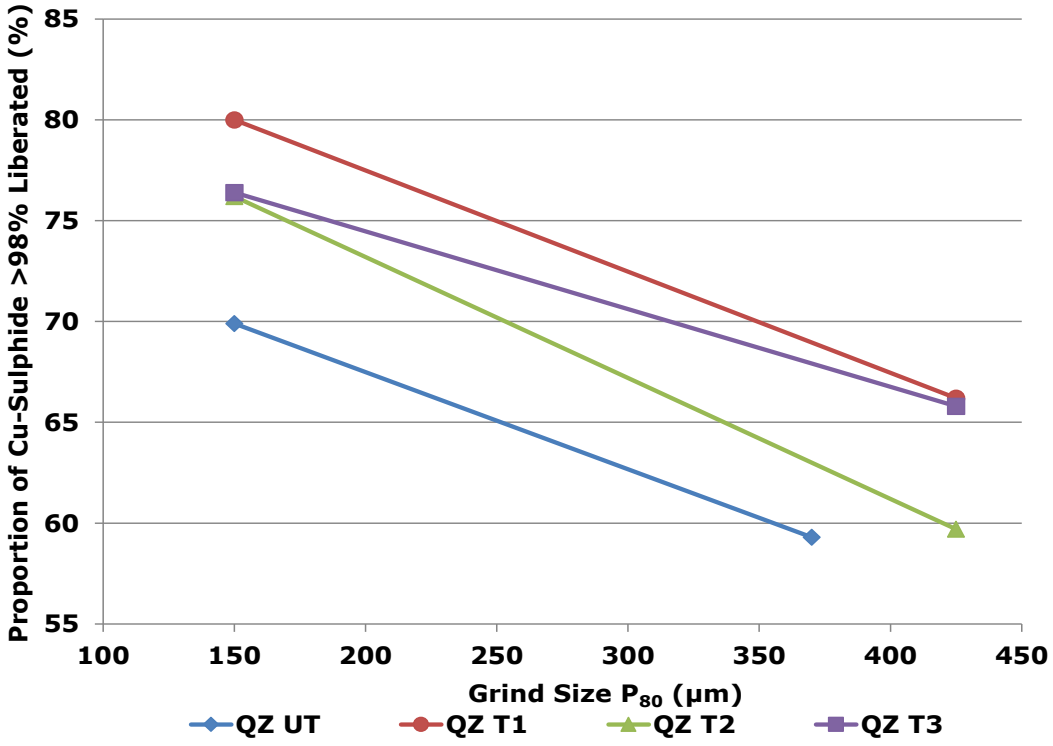


Figure 5.14: Cu-sulphide liberation (>98%) comparison for QZ untreated and treated samples at 150, 370 and 425 µm grind sizes.

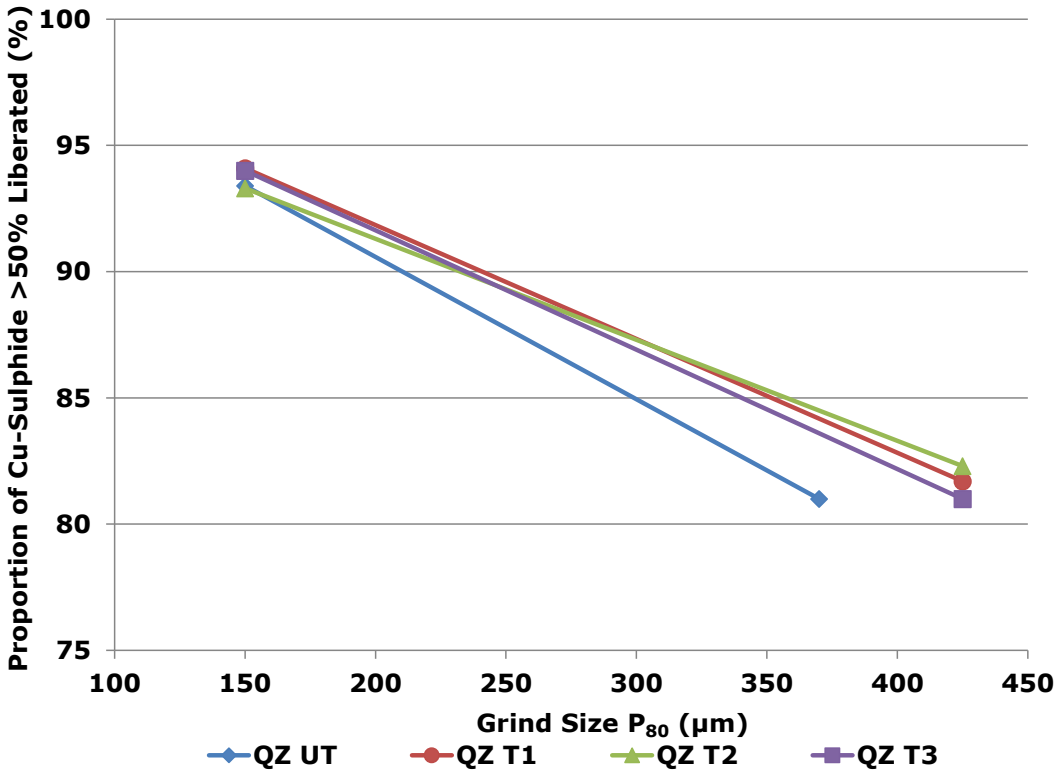


Figure 5.15 Cu-sulphide liberation (>50%) comparison for QZ untreated and treated samples at 150, 370 and 425 µm grind sizes.

Similar to the MZ ore, the effect of splitting the high-grade middlings particles is seen in the changes in mineral locking for Cu-sulphide:NSG binary particles between untreated and treated samples. A clear reduction in the proportion of Cu-sulphides occurring in binary particles with NSG is observable in Figure 5.16. The splitting in Cu-sulphide:NSG binary particles results in the higher proportions of >98% liberated Cu-sulphide observed in the microwave treated samples. The mineral locking data for Cu-sulphides with pyrite shown in Figure 5.17 is inconclusive, showing no clear difference between untreated and treated samples. There is however, a minor observable difference between untreated and treated samples in the proportions of Cu-sulphide minerals occurring in multiphase particles, as shown in Figure 5.18. This could be interpreted as preferential breakage occurring of these complex multi-mineral particles following microwave treatment.

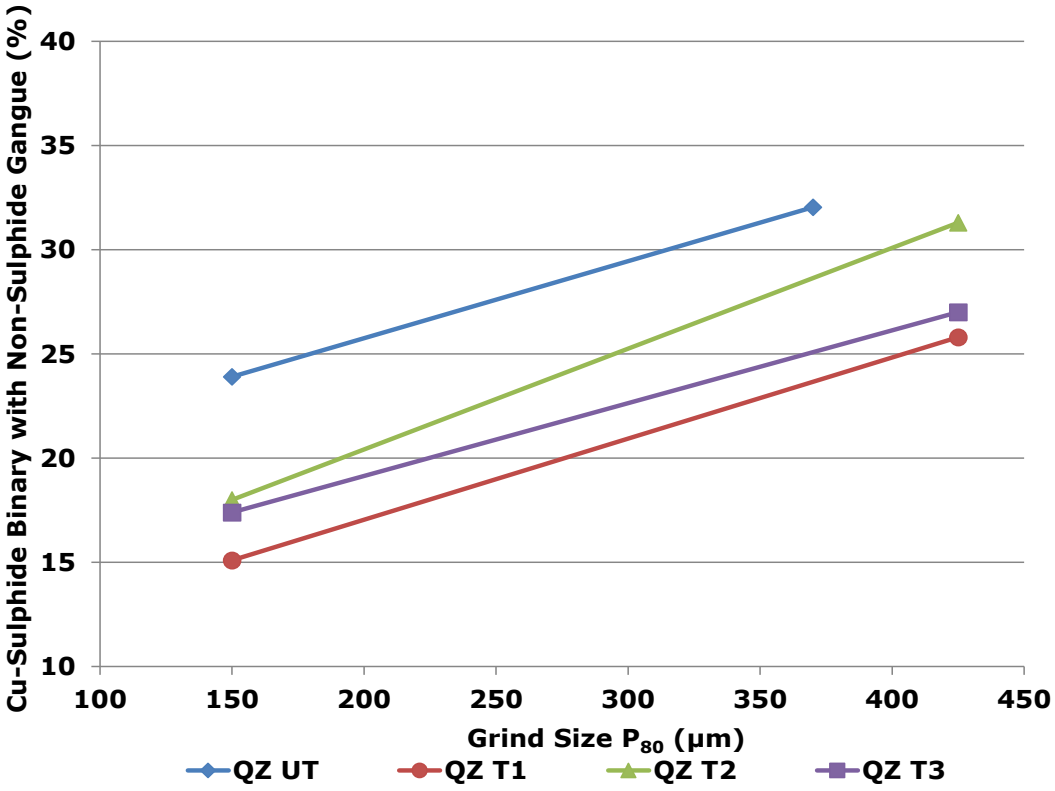


Figure 5.16 QZ ore mineral locking data for Cu-sulphides occurring in binary particles with non-sulphide gangue.

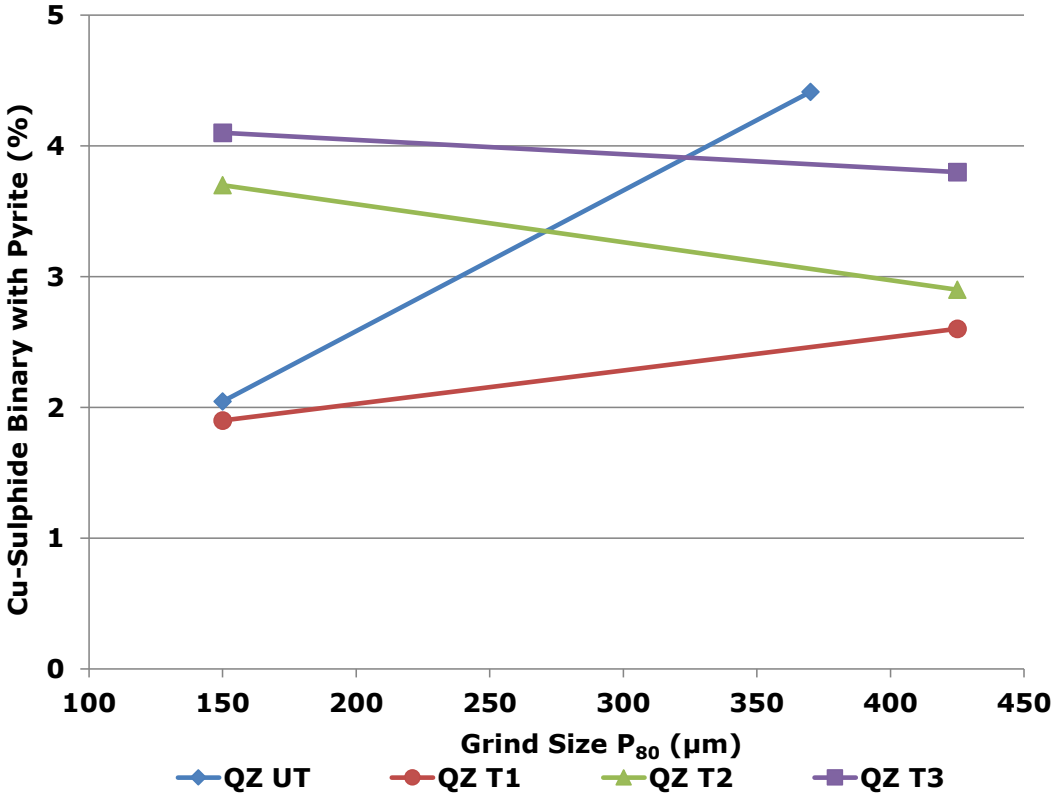


Figure 5.17 QZ ore mineral locking data for Cu-sulphides occurring in binary particles with pyrite.

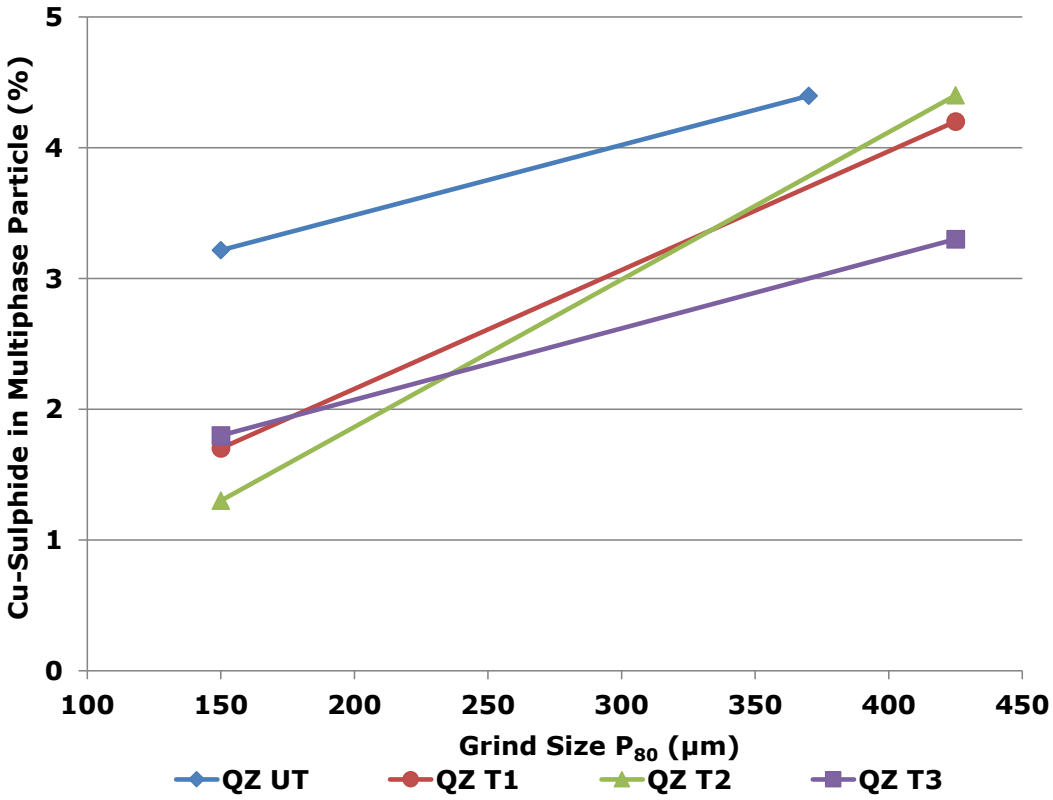


Figure 5.18 QZ ore mineral locking data for Cu-sulphides occurring in multiphase particles.

Despite QZ ore having only very small room for improvement in terms of enhancing liberation of Cu-sulphide minerals through microwave treatment, splitting of high-grade middlings and increases in the proportion of Cu-sulphides reporting to the >98% liberated class were observed. This indicates that preferential breakage is occurring following microwave treatment due to the formation of micro-fractures around the grain boundaries of microwave heating minerals in the ore.

5.5.5 Summary of Liberation Results

Figure 5.19 and Figure 5.20 show the relationship between the beneficial change in the >98% liberated Cu-sulphide class resulting from the microwave treatments conducted at varying microwave doses and power densities. It is important to remember that the beneficial change being reported for the microwave treated grinds with a P_{80} of 425µm, is in comparison to a P_{80} 350µm grind for the untreated sample. A greater beneficial change in Cu-sulphide liberation is

observed for both ores at the finer grind than for the coarser grind. This suggests that the effects of microwave treatments can potentially be exploited for finer grained ores which required grinding to 150μm, or possibly finer. It can be clearly identified in these figures that the threshold at which liberation enhancement occurs for both MZ and QZ ores is equal to or less than a microwave power density of $3.3x10^6W/m^3$, and a total microwave energy input of 0.7kWh/t. Anomalous results produced for the QZ T2 treatment are potentially related to the inherent textural characteristics of this particular sample making it harder to liberate. The results could also be interpreted as being due to a less effective microwave treatment being performed for the QZ T2 sample, in comparison to the T1 and T3 samples, potentially related to arcing in the applicator affecting the delivery of microwave power into the ore.

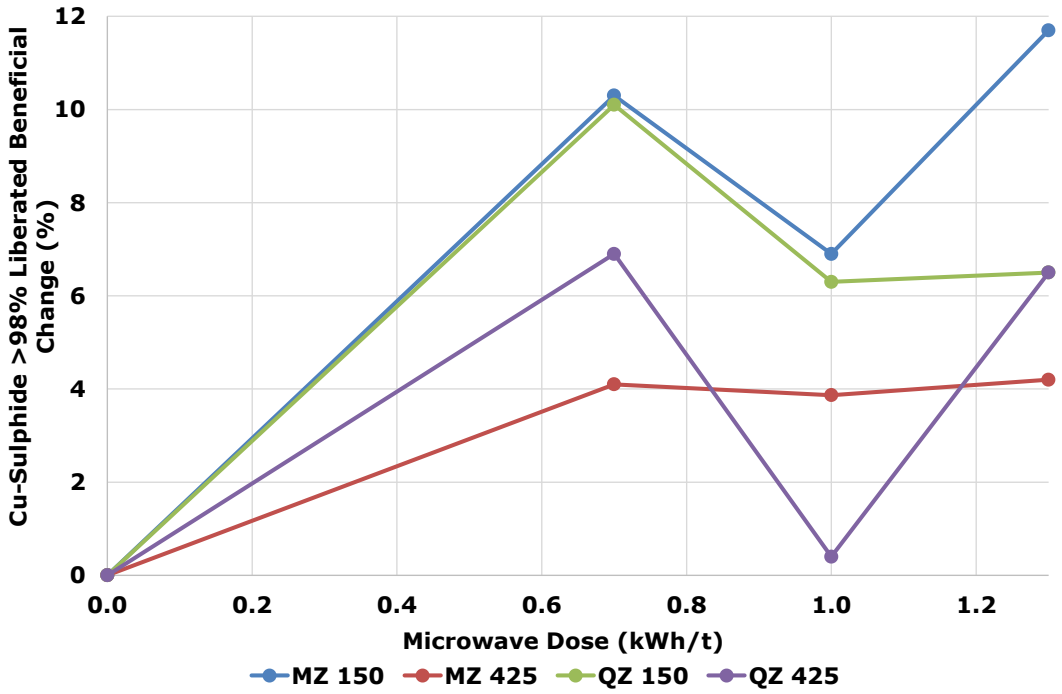


Figure 5.19 Beneficial change in >98% liberated Cu-sulphides at varying microwave treatment doses.

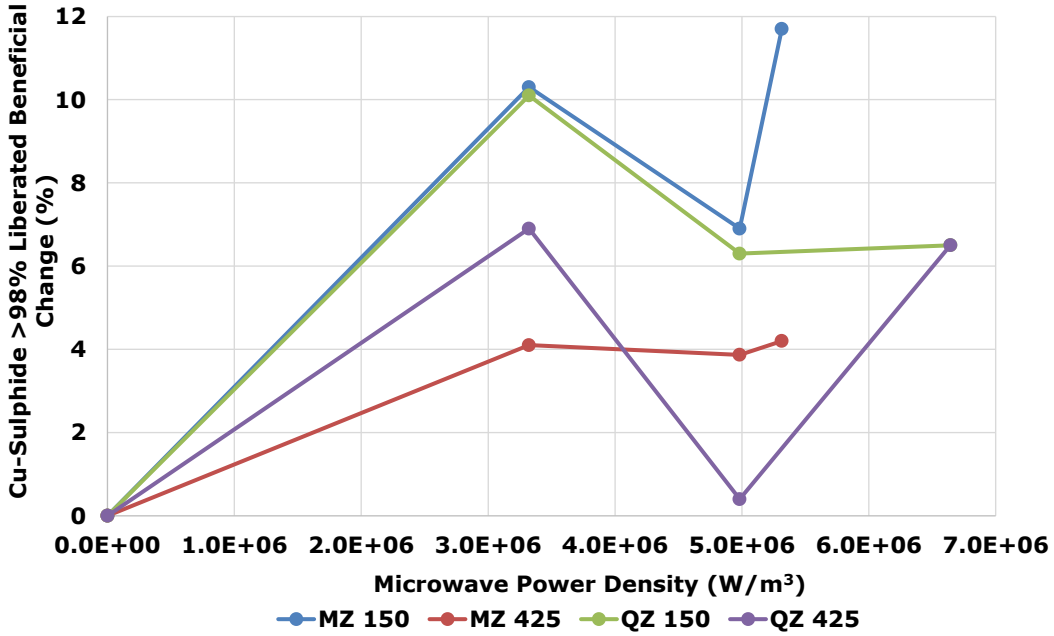


Figure 5.20 Beneficial change in >98% liberated Cu-sulphides at varying microwave treatment power densities.

5.6 Comminution Testing

5.6.1 Introduction

To investigate the comminution benefits achieved by the microwave treatments of MZ and QZ ores, untreated and microwave treated samples of each ore were subjected to comminution testing using the JK GeM Ci test and the Bond Ball Mill Work index test. If the high power microwave treatments have altered the properties of the ores through the generation and propagation of micro and macro-fractures in the ore fragments, then it could be expected that the microwave treated samples would perform better in comminution tests compared to the untreated control samples.

5.6.2 Sample Preparation and Testing Procedure

JK GeM Ci testing was conducted on representative 30kg sub-samples that were split from the 500kg bulk sample of the untreated and three microwave treated samples of the MZ and QZ ore. Sub-samples were further split into 10kg batches for Ci testing, which was conducted in triplicate for each sample to allow for the determination of confidence

levels by t-test. Each of the sub-samples were screened to produce a -31.5+26.5mm ore fragment size fraction, which was then crushed in a jaw crusher with a CSS of 11.6mm. The crusher CSS was set to achieve a fixed size reduction ratio of 2.5, based on the geometric mean ore fragment size to crusher CSS. As detailed in Section 4.5.1, the test produces three key results; two indices that are defined as CRU and GRD, and the percentage of material passing a 4.75mm sieve after crushing. In simple terms, the GRD index relates to the 'grindability' breakage behaviour of an ore, which in a microwave treatment context could be changed through the generation of fractures which alter the ore matrix of a microwave treated sample. The CRU index reflects the impact breakage response of an ore, and indicates the influence of microwave induced fractures on the 'crushability' of ore samples following microwave treatment.

An additional 30kg sub-sample was spilt from the bulk for BBMWi testing, also conducted in triplicate using three 10kg sub-samples. The BBMWi test was modified in this investigation, as it was shown that the microwave treated samples typically yielded a finer crushing product size distribution compared to the untreated sample. This was determined as being due to the impact of the microwave treatment, and was evidenced by a higher percent of crushed sample passing 4.75mm in Ci testing. To directly compare the work index of the untreated and microwave treated samples, it was necessary to artificially alter the BBMWi test feed size distribution of the microwave treated samples to be the same as the untreated sample. This modification ensured that the work index value may be used as a true comparison of any change in ore competency, and not as a result of different feed size distributions. Each size fraction was carefully adjusted to have less than a 1% relative difference to the percent retained in the same size fraction of the untreated control sample. BBMWi testing was conducted following the procedure describe in Section 4.5.2, in order to measure the specific energy required (kWh/t) to reduce the untreated and treated samples from their

original feed size to 80% passing size of 160µm, using a closing sieve size in the Work Index calculations of 212µm.

5.6.3 JK GeM Crushing Index Test Results

The results produced from Ci testing of untreated and microwave treated MZ and QZ ores are shown in Table 5.7. All the tests were conducted in triplicate, except the MZ T2 sample for which sufficient material was not available following an error during testing, and the mean results for each test outcome are shown with their respective standard deviation and coefficient of variance. The beneficial change of each index and the %-4.75mm material for the microwave treated samples in relation to the untreated control sample has also been presented.

Ore	Sample	GRD			CRU			%-4.75mm			Beneficial Change (%)			Confidence Level (%)		
		Mean	Std Dev.	CoV (%)	Mean	Std Dev.	CoV (%)	Mean	Std Dev.	CoV (%)	GRD	CRU	% - 4.75 mm	GRD	CRU	%- 4.75 mm
MZ	UT1	0.577	0.017	2.9	2.99	0.13	4.4	11.90	0.40	3.6						
	T1	0.603	0.006	0.9	3.09	0.08	2.5	16.20	0.10	0.7	-4.6	3.3	36.7	94	69	100
	T2	0.529	-	-	3.20	-	-	18.40	-	-	8.3	7.0	54.7	99	95	100
	T3	0.545	0.039	7.2	3.00	0.16	5.3	16.20	0.60	3.7	5.4	0.3	36.4	73	6	100
QZ	UT	0.493	0.006	0.8	2.94	0.17	5.9	11.80	0.70	6.1						
	T1	0.467	0.006	1.4	3.11	0.15	4.7	15.90	0.40	2.3	5.4	5.9	35.3	100	75	100
	T2	0.470	0.010	2.0	3.14	0.10	3.1	15.70	0.50	3.0	4.7	6.9	33.5	98	85	100
	T3	0.473	0.015	2.5	3.08	0.23	7.6	15.50	1.10	7.3	4.1	4.8	32.2	90	55	99

Table 5.7 JK GeM Ci test results

5.6.3.1 MZ Ore

Ci test results for the MZ ore show benefits achieved from the microwave treatments in both GRD and CRU indices, and in the percentage of material passing 4.75mm after crushing. GRD results show a change of 8.3% for the MZ T2 sample, and 5.4% for the MZ T3 sample, compared to the MZ UT1 sample. The GRD index for the MZ T1 sample showed a detrimental change compared to the untreated sample. Since the MZ T1 sample possesses similar mineralogy to the other MZ samples, this result suggests that at the lower microwave dose used for this treatment, a change in the breakage response of the ore is observed compared to samples that received higher dose

treatments. This finding for the MZ T1 sample potentially marks a threshold microwave energy input level at which the response of the ore matrix to the microwave treatment results in a different breakage outcome for the ore following crushing. CRU index results indicating a change in ore impact breakage response, show beneficial changes of 3.3% and 7% for the MZ T1 and MZ T2 samples respectively. The MZ T3 sample showed only a very minor 0.3% beneficial change at very low confidence levels.

Changes were seen at statistically significant confidence levels for all microwave treated MZ samples in terms of the percentage of material passing a 4.75mm sieve after crushing. This indicates that the properties of the ore have been altered by the microwave treatment, and a finer product size distribution is produced for treated ores following the same crushing conditions, as can be clearly seen in Figure 5.21.

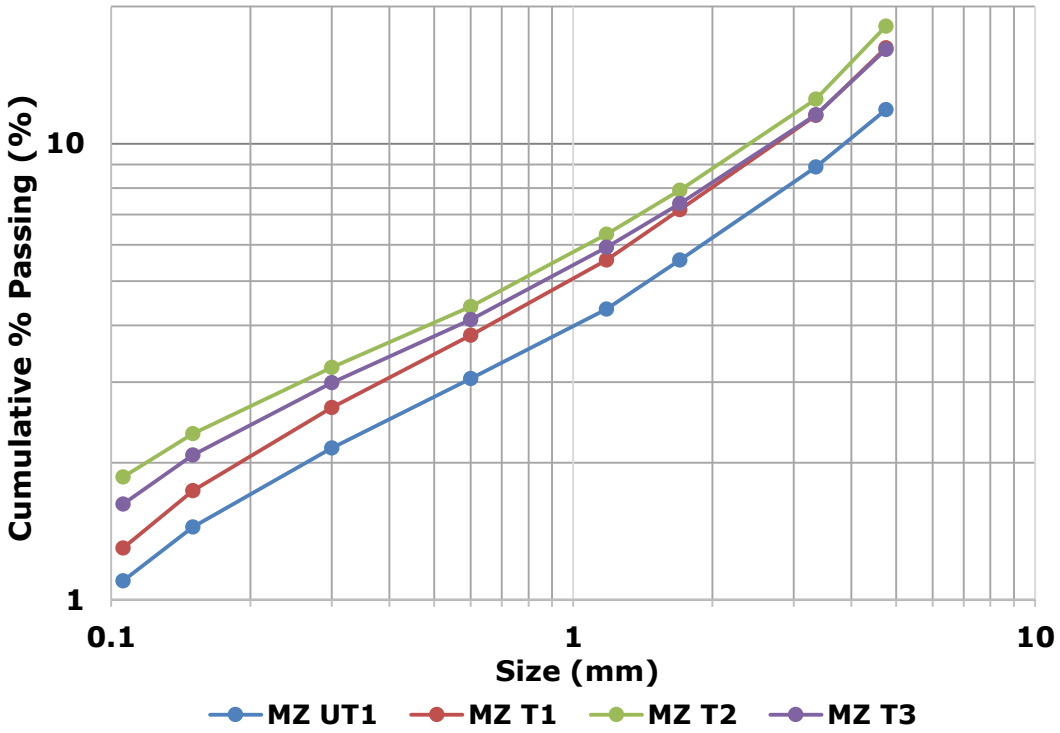


Figure 5.21 JK GeM Ci test -4.75mm product size distributions for MZ samples

Similar to the outcomes seen in the results of the MZ ore mineral liberation analysis, there appears to be no clear indication that increases in microwave energy input correspond with achieving greater comminution benefits from the microwave treatments. As beneficial changes in comminution test results were observed for all treated MZ ores, it could be surmised that changes in ore breakage response and ore strength reductions are achievable for an ore of this mineralogy at microwave treatment conditions of equal to or less than $3.3x10^6 W/m^3$ and 0.7kWh/t. The detrimental GRD result and low confidence CRU benefit of only 3.3% for the MZ T1 lowest energy microwave treated sample, do suggest that the threshold at which comminution benefits can be achieved for this ore, is potentially ~0.7kWh/t. The significant changes observed in %-4.75mm material following crushing suggest that the microwave treatments have resulted in the propagation of fracturing through the MZ ore fragments, resulting in both ore strength reductions, and more effective size reduction during crushing of microwave treated ores.

5.6.3.2 QZ Ore

Ci test results for the QZ ore show relatively consistent changes in both GRD and CRU indices, and in percentage of material passing 4.75mm. Changes in GRD index for the microwave treated ores of 4.1-5.4% were achieved at >90% confidence levels. 4.8-6.9% changes in CRU were also observed, although confidence levels on these results were lower (<85%), and results could not be deemed significant. Beneficial changes shown for %-4.75mm material following microwave treatments were also very consistent, with the treated samples producing 32.2-35.3% more -4.75mm material after crushing than the untreated sample. The consistency in these results can be seen in the -4.75mm particle size distribution data for QZ ore shown in Figure 5.22.

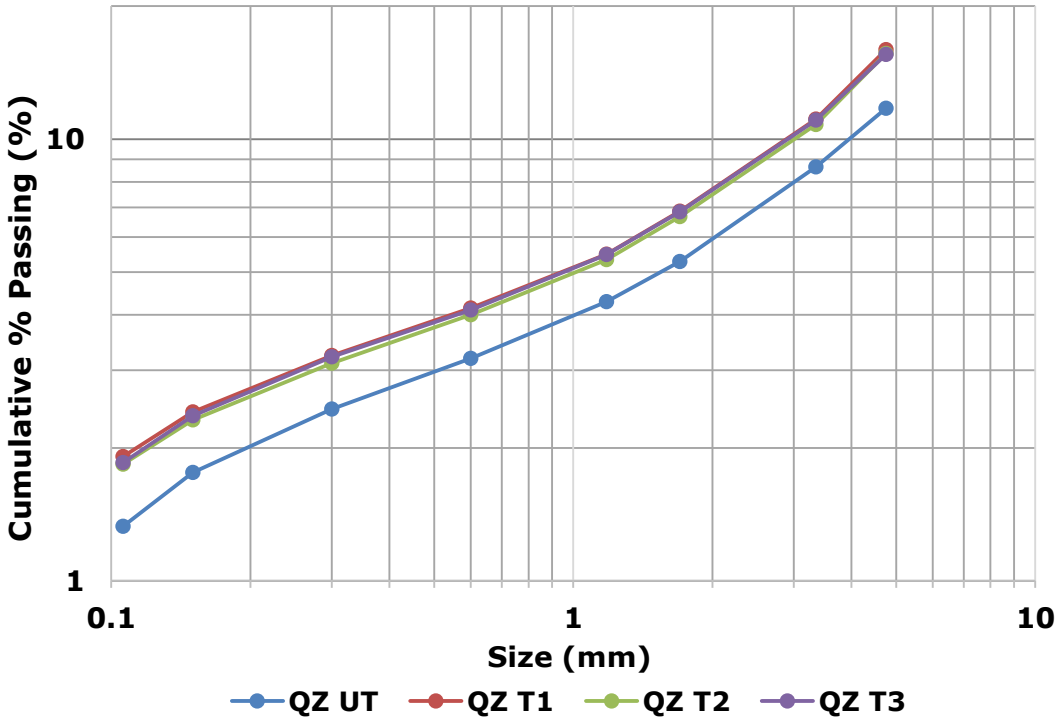


Figure 5.22 JK GeM Ci test -4.75mm product size distributions for QZ samples

The GRD and CRU index changes in the treated samples suggest that changes in both the grindability and crushability of the ore have occurred through the generation and propagation of micro and macro-fractures during the microwave treatments. The consistency in the comminution benefits achieved at the three different microwave treatment energy inputs for the QZ ore, clearly illustrates the phenomenon where, once a certain microwave energy input threshold is crossed, the input of further microwave energy produces no or minimal additional benefit. This finding is consistent with those of several researchers, which indicate that large reductions in ore competency can be achieved with short treatment durations, with diminishing returns seen with increases in the total microwave energy input beyond a certain threshold level (Kingman and Rowson, 1997; Kingman et al., 2000b; Vorster et al., 2001; Batchelor et al., 2015). The Ci test results for the QZ ore show, even more clearly than for the MZ ore, that for an ore possessing these mineralogical characteristics, microwave treatment conditions of equal to or less than $3.3x10^6 W/m^3$ and 0.7kWh/t are sufficient for changes in the breakage response of the ore to be achieved in laboratory testing.

5.6.4 Bond Ball Mill Work Index Test Results

The results produced from BBMWi testing of untreated and microwave treated MZ and QZ ores are shown in Table 5.8. All the tests were conducted in triplicate, and the mean BBMWi results for each sample are shown with their respective standard deviations and co-efficients of variance (CoV). That the co-efficients of variance of the BBMWi results for each of the samples are below the industry standard of 3.4% (Bailey et al., 2009), suggest that the changes in BBMWi have occurred as a result of the microwave treatments, rather than being due to variability in the data. The beneficial change in BBMWi for the microwave treated samples is shown in comparison to the untreated sample.

Ore	Sample	F_{80} (µm)		P_{80} (µm)		Gbp (g/rev)		BBMWi (kWh/t)			Beneficial Change (%)	Confidence Level (%)
		Mean	Std Dev.	Mean	Std Dev.	Mean	Std Dev.	Mean	Std Dev.	CoV (%)		
MZ	UT1	2140	37	156	0.6	2.03	0.03	13.69	0.17	1.3		
	T1	2112	14	157	0.6	2.28	0.03	12.50	0.10	0.8	8.7	100
	T2	2135	21	157	0.6	2.18	0.04	13.00	0.21	1.6	5.0	99
	T3	2134	17	158	1.0	2.26	0.03	12.69	0.11	0.8	7.3	100
QZ	UT	2061	16	161	0.6	3.39	0.10	9.27	0.21	2.3		
	T1	2038	3	162	0.6	3.45	0.05	9.19	0.08	0.9	0.9	44
	T2	2057	24	161	0.6	3.50	0.03	9.03	0.06	0.7	2.5	86
	T3	2047	3	162	0.6	3.42	0.02	9.23	0.02	0.3	0.4	24

Table 5.8 BBMWi test results, Gbp = ball mill grindability, (g/rev), P_{80} = size at which 80% of the product passes, (µm), F_{80} = size at which 80% of the feed passes, (µm).

5.6.4.1 MZ Ore

BBMWi test results for the MZ ore show that with BBMWi values for the untreated ore of 13.69kWh/t, it is inherently a medium-hard strength ore, considering the ranges described in Section 4.5.2. BBMWi benefits of 8.7%, 5.0% and 7.3% were achieved for the MZ T1, T2 and T3 samples respectively at a statistically significant level of confidence, compared to the untreated sample. These benefits indicate that significant reductions in ore grinding energy consumption could be achieved through the microwave treatment of MZ ore. Similar to the Ci test results, it can be seen that no clear relationship exists between

increases in microwave treatment energy input and the benefits achieved.

5.6.4.2 QZ Ore

BBMWi test results for the QZ ore show that the untreated sample possesses a BBMWi of 9.27kWh/t, indicating that it behaves as quite a soft ore during comminution compared to the MZ ore. Benefits of 0.4-2.5% were achieved in terms of BBMWi reductions in microwave treated QZ samples, and could not be deemed as statistically significant. This outcome indicates that fractures in the ore induced during the microwave treatment were largely utilised in achieving the crushing benefits seen for the QZ treated samples in Ci testing. Similar to what was seen for the QZ untreated sample with regards to already exhibiting very high liberation of Cu-sulphides after grinding, the QZ untreated sample is already quite a soft and easily comminutable ore. As such, the potential for further weakening an already soft ore is quite limited. Interestingly, it is the hard and brittle dominant gangue minerals of the ore that suggest it would be it amenable to microwave treatment, that also mean it fractures readily and is characterised as being soft in terms of its comminution behaviour. In contrast, the MZ ore which was deemed to have a less amenable gangue composition for microwave treatment, is actually a harder ore in comminution, and subsequently has a greater potential for benefits in ore strength reduction to be achieved.

5.6.5 Summary of Comminution Test Results

It has been shown by the comminution test results that changes in ore strength reduction and improved grindability of both MZ and QZ ores are achievable at equal to or less than a microwave power density of $3.3x10^6 W/m^3$ and a total microwave energy input of 0.7kWh/t. This finding is the same as was observed for the mineral liberation results, and is shown for the MZ ore in Figure 5.23 and Figure 5.24, and for the QZ ore in Figure 5.25and Figure 5.26. The one inconsistency in

this set of results is the detrimental change in GRD observed in the MZ T1 lowest energy treatment. It is theorised that the microwave treatment energy and power density conditions used for this treatment, are potentially approaching a threshold at which a different change in the breakage response of the ore is being observed. This theory will be investigated further later in this study.

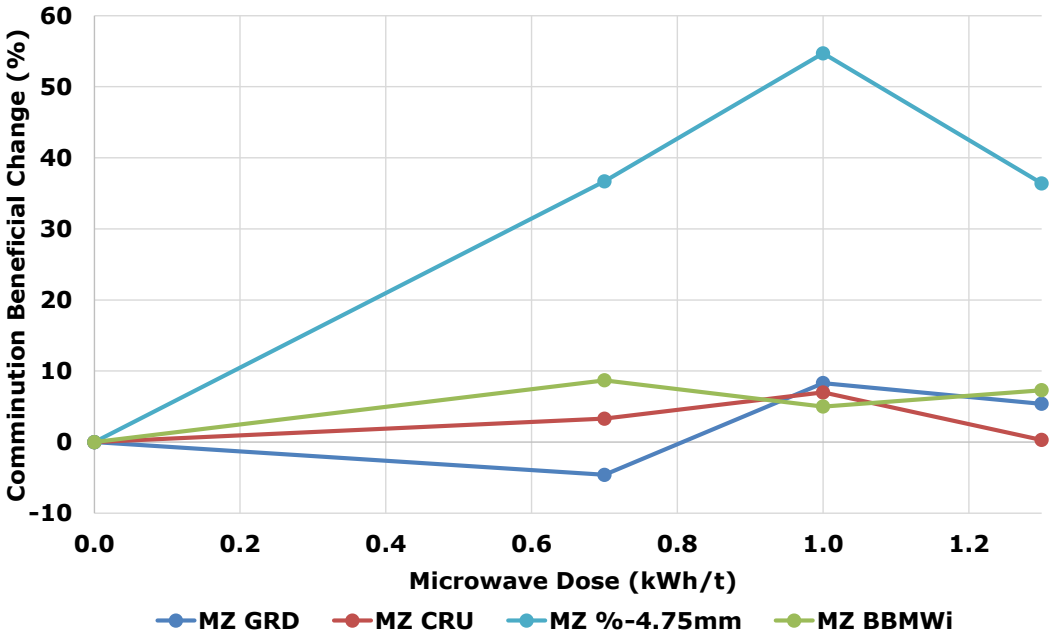


Figure 5.23 Beneficial change in comminution test results at varying microwave treatment doses for MZ ore.

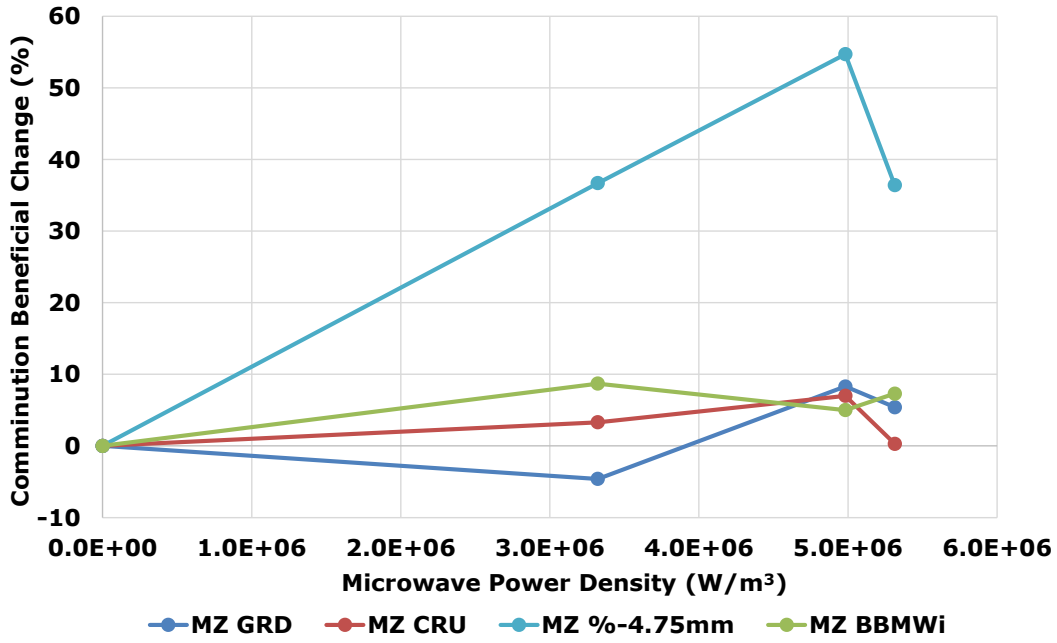


Figure 5.24 Beneficial change in comminution test results at varying microwave treatment power densities for MZ ore.

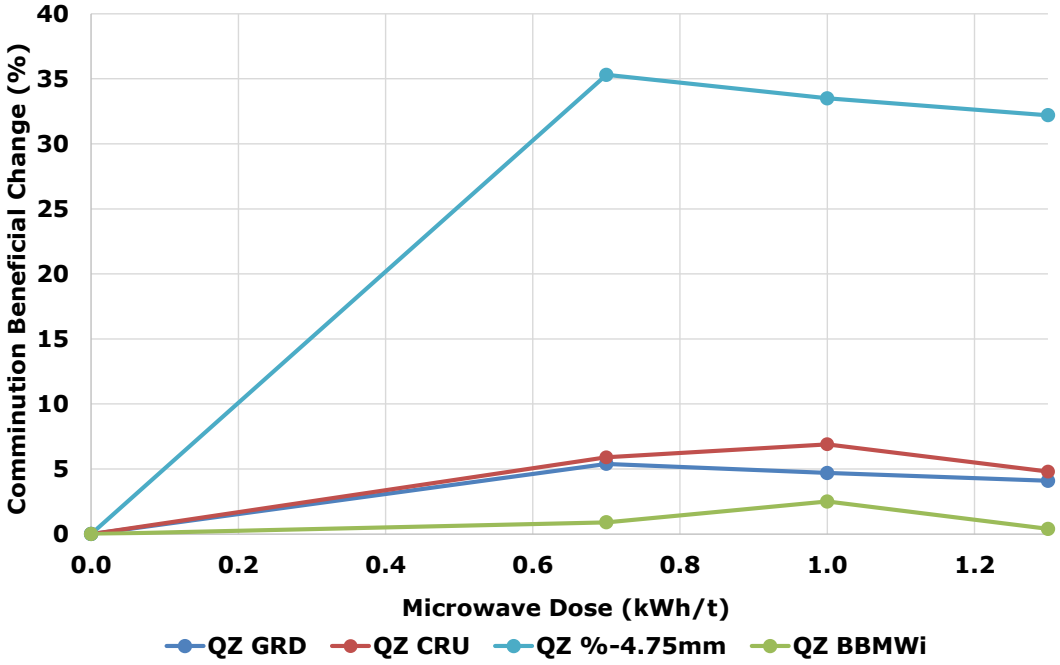


Figure 5.25 Beneficial change in comminution test results at varying microwave treatment doses for QZ ore.

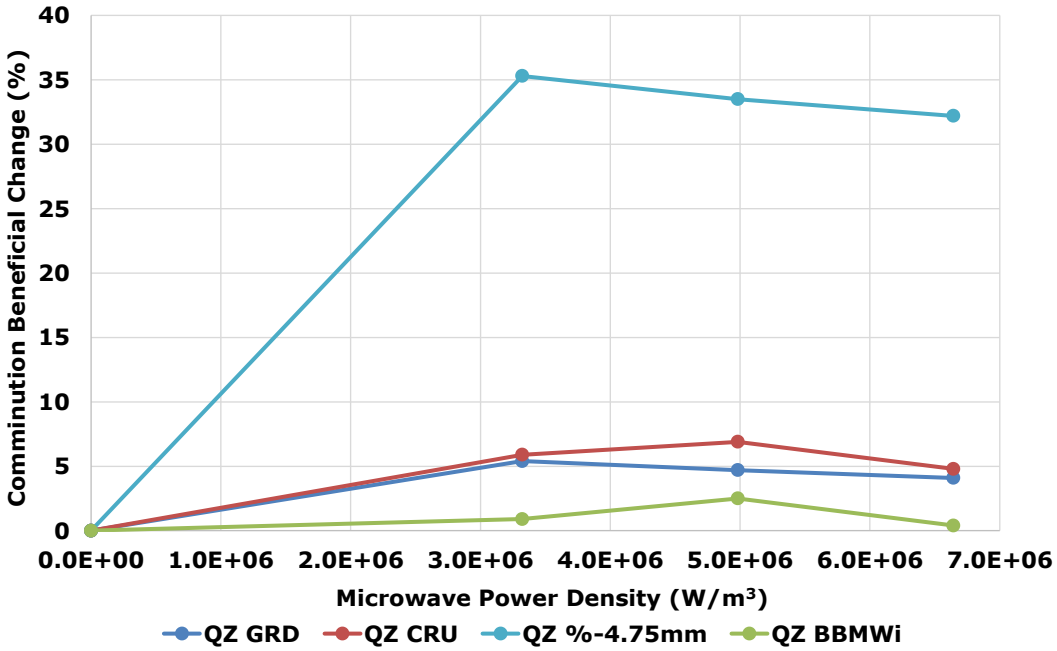


Figure 5.26 Beneficial change in comminution test results at varying microwave treatment power densities for QZ ore.

5.7 SUMMARY

The primary aim of this chapter has been to investigate how the mineralogical characteristics of an ore influences the mineral liberation and comminution benefits achieved through high power microwave treatments. It also sought to elucidate how changes in microwave power and microwave energy input, or 'dose', can influence the benefits achieved by the treatments. Through conducting an experimental program involving a series of microwave treatments of two mineralogically different ores at varying power densities and total energy inputs, a number a findings have been derived based on the liberation and comminution benefits achieved.

At the microwave treatment conditions used in producing the MZ and QZ treated ore samples, there are only marginal observable differences in the benefits achieved that can be attributed to variations in the mineralogy of the different ores. The MZ ore, having twice the abundance of sulphide heating minerals, three times the abundance of total heating minerals, and a coarser pyrite native grain size, has

shown marginally better liberation improvements in the >98% and >50% Cu-sulphide liberation classes. MZ ore also performed slightly better than the QZ ore in terms of splitting of the middlings particles, as evidenced by the greater reductions observed in Cu-sulphide:NSG binary particles in the treated samples. The potential for better liberation improvements in the QZ treated samples is hindered by the fact that Cu-sulphides in the ore already show very high levels of liberation in the untreated ore.

A comparison of Ci test results shows that the changes achieved for the MZ T2 treatment show the greatest benefits of all the treatments on both ores, however the results across the three different treatment conditions for MZ ore are quite variable. The Ci test results for the QZ ore consistently show beneficial changes at all microwave treatment conditions. The BBMWi results clearly show significant benefits have been achieved for the MZ ore as a result of the microwave treatments, while only marginal changes were seen in BBMWi for the QZ ore at low confidence levels. As the QZ ore is relatively soft in terms of BBMWi compared to the MZ ore, there is smaller room for improvement in terms of beneficial reductions in BBMWi from microwave treatments.

The results achieved in this study show good agreement with the small batch laboratory experiments performed by Batchelor et al. (2016). In that study, a porphyry copper ore was treated at 15kW in a single mode applicator with approximately 2kWh/t total energy input provided by two passes of 1kWh/t each, which is a comparable treatment process to the dual applicator configuration adopted in the pilot system. The results showed that the grind size for the microwave treated ore could be increased by 50-60µm and achieve equivalent liberation of Cu-sulphide minerals. Bond work index was also shown to be reduced by 4-8% in the treated sample compared to the untreated sample. In the ore use in the study, the copper and iron sulphides were highly associated with each other, and notable changes in mineral locking behaviour were observed following microwave treatment and grinding. In comparison, the ore used in this

investigation had a relatively small proportion of binary particles with pyrite (<5%) and the coarse ore characterisation indicated that copper and iron sulphides were not highly associated in the MZ and QZ ores. As such, in comparison to the ores assessed by Batchelor et al. (2016), there was less scope for improvement in copper and iron sulphide locking behaviour for these two ore types.

It is difficult to differentiate the performance of the two ores tested in this investigation based on a comparison between variations in the mineralogy of the different ores, and the benefits achieved from the microwave treatments. It is suggested that both ores have shown benefits in terms of improvements in Cu-sulphide mineral liberation and comminution performance, as it has been shown from the coarse ore characterisation that both ores possess characteristics that render them highly amenable to beneficial microwave treatment outcomes, based on previously identified mineralogical criteria (Kingman et al., 2000b; Batchelor et al., 2015).

In terms of assessing the influence of microwave power density and total microwave energy input on the benefits achieved from the microwave treatments of MZ and QZ ores, it has been shown that all treatments conducted were beyond the microwave power density and dose thresholds for both mineral liberation and comminution benefits to be achieved. The results in this chapter indicate that beneficial changes in Cu-sulphide mineral liberation and changes in ore breakage response, can be achieved for the MZ and QZ ores used in this study at equal to or less than a microwave power density of $3.3x10^6 W/m^3$ and a total microwave energy input, or dose, of 0.7kWh/t. This is a major finding in the context of the study of the microwave treatment of copper ores, in that it extends downwards the microwave energy input threshold values at which mineral liberation and comminution benefits can be achieved, from those previously reported in the literature.

CHAPTER 6 - ANALYSIS AND QUANTIFICATION OF FRACTURING IN MICROWAVE TREATED ORES

6.1 INTRODUCTION

One of the key aims highlighted for this research project was to develop the understanding of the generation and propagation of fractures in microwave treated ores. The characterisation and quantification of fractures resulting from the microwave treatment process required the development of a new experimental method, and the application of this method to assessing the benefits of microwave treatment in terms of ore fracturing. The fluorescent dye impregnation method that was developed and employed in this investigation is detailed in Section 4.6.

It was identified by Wills and Atkinson (1993) that the speed of fracture propagation in an ore, which is related to the rate of strain, can influence whether random or non-random breakage takes place during comminution. It was suggested that lower energy inputs and a subsequently slower strain rate during comminution, would promote stable fracture propagation and exploit grain boundary weaknesses more effectively than high energy and fast-strain processes. This would result in intergranular fracturing and enhanced mineral liberation by detachment of Cu-sulphide grains from the gangue. The authors further suggested that comminution conducted through the slow application of pressure to an ore, rather than by rapid impact events, can create residual internal stresses which can cause cracking to occur around grains during a subsequent relaxation phase in the material.

In contrast, both numerical modelling studies (Whittles et al., 2003; Jones et al., 2007; Ali and Bradshaw, 2009; Ali, 2010; Wang and Djordjevic, 2014) and experimental investigations (Kingman et al., 2004a; Rizmanoski, 2011; Batchelor et al., 2015) of the microwave

treatment of ores have suggested that the rapid application of high power microwaves over a short treatment duration results in the greatest benefits in terms of ore fracture, and subsequent improvements in mineral liberation and comminution performance.

It has been previously suggested in this study that, in the context of the microwave treatment of ores, two thresholds exist in terms of the benefits achieved by the treatment. The first threshold is where intergranular micro-fractures are generated and liberation enhancement occurs. The second threshold is where, at higher microwave power or energy inputs, the micro-fractures propagate and link together to form macro-fractures, resulting in ore strength reductions. This chapter will assess the development of micro and macro-fractures in MZ, QZ and QX ore fragments as a result of microwave treatments conducted at varying microwave power and energy inputs, and investigate how observed degrees of ore fracturing relate to the mineral liberation and comminution benefits achieved from the treatments.

6.1.1 Sample Preparation and Testing Procedure

Fracture analysis was conducted on representative samples of MZ, QZ and QX ores, comprising 50 fragments (nominally -50.8+25.4mm) of both untreated and microwave treated samples that were split from the original bulk samples produced for mineral liberation analysis and comminution testing in the previous chapter. All fragments were washed in water to remove surface debris and dried overnight in a 40°C oven, prior to being placed in the sample mounts. Samples were subjected to preparation by dye penetration and fluorescent imaging of fractures according to the method described in detail in Section 4.6.2. An untreated sample was prepared and analysed for each ore to act as a control sample, and the microwave treated samples shown in Table 6.1 were also prepared and analysed. The low (T1) and high (T3) energy microwave treatments for the MZ and QZ ores were selected for analysis, as were the three treated QX ore samples. Results of

fracture area, fracture density and fracture length were produced for each microwave treated sample, and compared to the inherent fracture characteristics that were determined for the untreated sample.

Ore	Sample	Microwave Treatment System	Throughput (t/h)	Total Microwave Power (kW)	Treatment Energy 'Dose' (kWh/t)	Power Density in Applicator (W/m^3)
MZ	T1	Pilot	150	2 x 50	**0.7**	3.3x10^6
	T3	Pilot	120	2 x 80	**1.3**	5.3x10^6
QZ	T1	Pilot	150	2 x 50	**0.7**	3.3x10^6
	T3	Pilot	150	2 x 100	**1.3**	6.6x10^6
QX	T1	Pilot	150	2 x 50	**0.7**	3.3x10^6
	T2	Pilot	100	2 x 75	**1.5**	5.0x10^6
	T3	Pilot	60	2 x 65	**2.2**	4.3x10^6

Table 6.1 Microwave treated samples selected for fracture analysis.

6.2 Inherent Fracture Characteristics

It was important to first determine the inherent, or natural fracture characteristics of the untreated ores to act as a baseline for comparison. The prevalence of fractures in an ore prior to microwave treatment may also have an impact on the benefits achieved. Microwave treatments may lead to fracture formation and propagation from existing planes of weakness within an ore, and it could be argued that higher levels of inherent fracturing are beneficial for the process. However, pre-existing weaknesses in the ore would have required the least energy to be re-activated during conventional comminution processes, so it is suggested that lower levels of inherent fracturing may be more favourable in terms of the potential benefits achievable from the microwave treatments.

6.2.1 MZ Ore

As was determined from the coarse ore characterisation in the previous chapter, MZ ore possesses a pyrite native grain size D_{80} of ~350µm, and a Cu-sulphide native grain size D_{80} of ~240µm. Sulphide mineralisation tends to occur in vein structures, and

sometimes as granular clusters within the fragments. Visual observations of inherent fracturing in untreated MZ ore shows pre-existing fractures occurring adjacent to sulphides within some fragments. These fractures have potentially formed in pre-existing regions of weakness in the ore due to geodynamic processes impacting the orebody after formation, through the impacts of blasting prior to mining, or during crushing to produce the -50.8+25.4mm fragments. While the majority of untreated MZ ore fragments do not show pre-existing fractures, the fragments that are fractured tend to also be highly mineralised with coarse and granular pyrite. This finding is consistent with the observations made regarding the contributing influence of pyrite to the initiation of fractures in Section 2.3.4. Figure 6.1 shows an example of a highly mineralised MZ untreated fragment with its associated fluorescent fracture image. The network of inherent fractures in this fragment are clearly observed to be associated with the distribution of sulphide mineralisation in the fragment.

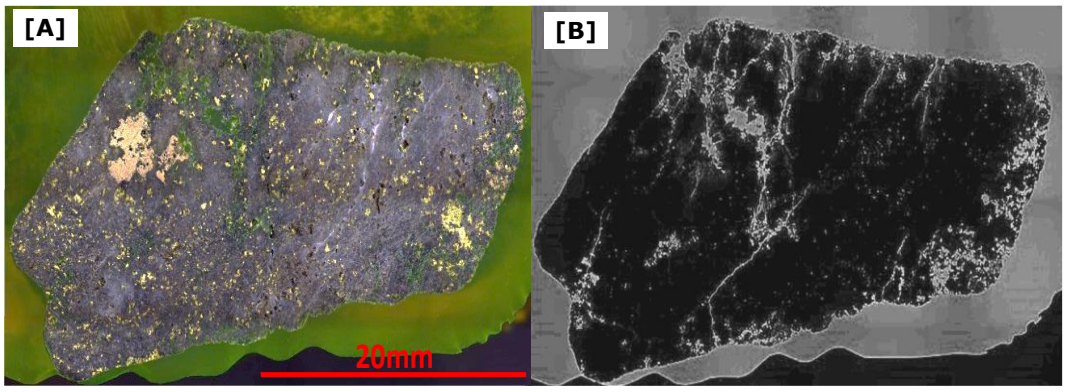


Figure 6.1 Example of pre-existing fractures in a highly mineralised untreated MZ fragment, [A] Reflected light image [B] Fluorescent light image.

6.2.2 QZ Ore

Textural characteristics of sulphide heating minerals within the QZ ore sample are predominantly disseminated and granular, possessing a native grain size D_{80} of ~260µm for Cu-sulphides and ~265µm for pyrite. Mineralisation tends to be disseminated throughout the ore, or sometimes concentrated along fracture planes within the fragments. Untreated QZ ore is observably more inherently fractured than the

untreated MZ ore. This is most likely due to the brittle nature of the gangue, which allows for the initiation and propagation of fractures to occur more readily than in MZ ore. These brittle or 'soft' characteristics of QZ ore were also observed in the BBMWi test results in the previous chapter. Pre-existing fractures in the ore tend to occur as relatively linear cracks, rather than the complex fracture networks observed in MZ ore, and are either continuous across the entire fragment, or terminate within the fragment. These inherent fracture characteristics suggest that QZ ore has a propensity towards macro-fracture formation and propagation. Figure 6.2 shows an example image of characteristic fracturing in an untreated QZ ore fragment. Fractures are observed to occur either indiscriminately in fragments with relatively homogeneously disseminated sulphides, or associated with vein-like sulphide features in the ore.

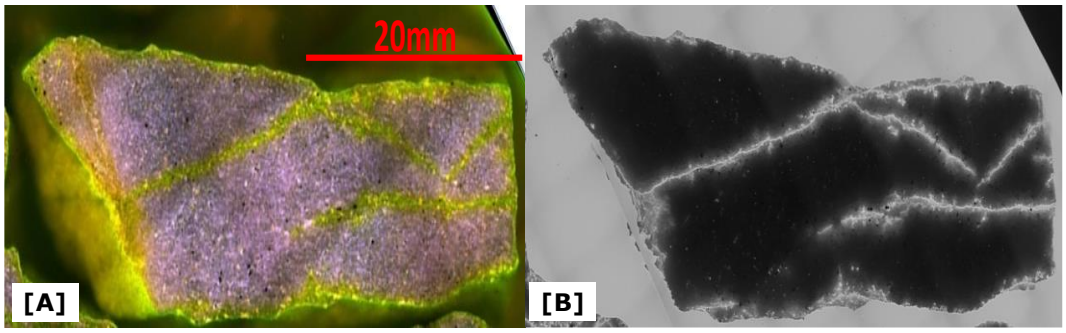


Figure 6.2 Example of characteristic pre-existing fractures in an untreated QZ fragment with fine disseminated sulphide grains (appearing as small black grains in image [A]). [A] Reflected light image [B] Fluorescent light image.

6.2.3 QX Ore

Similar to the QZ ore, the textural characteristics of sulphide heating minerals within QX ore are predominantly disseminated and granular, possessing a native grain size D_{80} of ~320µm for pyrite and ~145µm for Cu-sulphides, although the Cu-sulphide abundance is very low (<~0.3wt%). Inherent fracturing in QX ore fragments is similar in nature and appearance to fractures observed in QZ ore. It is however, of lower abundance, and appears to occur in association with coarse granular pyrite grains. Figure 6.3 shows an example image of fracturing associated with coarse sulphide grains in a QX ore fragment.

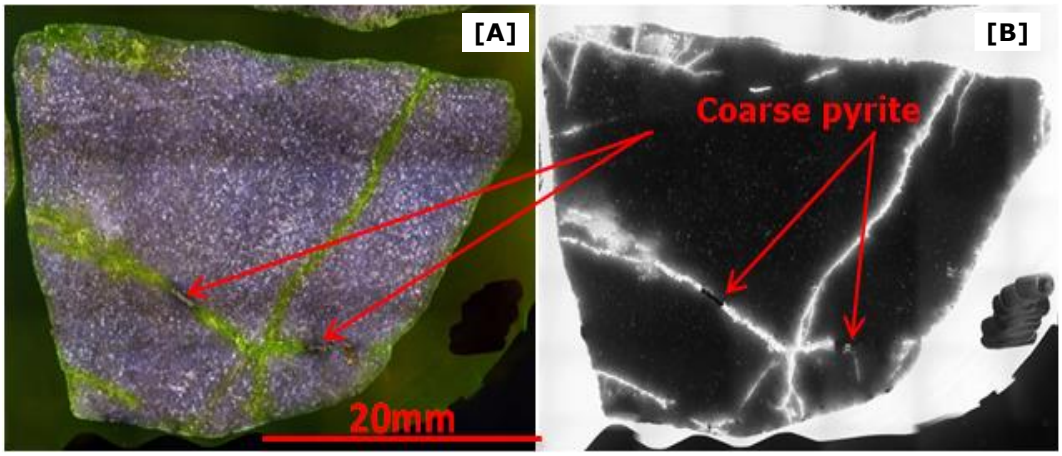


Figure 6.3 Example of pre-existing fractures in an untreated QX fragment which appear to be associated with coarse granular pyrite grains.

6.3 Fracture Length

Cumulative fracture length distributions were determined for untreated and microwave treated samples for each of the ores. It would be expected that if a microwave treatment has resulted in the generation of new macro-fractures in a sample, or the propagation and extension of inherent fractures, then the fracture length D_{50} and D_{80} would increase relative to the untreated sample. A comparison of the fracture length distributions for the untreated samples of each of the ores is shown in Figure 6.4. The differences observed in inherent fracture characteristics between the three ores can be clearly seen in the variations in fracture length distributions.

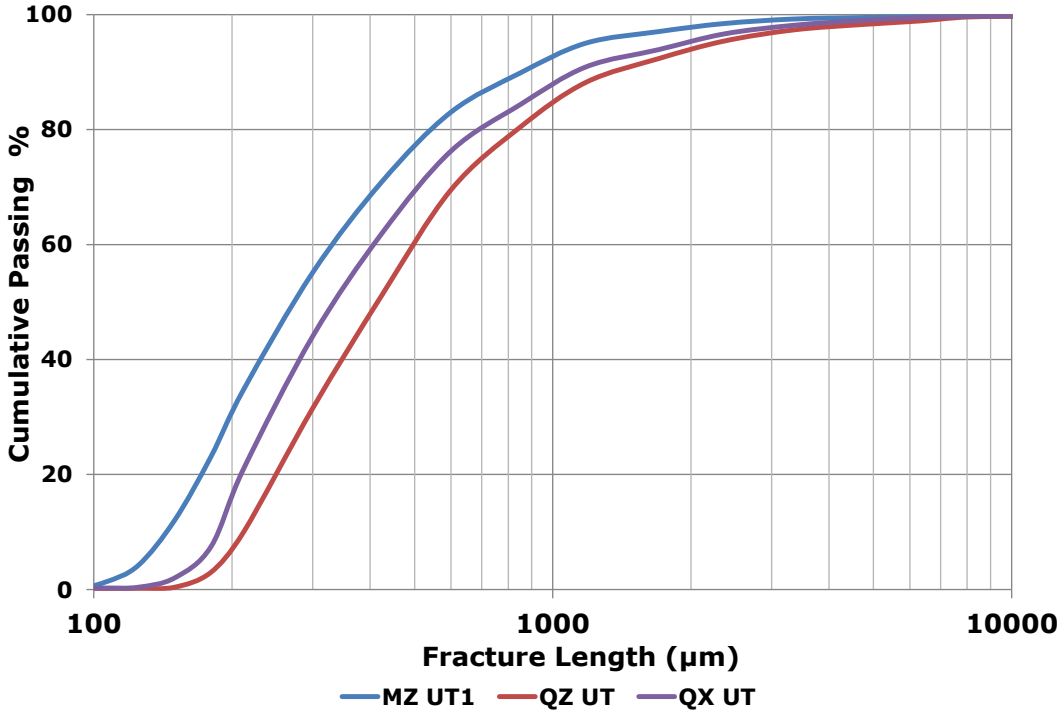


Figure 6.4 Fracture length distributions for untreated MZ, QZ and QX samples.

6.3.1 MZ Ore

Cumulative fracture length distributions are shown for untreated and treated MZ ore samples in Figure 6.5. Minor differences between the distributions of fracture lengths of the UT1 and T1 samples indicate that significant macro-fracturing was not caused by the microwave treatment. This is consistent with the findings from the previous chapter where the MZ T1 sample showed no significant benefit in the Ci test CRU index, which is an indication of ore crushability. In contrast, the T3 sample which received the higher microwave dose shows a significant increase in fracture length distribution compared to the UT1 and T1 samples. This result indicates that the T3 sample contains a greater proportion of longer fractures than the UT and T1 samples. These results indicate that while the T1 lower energy treatment had only a minor influence on the length of fractures in the sample, the higher energy T3 treatment generated an increased proportion of longer fractures compared to the UT sample. While benefits have been observed for the MZ T1 sample in terms of mineral liberation and grindability, these results indicate that MZ ore requires

microwave energy input of >0.7kWh/t, or microwave power density >3.3x10^6 W/m^3 to promote an observable increase in fracture length distribution.

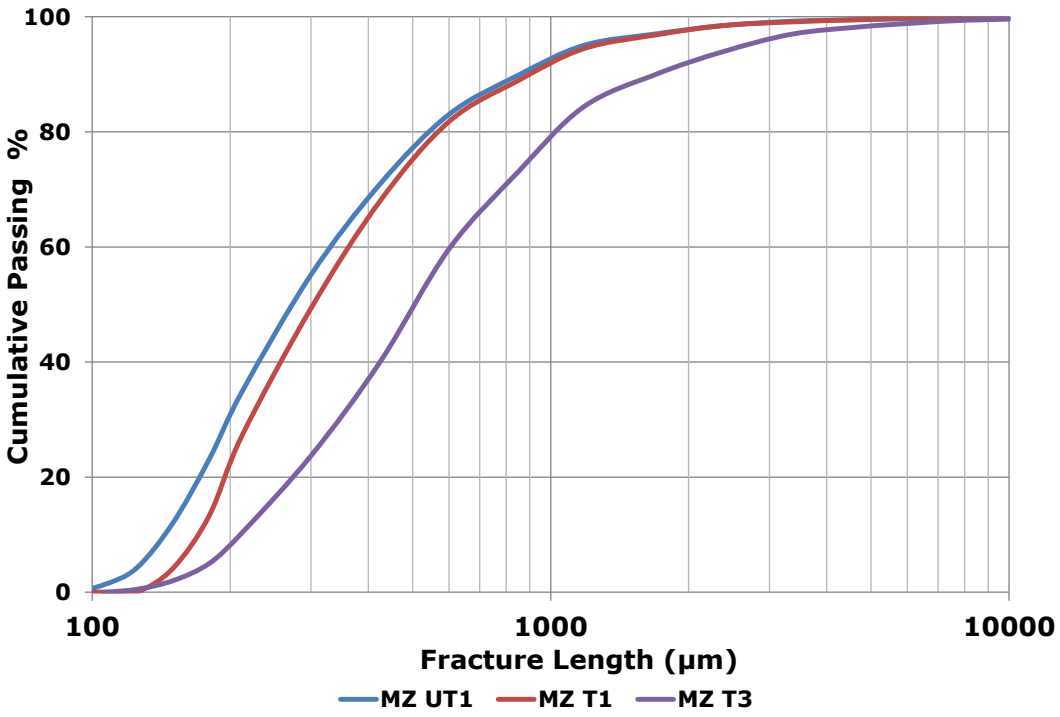


Figure 6.5 Fracture length distribution for MZ UT, T1 and T3 samples.

6.3.2 QZ Ore

Cumulative fracture length distributions shown for untreated and treated QZ ore samples in Figure 6.6, indicate similar increases in fracture length for both the T1 and T3 samples when compared to the untreated sample. The QZ UT sample possesses a fracture feature length D_{80} of ~840µm, and the T1 and T3 of ~950µm and ~970µm respectively. The results indicate that the microwave treated QZ samples possess only a slightly greater proportion of longer fractures than the untreated sample. It is suggested that this may be due to the untreated QZ ore already being highly fractured, with only minimal potential for additional fracture benefits to be achieved, similar to the outcomes observed for this ore in BBMWi testing in the previous chapter. These results indicate that for the QZ ore, a microwave energy input of 0.7kWh/t at a microwave power density of 3.3x10^6

W/m^3 is sufficient to affect an increase in fracture length distribution, while further energy input beyond this level produces minimal further measurable benefits in terms of fracture length.

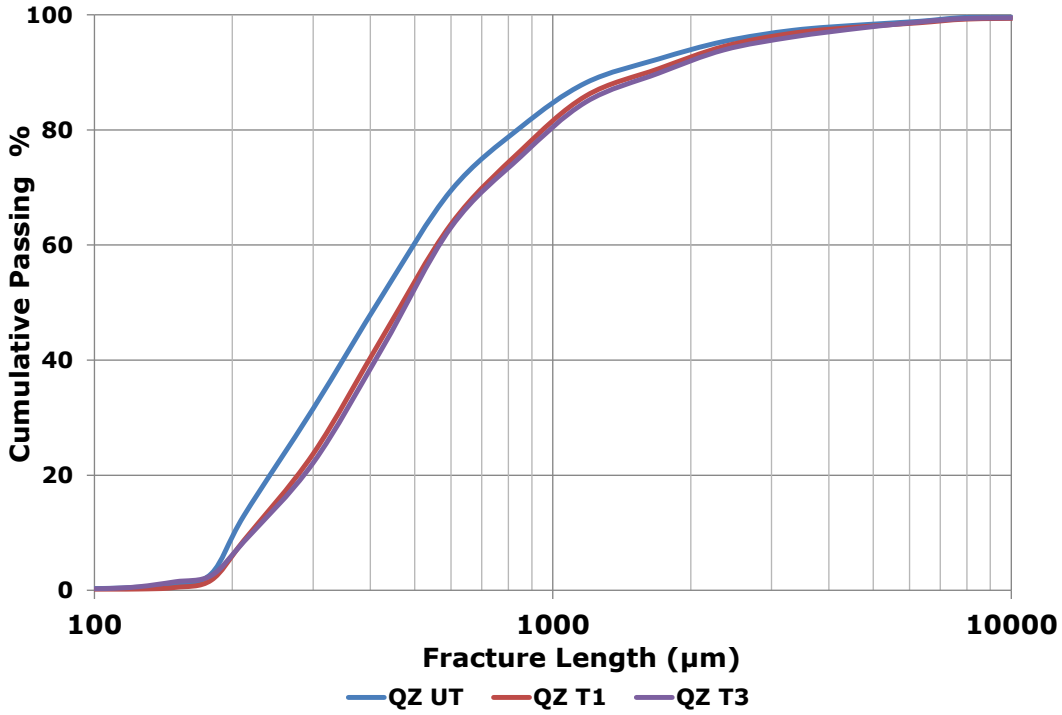


Figure 6.6 Fracture length distribution for QZ UT, T1 and T3 samples.

6.3.3 QX Ore

Cumulative fracture length distributions are shown for untreated and treated QX ore samples in Figure 6.7, and indicate a similar increase in fracture feature length distribution for all treated samples compared to the untreated sample. QX UT shows a fracture feature length D_{80} of ~680µm, while the microwave treated samples have a length D_{80} of ~840-860µm. Similar to the findings for the QZ ore, this result indicates that all the QX microwave treated samples show a consistently larger proportion of longer fractures than the untreated sample, irrespective of the treatment dose they received. This data indicates that for QX ore, treatment energy of 0.7kWh/t, or potentially even lower, can promote longer fractures in treated samples.

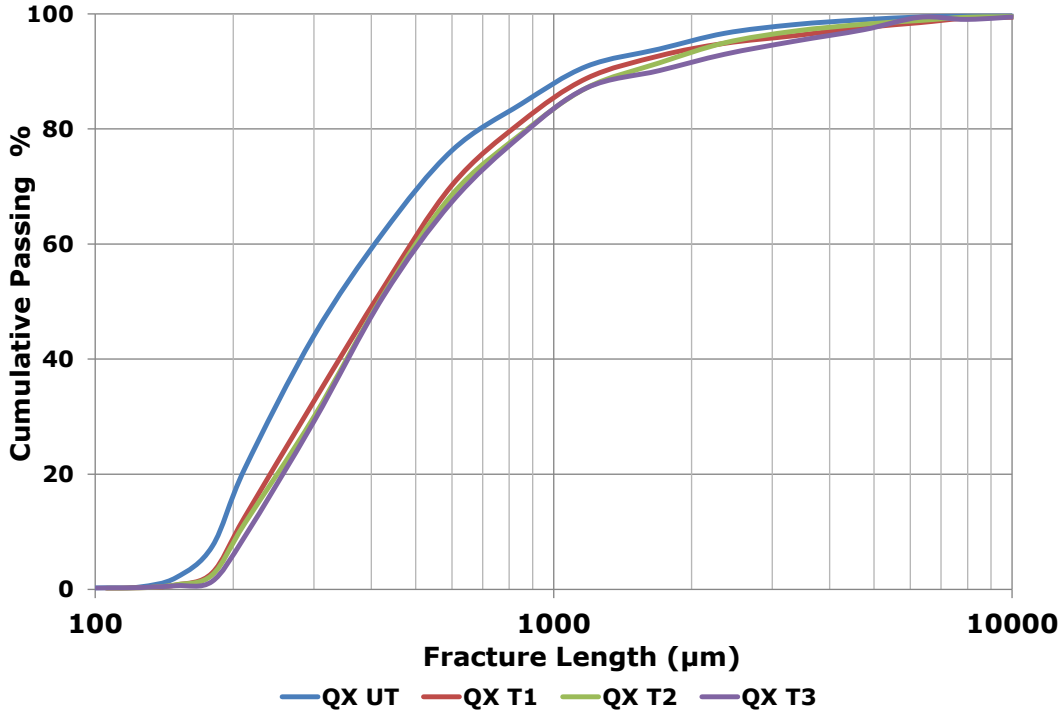


Figure 6.7 Fracture length distribution for QX UT, T1, T2 and T3 samples.

6.3.4 Statistical Analysis

Statistical analysis was conducted for the cumulative fracture length distributions for each ore, to determine whether the observable differences between the distributions could be considered as being significant. After assessing and trialling several methods, the Kolmogorov-Smirnov test (K-S test) was determined to be an appropriate and applicable tool to assess whether the cumulative fracture length distributions of the untreated and microwave treated samples for each ore are significantly different from each other.

The K-S test is a non-parametric test that can be easily applied to compare the empirical distribution functions for two samples to determine whether they have the same distribution, or if their distributions can be considered to be significantly different (Smirnov, 1948; Sprent and Smeeton, 2016). The two sample K-S test is based on measuring the maximum distance (D) between the continuous cumulative distributions for two datasets, and comparing it to a critical distance (D-crit) that can be determined from a K-S table of critical

values, obtained through Monte Carlo calculations, for a desired confidence level. In comparing two distributions, if D>D-crit at a desired confidence level (i.e. >95% or >99%), then the difference between the distributions can be considered to be significant at that confidence level. Detailed justification for the use of the K-S test over the Chi^2 test or other alternative methods can be found in Massey (1951) and Lilliefors (1967), where the authors state it to be a powerful statistical test for comparing population distributions. Importantly, the findings from the K-S test make sense in the context of this investigation, when observed in conjunction with the graphical representations of the distributions in Figure 6.5, Figure 6.6 and Figure 6.7. Results from the application of the K-S test to comparing the fracture length distributions between the samples for each ore are shown in Table 6.2, Table 6.3 and Table 6.4.

K-S tests comparing each of the MZ samples, indicates that differences observed between the distributions can be considered as being significant at >95% and >99% confidence levels.

MZ			
Criteria	**UT vs T1**	**UT vs T3**	**T1 vs T3**
D	0.1484	0.3145	0.2797
D crit	0.0227	0.0222	0.0219
Significant (>95% confidence)	**Yes**	**Yes**	**Yes**
Significant (>99% confidence)	**Yes**	**Yes**	**Yes**

Table 6.2 K-S test outcomes for comparisons between MZ samples

K-S tests comparing each of the QZ samples, indicate that differences observed between the distributions for the UT v T1, and UT v T3 samples, can be considered as being significant at >95% and >99% confidence levels. Distributions for the T1 and T3 samples were not shown to be significantly different at either confidence level, which can also be observed in the very close similarity between these distributions in Figure 6.6.

QZ			
Criteria	**UT vs T1**	**UT vs T3**	**T1 vs T3**
D	0.0785	0.0941	0.0183
D crit	0.0245	0.0257	0.0259
Significant (>95% confidence)	**Yes**	**Yes**	**No**
Significant (>99% confidence)	**Yes**	**Yes**	**No**

Table 6.3 K-S test outcomes for comparisons between QZ samples

K-S tests comparing each of the QX samples, indicate that differences observed between the distributions for the UT v T1, UT v T2, and UT v T3 samples, can be considered as being significant at >95% and >99% confidence levels. At the >99% confidence level, the T1 v T2, and T2 v T3, could not be considered as significantly different. At the lower >95% confidence level however, distributions for all of the microwave treated samples were considered significantly different when compared to each other. This indicates that, while minor observable differences between the T1, T2 and T3 distributions seen in Figure 6.7 are discerned at the >95% confidence level, they are not considered significant with >99% confidence.

QX						
Criteria	**UT vs T1**	**UT vs T2**	**UT vs T3**	**T1 vs T2**	**T1 vs T3**	**T2 vs T3**
D	0.1201	0.1411	0.1540	0.0273	0.0352	0.0229
D crit	0.0252	0.0237	0.0202	0.0260	0.0228	0.0211
Significant (>95% confidence)	**Yes**	**Yes**	**Yes**	**Yes**	**Yes**	**Yes**
Significant (>99% confidence)	**Yes**	**Yes**	**Yes**	**No**	**Yes**	**No**

Table 6.4 K-S test outcomes for comparisons between QX samples

Data tables used in determining D and D-crit values used in the K-S tests are shown in APPENDIX C.

Beneficial changes in fracture length D_{80} for each of the microwave treated samples are shown in relation to microwave dose in Figure 6.8, and microwave power density in Figure 6.9. These figures illustrate that for MZ ore, only a minor observable benefit is achieved by the T1 treatment at 0.7kWh/t and $3.3x10^6W/m^3$, while a significant increase in fracture length is achieved by the T3 treatment. This suggests that, while the T1 treatment has shown improvements in both Cu-sulphide liberation and reductions in BBMWi, the treatment does not appear to have generated significant macro-fractures throughout the ore fragments. The QZ and QX ores both show benefits in terms of increased fracture length D_{80} for the T1 treatment. Beyond this microwave power density and energy input however, diminishing returns are observed, similar to what was observed for the QZ ore in comminution testing, and consistent with the findings of previous researchers (Kingman and Rowson, 1997; Kingman et al., 2000b; Vorster et al., 2001; Batchelor et al., 2015). This result indicates that for quartzitic ore types such as the QZ and QX ores used in this study, microwave treatments of equal to or less than a microwave power density of $3.3x10^6W/m^3$ and a total microwave dose of 0.7kWh/t are sufficient for macro-fracturing to be achieved.

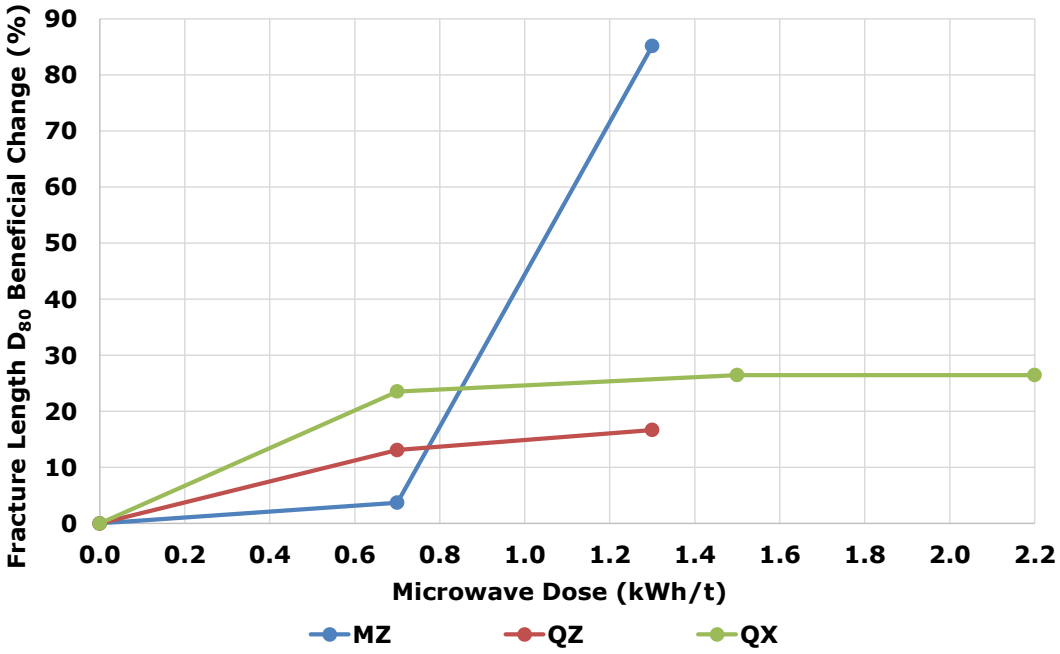


Figure 6.8 Beneficial change in fracture length D_{80} at varying microwave treatment doses.

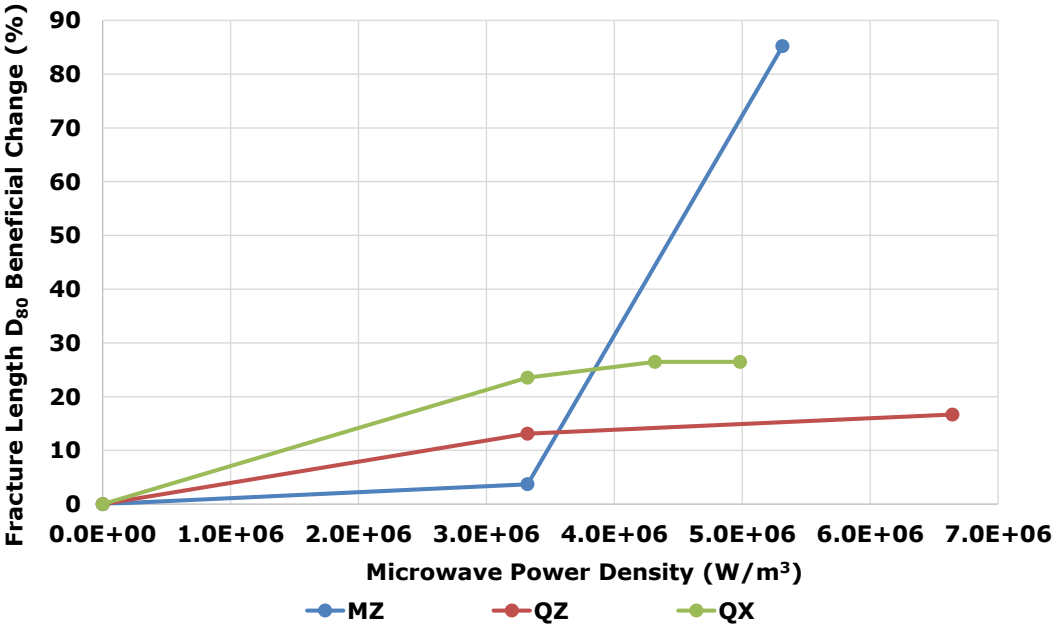


Figure 6.9 Beneficial change in fracture length D_{80} at varying microwave treatment power densities.

6.4 Fracture Area

Analysis of fracture area was conducted for all untreated and microwave treated samples, based on the total measured surface area of all fractures (>~100µm fracture length) in a sample, as a percentage of the total measured fragment surface area. The area abundance measurement provides a 'bulk' assessment of changes in fracture area between untreated and treated samples of each ore, and results are shown in Table 6.5.

Ore	Sample	Fracture Area - All Fractures				
		Total Sample Area (cm^2)	Fragment Area %	Fracture Area (cm2)	Fracture Area %	Beneficial Change %
MZ	UT1	476.63	97.44%	12.20	2.56%	
	T1	475.95	97.62%	11.33	2.38%	-7.0%
	T3	467.97	96.78%	15.07	3.22%	25.8%
QZ	UT	423.91	95.18%	20.44	4.82%	
	T1	412.20	93.60%	26.40	6.40%	32.8%
	T3	384.14	93.55%	24.76	6.45%	33.8%
QX	UT	537.11	97.26%	14.69	2.74%	
	T1	484.14	96.18%	18.52	3.82%	39.8%
	T2	457.95	95.40%	21.06	4.60%	68.1%
	T3	672.37	95.21%	32.20	4.79%	75.1%

Table 6.5 Total sample surface area and the total area of fractures measured in each sample.

Similar to the Ci test GRD results, the MZ ore shows an apparently detrimental change between the UT and T1 samples. This supports the theory that a microwave treatment with a power density of $3.3x10^6 W/m^3$ and a total microwave energy input of 0.7kWh/t is approaching the minimum threshold at which benefits in ore strength reduction may achievable for MZ ore. An increase in fracture area of 25.8% was observed in the MZ T3 sample compared to the untreated. Both microwave treated QZ samples show a similar increase in total measured fracture area of 32.8% and 33.8% respectively, compared to the untreated QZ sample. QX treated samples showed increases in total measured fracture feature area corresponding with increases in microwave treatment energy input. The QX T1, T2 and T3 samples showed respective increases of 39.8%, 68.1% and 75.1%, when compared to the untreated sample, indicating that for this ore, the additional energy input beyond 0.7kWh/t resulted in an increase in fracture area.

Analysis of fracture area was also conducted for all samples, based on the total measured area of what could be considered to be macro-fractures (>~1mm fracture length), and is shown in Table 6.6. This was conducted to investigate whether any of the three different ores indicated a propensity towards macro-fracture development with increasing microwave treatment power density or dose.

Ore	Sample	Fracture Area - Fractures >1mm Length				
		Total Sample Area (cm^2)	Fragment Area %	Fracture Area (cm2)	Fracture Area %	Beneficial Change %
MZ	UT1	476.63	98.36%	7.84	1.64%	
	T1	475.95	98.54%	6.95	1.46%	-11.2%
	T3	467.97	97.28%	12.74	2.72%	65.4%
QZ	UT	423.91	96.21%	16.05	3.79%	
	T1	412.20	94.71%	21.79	5.29%	39.6%
	T3	384.14	94.47%	21.26	5.53%	45.9%
QX	UT	537.11	98.06%	10.40	1.94%	
	T1	484.14	96.98%	14.61	3.02%	55.9%
	T2	457.95	96.38%	16.59	3.62%	87.1%
	T3	672.37	96.36%	24.45	3.64%	87.8%

Table 6.6 Total sample surface area and the total area of fractures >1mm in length measured in each sample.

While the MZ ore again showed a detrimental change in macro-fracture area between the untreated and T1 samples, the T3 sample showed a 65.4% relative increase in measured macro-fracture area compared to the untreated MZ sample. This result supports the fracture length distribution data for MZ ore which indicated an increased proportion of longer fractures in the T3 sample. Both the T1 and T3 QZ treated samples showed increases in macro-fracture area of 39.6% and 45.9% respectively when compared to the untreated sample which is consistent with the fracture length distribution results for this ore. The QX T1 sample showed an increase in measured fracture area of 55.9%, and the T2 and T3 samples similar increases of 87.1% and 87.8% respectively, compared to the untreated QX ore sample.

Both QX and MZ ores show an increase in macro-fracture area between the 0.7kWh/t T1 treatments, and the 1.3kWh/t T3 microwave treated samples. This is potentially related to the higher pyrite content in both of these ores, as discussed previously in Section 2.3.4. Pyrite abundance, grain size and associations with hard gangue minerals have been shown to be contributing factors to macro-fracturing of ores during microwave treatment. Pyrite has a modulus of elasticity that is much higher than chalcopyrite and typical gangue minerals such as quartz, feldspars, micas, and carbonates (Mavko et al., 2009; Djordjevic, 2014). Thermal expansion of pyrite during the 1.3kWh/t microwave treatments appears to be sufficient to cause

disruption of the ore matrix and promote macro-fracturing to occur more readily than in the lower energy 0.7kWh/t treatments.

The beneficial changes observed in total fracture area are shown in relation to microwave dose and microwave power density in Figure 6.10 and Figure 6.11 respectively. Similar to the findings for fracture length, MZ ore shows no benefit from the T1 treatment and a beneficial increase in fracture area as a result of the T3 treatment. The QZ ore shows a benefit from the T1 treatment and no further benefits from the higher power and higher energy T3 treatment. Interestingly, the QX ore shows increasing benefits in total fracture area with increases in both microwave dose and power density up to the T3 treatment at 2.2kWh/t and $5.0x10^6W/m^3$. This suggests that, while the fractures may not be increasing in length beyond the T1 treatment conditions, additional fractures are being generated at the higher dose and power density T2 and T3 treatment conditions. This is potentially attributable to the higher abundance of pyrite within the QX ore compared to the QZ ore.

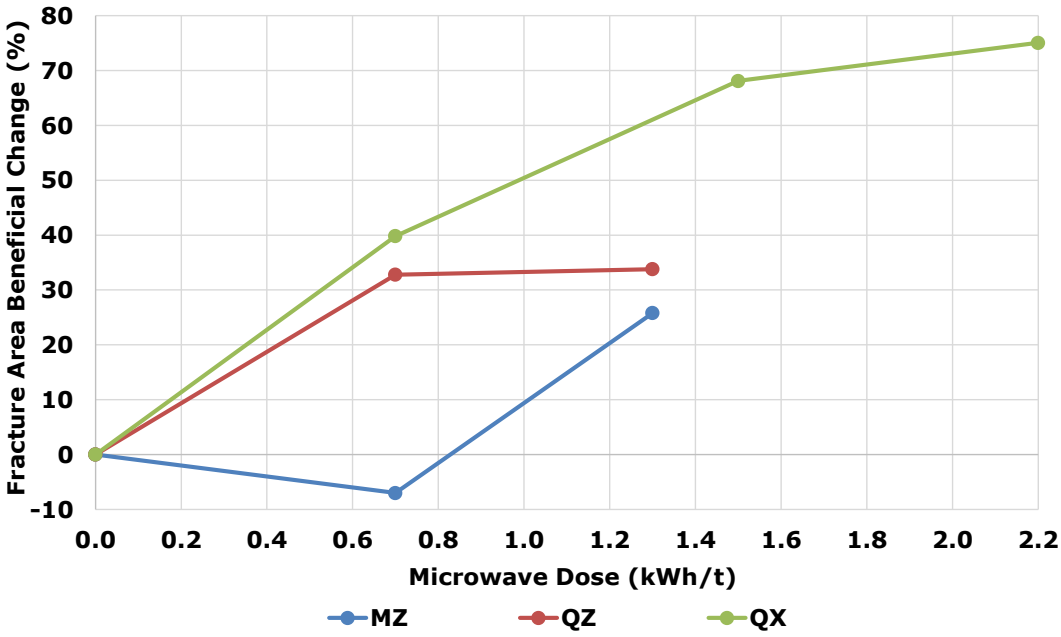


Figure 6.10 Beneficial change in total fracture area at varying microwave treatment doses.

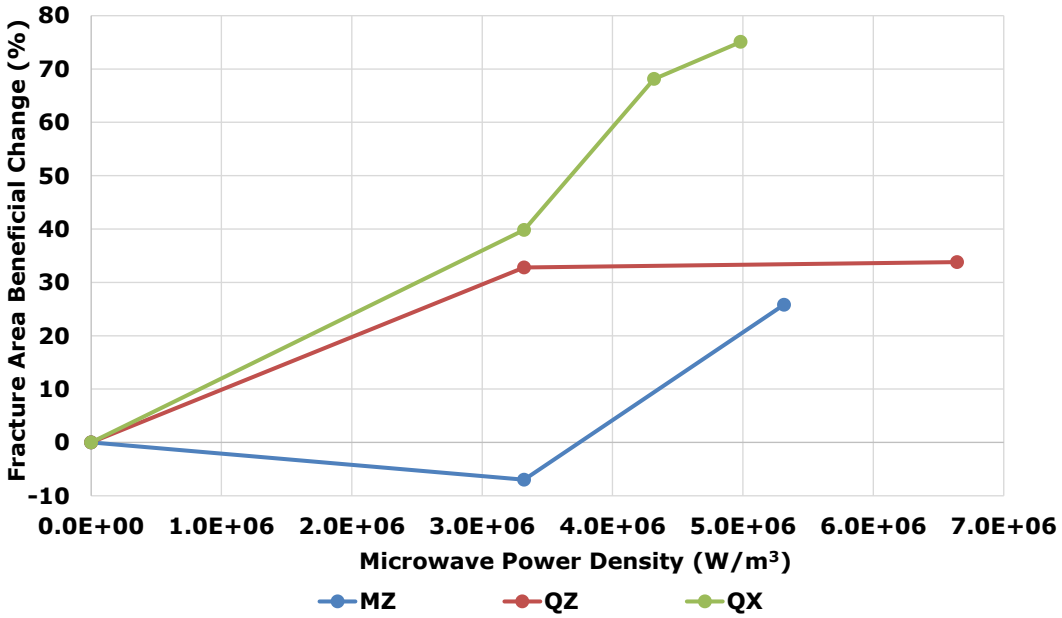


Figure 6.11 Beneficial change in total fracture area at varying microwave treatment power densities.

6.5 Fracture Density

Fracture density results were analysed to investigate whether new fractures are being induced in the microwave treated samples, in addition to the activation or extension of pre-existing fractures within the ore fragments. Fracture density results are based on the total number of fracture features of a given length range, taking into account the total fragment surface area measured for each sample. Fracture density results shown in Table 6.7 detail the number (n) of fractures per square centimetre (n/cm^2) for <1mm length fractures, 1mm-5mm length fractures, and >5mm length fractures.

Ore	Sample	Total Fracture Number (n)				Total Sample Area (cm^2)	Fracture Density (n/cm^2)			
		<1mm Fracture Length	1-5mm Fracture Length	>5mm Fracture Length	Total Number		<1mm Fracture Length	1-5mm Fracture Length	>5mm Fracture Length	Total Fracture Density
MZ	UT1	5891	1038	59	6988	476.63	12.36	2.18	0.12	14.66
	T1	6333	1001	66	7400	475.95	13.31	2.10	0.14	15.55
	T3	7021	1004	87	8112	467.97	15.00	2.15	0.19	17.33
QZ	UT	4692	1408	160	6260	423.91	11.07	3.32	0.38	14.77
	T1	4242	1603	176	6021	412.20	10.29	3.89	0.43	14.61
	T3	3373	1512	174	5059	384.14	8.78	3.94	0.45	13.17
QX	UT	5690	1266	120	7076	537.11	10.59	2.36	0.22	13.17
	T1	3519	1236	180	4935	484.14	7.27	2.55	0.37	10.19
	T2	4529	1426	168	6123	457.95	9.89	3.11	0.37	13.37
	T3	10309	2239	209	12757	672.37	15.33	3.33	0.31	18.97

Table 6.7 Fracture density results; (N) number of fractures per unit measured surface area (cm^2).

MZ ore fracture density results for >5mm fractures show an increase between the untreated and T3 samples, with only a minimal change observed between the untreated and T1 samples. MZ ore showed only minor variation in fracture density between untreated and microwave treated samples for 1-5mm length fracture. This data indicates the introduction of additional macro-fractures in MZ ore from the T3 treatment, and supports the findings of the fracture length and area results. The MZ ore also showed an increase in fracture density of <1mm fractures in the microwave treated samples. This indicates that increased micro-fracture is occurring in the microwave treated samples, which is consistent with the benefits achieved in the treated MZ ore in terms of mineral liberation and BBMWi.

Results for the QZ ore show a similar increase in fracture feature density for both >5mm and 1-5mm length features in the T1 and T3 treated samples when compared to the untreated sample. QZ ore does however show a lower density of <1mm fractures in the microwave treated samples. This result is interpreted as being due to the linking together of micro-fractures during the microwave treatment to form macro-fractures, with the resultant effect of reducing the density of <1mm fractures in the treated samples. This effect is observable in Figure 6.12, and is conceptually similar to the splitting and redistribution of the middlings particles in the mineral liberation analysis in the previous chapter. The microwave treatment process

propagates the <1mm fractures and links them together to form longer fractures. This is observed as a redistribution of fractures from the <1mm fracture class to the 1-5mm and >5mm fracture classes.

Microwave treated samples of the QX ore show progressive increases in 1-5mm feature density compared to the untreated sample, in line with increases in the microwave treatment dose and power density. Conversely, the >5mm feature length density results show greater benefits at lower microwave dose and power density treatment conditions, while the T3 sample which received the highest microwave dose and power density shows a smaller density increase when compared to the untreated sample. This could be interpreted as occurring due to the linking up of macro-fractures in the higher energy T3 treatment, resulting in longer fractures of lower density.

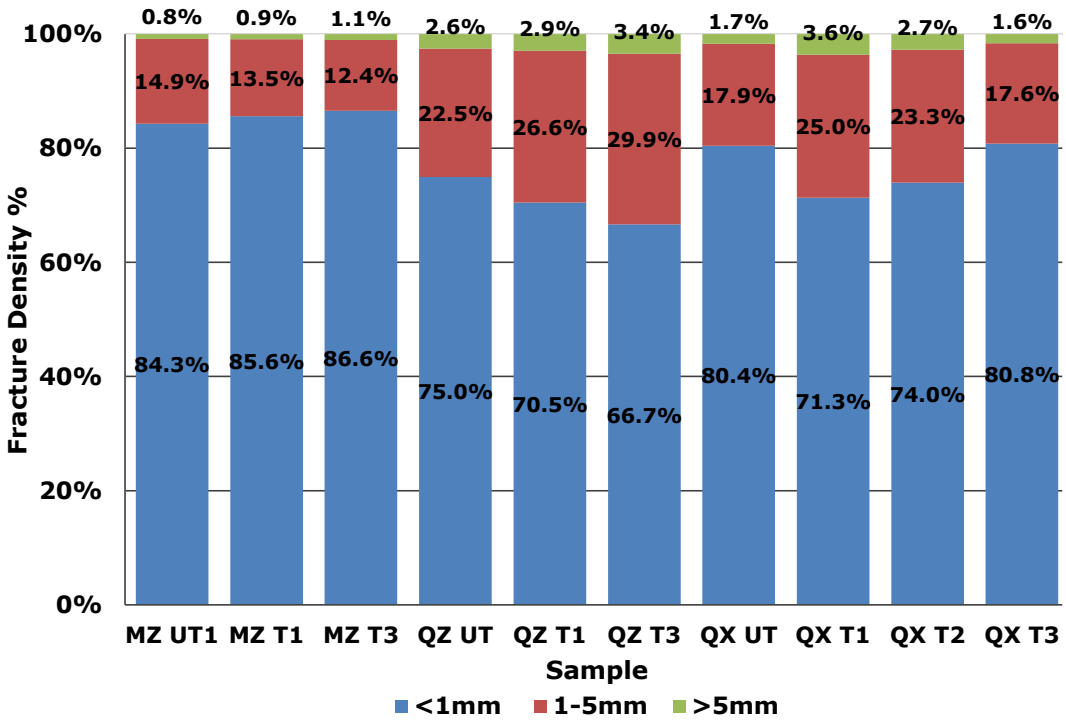


Figure 6.12 Percentage contribution of fracture length classes to total fracture density.

The beneficial changes observed in the density of 1-5mm fractures are shown in relation to microwave dose and microwave power density in Figure 6.13 and Figure 6.14. It can be observed in these figures that

benefits in terms of increase density of 1-5mm fractures can be achieved for MZ and QZ ores at a microwave power density of $3.3x10^6W/m^3$ and a total microwave dose of 0.7kWh/t. QX ore shows a continued increase in the density of 1-5mm fractures up to, and potentially beyond, a microwave power density of $5.0x10^6W/m^3$ and a total microwave dose of 2.2kWh/t.

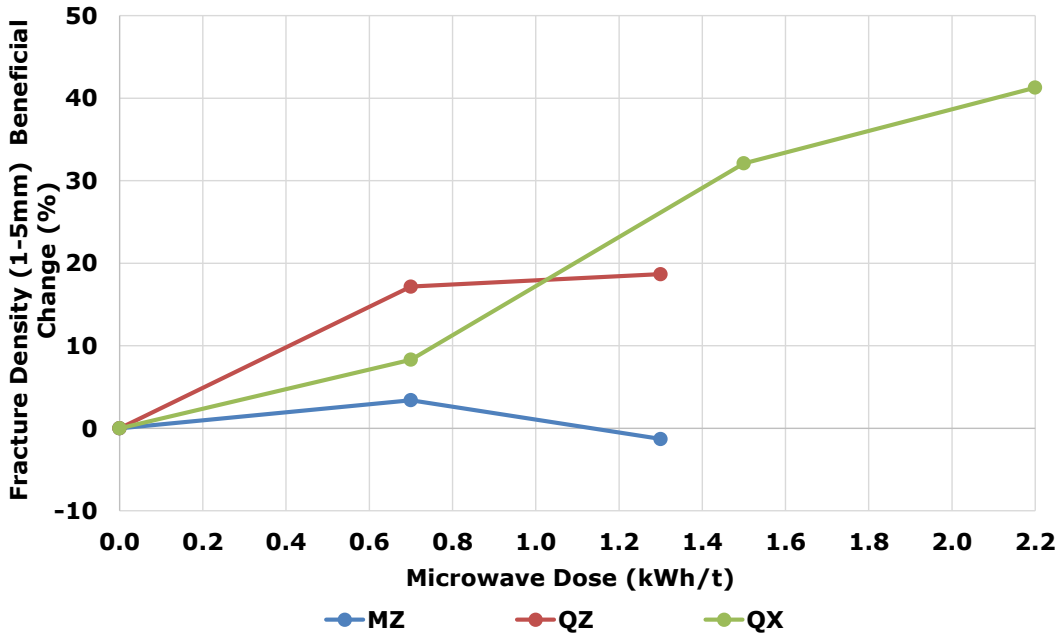


Figure 6.13 Beneficial change in fracture density (1-5mm fractures) at varying microwave treatment doses.

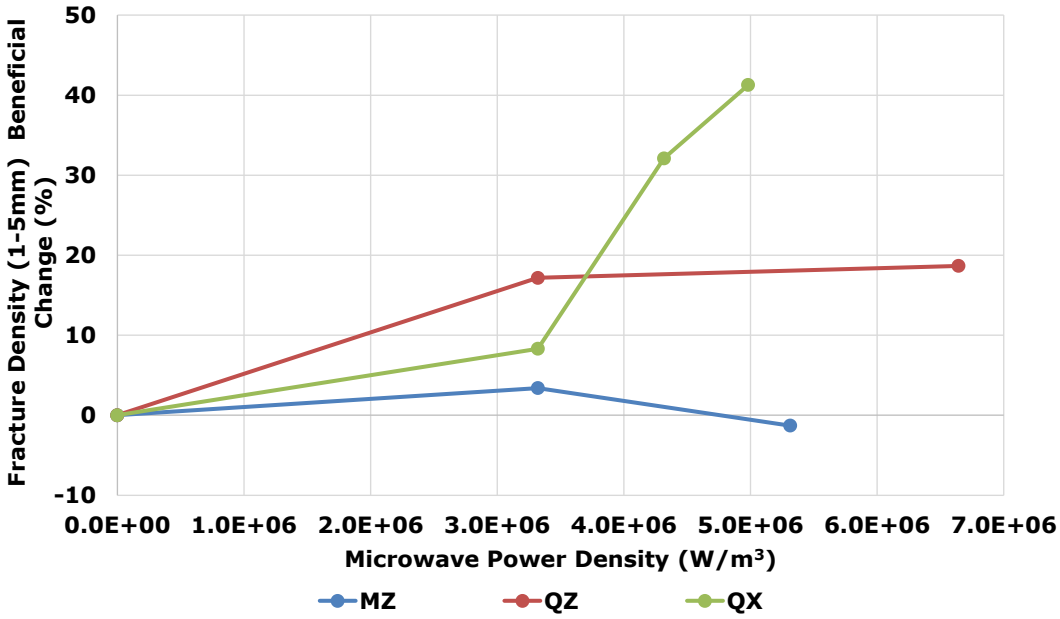


Figure 6.14 Beneficial change in fracture density (1-5mm fractures) at varying microwave treatment power densities.

Beneficial changes observed in the density of >5mm fractures are shown in relation to microwave dose and microwave power density in Figure 6.15 and Figure 6.16. While MZ and QZ treated samples show increased density of >5mm fractures with increases in microwave dose and power density, the QX treated samples appear to reach a peak density at between 0.7-1.5kWh/t and $3.3x10^6$ -$4.3x10^6 W/m^3$ before the density diminishes due to the linking together of fractures, reducing the total number and subsequently the density.

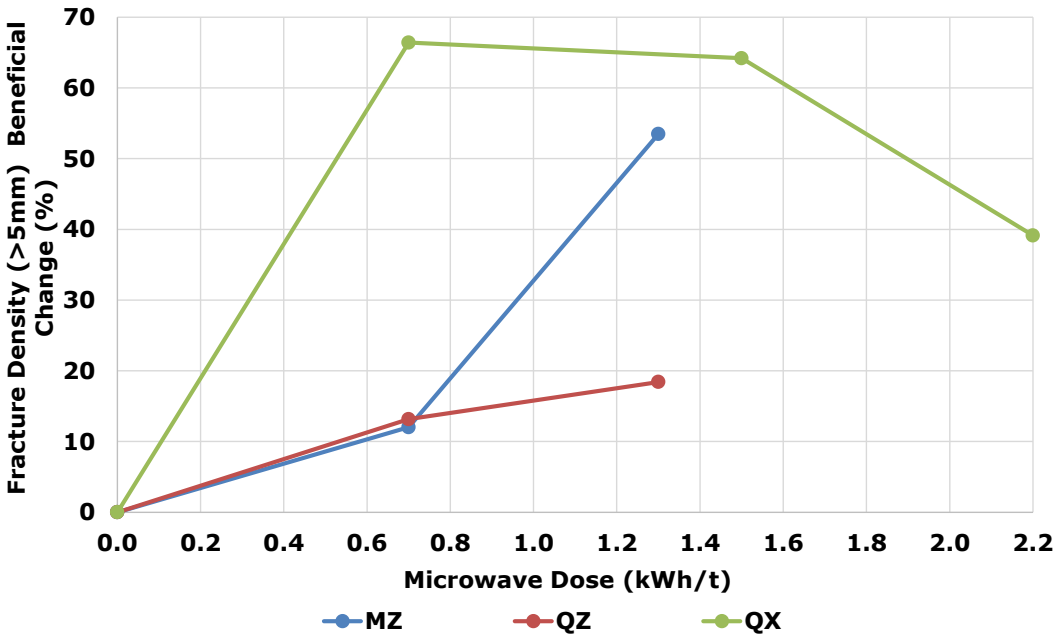


Figure 6.15 Beneficial change in fracture density (>5mm fractures) at varying microwave treatment doses.

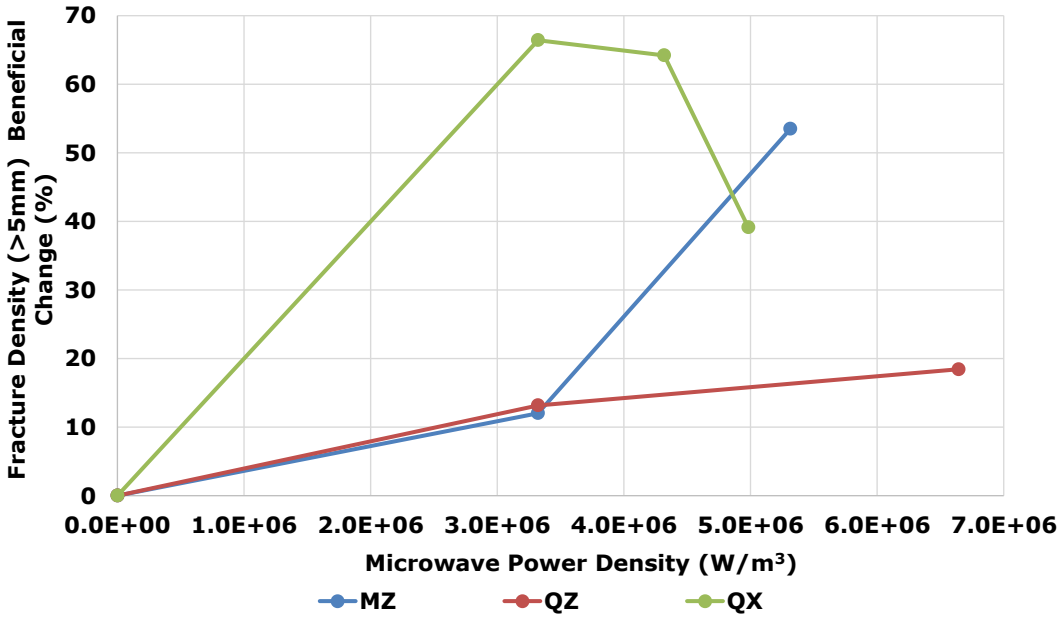


Figure 6.16 Beneficial change in fracture density (>5mm fractures) at varying microwave treatment power densities.

6.6 Comparison to Mineral Liberation and Comminution Results

A summary of the fracture analysis results highlighting the beneficial change between the untreated and microwave treated samples is shown in Table 6.8. These results will be compared to results from comminution and liberation testing conducted in the previous chapter for MZ and QZ ores to investigate whether comminution and liberation benefits can be related to changes in ore fracturing in microwave treated samples.

Ore	Sample	Fracture Area				Fracture Density				Fracture Length	
		Total Area %	Beneficial Change %	Area (>1mm) %	Beneficial Change %	1-5mm Fractures (N/cm²)	Beneficial Change %	>5mm Fractures (N/cm²)	Beneficial Change %	Length D_{80} (µm)	Beneficial Change %
MZ	UT1	2.56		1.64		2.18		0.12		540	
	T1	2.38	-7.0%	1.46	-11.2%	2.10	-3.4%	0.14	12.0%	560	3.7%
	T3	3.22	25.8%	2.72	65.4%	2.15	-1.3%	0.19	53.5%	1000	85.2%
QZ	UT	4.82		3.79		3.32		0.38		840	
	T1	6.40	32.8%	5.29	39.6%	3.89	17.2%	0.43	13.2%	950	13.1%
	T3	6.45	33.8%	5.53	45.9%	3.94	18.7%	0.45	18.4%	980	16.7%
QX	UT	2.74		1.94		2.36		0.22		680	
	T1	3.82	39.8%	3.02	55.9%	2.55	8.3%	0.37	66.4%	840	23.5%
	T2	4.60	68.1%	3.62	87.1%	3.11	32.1%	0.37	64.2%	860	26.5%
	T3	4.79	75.1%	3.64	87.8%	3.33	41.3%	0.31	39.1%	860	26.5%

Table 6.8 Summary of fracture analysis results

A comparison between the beneficial change in sample fracture characteristics and the beneficial change in comminution test results for the microwave treated samples, relative to the untreated samples, is shown in Figure 6.17.

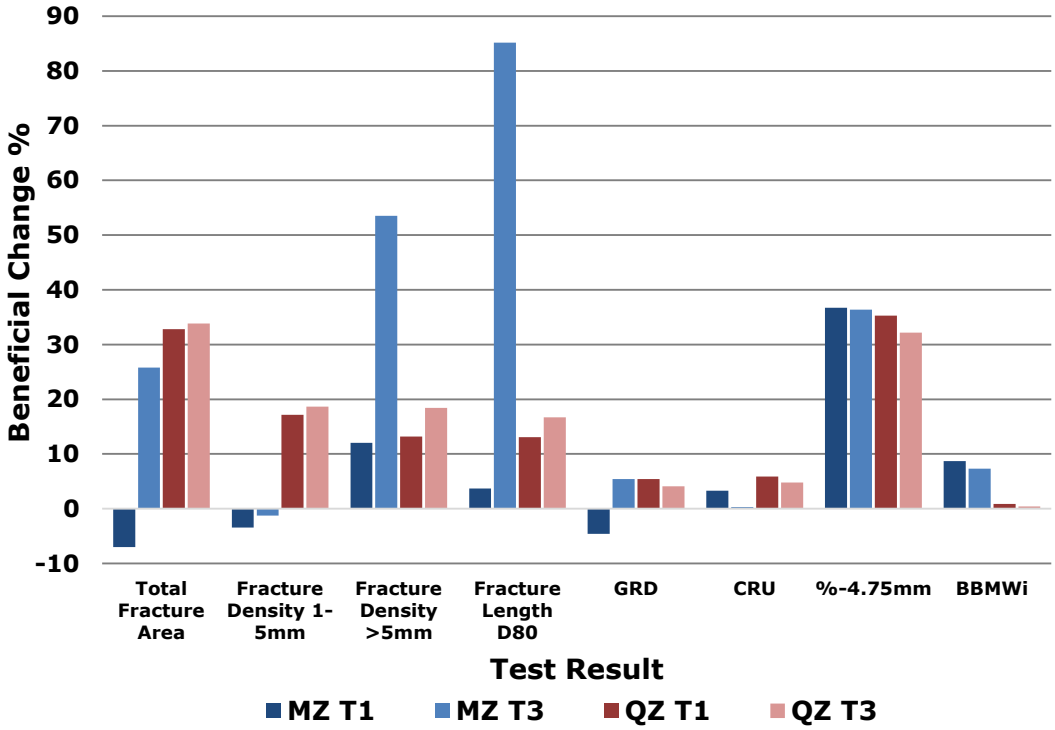


Figure 6.17 Comparison of fracture analysis results with comminution test results showing % beneficial change from the untreated sample for each test following microwave treatment.

While the MZ T1 sample showed minimal change in observable fracture properties following microwave treatment, it showed benefits in both %-4.75mm material in Ci testing, and in BBMWi. This indicates that while no significant observable changes in macro-fracturing were observable from the T1 treatment, weakening within the ore matrix is still occurring due to propagation of intergranular micro-fractures, resulting in ore strength reductions and comminution benefits. The MZ T3, QZ T1 and QZ T3 samples all showed positive changes in terms of sample fracture properties following microwave treatment, which generally translated into improvements in the Ci test results compared with their respective untreated samples.

While QZ T1 and T3 samples both showed increased fracture and changes in Ci test indices, they showed only minimal benefits in BBMWi. This may be due to any potential benefits from increased fracturing in QZ ore being realised during crushing of the ore to -3.35mm in order to conduct the BBMWi test. Also, as previously mentioned, the QZ untreated ore is already quite a soft and easily comminutable ore, and subsequently the potential for benefits to be seen in BBMWi are quite limited. These results suggest that greater comminution benefits for quartzitic ores may be achieved through microwave treatment and breakage of the ore at coarser fragment sizes of >50mm.

Mineral liberation analysis was conducted for MZ and QZ ores in the previous chapter to investigate the Cu-sulphide liberation benefits achievable through microwave treatment. Liberation analysis results have been compared to fracture analysis results to investigate the relationship between changes in ore fracture properties and enhancements in the liberation of Cu-sulphides from microwave treatments. A comparison between the beneficial change in fracture characteristics, and the beneficial change in the >98% liberated Cu-sulphide class for the microwave treated samples is shown in Figure 6.18.

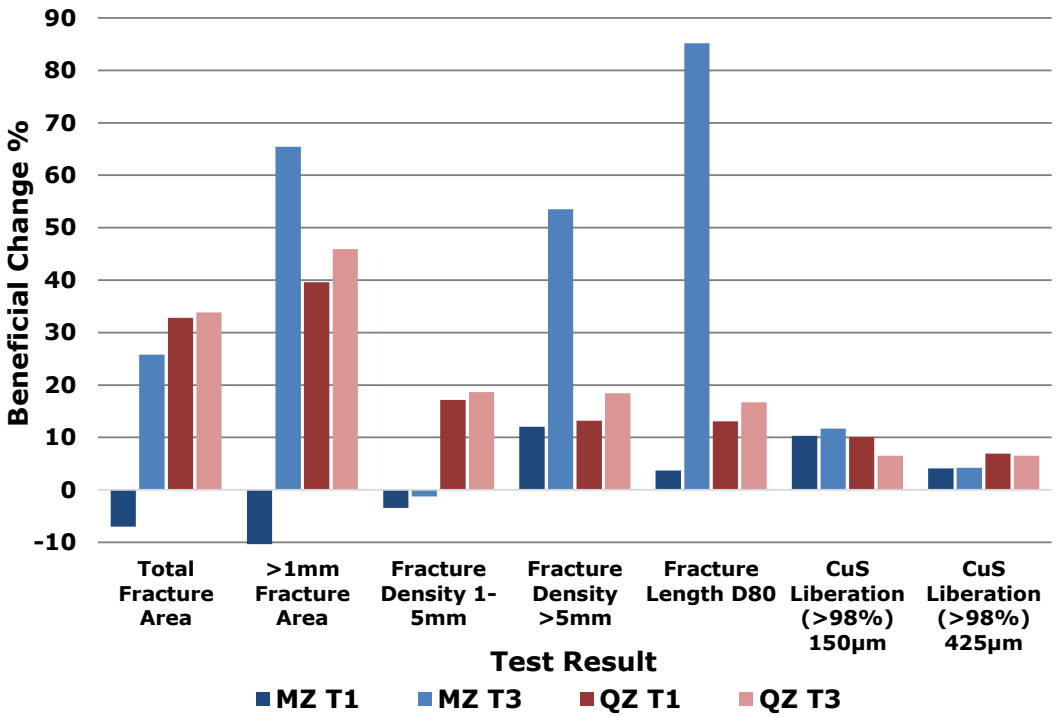


Figure 6.18 Comparison of fracture analysis results with Cu-sulphide mineral liberation results.

While the MZ T1 sample showed minimal increase in fracturing, it showed liberation improvements in the >98% Cu-sulphide liberation classes for both the fine and coarse grinds. This again supports the assertion that changes in the ore matrix are occurring when MZ ore is treated at a microwave power density of $3.3x10^6 W/m^3$ and a microwave dose of 0.7kWh/t. It is suggested that at these microwave treatment conditions, intergranular micro-fracturing is occurring around Cu-sulphide grains which are beyond the capability of the dye penetration technique to resolve.

Both QZ T1 and T3 microwave treated samples showed relatively consistent improvements in Cu-sulphide liberation compared to the untreated QZ sample, which correspond with consistent benefits seen in fracture analysis. This finding continues to support the suggestion that for QZ ore, microwave energy input beyond 0.7kWh/t, or microwave power density greater than $3.3x10^6 W/m^3$ deliver no further benefits in either Cu-sulphide liberation or fracturing.

6.7 SUMMARY

The aim of this chapter was to develop the understanding of the generation and propagation of fractures in microwave treated ores through the characterisation and quantification of fractures produced during the microwave treatment process. This required the development of a new experimental method for imaging and quantifying fractures in ore fragments, and the application of the method to the analysis of untreated and microwave treated ore samples. The results presented in this chapter support the findings of the mineral liberation analysis and comminution testing outcomes from the previous chapter. The fracture analysis results clearly show that benefits achieved in Cu-sulphide liberation and comminution testing can be attributed to the increases in fracturing observed as a result of microwave treatments.

Results for MZ ore showed only minor observable additional fracturing from the T1 treatment, however the T3 treatment showed increases to measured fracture length, area, and density of >5mm fractures in the sample. The MZ T1 sample showed improvements in both BBMWi testing and liberation analysis, despite only minor observable increases in fracture. MZ T3 showed improvements in both liberation and comminution results, as expected due to the observed increase in fracturing. The results presented for MZ ore in this chapter support the assertion that a microwave power density of $3.3x10^6 W/m^3$ and a microwave dose of 0.7kWh/t is sufficient for liberation and comminution benefits to be achieved, however higher levels of macro-fracturing are observed at a microwave power density of $5.3x10^6 W/m^3$ and a microwave dose of 1.3kWh/t.

Results for the QZ ore presented in this chapter show consistent increases in fracture length, area and density for both the T1 and T3 microwave treatments. This supports the suggestion that a microwave treatment dose of 0.7kWh/t and power density of $3.3x10^6 W/m^3$ is sufficient to introduce additional fractures in QZ ore, and that the

application of additional power or energy does not appear to induce further benefits in terms of fracturing of the ore fragments. QZ microwave treated samples both showed consistent benefits in Cu-sulphide liberation and comminution testing, which are consistent with the trends observed in the fracture analysis results.

Consistent increases in fracture length were observed in each of the treated QX ore samples, irrespective of microwave treatment conditions. Fracture area, and the density of 1-5mm length features in treated QX ore, appear to increase in line with increasing microwave treatment dose and power density. The density of >5mm fractures, or what could be considered as macro-fractures, does not observe this trend, and shows a reduction in fracture density for the T3 treatment. This indicates that linking up of macro-fractures is occurring, resulting in longer fractures of lower density. Overall, QX ore showed the greatest beneficial change in terms of fracturing as a result of microwave treatments. This is most likely due to QX ore possessing a highly amenable mineralogy and texture, with a sufficient abundance of coarse and granular pyrite, distributed relatively homogeneously throughout a gangue comprised predominantly of hard and brittle quartz.

The results presented in this chapter show that microwave treatments can induce additional beneficial fracturing in amenable ores. The beneficial fracture outcomes can also be seen to correspond with benefits achieved in Cu-sulphide liberation, and comminution testing by JK GeM Ci and BBMWi methods.

CHAPTER 7 – INVESTIGATING THE INFLUENCE OF POWER DENSITY AND ENERGY INPUT ON THE MICROWAVE TREATMENT OF COPPER ORES

7.1 INTRODUCTION

As presented in detail in the literature review conducted in Chapter 2, a number of previous researchers have investigated the influence of microwave power density and energy input on the beneficial outcomes achievable from the microwave treatment of ores in terms of enhanced mineral liberation and reductions in ore strength. Early work involving the use of low power microwaves (i.e. <3kW) in multimode applicators, required longer treatment durations for benefits to be achieved, and subsequently resulted in total microwave energy inputs of typically much greater than 10kWh/t that were not economically feasible (Walkiewicz et al., 1991; Kingman and Rowson, 1997; Kingman et al., 2000b; Vorster et al., 2001). Recent research by Marion et al. (2016) continues to support these early findings through microwave treatments of a copper-nickel sulphide ore using microwave power inputs of 3kW at 2.45Ghz in a multimode cavity. While a treatment duration of 60 seconds resulted in a 22% reduction in Bond Work Index for the ore and improvements in flotation recovery, the microwave energy input of 200kWh/t was deemed by the authors to be economically unviable.

The consistent finding of early experimental and theoretical studies into the microwave treatment of ores was that achieving a high microwave power density (W/m^3) over a rapid heating interval is vital for the development of high thermal stresses and subsequent microwave-induced fracturing. The use of higher microwave power of 15kW at 2.45GHz using a single mode cavity by Kingman et al. (2004b), demonstrated that ore strength reductions and improvements in Cu-sulphide mineral liberation could be achieved with a total microwave energy input of 0.83kWh/t. This is the lowest microwave

dose at which mineral liberation benefits have been previously reported for the microwave treatment of a copper ore. An investigation by Batchelor et al. (2015) showed benefits in ore strength reductions in a highly amenable lead-zinc ore, as measured by Point Load test, resulting from microwave treatment with 20kW power at 2.45GHz in a single mode cavity at a microwave dose of 0.5kWh/t. This is the lowest total microwave energy input at which comminution benefits have been previously reported in the literature for any ore type.

Experimental work conducted in this investigation, and presented in Chapters 5 and 6, has shown that benefits in Cu-sulphide mineral liberation and ore comminution, as measured by JK GeM Ci and BBMWi testing, are achievable for the amenable MZ and QZ copper ores at microwave energy inputs of 0.7kWh/t. These findings were supported by the fracture analysis investigation, which showed that at microwave energy inputs of 0.7kWh/t, additional beneficial fracturing was observable in microwave treated QZ and QX ores. It was identified however, that despite MZ ore showing a beneficial change in Cu-sulphide mineral liberation and changes in ore breakage response at a microwave treatment energy of 0.7kWh/t, at this dose minimal additional macro-fracturing was observed in the treated ore. These findings suggested that MZ ore was potentially approaching the minimum microwave energy input threshold at which benefits achieved from the treatments may begin to diminish. As such, MZ ore was selected for an additional set of microwave treatments at lower total microwave energy inputs, to investigate the minimum microwave dose threshold at which mineral liberation benefits or changes in the breakage behaviour of the ore can be achieved.

The aim of this chapter will be to investigate the relationship between microwave power density and microwave energy input for MZ ore, and to determine the lowest microwave treatment dose (kWh/t) at which measurable beneficial changes can be observed.

7.2 MICROWAVE TREATMENTS

7.2.1 Introduction

The low dose microwave treatments of MZ ore conducted to meet the aims of this chapter were performed using the microwave treatment batch system. As described in detail in Section 4.3.2, the batch system is a laboratory-based pilot plant, capable of treating ore samples of up to 60kg, at between 10-300t/h equivalent throughput, with between 60-200kW of microwave power at a frequency of 896MHz. The design of the system enables higher treatment throughputs to be achieved, with a maximum throughput equivalent of 300t/h for a treatment tube of 150kg total mass. This higher throughput feature of the batch system allows for lower total energy treatments to be conducted than in the pilot system, while still maintaining high microwave power input to the sample. The batch system is capable of performing a microwave treatment of up to a 60kg ore sample at a total microwave energy input of as low as 0.2kWh/t. This capability of the batch system will be critical to achieving the aims of this phase of the investigation.

7.2.2 Microwave Treatment Conditions

A 300kg sample of -50.8+25.4mm ore fragments was representatively split from the bulk stock of the same MZ ore treated and analysed in Chapters 5 and 6. This 300kg sub-sample was further split by RSD into five individual 60kg sub-samples. One of the sub-samples remained untreated to act as a control sample, and was designated as MZ UT2. The four remaining samples were subjected to microwave treatment using the batch system. MZ ore fines (<5mm) were utilised as void filling material in the sample treatment tube, as in the pilot system, to replicate the treatment conditions applied to the ore in the previous treatments, and to minimise the potential for arcing during treatment. Ore and fines were blended out of the batch system feed hoppers into the treatment tube to produce a homogeneously distributed 40:60 ore to fines ratio. The untreated sample was also

loaded and unloaded from the batch system treatment tube to replicate the materials handling conditions experienced by the microwave treated samples.

A program of four additional microwave treatments was performed for the MZ ore, with the different treated samples designated as T4, T5, T6 and T7. These designations were used to follow on from the T1, T2 and T3 treated samples produced previously for MZ ore in this investigation. The microwave treatment conditions used in producing the MZ treated samples required to address the proposed aims of this phase of the investigation are detailed in Table 7.1.

Ore	Sample	Microwave Treatment System	Throughput (t/h)	Total Microwave Power (kW)	Treatment Energy 'Dose' (kWh/t)	Power Density in Applicator (W/m^3)
MZ	**T4**	Batch	300	2x30	**0.2**	$2.0x10^6$
	T5	Batch	180	2x30	**0.3**	$2.0x10^6$
	T6	Batch	300	2x50	**0.3**	$3.3x10^6$
	T7	Batch	240	2x80	**0.7**	$5.3x10^6$

Table 7.1 Microwave treatment conditions for MZ ore low dose treatments.

The MZ T4 treatment conditions produce the lowest possible microwave dose achievable with the batch treatment system of 0.2kWh/t. The MZ T5 and T6 treatments result in the sample being subjected to the same microwave dose of 0.3kWh/t, however the microwave power density and sample throughput varies between the treatments. These treatment conditions were chosen to investigate whether differences in the benefits achieved can be observed from treatments of the same total microwave energy input performed at different microwave power densities. The MZ T7 treatment conditions were selected to match the microwave power density of the MZ T3 treatment at half the microwave dose, and to match the microwave dose of the MZ T1 treatment at a higher power density. These additional treatments of MZ ore will allow for the investigation of the relationship between microwave dose and microwave power density on the benefits achieved from the treatments, and for assessing the

minimum microwave dose at which Cu-sulphide mineral liberation and comminution benefits can be achieved for MZ ore.

7.3 Mineral Liberation Analysis

7.3.1 Introduction

In order to assess the impacts of the lower dose microwave treatments on the liberation of Cu-sulphide minerals in MZ ore, both the untreated and microwave treated samples were subjected to analysis by MLA automated mineralogy.

7.3.2 Sample Preparation and Analysis Procedure

The 60kg samples of the untreated and each of the microwave treated samples were stage crushed following comminution testing describe in the next section, using a consistent closed size setting of ~1mm in a laboratory jaw crusher to ensure consistent breakage conditions. The crusher products were split by RSD to produce representative 1kg sub-samples for batch grinding. Grinding was performed in a laboratory rod mill which was operated at 60wt% solids and 70% critical speed (68rpm). A series of rod mill calibration grinds were conducted at 2min, 4min, 8 min and 16min durations in order to determine the grind time required to achieve a target grind P_{80} of 290µm for the untreated and microwave treated samples. The target grind size P_{80} of 290µm was selected as it is 50µm coarser than the Cu-sulphide grain size D_{80} of 240µm, based on the MZ coarse ore characterisation conducted in Chapter 5. The selection of this grind size will allow for the observation of preferential liberation occurring of Cu-sulphides in the microwave treated samples at, or close to, their native grain size in the ore. It will also minimise the possibility of any benefits achievable through alterations of the ore matrix as a result of the microwave treatments, being eliminated or negated through over-grinding of the ore. The milled samples were then wet and dry sieved into the √2 series, and prepared for mineralogical analysis by MLA using the XBSE

measurement mode, as described in Section 4.4.3.3. Particle size distributions for the untreated and each of the low dose microwave treated samples are shown in Figure 7.1. This highlights the accuracy of the grinding performed in order to produce particulate samples for mineral liberation analysis. This grinding accuracy ensures that any differences observed in Cu-sulphide liberation are a function of differences in the ore samples, rather than differences in sample particle size distribution. Details of grinding calibrations are included in Appendix A.

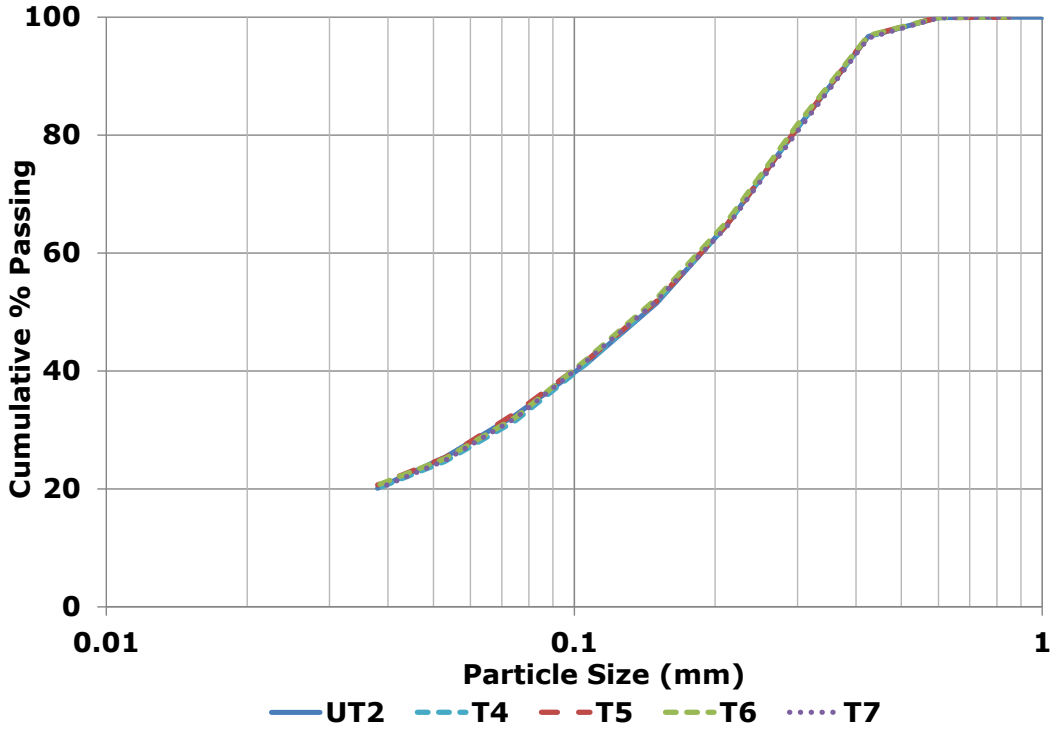


Figure 7.1 Particle size distribution of P_{80} 290µm target grinds for mineral liberation analysis.

7.3.3 Results

The grouped modal mineralogy for the MZ ore samples used in this phase of the investigation is shown in Table 7.2. The mineralogy of the untreated and treated samples produced for this series of experiments is very consistent with the MZ ore samples analysed in Chapter 5, which demonstrates good sampling from the bulk ore material. Consistency is also observed between each of the untreated and microwave treated samples analysed for this series of

experiments, demonstrating good sub-sampling practice. As the abundance of microwave heating minerals and the gangue composition are very similar to the initial MZ samples, any differences in the benefits achieved can be deemed to have resulted from the different microwave treatment conditions employed, rather than variations in sample mineralogy. All samples have an abundance of sulphide heaters of between 5.44-5.58 wt%, and a total microwave heating mineral abundance of between 6.24-6.35 wt%. The gangue is comprised predominantly of quartz, feldspar and micas, with ~70% of the gangue composed of hard minerals, and ~22% composed of soft minerals.

MZ Ore Grouped Mineral Abundance (wt %)									
Grouped Minerals			UT2	T4	T5	T6	T7	AVE	Std Dev.	CoV %
Good Heaters	Copper Sulphides	Chalcopyrite	1.05	1.08	1.02	0.99	1.10	1.05	0.04	4
		Other Cu Sulphides	0.07	0.06	0.06	0.06	0.06	0.06	0.01	10
	Other Sulphides	Pyrite	4.41	4.28	4.41	4.45	4.32	4.37	0.07	2
		Other Sulphides	0.05	0.03	0.03	0.03	0.01	0.03	0.01	41
	Non-sulphide	Montmorillonite	0.77	0.80	0.76	0.78	0.81	0.78	0.02	2
Other Heaters		Iron Oxides	0.22	0.24	0.41	0.32	0.19	0.28	0.09	33
Non-heating Gangue	Hard Gangue Mohs ≥6	Quartz	40.08	40.65	38.81	39.46	39.20	39.64	0.73	2
		Feldspar	28.76	28.28	29.96	29.11	29.13	29.05	0.62	2
		Other Hard	1.86	1.77	1.61	1.79	2.02	1.81	0.15	8
	Soft Gangue Mohs <6	Micas	21.93	22.05	22.13	22.21	22.46	22.16	0.20	1
		Carbonates	0.35	0.25	0.28	0.24	0.25	0.27	0.05	17
		Other Soft	0.00	0.00	0.00	0.00	0.00	0.00	0.00	0
	Others		0.45	0.53	0.52	0.55	0.45	0.50	0.05	9
	Total		**100**	**100**	**100**	**100**	**100**	**100**		
	All Sulphide Heaters		5.58	5.44	5.52	5.53	5.49	5.51	0.05	1
	Good Heaters		6.35	6.24	6.28	6.31	6.30	6.30	0.04	1
	All Heaters		6.57	6.48	6.69	6.63	6.49	6.57	0.09	1
	Hard Gangue Minerals		70.70	70.70	70.38	70.36	70.35	70.50	0.18	0
	Soft Gangue Minerals		22.28	22.30	22.41	22.45	22.71	22.43	0.17	1

Table 7.2 MZ ore grouped mineral abundance for untreated and low dose treated samples. [Other Cu-Sulphides comprises bornite, chalcocite, covellite; Other Sulphides comprises molybdenite, sphalerite; Iron Oxides comprises magnetite, hematite; Other Hard comprises zircon, pyroxenes/amphiboles, apatite; Other Soft comprises talc, gypsum fluorite; Micas comprises muscovite, phlogopite, biotite, chlorite; Carbonates comprises calcite, dolomite, siderite.]

The distributions of Cu-sulphide minerals by liberation class for the MZ ore lower dose treatments at the target grind P_{80} of 290µm are shown in Figure 7.2. The MZ T5 sample shows the greatest change in Cu-sulphide reporting to the >98% liberated class, with a 4.5% increase compared to the untreated sample. The T6 and T7 samples show

minor positive changes in the >98% liberated Cu-sulphide class of 1.8% and 2.3% respectively. The lowest dose T4 sample shows only a very minor 0.5% increase in the proportion of Cu-sulphides reporting to the >98% liberated class.

As was observed for MZ ore in Chapter 5, increases seen in the >98% liberated class as a result of microwave treatment correspond with decreases in the proportion of Cu-sulphides reporting to the 50-98% liberated high-grade middlings class and the 10-50% liberated low-grade middlings class. This finding is consistent with the previous observations that Cu-sulphides are being redistributed to higher liberation classes as a result of splitting of the low and high grade middlings binary and multiphase particles. This indicates that, even at the low doses used in this series of treatments, the properties of the MZ ore have been altered, and preferential liberation of Cu-sulphide minerals is occurring due to the generation of intergranular micro-fractures.

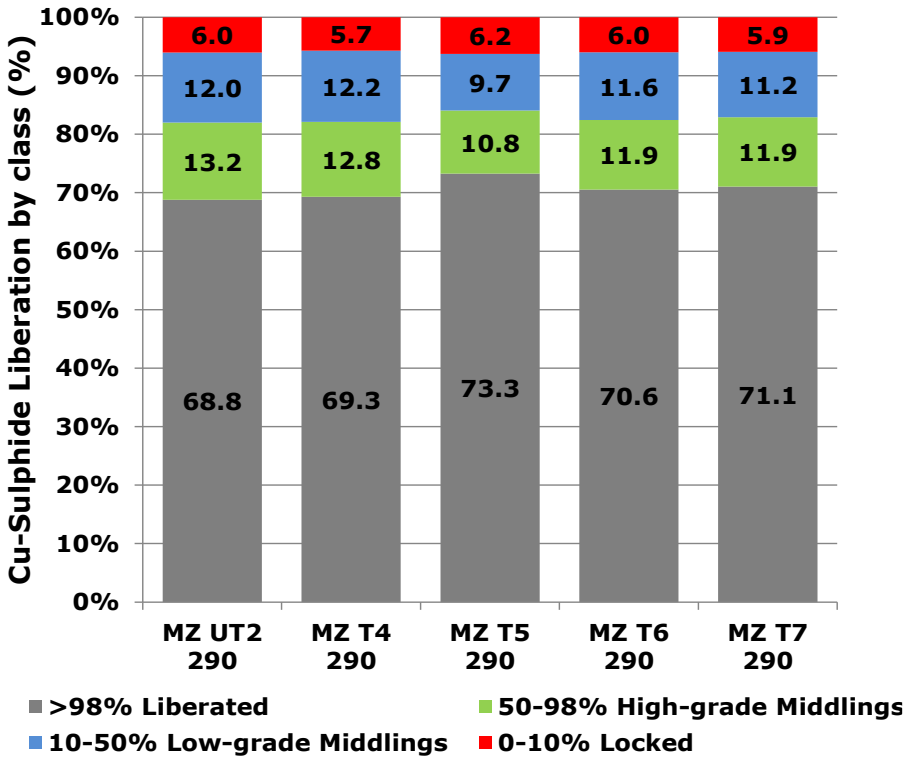


Figure 7.2 MZ ore Cu-sulphide distribution by liberation class.

When the Cu-sulphide liberation results for this series of treatments are presented as 5% liberation classes, as shown in Figure 7.3, it can be clearly observed that the MZ T5 treatment resulted in the greatest benefit in Cu-sulphide mineral liberation compared to the untreated MZ UT2 sample. A gradual increase is observed in the difference between the MZ UT2 and MZ T5 liberation distribution from the 35-40% class through to the 100% class, indicating the redistribution of particles into the higher liberation classes as a result of splitting of the middlings particles. A similar, although less pronounced effect is also observable for the MZ T7 sample, while the MZ T6 samples shows only a very minor and relatively consistent increase across the liberation distribution. Only a very minor difference in liberation distribution is observed for the MZ T4 sample compared to the MZ UT2 sample, occurring mainly in liberation classes greater than the 80-85% classes. This suggests that for the MZ T4 treatment, splitting of the middlings particles is not occurring, which indicates that the very low dose of 0.2kWh/t has not sufficiently altered the ore matrix through the generation and propagation of intergranular micro-fractures for preferential liberation to take place.

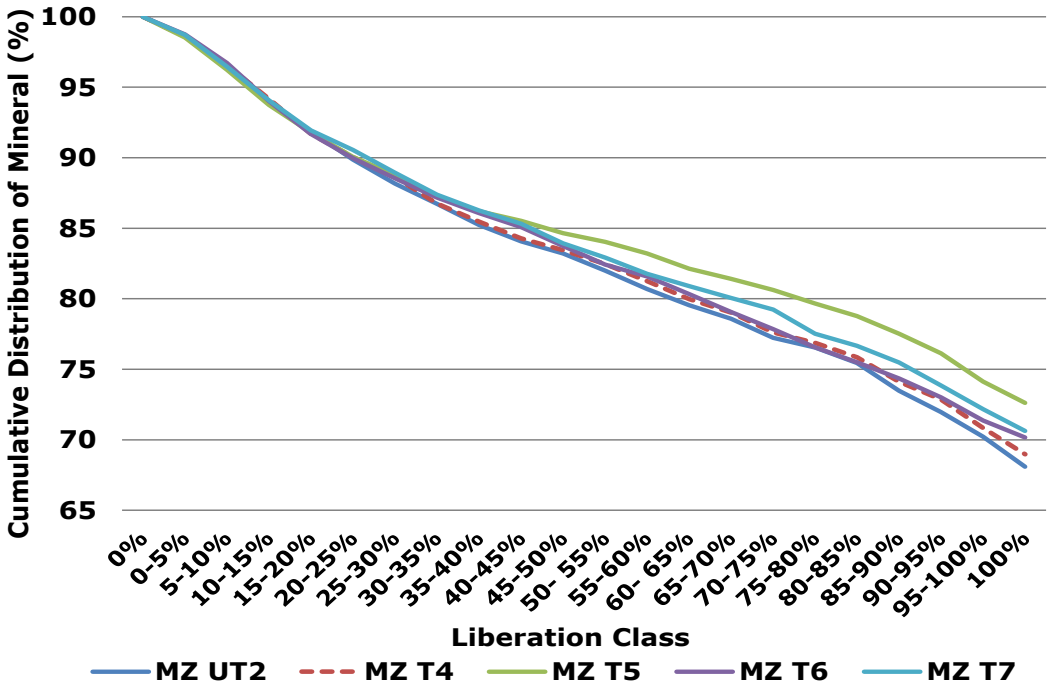


Figure 7.3 MZ ore Cu-sulphide distribution by 5% liberation classes for low dose treatments.

The degree of unlocking or liberation of Cu-sulphides from binary and multiphase particles can be determined through assessments of Cu-sulphide mineral locking data produced by the MLA. Mineral locking data for Cu-sulphides occurring as binary particles with non-sulphide gangue (NSG) minerals, as a binary particle with pyrite, or in a multiphase particle, is shown in Figure 7.4. As expected from the Cu-sulphide liberation results, the MZ T5 sample showed the greatest change in mineral locking as a binary particle with NSG compared to the untreated sample, with a 4% reduction. The MZ T4, T6 and T7 samples all showed only minimal (~1%) change in Cu-sulphide:NSG binary particles. Minimal change is observed in the Cu-sulphide:pyrite binary particles and multiphase particles between the untreated and all microwave treated samples, although there is a relatively low abundance of these types of locked particles able to be spilt.

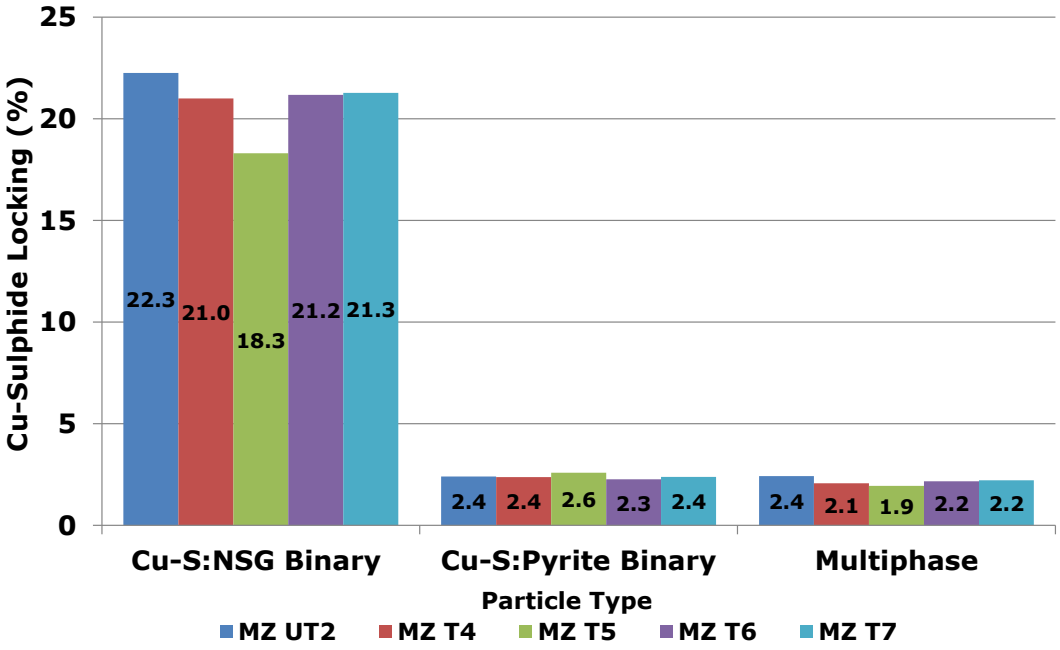


Figure 7.4 Cu-Sulphide (Cu-S) mineral locking results for MZ ore low dose treatments.

A detailed analysis of the locking behaviour of Cu-sulphides with NSG minerals is shown in Figure 7.5. NSG minerals have been separated into 'Hard' and 'Soft' mineral groupings to investigate whether preferential particle splitting is observable. While these results confirm that the MZ T5 treatment was the most effective at splitting of binary and multiphase particles comprising Cu-sulphide minerals with NSG,

the results do not show a clear preference for particle splitting based on the hardness characteristics of the NSG minerals. This finding suggests that, at low microwave doses of less than 0.7kWh/t, enhanced particle splitting and subsequent improvements in liberation can be achieved in an ore comprising a 'soft' gangue mineral component.

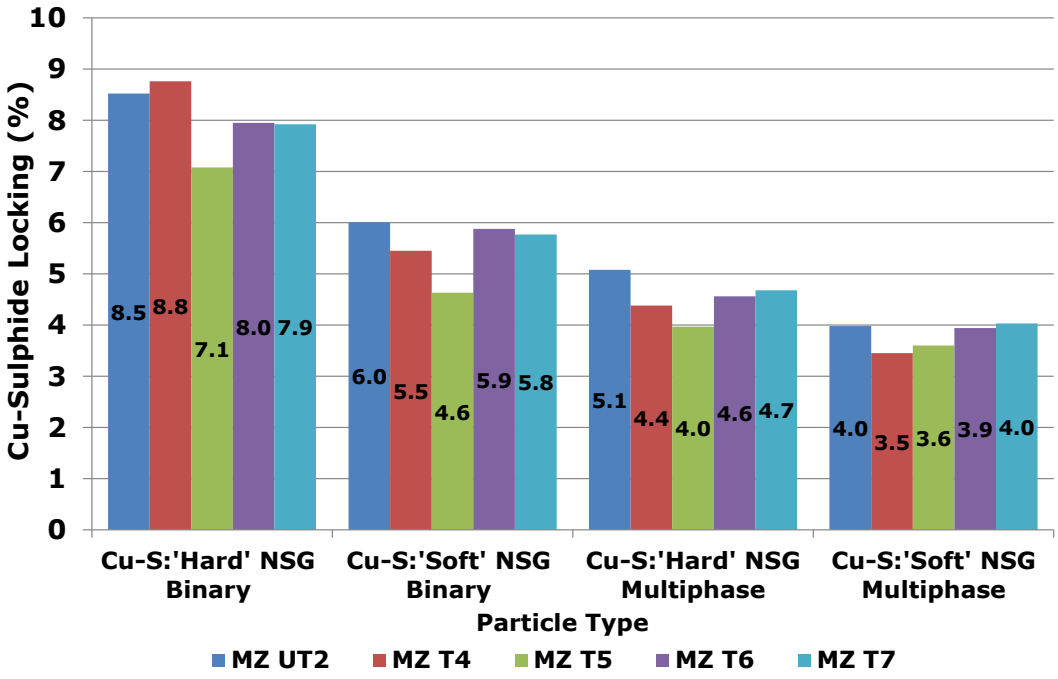


Figure 7.5 Cu-Sulphide (Cu-S):Non-Sulphide Gangue (NSG) mineral locking results for MZ ore low dose treatments.

In contrast to the liberation results achieved for the MZ UT1, T1, T2 and T3 samples assessed in Chapter 5, which showed no clearly observable difference between the liberation results for samples treated at different energy inputs >0.7kWh/t, the results from this series of treatments does show variation in liberation of Cu-sulphides with changes in microwave treatment conditions. Interestingly, it is not the highest microwave dose or power density treatment which resulted in the greatest beneficial change in Cu-sulphide mineral liberation. It was expected that the T7 treatment conditions of 0.7kWh/t and $5.3x10^6 W/m^3$ would have resulted in the greatest benefits in Cu-sulphide mineral liberation from the microwave treatment, as this dose and power density were both shown to achieve

beneficial outcomes in mineral liberation in Chapter 5. This finding suggests that the rate of sample throughput, and subsequently the residence time of the sample in the applicator, may have an influence on the effectiveness of a microwave treatment. In addition to there being a microwave power density and energy input threshold below which microwave treatment benefits diminish, there may also be a throughput threshold which influences the effectiveness of a treatment. Above a certain throughput, or below a corresponding residence time threshold, the sample may not spend sufficient time in the applicator for adequate microwave absorption and thermal expansion to take place. This would minimise the formation of stresses within the ore matrix, limiting the generation and propagation of micro and macro-fractures within the ore fragments.

These liberation results are consistent with the observations of Wills and Atkinson (1993), that a slower application of strain during comminution promotes stable fracture propagation and exploits grain boundary weaknesses more effectively than higher energy and faster strain processes. Stable crack propagation along grain boundaries has been shown to be most effective at lower velocities, unlike in conventional comminution processes where high strain rates cause unstable crack propagation, leading to random transgranular fracturing (Meredith and Atkinson, 1983). Comminution conducted through the slow application of pressure to an ore, rather than by rapid application of energy, can create residual internal stresses which can cause cracking to occur around grains during a subsequent relaxation phase. Where comminution energy is transmitted rapidly to the ore, the material has little time to absorb the strain energy, and no material relaxation phase cracking will occur. This slow strain mechanism is employed by High Pressure Grinding Rolls, where it has been shown that a longer exposure to the compressive forces between the rolls more effectively exploits grain boundary weaknesses during comminution. This slow strain comminution also more effectively generates intergranular micro-fractures throughout the ore, which has

been shown to lead to improvements in mineral liberation following HPGR crushing (Baum et al., 1997).

The relationship between the beneficial change in the >98% liberated Cu-sulphide class and microwave dose is shown for all MZ ore microwave treatments in Figure 7.6. It should be re-iterated here that the beneficial change shown for the MZ 425µm grind is a comparison between a grind P_{80} of 370µm for the UT1 untreated sample with a grind P_{80} of 425µm for the T1, T2 and T3 treated samples. Interpolation of the Cu-sulphide liberation results for the microwave treated samples to a grind P_{80} of 370µm was considered for comparison against the untreated sample, however, the assumption of a linear relationship between liberation results at different grind sizes could not be supported with the current data. Further work in this field could investigate this relationship between grind size and mineral liberation for microwave treated ores to study this relationship in greater depth.

Two key observations can be made from Figure 7.6. Firstly, that microwave treatments conducted at throughputs <200t/hr result in greater beneficial changes in Cu-sulphide mineral liberation than treatments conducted at faster throughputs >200t/hr. This is clearly illustrated by a comparison between the 180t/hr T5 treatment at 0.3kWh/t, and the 300t/hr T6 treatment at the same microwave dose. Despite the T6 treatment receiving a higher microwave power density to achieve the required dose at the 300t/hr throughput, the T5 treatment showed the greater beneficial change in Cu-sulphide liberation. The second observation, which is arguably more important in the context of this investigation, is that a beneficial change in Cu-sulphide mineral liberation has been achieved for MZ ore at a total microwave energy input of 0.3kWh/t. This is a significant finding, considering the lowest reported microwave energy input at which mineral liberation benefits have been achieved previously for a copper ore is 0.83kWh/t (Kingman et al., 2004b). This outcome indicates that scale-up of the process to industrially relevant throughputs (i.e.

>10,000 t/h) could potentially be achieved using existing microwave generator technology to produce the required microwave treatment dose, eliminating the need for the development of higher power generators producing over 100kW of microwave power.

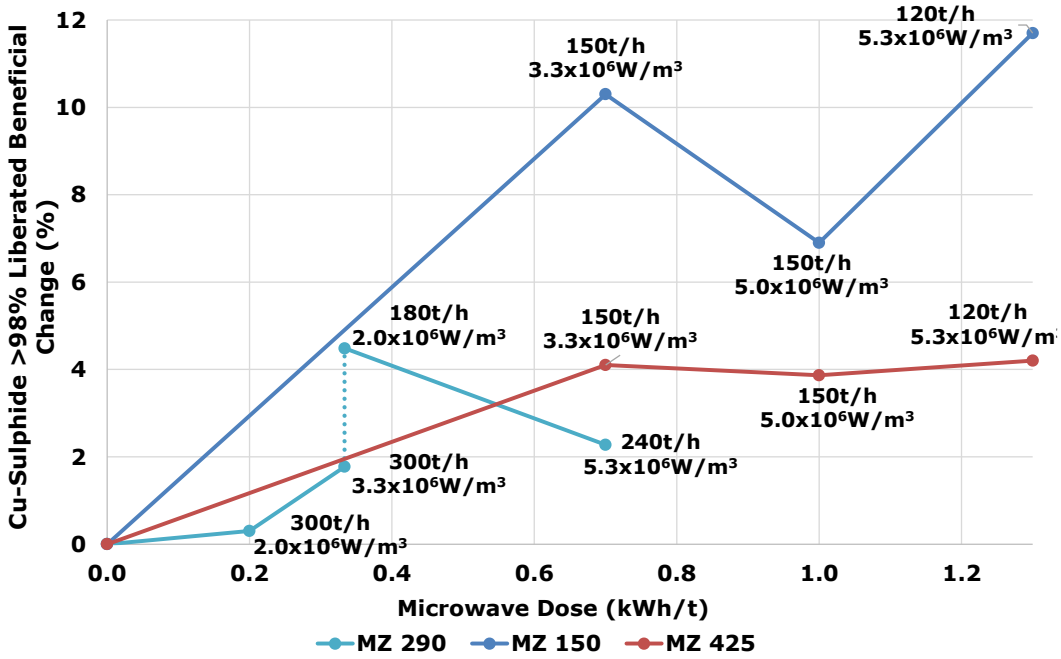


Figure 7.6 Beneficial change in >98% liberated Cu-sulphides for MZ ore at varying microwave treatment doses. The dashed line connects treatments of the same dose and different power density. Data labels show throughputs and microwave power density at each treatment dose.

The relationship between the beneficial change in the >98% liberated Cu-sulphide class and microwave power density is shown for all microwave treatments conducted for MZ ore in Figure 7.7. The key observation from this figure is that a beneficial change can be achieved in Cu-sulphide liberation in MZ ore at a microwave power density of $2.0x10^6W/m^3$, if conducted at a throughput which results in a microwave dose of 0.3kWh/t, as for the MZ T5 treatment. The same power density treatment at a higher throughput, and subsequently lower microwave dose of 0.2kWh/t, as for the MZ T4 treatment, showed only very minor beneficial change in Cu-sulphide mineral liberation.

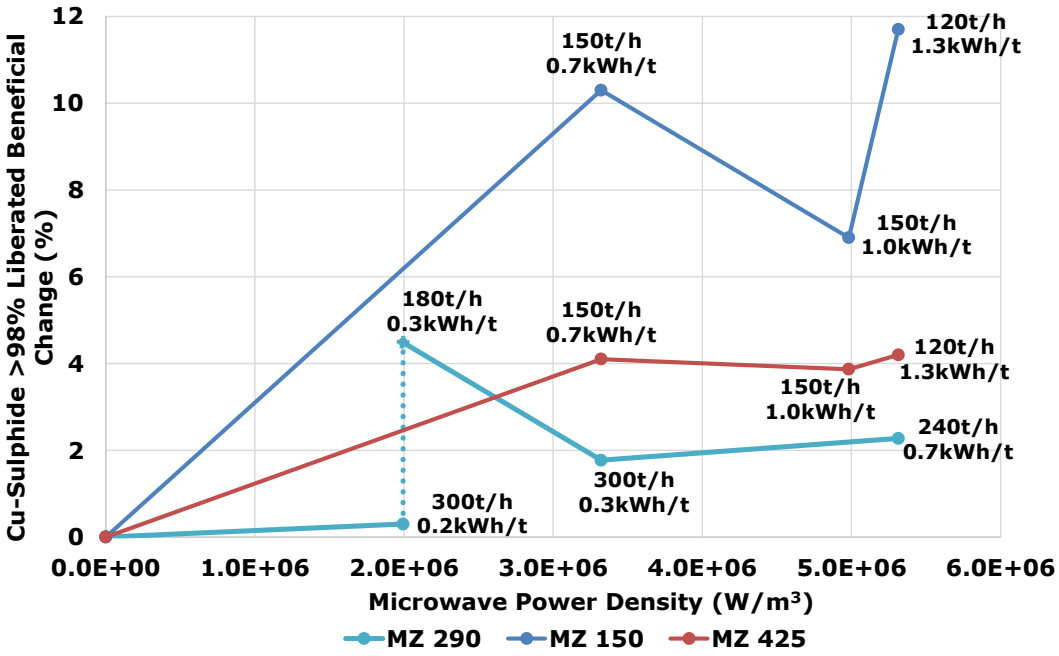


Figure 7.7 Beneficial change in >98% liberated Cu-sulphides for MZ ore at varying microwave treatment power densities. The dashed line connects treatments of the same power density and different dose. Data labels show throughput and microwave dose at each treatment power density.

Given that the microwave applicators used in both the pilot system and batch system have the same internal height dimension of 121mm, samples treated in both systems will travel a combined total of 242mm inside a microwave applicator during a dual applicator treatment. With knowledge of the sample velocities (mm/s) required in order to achieve the targeted throughputs, it is possible to calculate the total microwave applicator residence duration experienced by each microwave treated sample. The total microwave applicator residence durations, and their corresponding throughputs and treatment velocities, are shown for all MZ ore microwave treatments in Table 7.3.

Ore	Sample	Microwave Treatment System	Throughput (t/h)	Sample Treatment Velocity (mm/s)	Total Applicator Residence Duration (sec)
MZ	T1	Pilot	150	750	0.32
	T2	Pilot	150	750	0.32
	T3	Pilot	120	600	0.40
	T4	Batch	300	1500	0.16
	T5	Batch	180	930	0.26
	T6	Batch	300	1500	0.16
	T7	Batch	240	1200	0.20

Table 7.3 MZ ore microwave treatment throughput, sample velocity and applicator residence duration.

The relationship between the beneficial change in the >98% liberated Cu-sulphide class and microwave applicator residence duration is shown for all microwave treatments conducted for MZ ore in Figure 7.8. It can be observed in this figure that shorter applicator residence durations, and subsequently higher sample throughputs, appear to result in a diminished beneficial change in Cu-sulphide liberation. These results suggest that for MZ ore, a minimum applicator residence duration of ~0.25 seconds is required for substantial liberation benefits to be achieved.

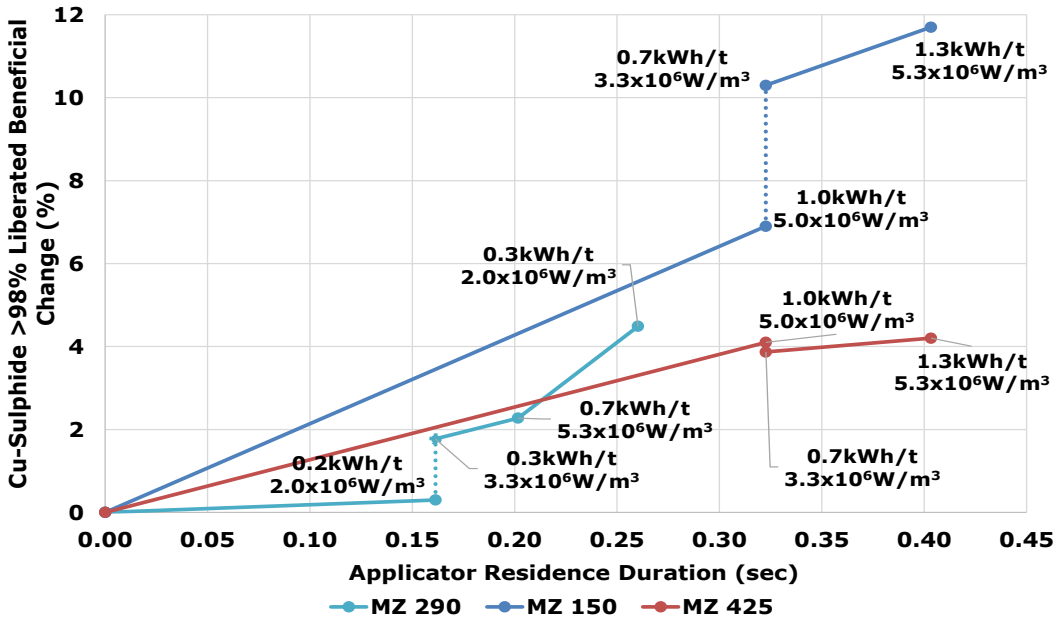


Figure 7.8 Beneficial change in >98% liberated Cu-sulphides for MZ ore at varying microwave applicator residence durations. The dashed line connects treatments of the same duration. Data labels show the microwave dose and power density corresponding with each treatment duration.

Analysis of the results for all microwave treated MZ ore samples has shown that Cu-sulphide mineral liberation benefits can be achieved at a microwave power density of $2.0x10^6W/m^3$, and a microwave dose of 0.3kWh/t, provided that the throughput rate allows the sample a total residence duration of ≥~0.25 seconds in the microwave applicators for sufficient thermal expansion of heating minerals to occur, and intergranular micro-fractures to be generated.

7.4 COMMINUTION TESTING

7.4.1 Introduction

Comminution testing of microwave treated MZ ore samples in Chapter 5 showed that changes in ore breakage behaviour are achievable at a microwave power density of $3.3x10^6W/m^3$ and a total microwave energy input of 0.7kWh/t. An inconsistency in this set of results was the detrimental effect observed in the Ci test GRD result for the MZ T1 lowest energy treatment. It was suggested that the microwave treatment conditions used for this treatment have potentially reached a threshold at which a different change in ore breakage characteristics may be observed. In order to investigate whether a microwave treatment power density or dose threshold has indeed been reached, microwave treated MZ ore samples produced for this phase of the investigation will be subject to comminution testing by JK GeM Crushing Index testing and Bond Ball Mill Work Index testing. The aim of these tests will be to determine whether measurable changes in ore impact breakage response and grindability can still be observed in lower power density and lower dose treatments of MZ ore.

7.4.2 Sample Preparation and Testing Procedure

Comminution testing conducted in this phase of the investigation was designed to replicate the tests performed in Chapter 5 in order to ensure comparability between the results. JK GeM Ci testing was conducted on -31.5+26.5mm ore fragments that were screened out of

the 60kg untreated and microwave treated MZ ore samples. The -31.5+26.5mm size class represents the largest proportion of mass within the nominally -50.8+25.4mm sample fragment size class used for microwave treatments in this study. Approximately 15kg of screened -31.5+26.5mm size fragments were produced for each sample, and these samples were then spilt by RSD to produce three ~5kg samples for the untreated and each of the microwave treated samples. Ci testing was conducted in triplicate for the untreated and each microwave treated sample to allow for the determination of confidence levels by t-test. Samples were crushed in a laboratory jaw crusher with a closed size setting of 11.6mm to achieve a fixed size reduction ratio of 2.5, based on the geometric mean ore fragment size to crusher CSS. As described previously, the Ci test produces three key results; the CRU and GRD indices, and the percentage of material passing a 4.75mm sieve after crushing.

Following completion of the Ci crushing tests, the crushed -31.5+26.5mm material was re-combined with the rest of the original sample and the entire 60kg sample was stage crushed to a CSS of 1mm. It is from this sample that 1kg representative sub-samples were split using RSD for mineral liberation analysis conducted in the previous section. 1kg representative sub samples were also produced for BBMWi testing.

The BBMWi testing procedure used in Chapter 5 was replicated for the samples produced in this phase of the investigation. Again, it was necessary to artificially alter the BBMWi test feed size distribution of the microwave treated samples to be the same as the untreated sample, to ensure that the work index value may be used as a true comparison of any change in ore competency, and is not due to differences in initial feed size distributions. BBMWi testing followed the same procedure as previously described to measure the specific energy required (kWh/t) to reduce the untreated and treated samples from their original feed size to 80% passing size of 160µm, using a closing sieve size in the Work Index calculations of 212µm.

7.4.3 JK GeM Crushing Index Test Results

The results produced from Ci testing of untreated and microwave treated MZ ores are shown in Table 7.4. All the tests were conducted in triplicate, and the mean results for each test outcome are shown with their respective standard deviations and co-efficients of variance (CoV). The percentage change of each result for the microwave treated samples in relation to the untreated control sample is also shown.

Ore	Sample	GRD			CRU			%-4.75mm			Beneficial Change (%)			Confidence Level (%)		
		Mean	Std Dev.	CoV (%)	Mean	Std Dev.	CoV (%)	Mean	Std Dev.	CoV (%)	GRD	CRU	% - 4.75 mm	GRD	CRU	%- 4.75 mm
MZ	UT2	0.504	0.025	4.9	2.883	0.12	4.3	15.68	0.35	2.2						
	T4	0.519	0.009	1.8	3.041	0.18	5.9	15.57	0.62	4.0	-3.0	5.5	-0.8	80	87	61
	T5	0.532	0.004	0.8	3.171	0.16	5.0	15.61	0.17	1.1	-5.7	10.0	-0.5	94	97	62
	T6	0.527	0.017	3.2	3.058	0.04	1.4	15.77	0.74	4.7	-4.7	6.1	0.5	88	96	57
	T7	0.530	0.003	0.6	3.114	0.10	3.3	15.70	0.37	2.4	-5.1	8.0	0.1	92	93	53

Table 7.4 JK GeM Ci test results for MZ ore low dose treatments.

Ci test results for the MZ ore low dose treatments show a relatively consistent detrimental change in GRD index values for all microwave treated samples when compared to the untreated MZ UT2 sample. This finding is consistent with the Ci test GRD result of the MZ T1 treatment presented in Chapter 5 which also saw a detrimental change in GRD index. This is an interesting finding in that it shows that at microwave treatment doses of less than or equal to 0.7kWh/t, a different change in ore breakage behaviour is observed as a result of microwave treatments than at microwave doses greater than 0.7kWh/t. As previously stated, a detrimental change in GRD value does not indicate that a microwave treated sample performs worse during comminution than the untreated sample. It does, however, show that the crushing response of MZ ore is different after being subjected to lower (≤0.7kWh/t) dose microwave treatments compared to higher (>0.7kWh/t) dose treatments. This suggests that the lower dose microwave treatments altered the physical properties of the ore matrix in a different way than the higher dose treatments, leading to a measurable change in ore breakage behaviour. CRU index results

show a change of between 5.5-10% for the treated samples compared to the untreated sample at high confidence levels. This indicates that a change in the impact resistance of MZ ore has also occurred as a result of the lower dose microwave treatments.

The MZ T5 treated sample, which showed the greatest beneficial change in Cu-sulphide mineral liberation, also showed the greatest changes in both GRD and CRU indices. This finding indicates that the generation of fracturing and physical alteration of the properties of MZ ore resulting from a treatment with a microwave dose of 0.3kWh/t at a power density of $2.0x10^6 W/m^3$, achieved a change in the breakage behaviour of the ore that promoted an enhancement of the liberation of Cu-sulphide minerals during subsequent grinding. Surprisingly, the MZ T4 sample, which received the lowest microwave treatment dose of 0.2kWh/t, showed changes in GRD and CRU indices of -3.0% and 5.5% respectively. This suggests that, while the MZ T4 treatment did not result in a measurable beneficial change in Cu-sulphide liberation, these microwave treatment conditions were still able to affect the breakage characteristics of the ore compared to an untreated sample.

7.4.4 Bond Ball Mill Work Index Test Results

The results produced from BBMWi testing of the MZ ore untreated UT2 sample and the low dose microwave treated MZ ore samples are shown in Table 7.5. Unfortunately, due to time and equipment constraints, testing in triplicate was not able to be conducted for this phase of the investigation in the required timeframe, however a single BBMWi test was completed for the untreated and each of the low dose microwave treated samples. The beneficial change in BBMWi for the microwave treated samples is also shown in comparison to the untreated sample.

Ore	Sample	F_{80} (µm)	P_{80} (µm)	Gbp (g/rev)	BBMWi (kWh/t)	Beneficial Change (%)
MZ	UT2	1526	165	2.57	12.67	
	T4	1526	168	2.68	12.36	2.4
	T5	1526	167	2.58	12.74	-0.6
	T6	1526	167	2.64	12.46	1.6
	T7	1526	166	2.59	12.65	0.2

Table 7.5 BBMWi test results, Gbp = ball mill grindability, (g/rev), P_{80} = size at which 80% of the product passes, (µm), F_{80} = size at which 80% of the feed passes, (µm).

The BBMWi test results for the low dose MZ ore treatments showed that the UT2 sample returned a BBMWi value of 12.67kWh/t. BBMWi beneficial energy reductions of 2.4% and 1.6% were recorded for the MZ T4 and T6 samples, the T5 sample showed a slightly worse result than the untreated UT2 sample, while the T7 sample essentially showed no change.

These results are inconsistent with the trends observed for this series of microwave treated samples with regards to the beneficial changes seen in Cu-sulphide mineral liberation and changes in ore breakage characteristics shown by Ci testing. The results are also inconsistent with the microwave treatment conditions employed in this series of tests. It would have been expected that the MZ T5 sample, which has shown the greatest benefit in Cu-sulphide mineral liberation and the greatest change in ore breakage response as a result of microwave treatment, would also return the greatest reduction in grinding energy as measured by BBMWi. Since only a single BBMWi test has been completed for each sample, the reliability of the results and the confidence levels of the comparisons with the untreated sample were not able to be assessed. As such, these results have been deemed to be inconclusive and no reliable outcomes can be observed. Additional replicate BBMWi testing of these samples could be conducted in future work to improve the statistical reliability of these results and verify the outcomes.

7.5 SUMMARY

The overall aim of the microwave treatments and analysis conducted in this chapter, has been to investigate the influence that microwave power density and energy input have on the benefits achieved in terms of enhanced Cu-sulphide mineral liberation, and improvements in ore comminution performance. Through conducting a series of additional lower dose microwave treatments of MZ ore than those performed in Chapter 5, a wider range of microwave doses and power densities were able to be compared for a single ore. Through analysis of the benefits achieved by these microwave treatments in comparison to the untreated ore, it was possible to determine a minimum threshold for microwave power density and dose at which Cu-sulphide mineral liberation benefits could be achieved for MZ ore.

An additional important finding from this series of experiments was the influence that sample throughput, or in other terms the residence duration of the sample within the applicators during treatment, has on the effectiveness of the microwave treatment. It was observed that a minimum applicator residence duration appears to exist, below which mineral liberation benefits from the microwave treatment appear to diminish.

It has been suggested by previous researchers using both numerical modelling studies and experimental investigations, that a key factor in achieving benefits from the microwave treatment of an ore is the rapid application of a high microwave power density (W/m^3) over a short treatment duration (Whittles et al., 2003; Kingman et al., 2004a; Jones et al., 2007; Ali and Bradshaw, 2009; Rizmanoski, 2011; Wang and Djordjevic, 2014; Batchelor et al., 2015). In contrast, Wills and Atkinson (1993) suggest that lower power and energy inputs, and a slower application of strain during comminution, promotes stable fracture propagation and exploits grain boundary weaknesses more effectively than faster applications of strain at higher power and energy.

The Cu-sulphide mineral liberation results in this chapter showed that a beneficial change can be achieved in a microwave treated MZ sample at a microwave power density of $2.0x10^6 W/m^3$, and a microwave dose of 0.3kWh/t. Interestingly, it was not the highest power and most rapid treatment which resulted in the greatest liberation benefits. The MZ T5 treated sample showed the greatest improvement in Cu-sulphide mineral liberation as a result of the most effective splitting of high-grade and low-grade middlings particles in the ore, as evidenced by the changes observable in Cu-sulphide:NSG mineral locking. This improvement in mineral liberation also corresponded with the greatest observable changes in ore breakage behaviour resulting from the microwave treatments, as shown by changes in GRD and CRU indices from Ci testing.

The findings in this chapter support the theory that for the microwave treatment of MZ ore, lower microwave power and energy input at a slower application rate, results in the greatest beneficial changes in Cu-sulphide mineral liberation due to changes in the breakage behaviour of the ore. That the equal lowest power density, and longest applicator duration treatment showed the greatest improvement, supports the theory that slow and stable fracture propagation promotes intergranular fracturing and liberation by detachment more effectively than rapid high power microwave treatments of MZ ore.

CHAPTER 8 - CONCLUSIONS AND FURTHER WORK

8.1 INTRODUCTION

Over the past two decades, the high power microwave treatment of ores has been shown by several researchers to have the potential of being a novel step-changing comminution technology. The ability of microwave energy to rapidly and selectively heat certain minerals within an ore, and generate and propagate intergranular fractures at grain boundaries, has been shown to be an innovative process for reducing ore strength and enhancing mineral liberation.

Through a detailed review of the relevant literature, it was identified that, while the understanding of the process of the microwave treatment of ores has developed significantly over recent years, fundamental knowledge of how mineralogical and textural characteristics of different ores influences their amenability to microwave treatment is still limited. Previous work in the field of understanding the microwave treatment of ores has also been primarily concerned with testing the downstream mineral processing benefits achievable from the technology, rather than directly measuring the impact of the treatment on ore fracturing. While theoretical modelling studies have investigated fracture mechanisms on simple binary mineral systems, the understanding of the nature of fractures induced by microwave treatments in complex multi-mineral ores was also identified as a gap existing in the current knowledge.

The overall aim of this experimental investigation has been to make an original and distinct contribution towards addressing these existing gaps in the current state of knowledge through the application of both existing and newly developed microwave treatment processes and analytical methods. It has done so by investigating the relationship between the mineralogical characteristics of three different copper ores from a single deposit, with the comminution and mineral liberation

benefits achieved, and the generation and propagation of ore fracturing resulting from high power microwave treatments. This study has also sought to advance this field of knowledge through investigating the minimum microwave energy input threshold at which measurable benefits in ore comminution or mineral liberation are achievable following an expanded range of microwave treatment conditions for a single ore.

The capabilities of the innovative microwave treatment systems developed at the University of Nottingham have, for the first time, allowed for the application of a range of previously unattainable microwave treatment conditions. The extensive use of Mineral Liberation Analyser (MLA) and QEMScan automated mineralogy systems has also allowed for detailed coarse ore characterisation studies, and an unprecedented level of comprehensive analysis of mineral liberation benefits to be conducted for microwave treated ores. The unique application of the JK GeM Crushing Index comminution test as a method of assessing the 'bulk' changes in the ore breakage characteristics of microwave treated ores also represents a novel method of assessing the benefits achieved. The adaptation and application of dye-penetration fracture analysis and quantification to the assessment of fracturing in microwave treated ores in this investigation also represents an innovative contribution to this field of knowledge.

Through the completion of the series of specific experimental objectives, and detailed analysis and interpretation of the results produced, a number of key conclusions can be drawn which provide a novel contribution to the understanding of the microwave treatment of copper ores. This chapter will summarise the key outcomes achieved from this investigation, describe how the study has advanced the state of knowledge of the field, and present new potential avenues for further novel work in this field.

8.2 The Influence of Ore Mineralogy on Microwave Treatment Benefits

Experimental investigations conducted to address the initial aim of this study regarding the influence of mineralogy on the beneficial outcomes achievable through microwave treatment were presented in Chapter 5. A series of high power microwave treatments were conducted at previously unattainable treatment conditions for MZ, QZ, and QX copper ores, which were shown to possess differences in relevant mineralogical and textural amenability characteristics. The benefits achieved from the treatments, in terms of improved comminution behaviour and mineral liberation, were assessed and compared between the ores, and related to both coarse ore mineralogy, and microwave treatment conditions. In contrast to previous studies which employed <30kW microwave power, predominantly in multimode cavities, the samples for this investigation were treated with up to 200kW total microwave power in a single mode resonant applicator. The capability of the microwave treatment pilot system in achieving high sample throughputs of up to 150t/h, allowed for testing the comminution and mineral liberation benefits achieved from total microwave energy inputs of between 0.7-1.3kWh/t, which was lower than for previous studies reported in the literature, due to the unprecedented capabilities of the system.

At the microwave treatment conditions used in producing the MZ and QZ treated ore samples assessed in Chapter 5, there are only marginal observable differences in the benefits achieved that can be attributed to variations in the mineralogy of the different ores. It is difficult to differentiate the performance of the two ores tested in this investigation based on a comparison between variations in the mineralogy of the different ores, and the benefits achieved from the microwave treatments. The results from this study show that both ores have achieved benefits in terms of improvements in Cu-sulphide mineral liberation and comminution performance, as it has been shown from detailed coarse ore characterisation studies that both ores

possess characteristics that render them highly amenable to beneficial microwave treatment outcomes. MZ ore, with twice the abundance of sulphide heating minerals, three times the abundance of total heating minerals, and a coarser pyrite native grain size, did result in marginally better liberation improvements in the >98% and >50% Cu-sulphide liberation classes compared to QZ ore, despite having a 'softer' and less amenable gangue composition. MZ ore also performed slightly better than QZ ore in terms of splitting of the middlings particles, as shown by the greater reductions observed in Cu-sulphide:NSG binary particles in the treated samples. The potential for better Cu-sulphide mineral liberation improvements in the QZ treated samples was hindered by the fact that Cu-sulphides in the ore already show very high levels of liberation in the untreated ore.

Ci test results for the QZ ore consistently showed changes in ore breakage characteristics at all microwave treatment conditions, while only marginal changes were seen in BBMWi for the QZ ore at low confidence levels. As QZ ore was shown to be relatively soft in terms of BBMWi compared to MZ ore, there was less room for improvement in terms of potential beneficial reductions in BBMWi from microwave treatments. Ci test results also showed that the MZ T2 treatment achieved the greatest change in ore breakage response of all the treatments on both ores, however the results across the three different treatment conditions for MZ ore are quite variable. The BBMWi results also clearly showed significant benefits have been achieved for the MZ ore in terms of reductions in grinding energy requirements as a result of the microwave treatments.

The findings from this experimental program suggest that, despite the limited research presented in the literature, the understanding of the mineralogical and textural characteristics of a copper ore that render it amenable to beneficial microwave treatment are well understood and defined at an applied level. This study has made a new contribution to the knowledge of the influence of mineralogy on the microwave treatment of ores through the experimental validation of hypothesised

amenability characteristics proposed by previous researchers, and presented in Chapter 2.

8.3 The Influence of Microwave Treatment on Ore Fracture

The second key aim of this investigation was to address a previously neglected field of understanding through attempting to experimentally quantify the generation and propagation of fractures in microwave treated ores. The characterisation and quantification of fractures resulting from the microwave treatment process was assessed through the development of a novel experimental method, and the first application of this type of method to assessing the benefits of microwave treatment in terms of ore fracturing. X-ray micro-tomography was also considered as a potential new method for addressing this research aim, however, following a series of test scans, the required image voxel resolution proposed for fractures to be observable resulted in impractical measurement times and costs.

Importantly, the results produced in this novel experimental investigation, which is presented in detail in Chapter 6, support the findings of the mineral liberation analysis and comminution testing outcomes from Chapter 5. The fracture analysis results for MZ and QZ ores clearly show for the first time, that benefits achieved in Cu-sulphide liberation and comminution testing can be attributed to quantifiable increases in fracturing observed as a result of microwave treatments. The results presented for MZ ore in this chapter showed that, while a microwave power density of $3.3x10^6 W/m^3$ and a microwave dose of 0.7kWh/t is sufficient for liberation and comminution benefits to be achieved, higher levels of macro-fracturing can be observed at a microwave power density of $5.3x10^6 W/m^3$ and a microwave dose of 1.3kWh/t. Results for the QZ ore showed consistent increases in fracture length, area and density for both microwave treatment conditions assessed. This finding supports the suggestion that a microwave treatment dose of 0.7kWh/t and power

density of $3.3x10^6 W/m^3$ is sufficient to introduce additional fractures in QZ ore, and that the application of additional power or energy does not appear to induce further benefits in terms of fracturing of the ore fragments over the range of microwave treatment conditions tested. QZ microwave treated samples had previously shown consistent benefits in Cu-sulphide liberation and comminution testing, which are consistent with the trends observed in the fracture analysis results.

Overall, QX ore showed the greatest beneficial change in terms of fracturing as a result of microwave treatments. This is most likely due to QX ore possessing a highly amenable mineralogy and texture, with a sufficient abundance of coarse and granular pyrite, distributed relatively homogeneously throughout a gangue comprised predominantly of hard and brittle quartz. This finding represents a development in the understanding of the role of pyrite in the initiation and propagation of macro-fractures in an ore resulting from high power microwave treatment.

In summary, the results produced using the novel fracture analysis and quantification method to address the second aim of this investigation, have quantifiably shown for the first time that microwave treatments can induce additional beneficial fracturing in ores possessing amenable mineralogical characteristics. An additional contribution to the field is that beneficial fracture outcomes have been shown to correspond with benefits achieved in Cu-sulphide liberation, and comminution testing by JK GeM Ci and BBMWi methods. The results also illustrated for the first time that benefits in mineral liberation and changes in ore breakage behaviour could be achieved in an ore that did not showed a measurable change in fracturing due to microwave treatment. This finding suggests that intergranular micro-fractures, which proved to be beyond the capability of the newly developed method to resolve, rather than macro-fractures, potentially make a greater contribution to the enhancement of Cu-sulphide mineral liberation and changes in ore breakage characteristics resulting from microwave treatments.

8.4 The Influence of Microwave Energy Input and Power Density on Treatment Benefits

Experimental work conducted in this investigation, and presented in detail in Chapters 5 and 6, provided the first demonstration that benefits in Cu-sulphide mineral liberation, changes in ore breakage behaviour as measured by JK GeM Ci testing, and reductions in grinding energy consumption as measured by BBMWi testing, are achievable for highly amenable copper ores at microwave energy inputs of 0.7kWh/t. These findings were supported by the novel fracture analysis investigation, which showed that at microwave energy inputs of 0.7kWh/t, additional beneficial fracturing was observable in microwave treated QZ and QX ores. It was identified however, that despite MZ ore showing a beneficial change in Cu-sulphide mineral liberation and changes in ore breakage response at a microwave treatment energy of 0.7kWh/t, at this dose minimal additional macro-fracturing was observed in the treated ore. MZ ore was therefore selected for an additional set of microwave treatments at lower total microwave energy inputs than have previously been tested, to investigate the minimum microwave dose threshold at which benefits in mineral liberation and changes in ore breakage behaviour are achievable. The final aim in this investigation was to study the relationship between microwave power density and microwave energy input for MZ ore, and to determine the lowest microwave treatment dose (kWh/t) at which measurable beneficial changes were observable.

Through performing a series of additional lower dose microwave treatments of MZ ore than those conducted in Chapter 5, and lower than has been reported by previous researchers in the field, an expanded range of microwave doses and power densities were able to be assessed for MZ ore. After assessing the benefits achieved by these microwave treatments in comparison to the untreated ore, it was possible to assess the minimum threshold for microwave power density and dose at which Cu-sulphide mineral liberation benefits and changes

in ore breakage could be achieved for MZ ore. An additional novel finding that resulted from this series of microwave treatments was the influence that sample throughput, or residence duration of the sample within the applicators during treatment, has on the effectiveness of the treatment. The results indicated that a minimum applicator residence duration appears to exist, and that below a certain residence duration threshold, the benefits resulting from the microwave treatment appear to diminish.

Cu-sulphide mineral liberation results showed that a beneficial change can be achieved for microwave treated MZ ore at a microwave power density of $2.0x10^6 W/m^3$, and a microwave dose of 0.3kWh/t. It was not however, the highest power and most rapid treatment that resulted in the greatest beneficial change in Cu-sulphide mineral liberation. This finding supports a new theory that, for the microwave treatment of MZ ore, lower microwave power and energy input at a slower application rate, results in the greatest beneficial changes. That the equal lowest power density, and longest applicator duration treatment showed the greatest improvements in mineral liberation and greatest changes in ore breakage response, supports the theory that slow and stable fracture propagation promotes intergranular micro-fracturing more effectively than more rapid and higher power microwave treatments of MZ ore. The treatment conditions for total microwave energy input at which mineral liberation benefits have been shown to be achievable in this study, are lower than conditions previously reported in the literature for any ore type, with these findings advancing the understanding of the application of high power microwave treatments to improving comminution performance.

8.5 Recommendations for Further Work

The conclusions derived from this experimental investigation have provided an original and distinct contribution to addressing the existing gaps in the fundamental knowledge of the microwave treatment of copper ores, and have advanced the understanding of the application

of the process to enhancing ore comminution. There are, however, several areas where additional investigations may further advance the fundamental understanding of the microwave treatment of ores, and progress the development and commercialisation of the technology.

- Rather than continuing to use Mohs scale as a simple measure of mineral 'hardness' to assess ore amenability, investigations could be conducted into assessing whether Modulus of Elasticity values are a better representation of mineral response to applied stresses during microwave treatment. This could lead to the development of a 'bulk' ore elasticity rating which would present a novel avenue for furthering the development of ore amenability assessments for beneficial microwave treatment.

- Improvements in High Performance Computing could lead to more advanced modelling and simulations of complex multi-mineral assemblages during microwave treatment than have previously been able to be performed. Advancing beyond the binary models previously employed would allow for a fundamental assessment of mineral assemblages that are more representative of real ores.

- Advances in high-speed synchrotron based x-ray micro-tomography (XMT) could enable in situ dynamic assessments of ore fragments undergoing microwave treatment. The application of real-time, high-speed 3D imaging of ore fragments under microwave radiation would present a novel method of further advancing the understanding of the mechanisms of ore fracturing during microwave treatment. This could be conducted using either real ore or synthetically produced fragments.

- The results achieved in this study suggest that the investigation of a wider range of copper ores with varying mineralogical and

textural characteristics, or amenable ores of differing commodities, is warranted at low microwave treatment doses of 0.3-0.7kWh/t. This would allow for an assessment of whether this newly determined minimum energy threshold at which benefits can be achieved, also applies to other ores.

- An assessment of the impact that unprecedentedly low microwave treatment dose requirements of potentially <0.5kWh/t has on the scale-up of the technology to industrially relevant throughputs would be beneficial in advancing the commercial or industrial scale development of the technology.

- An investigation into other novel applications of the microwave treatment of ores that exploits the particle 'splitting' capabilities of the fracture mechanism would also be a potentially valuable avenue of enquiry. Such as whether microwave treatments can be used to enhance the separation of penalty element bearing minerals during production of a mineral concentrate, where these minerals occur in association with microwave heating minerals within an ore.

- Investigate whether the microwave treatment process can be applied to transforming the processing economics of ores that are currently unable to be economically exploited using conventional comminution methods.

REFERENCES

AGILENT 2006. Basics of measuring the dielectric properties of materials. *Agilent Technologies: Santa Clara, CA, USA*.

AL-HARAHSHEH, M., KINGMAN, S., HANKINS, N., SOMERFIELD, C., BRADSHAW, S. & LOUW, W. 2005. The influence of microwaves on the leaching kinetics of chalcopyrite. *Minerals Engineering,* 18**,** 1259-1268.

AL SAYEGH, H. 2012. *Microwave pyrolysis of forestry waste.* PhD Thesis, University of Nottingham.

ALI, A. Y. 2010. *Understanding the Effects of Mineralogy, Ore Texture and Microwave Power Delivery on Microwave Treatment of Ores.* PhD, University of Stellenbosch.

ALI, A. Y. & BRADSHAW, S. M. 2009. Quantifying damage around grain boundaries in microwave treated ores. *Chemical Engineering and Processing: Process Intensification,* 48**,** 1566-1573.

ALI, A. Y. & BRADSHAW, S. M. 2010. Bonded-particle modelling of microwave-induced damage in ore particles. *Minerals Engineering,* 23**,** 780-790.

ALI, A. Y. & BRADSHAW, S. M. 2011. Confined particle bed breakage of microwave treated and untreated ores. *Minerals Engineering,* 24**,** 1625-1630.

AMANKWAH, R. K., KHAN, A. U., PICKLES, C. A. & YEN, W. T. 2005. Improved grindability and gold liberation by microwave pretreatment of a free-milling gold ore. *Mineral Processing and Extractive Metallurgy,* 114**,** 30-36.

AMIRA 2009. *P843 Geometallurgical Mapping and Mine Modelling_Technical Report 03,* Brisbane, Australia.

ANDERSON, J. C. 1964. *Dielectrics,* Chapman & Hall, London.

ANDRES, U. 1989. Parameters of disintegration of rock by electrical pulses. *Powder Technology,* 58**,** 265-269.

ANDRES, U. 2010. Development and prospects of mineral liberation by electrical pulses. *International Journal of Mineral Processing,* 97**,** 31-38.

ANDRES, U. T. 1977. Liberation study of apatite-nepheline ore comminuted by penetrating electrical discharges. *International Journal of Mineral Processing,* 4**,** 33-38.

ANGEL, R. J., JACKSON, J. M., REICHMANN, H. J. & SPEZIALE, S. 2009. Elasticity measurements on minerals: a review. *European Journal of Mineralogy,* 21**,** 525-550.

ATKINSON, B. 1975. Experimental deformation of polycrystalline pyrite; effects of temperature, confining pressure, strain rate, and porosity. *Economic Geology,* 70**,** 473-487.

AYDOĞAN, N. A., ERGÜN, L. & BENZER, H. 2006. High pressure grinding rolls (HPGR) applications in the cement industry. *Minerals Engineering,* 19**,** 130-139.

BAILEY, C., LANE, G., MORRELL, S. & STAPLES, P. What can go wrong in comminution circuit design. Proceedings of the 10th Mill Operatirs' Conference, Adelaide, SA, 2009.

BATCHELOR, A. 2013. *Microwave Treatment of Ores.* PhD, University of Nottingham.

BATCHELOR, A. R., JONES, D. A., PLINT, S. & KINGMAN, S. W. 2015. Deriving the ideal ore texture for microwave treatment of metalliferous ores. *Minerals Engineering,* 84**,** 116-129.

BATCHELOR, A. R., JONES, D. A., PLINT, S. & KINGMAN, S. W. 2016. Increasing the grind size for effective liberation and flotation of a porphyry copper ore by microwave treatment. *Minerals Engineering,* 94**,** 61-75.

BATTERHAM, R. 2011. Trends in comminution driven by energy. *Advanced Powder Technology,* 22**,** 138-140.

BATTERHAM, R. J. 2013. Major Trends in the Mineral Processing Industry. *BHM Berg- und Hüttenmännische Monatshefte,* 158**,** 42-46.

BATTERSBY, M. J. G., KELLERWESSEL, H. & OBERHEUSER, G. Important advances in the development of high pressure rolls comminution for the minerals industry. AusIMM Extractive Metallurgy Conference, 1992. 159-165.

BAUM, W. & AUSBURN, K. 2011. HPGR comminution for optimization of copper leaching. *Minerals and Metallurgical Processing,* 28**,** 77.

BAUM, W., PATZELT, N. & KNECHT, J. 1997. Metallurgical benefits of high pressure roll grinding for gold and copper recovery. *Comminution Practices, ed. Kawatra, KS, Society for Mining, Metallurgy, and Exploration, Inc.(SME)***,** 111-116.

BECKER, M., DYANTYI, N., BROADHURST, J. L., HARRISON, S. T. L. & FRANZIDIS, J. P. 2015. A mineralogical approach to evaluating laboratory scale acid rock drainage characterisation tests. *Minerals Engineering,* 80**,** 33-36.

BLUHM, H., FREY, W., GIESE, H., HOPPÉ, P., SCHULTHEIß, C. & STRÄßNER, R. 2000. Application of pulsed HV discharges to material fragmentation and recycling. *IEEE Transactions on Dielectrics and Electrical Insulation,* 7**,** 625-636.

BOND, F. C. 1952. The 3rd theory of comminution. *Transactions of the American Institute of Mining and Metallurgical Engineers,* 193**,** 484-494.

BŐTTCHER, C. 1952. Theory of electric polarisation. *Houston: Elsevier*.

BRADSHAW, D. The role of process mineralogy in improving the process performance of complex sulphide ores. Proceedings of the XXVII International Mineral Processing Congress, 2014. 1-23.

BRADSHAW, S., LOUW, L., VAN DER MERWE, C., READER, H., KINGMAN, S., CELUCH, M. & KIJEWSKA, W. 2007. Techno-economic considerations in the commercial microwave processing of mineral ores. *Journal of Microwave Power and Electromagnetic Energy,* 40**,** 228-240.

BRITISH-STANDARDS, 2011, BS EN 60519-6:2011, Safety in electroheat installations. Specifications for safety in industrial microwave heating equipment, BSI London

BROCH, E. & FRANKLIN, J. A. 1972. The point-load strength test. *International Journal of Rock Mechanics and Mining Sciences and,* 9**,** 669-676.

BROUGH, C. P., WARRENDER, R., BOWELL, R. J., BARNES, A. & PARBHAKAR-FOX, A. 2013. The process mineralogy of mine wastes. *Minerals Engineering,* 52**,** 125-135.

BROZ, M. E., COOK, R. F. & WHITNEY, D. L. 2006. Microhardness, toughness, and modulus of Mohs scale minerals. *American Mineralogist,* 91**,** 135-142.

BUSHELL, C. 2011. A new SEM–EDS based automated mineral analysis solution for PGM-bearing ores and flotation products. *Minerals Engineering,* 24**,** 1238-1241.

BUTTRESS, A., KATRIB, J., JONES, D., BATCHELOR, A., CRAIG, D., ROYAL, T., DODDS, C. & KINGMAN, S. 2016. Towards large scale microwave treatment of ores: Part 1 – Basis of design, construction and commissioning. *Minerals Engineering,* In Review.

CEEC 2012a. *The CEEC Roadmap for Eco-Efficient Comminution*.Available: http://www.ceecthefuture.org/resource-center/ceec-roadmap/.

CEEC 2012b. Comminution: waging war on Watts. *Mining World.* Tradelink Publications.

CHARIKINYA, E., BRADSHAW, S. & BECKER, M. 2015. Characterising and quantifying microwave induced damage in coarse sphalerite ore particles. *Minerals Engineering,* 82**,** 14-24.

CHEN, T. T., DUTRIZAC, J. E., HAQUE, K. E., WYSLOUZIL, W. & KASHYAP, S. 1984. The relative transparency of minerals to microwave radiation. *Canadian Metallurgical Quarterly,* 23**,** 349-351.

CHURCH, R. H., WEBB, W. E. & SALSMAN, J. B. 1988. *Dielectric properties of low-loss minerals*.

CLARKE, A. J. & WILLS, B. A. 1989. Technical note Enhancement of cassiterite liberation by high pressure roller comminution. *Minerals Engineering,* 2**,** 259-262.

COOKE, D. R., HOLLINGS, P. & WALSHE, J. L. 2005. Giant porphyry deposits: Characteristics, distribution, and tectonic controls. *Economic Geology,* 100**,** 801-818.

COWEN, R. 2000. *Exploiting the earth*.

COX, B. 2015. *Human Universe,* William Collins, London.

CROWSON, P. 2012. Some observations on copper yields and ore grades. *Resources Policy,* 37**,** 59-72.

CURRY, J. A., ISMAY, M. J. L. & JAMESON, G. J. 2014. Mine operating costs and the potential impacts of energy and grinding. *Minerals Engineering,* 56**,** 70-80.

DANIEL, M. J. & LEWIS-GRAY, E. 2011. Comminution efficiency attracts attention. *AusIMM Bulletin***,** 20-24+29.

DEER, W. A., HOWIE, R. A. & ZUSSMAN, J. 2013. *An introduction to the rock-forming minerals,* 3rd Edition, Mineralogical Society, London.

DIAO, Z. J., ZHAO, Y. M., DUAN, C. L., SUN, S. & XU, F. 2013. Fundamental study of fragmentation of waste printed circuit boards by a high voltage pulse. *Zhongguo Kuangye Daxue Xuebao/Journal of China University of Mining and Technology,* 42**,** 817-823.

DJORDJEVIC, N. 2010. Improvement of energy efficiency of rock comminution through reduction of thermal losses. *Minerals Engineering,* 23**,** 1237-1244.

DJORDJEVIC, N. 2014. Recovery of copper sulphides mineral grains at coarse rock fragments size. *Minerals Engineering,* 64**,** 131-138.

DRINKWATER, D., NAPIER-MUNN, T. & BALLANTYNE, G. Energy reduction through eco-efficient comminution strategies. 26th International Mineral Processing Congress, IMPC 2012: Innovative Processing for Sustainable Growth, 2012a New Delhi. 1223-1229.

DRINKWATER, D., NAPIER-MUNN, T. & BALLANTYNE, G. Energy reduction through eco-efficient comminution strategies. 2012b. 1223-1229.

DS, 2002, DS 423.39, Testing of concrete - Production of fluorescence impregnated plane sections, Denmark

EBERHART, M. 2007. *Feeding the Fire: the lost history and uncertain future of mankind's energy addiction,* Crown.

ESA 2013. Planck CMB. ESA and the Planck Collaboration.

EVANS, C. L., WIGHTMAN, E. M., MANLAPIG, E. V. & COULTER, B. L. 2011. Application of process mineralogy as a tool in sustainable processing. *Minerals Engineering,* 24**,** 1242-1248.

FANDRICH, R., GU, Y., BURROWS, D. & MOELLER, K. 2007a. Modern SEM-based mineral liberation analysis. *International Journal of Mineral Processing,* 84**,** 310-320.

FANDRICH, R., GU, Y., BURROWS, D. & MOELLER, K. 2007b. Modern SEM-based mineral liberation analysis. *International Journal of Mineral Processing,* 84**,** 310-320.

FEI 2013. MLA Software suite. 3.1.3.612 ed. Hillsboro.

FILIPPOU, D. & KING, M. G. 2011. R&D prospects in the mining and metals industry. *Resources Policy,* 36**,** 276-284.

FITZGIBBON, K. E. & VEASEY, T. J. 1990. Thermally assisted liberation - a review. *Minerals Engineering,* 3**,** 181-185.

FUERSTENAU, D. W. & ABOUZEID, A. Z. M. 2002. The energy efficiency of ball milling in comminution. *International Journal of Mineral Processing,* 67**,** 161-185.

FUERSTENAU, D. W. & KAPUR, P. C. 1995. Newer energy-efficient approach to particle production by comminution. *Powder Technology,* 82**,** 51-57.

GAUDIN, A. M. 1939. *Principles of mineral dressing,* McGraw-Hill Book Co.

GAY, S. L. 1999. Numerical verification of a non-preferential-breakage liberation model. *International Journal of Mineral Processing,* 57**,** 125-134.

GAY, S. L. 2004. Simple texture-based liberation modelling of ores. *Minerals Engineering,* 17**,** 1209-1216.

GHORBANI, Y., MAINZA, A. N., PETERSEN, J., BECKER, M., FRANZIDIS, J. P. & KALALA, J. T. 2013. Investigation of particles with high crack density produced by HPGR and its effect on the redistribution of the particle size fraction in heaps. *Minerals Engineering,* 43–44**,** 44-51.

GIESE, J., SEWARD, D., GNOS, E. & KURZ, D. 2007. Comparative apatite fission track study of conventionally versus selFrag Lab fragmented samples. *Geochimica et Cosmochimica Acta,* 71**,** A322.

GORDON, R. B., BERTRAM, M. & GRAEDEL, T. E. 2006. Metal stocks and sustainability. *Proceedings of the National Academy of Sciences of the United States of America,* 103**,** 1209-1214.

GOTTLIEB, P., WILKIE, G., SUTHERLAND, D., HO-TUN, E., SUTHERS, S., PERERA, K., JENKINS, B., SPENCER, S., BUTCHER, A. & RAYNER, J. 2000. Using quantitative electron microscopy for process mineralogy applications. *JOM,* 52**,** 24-25.

GRIFFITH, A. A. 1921. The phenomena of rupture and flow in solids. *Philosophical transactions of the royal society of london. Series A, containing papers of a mathematical or physical character,* 221**,** 163-198.

GU, Y. 2003. Automated scanning electron microscope based mineral liberation analysis. *Journal of Minerals & Materials Characterization & Engineering,* 2**,** 33-41.

GU, Y. & NAPIER-MUNN, T. 1997. JK/Philips mineral liberation analyzer–an introduction. *Minerals Processing,* 97**,** 2.

GU, Y., SCHOUWSTRA, R. P. & RULE, C. 2014. The value of automated mineralogy. *Minerals Engineering,* 58**,** 100-103.

GY, P. M. 1976. The sampling of particulate materials — A general theory. *International Journal of Mineral Processing,* 3**,** 289-312.

HAMBLIN, W. H. & CHRISTIANSEN, E. H. 2004. *Earth's Dynamic Systems,* 10th, Pearson Education, New Jersey, USA.

HAMILTON, I. 2009. *The Development of Microwave Thermal Analysis (MWTA) and its application to the study of Carbons and other materials.* University of Huddersfield.

HARMSEN, J. H. M., ROES, A. L. & PATEL, M. K. 2013. The impact of copper scarcity on the efficiency of 2050 global renewable energy scenarios. *Energy,* 50**,** 62-73.

HARRISON, P. C. 1997. *A Fundamental Study of the Heating Effect of 2.45 GHz Microwave Radiation on Minerals*.

HARROP, P. J. 1972. *Dielectrics,* John Wiley & Sons.

HERBST, J. A., LO, Y. C. & FLINTOFF, B. 2003. Size Reduction and Liberation. *In:* FUERSTENAU, M. C. & HAN, K. N. (eds.) *Principles of Mineral Processing.* Colorado, USA: Society for Mining, Metallurgy and Exploration Ltd.

HERTWIG, A., MCCLELLAND, W. C., KITAJIMA, K., SCHERTL, H.-P., MARESCH, W. V., STANEK, K., VALLEY, J. W. & SERGEEV, S. A. 2016. Inherited igneous zircons in jadeitite predate high-pressure metamorphism and jadeitite

formation in the Jagua Clara serpentinite mélange of the Rio San Juan Complex (Dominican Republic). *Contributions to Mineralogy and Petrology,* 171**,** 48.

HOAL, K. O., STAMMER, J. G., APPLEBY, S. K., BOTHA, J., ROSS, J. K. & BOTHA, P. W. 2009. Research in quantitative mineralogy: Examples from diverse applications. *Minerals Engineering,* 22**,** 402-408.

HOLMAN, B. W. 1926. Heat treatment as an agent in rock breaking. *Trans IMM,* 26**,** 219.

HORNAIN, H., MARCHAND, J., AMMOUCHE, A., COMMÈNE, J. P. & MORANVILLE, M. 1996. Microscopic observation of cracks in concrete - A new sample preparation technique using dye impregnation. *Cement and Concrete Research,* 26**,** 573-583.

HSIH, C. S. & WEN, S. B. 1994. An extension of Gaudin's liberation model for quantitatively representing the effect of detachment in liberation. *International Journal of Mineral Processing,* 42**,** 15-35.

HUKKI, R. 1961. Proposal for a solomonic settlement between the theories of von Rittinger, Kick and Bond. *Trans. AIME,* 220**,** 403-408.

HUNT, J., BERRY, R. & BRADSHAW, D. 2011. Characterising chalcopyrite liberation and flotation potential: Examples from an IOCG deposit. *Minerals Engineering,* 24**,** 1271-1276.

ICSG 2015. *World Copper Factbook 2015,* International Copper Study Group, Lisbon.

ITASCA 2015. *FLAC Software,* ITASA Consulting Group.

JACKSON, B., REID, A. & WITTEMBERG, J. Rapid production of high quality polished sections for automated image analysis of minerals. Proceedings of the Australasian Institute for Mining and Metallurgy, 1984. 93-97.

JAMESON, G., NAM, S. & YOUNG, M. M. 1977. Physical factors affecting recovery rates in flotation. *Minerals Science and Engineering,* 9**,** 103-118.

JAMESON, G. J. 2012. The effect of surface liberation and particle size on flotation rate constants. *Minerals Engineering,* 36-38**,** 132-137.

JENIKE, A. W. 1964. Storage and flow of solids, bulletin no. 123. *Bulletin of the University of Utah,* 53.

JOHNSON, C., POWNCEBY, M. I. & WILSON, N. C. 2015. The application of automated electron beam mapping techniques to the characterisation of low grade, fine-grained mineralisation; potential problems and recommendations. *Minerals Engineering,* 79**,** 68-83.

JONES, D. A. 2004. *Understanding Microwave Treatment of Ores.* PhD, University of Nottingham.

JONES, D. A., KINGMAN, S. W., WHITTLES, D. N. & LOWNDES, I. S. 2005. Understanding microwave assisted breakage. *Minerals Engineering,* 18**,** 659-669.

JONES, D. A., KINGMAN, S. W., WHITTLES, D. N. & LOWNDES, I. S. 2007. The influence of microwave energy delivery method on strength reduction in ore samples. *Chemical Engineering and Processing: Process Intensification,* 46**,** 291-299.

JONES, M. P. 1987. *Applied Mineralogy: A Quantitative Approach,* Graham & Trotman, London.

KATRIB, J., BUTTRESS, A., BATCHELOR, A., DIMITRAKIS, G., JONES, D., DODDS, C. & KINGMAN, S. W. 2016. Routes to scale-up for high intensity continuous throughput microwave treatment of bulk materials. *Proceedings of the Royal Society A: Mathematical, Physical & Engineering Sciences*.

KICK, F. 1885. *The laws of proportional resistance and their applications,* Leipzig.

KING, R. P. 1994. Linear stochastic models for mineral liberation. *Powder Technology,* 81**,** 217-234.

KING, R. P. & SCHNEIDER, C. L. 1998. Mineral liberation and the batch communition equation. *Minerals Engineering,* 11**,** 1143-1160.

KINGMAN, S. & ROWSON, N. 1997. Applications of microwave radiation to enhance performance of mineral separation processes. *Richard Mozley Symposium, Falmouth, England.*

KINGMAN, S. W., JACKSON, K., BRADSHAW, S. M., ROWSON, N. A. & GREENWOOD, R. 2004a. An investigation into the

influence of microwave treatment on mineral ore comminution. *Powder Technology,* 146**,** 176-184.

KINGMAN, S. W., JACKSON, K., CUMBANE, A., BRADSHAW, S. M., ROWSON, N. A. & GREENWOOD, R. 2004b. Recent developments in microwave-assisted comminution. *International Journal of Mineral Processing,* 74**,** 71-83.

KINGMAN, S. W. & ROWSON, N. A. 1998. Microwave treatment of minerals - A review. *Minerals Engineering,* 11**,** 1081-1087.

KINGMAN, S. W., VORSTER, W. & ROWSON, N. A. 2000a. The effect of microwave radiation on the processing of Palabora copper ore. *Journal of The South African Institute of Mining and Metallurgy,* 100**,** 197-204.

KINGMAN, S. W., VORSTER, W. & ROWSON, N. A. 2000b. Influence of mineralogy on microwave assisted grinding. *Minerals Engineering,* 13**,** 313-327.

KITCHEN, R. 2001. *RF and Microwave Radiation Safety Handbook,,* 2nd, Newnes, Oxford, UK.

KNAB, L. I., WALKER, H. N., CLIFTON, J. R. & FULLER JR, E. R. 1984. Fluorescent thin sections to observe the fracture zone in mortar. *Cement and Concrete Research,* 14**,** 339-344.

KOBUSHESHE, J. 2010. *Microwave Enhanced Processing of Ores.* PhD, University of Nottingham.

KODALI, P., DHAWAN, N., DEPCI, T., LIN, C. L. & MILLER, J. D. 2011. Particle damage and exposure analysis in HPGR crushing of selected copper ores for column leaching. *Minerals Engineering,* 24**,** 1478-1487.

KOJOVIC, T., MICHAUX, S. P. & WALTERS, S. Development of new comminution testing methodologies for geometallurgical mapping of ore hardness and throughput. XXV International Mineral Processing Congress 2010, IMPC 2010, 2010. Australasian Institute of Mining and Metallurgy, 891-899.

LANE, G. R., JAHRAUS, M. & MELKER, M. Dye penetration techniques used to determine heap leach potential of a telluride bearing Cripple Creek breccia ore. Proceedings of the 38th Annual Meeting of the Canadian Mineral Processors. The Canadian Institute of Mining, Metallurgy and Petroleum, Ottawa, Ontario, 2006. 71-82.

LASTRA, R. 2007. Seven practical application cases of liberation analysis. *International Journal of Mineral Processing,* 84**,** 337-347.

LAUGESEN, P. Preparation of impregnated polished sections and thin sections, techniques. Sixth Canmet/ACI International Conference on Durability of Concrete, 2003 Thessaloniki, Greece.

LEIßNER, T., MÜTZE, T., BACHMANN, K., RODE, S., GUTZMER, J. & PEUKER, U. A. 2013. Evaluation of mineral processing by assessment of liberation and upgrading. *Minerals Engineering,* 53**,** 171-173.

LILLIEFORS, H. W. 1967. On the Kolmogorov-Smirnov Test for Normality with Mean and Variance Unknown. *Journal of the American Statistical Association,* 62**,** 399-402.

LITOROWICZ, A. 2006. Identification and quantification of cracks in concrete by optical fluorescent microscopy. *Cement and Concrete Research,* 36**,** 1508-1515.

LITTLE, L., MAINZA, A. N., BECKER, M. & WIESE, J. G. 2016. Using mineralogical and particle shape analysis to investigate enhanced mineral liberation through phase boundary fracture. *Powder Technology,* 301**,** 794-804.

LIU, L. X. & POWELL, M. 2016. New approach on confined particle bed breakage as applied to multicomponent ore. *Minerals Engineering,* 85**,** 80-91.

LOTTER, N. O. 2011. Modern Process Mineralogy: An integrated multi-disciplined approach to flowsheeting. *Minerals Engineering,* 24**,** 1229-1237.

LOTTER, N. O., KORMOS, L. J., OLIVEIRA, J., FRAGOMENI, D. & WHITEMAN, E. 2011. Modern Process Mineralogy: Two case studies. *Minerals Engineering,* 24**,** 638-650.

LOTTER, N. O., KOWAL, D. L., TUZUN, M. A., WHITTAKER, P. J. & KORMOS, L. 2003. Sampling and flotation testing of Sudbury Basin drill core for process mineralogy modelling. *Minerals Engineering,* 16**,** 857-864.

LOTTERMOSER, B. 2010. Sulfidic Mine Wastes. *Mine Wastes.* Springer Berlin Heidelberg.

MACDONALD, M., ADAIR, B., BRADSHAW, D., DUNN, M. & LATTI, A. D. Learnings from five years of on-site MLA at Kennecott

Utah copper corporation (myth busters through quantitative evidence). Proceedings of 10th International Congress for Applied Mineralogy (ICAM), 2012 Trondheim, Norway. Springer.

MARIANO, R. A., EVANS, C. L. & MANLAPIG, E. 2016. Definition of random and non-random breakage in mineral liberation - A review. *Minerals Engineering,* 94**,** 51-60.

MARION, C., JORDENS, A., MALONEY, C., LANGLOIS, R. & WATERS, K. E. 2016. Effect of microwave radiation on the processing of a Cu-Ni sulphide ore. *Canadian Journal of Chemical Engineering,* 94**,** 117-127.

MARTINS, S. 2016. Size–energy relationship in comminution, incorporating scaling laws and heat. *International Journal of Mineral Processing,* 153**,** 29-43.

MASSEY, F. J. 1951. The Kolmogorov-Smirnov Test for Goodness of Fit. *Journal of the American Statistical Association,* 46**,** 68-78.

MAVKO, G., MUKERJI, T. & DVORKIN, J. 2009. *The Rock Physics Handbook,* 2nd Ed., Cambridge University Press.

MAY, D., PRIOR, T., CORDELL, D. & GIURCO, D. 2012. Peak Minerals: Theoretical Foundations and Practical Application. *Natural Resources Research,* 21**,** 43-60.

MCGILL, S., WALKIEWICZ, J. & SMYRES, G. The effects of power level on the microwave heating of selected chemicals and minerals. MRS proceedings, 1988a. Cambridge Univ Press, 247.

MCGILL, S. L., WALKIEWICZ, J. W. & SMYRES, G. A. 1988b. The effects of power level on the microwave heating of selected chemicals and minerals. *MRS Proceedings,* 124**,** 247-252.

MEREDITH, P. G. & ATKINSON, B. K. 1983. Stress corrosion and acoustic emission during tensile crack propagation in Whin Sill dolerite and other basic rocks. *Geophysical Journal International,* 75**,** 1-21.

MEREDITH, R. J. 1998. *Engineers' handbook of industrial microwave heating,* IET.

METAXAS, A. C. & MEREDITH, R. J. 1983. *Industrial Microwave Heating,* Peter Peregrinus Ltd, London, United Kingdom.

MICHAUD, D. 2015. *Effect Of Primary Grind Size On Mineral Liberation* [Online]. Kamloops, BC, Canada: 911 Metallurgist.Available: https://www.911metallurgist.com/blog/effect-of-primary-grind-size-on-mineral-liberation [Accessed 29/11/2016 2016].

MICHAUX, S. P. 2013. *Experimental Protocol for the GeM Crushing Index,* AMIRA P843A Final Compendium of Results, Manual for comminution tests and tools, Brisbane, Australia.

MORRELL, S. 2004. An alternative energy–size relationship to that proposed by Bond for the design and optimisation of grinding circuits. *International Journal of Mineral Processing,* 74**,** 133-141.

MUDD, G. M. 2010. The Environmental sustainability of mining in Australia: key mega-trends and looming constraints. *Resources Policy,* 35**,** 98-115.

MUDD, G. M., WENG, Z. & JOWITT, S. M. 2013. A detailed assessment of global Cu resource trends and endowments. *Economic Geology,* 108**,** 1163-1183.

MWANGA, A., ROSENKRANZ, J. & LAMBERG, P. 2015. Testing of Ore Comminution Behavior in the Geometallurgical Context—A Review. *Minerals,* 5**,** 276-297.

NADOLSKI, S., KLEIN, B., KUMAR, A. & DAVAANYAM, Z. 2014. An energy benchmarking model for mineral comminution. *Minerals Engineering,* 65**,** 178-186.

NAPIER-MUNN, T. 2015. Is progress in energy-efficient comminution doomed? *Minerals Engineering,* 73**,** 1-6.

NAPIER-MUNN, T. J., MORRELL, S., MORRISON, R. D. & KOJOVIC, T. 1999. *Mineral Comminution Circuits: Their Operation and Optimisation,* Julius Kruttschnitt Mineral Research Centre, The University of Queensland, Brisbane, Australia.

NORGATE, T. & HAQUE, N. 2010. Energy and greenhouse gas impacts of mining and mineral processing operations. *Journal of Cleaner Production,* 18**,** 266-274.

NORGATE, T. & JAHANSHAHI, S. 2011. Reducing the greenhouse gas footprint of primary metal production: Where should the focus be? *Minerals Engineering,* 24**,** 1563-1570.

NORGATE, T. & WELLER, K. 1994. Selection and operation of high pressure grinding rolls circuits for minimum energy consumption. *Minerals Engineering,* 7**,** 1253-1267.

NORTHEY, S., MOHR, S., MUDD, G. M., WENG, Z. & GIURCO, D. 2014. Modelling future copper ore grade decline based on a detailed assessment of copper resources and mining. *Resources, Conservation and Recycling,* 83**,** 190-201.

PARBHAKAR-FOX, A., LOTTERMOSER, B. & BRADSHAW, D. 2013. Evaluating waste rock mineralogy and microtexture during kinetic testing for improved acid rock drainage prediction. *Minerals Engineering,* 52**,** 111-124.

PARBHAKAR-FOX, A. & LOTTERMOSER, B. G. 2015. A critical review of acid rock drainage prediction methods and practices. *Minerals Engineering,* 82**,** 107-124.

PAREKH, B. K., EPSTEIN, H. E. & GOLDBERGER, W. M. 1984. Novel Comminution Process Uses Electric and Ultrasonic Energy. *Mining Engineering,* 36**,** 1305-1309.

PARKER, T., SHI, F., EVANS, C. & POWELL, M. 2015. The effects of electrical comminution on the mineral liberation and surface chemistry of a porphyry copper ore. *Minerals Engineering,* 82**,** 101-106.

PHILLIPS, C., SMITH, T. & HARRISON, E. 1998. Alteration, metal zoning, and ore controls in the Bingham Canyon porphyry copper deposit. *Utah: Society of Economic Geologists Guidebook Series,* 29**,** 133-145.

PICKLES, C. A. 2009. Microwaves in extractive metallurgy: Part 2 – A review of applications. *Minerals Engineering,* 22**,** 1112-1118.

PIRRIE, D., ROLLINSON, G. K. & POWER, M. R. 2009. Role of automated mineral analysis in the characterisation of mining-related contaminated land. *Geoscience in South-West England,* 12**,** 162-170.

POKRAJCIC, Z., MORRISON, R. & JOHNSON, B. 2009. Designing for a reduced carbon footprint at Greenfield and operating comminution plants. *Recent Advances in Mineral Processing Plant Design*.

POWELL, M. Utilising orebody knowledge to improve comminution circuit design and energy utilisation. GeoMet 2013: The Second AusIMM International Geometallurgy Conference, 2013. The Australasian Institute of Mining and Metallurgy (AusIMM), 27-35.

POWELL, M. S. & MORRISON, R. D. 2007. The future of comminution modelling. *International Journal of Mineral Processing,* 84**,** 228-239.

PRIOR, T., GIURCO, D., MUDD, G., MASON, L. & BEHRISCH, J. 2012. Resource depletion, peak minerals and the implications for sustainable resource management. *Global Environmental Change,* 22**,** 577-587.

REDDY, S. M., JOHNSON, T. E., FISCHER, S., RICKARD, W. D. A. & TAYLOR, R. J. M. 2015. Precambrian reidite discovered in shocked zircon from the Stac Fada impactite, Scotland. *Geology,* 43**,** 899-902.

RINGOT, E. & BASCOUL, A. 2001. About the analysis of microcracking in concrete. *Cement and Concrete Composites,* 23**,** 261-266.

RIO TINTO 2014. *Presentation: Rio Tinto Copper,* London.Available: http://www.riotinto.com/documents/KUC_Site_Tour_24_June.pdf.

RIZMANOSKI, V. 2011. The effect of microwave pretreatment on impact breakage of copper ore. *Minerals Engineering,* 24**,** 1609-1618.

ROLLINSON, G. K., ANDERSEN, J. C. Ø., STICKLAND, R. J., BONI, M. & FAIRHURST, R. 2011. Characterisation of non-sulphide zinc deposits using QEMSCAN®. *Minerals Engineering,* 24**,** 778-787.

ROSARIO, P. P. & DROZDIAK, J. A. 2015. Creative and simpler HPGR circuits may increase their application even in the current restrictive financial environment. *SAG Conference.* Vancouver.

ROSS, J. 2010. *A Geometallurgical Study at the Bingham Canyon Mine, Utah Analyzing Mineralogical and Textural Paramteres Impacting Rock Breakage.* MSc, Colorado School of MInes.

S-TEAM. 2011.Available: http://www.s-team.sk/ [Accessed 03/11/2016.

SAHYOUN, C., ROWSON, N. A., KINGMAN, S. W., GROVES, L. & BRADSHAW, S. M. 2005. The influence of microwave pretreatment on copper flotation. *Journal of The South African Institute of Mining and Metallurgy,* 105**,** 7-13.

SAIREM. 2012. *Solid State Generators* [Online].Available: http://www.sairem.com/the-generators-44.html [Accessed 03/11/2016.

SALSMAN, J. B., WILLIAMSON, R. L., TOLLEY, W. K. & RICE, D. A. 1996. Short-pulse microwave treatment of disseminated sulfide ores. *Minerals Engineering,* 9**,** 43-54.

SANDMANN, D. 2015. *Method Development in Automated Mineralogy.* PhD Thesis, TU Bergakademie Freiberg.

SCHEDING, W., SHERRING, A., BINNS, D., PARKER, R. & WILLS, B. 1981. The effect of thermal pretreatment on grinding characteristics. *Camborne School of Mines Journal,* 81**,** 43.

SCHÖNERT, K. Aspects of the physics of breakage relevant to comminution. Fourth Tewksbury Symposium, University of Melbourne, 1979. 3.30.

SCHÖNERT, K. 1988. A first survey of grinding with high-compression roller mills. *International Journal of Mineral Processing,* 22**,** 401-412.

SCOTT, G., BRADSHAW, S. M. & EKSTEEN, J. J. 2008. The effect of microwave pretreatment on the liberation of a copper carbonatite ore after milling. *International Journal of Mineral Processing,* 85**,** 121-128.

SELFRAG, A. 2014. Creating shockwaves. *Inside Mining.*

SHIBATA, C., TAMAI, H., TANAKA, T. & WAKAMATSU, M. 1991. High-power (500-kW) CW magnetron for microwave heating. *Electrical Engineering in Japan,* 111**,** 94-101.

SILLITOE, R. H. 2002. Some metallogenic features of gold and copper deposits related to alkaline rocks and consequences for exploration. *Mineralium Deposita,* 37**,** 4-13.

SILLITOE, R. H. 2010. Porphyry Copper Systems. *Economic Geology,* 105**,** 3-41.

SMIRNOV, N. 1948. Table for Estimating the Goodness of Fit of Empirical Distributions. 279-281.

SMITH, C. 2015. *MicroHammer Prototype Phase II Liberation Data Assessment,* Perth, Australia, RIO-TINTO.

SOROUSHIAN, P., ELZAFRANEY, M. & NOSSONI, A. 2003. Specimen preparation and image processing and analysis techniques for automated quantification of concrete microcracks and voids. *Cement and Concrete Research,* 33**,** 1949-1962.

SPRENT, P. & SMEETON, N. C. 2016. *Applied nonparametric statistical methods,* CRC Press.

SVERDRUP, H. U., RAGNARSDOTTIR, K. V. & KOCA, D. 2014. On modelling the global copper mining rates, market supply, copper price and the end of copper reserves. *Resources, Conservation and Recycling,* 87**,** 158-174.

SYLVESTER, P. J. 2012a. Use of MLA for Mineralogical Studies.

SYLVESTER, P. J. 2012b. Use of the mineral liberation analyser (MLA) for mineralogical studies of sediments and sedimentary rocks. Mineralogical society of Canada.

TAVARES, L. M. 2005. Particle weakening in high-pressure roll grinding. *Minerals Engineering,* 18**,** 651-657.

THOSTENSON, E. T. & CHOU, T. W. 1999. Microwave processing: fundamentals and applications. *Composites Part A: Applied Science and Manufacturing,* 30**,** 1055-1071.

TROMANS, D. 2008. Mineral comminution: Energy efficiency considerations. *Minerals Engineering,* 21**,** 613-620.

UNITED NATIONS 2013. *United Nations - World Population Prospects: The 2012 Revision,* New York, NATIONS, U.Available: http://esa.un.org/wpp/Documentation/pdf/WPP2012_HIGHLIGHTS.pdf.

VAN DER WIELEN, K., WEH, A., GIESE, H. & KÄPPELER, J. High voltage breakage: A review of theory and applications. IMPC 2014 - 27th International Mineral Processing Congress, 2014.

VAN DER WIELEN, K. P., PASCOE, R., WEH, A., WALL, F. & ROLLINSON, G. 2013. The influence of equipment settings and rock properties on high voltage breakage. *Minerals Engineering,* 46-47**,** 100-111.

VAUGHAN, D. 1989. *Energy-dispersive X-ray microanalysis. An introduction,* Kevex Instruments, Inc, San Carlos CA.

VEASEY, T. J. & WILLS, B. A. 1991. Review of methods of improving mineral liberation. *Minerals Engineering,* 4**,** 747-752.

VIZCARRA, T. G., WIGHTMAN, E. M., JOHNSON, N. W. & MANLAPIG, E. V. 2010. The effect of breakage mechanism on the mineral liberation properties of sulphide ores. *Minerals Engineering,* 23**,** 374-382.

VON-HIPPEL, A. R. 1954. *Dielectrics and Waves,* MIT, Cambridge, MA.

VON DER LINDEN, E. 2006. Fundamental aspects of global metal markets: What drives the future demand? New mining capacities needed. *World of Mining - Surface and Underground,* 58**,** 243-246.

VON HIPPEL, A. R. 1954. *Dielectrics and waves,* MIT, Cambridge, MA.

VON MICHAELIS, H. Real and potential metallurgical benefits of HPGR in hard rock ore processing. Proceedings of the Randol Innovative Metallurgy Forum, 2005. 31-39.

VON RITTINGER, R. 1867. Textbook of mineral dressing. *Ernest and Korn*.

VORSTER, W. 2001. *The effect of microwave radiation on mineral processing.* PhD, The University of Birmingham.

VORSTER, W., ROWSON, N. A. & KINGMAN, S. W. 2001. The effect of microwave radiation upon the processing of Neves Corvo copper ore. *International Journal of Mineral Processing,* 63**,** 29-44.

WALKIEWICZ, J., LINDROTH, D. & CLARK, A. 1993. Grindability of taconite rod mill feed enhanced by microwave-induced cracking. *SME Annual Meeting.* Reno, Nevada.

WALKIEWICZ, J. W., KAZONICH, G. & MCGILL, S. L. 1988a. Microwave Heating Characteristics of Selected Minerals and

Compounds. *Minerals and Metallurgical Processing,* 5**,** 39-42.

WALKIEWICZ, J. W., KAZONICH, G. & MCGILL, S. L. 1988b. Microwave heating characterstics of selected minerals and compounds. *Mineral and Metallurgical Processing,* 5**,** 39-42.

WALKIEWICZ, J. W., LINDROTH, D. P. & MCGILL, S. L. 1991. Microwave assisted grinding. *IEEE Transactions on Industry Applications,* 27**,** 239-242.

WANG, E., SHI, F. & MANLAPIG, E. 2011. Pre-weakening of mineral ores by high voltage pulses. *Minerals Engineering,* 24**,** 455-462.

WANG, E., SHI, F. & MANLAPIG, E. 2012. Mineral liberation by high voltage pulses and conventional comminution with same specific energy levels. *Minerals Engineering,* 27-28**,** 28-36.

WANG, G., RADZISZEWSKI, P. & OUELLET, J. 2008. Particle modeling simulation of thermal effects on ore breakage. *Computational Materials Science,* 43**,** 892-901.

WANG, Y. 2015. Numerical modelling of heterogeneous rock breakage behaviour based on texture images. *Minerals Engineering,* 74**,** 130-141.

WANG, Y. & DJORDJEVIC, N. 2014. Thermal stress FEM analysis of rock with microwave energy. *International Journal of Mineral Processing,* 130**,** 74-81.

WEI, X. & GAY, S. 1999. Liberation modelling using a dispersion equation. *Minerals Engineering,* 12**,** 219-227.

WELSBY, S. D. D., VIANNA, S. M. S. M. & FRANZIDIS, J. P. 2010. Assigning physical significance to floatability components. *International Journal of Mineral Processing,* 97**,** 59-67.

WHITE, A. J. R. 1999. *Igneous Rocks Simplified,* University of Melbourne, Melbourne, Australia.

WHITTAKER, A. G. & MINGOS, D. M. P. 1994. Application of microwave heating to chemical syntheses. *Journal of Microwave Power and Electromagnetic Energy,* 29**,** 195-219.

WHITTAKER, G. 2007. *Microwave Heating Mechanisms [Online]* [Online].Available: http://www.tan-delta.com/mw_heating.html [Accessed 02/11/2016.

WHITTLES, D. N., KINGMAN, S. W. & REDDISH, D. J. 2003. Application of numerical modelling for prediction of the influence of power density on microwave-assisted breakage. *International Journal of Mineral Processing,* 68**,** 71-91.

WILLS, B. A. & ATKINSON, K. 1993. Some observations on the fracture and liberation of mineral assemblies. *Minerals Engineering,* 6**,** 697-706.

WILLS, B. A. & NAPIER-MUNN, T. J. 2006. *Mineral Processing Technology,* 7th Edition, Butterworth-Heinemann, Oxford, UK.

YATES, A. 1918. Effect of heating and quenching Cornish tin ores before crushing. *Trans IMM,* 28**,** 1918-1919.

YUTKIN, L. A. 1955. *Electrohydraulic Effect,* Mashgiz (State Scientific Technical Press for Machine Construction Literature), Moscow.

ZUO, W., SHI, F. & MANLAPIG, E. 2015a. Pre-concentration of copper ores by high voltage pulses. Part 1: Principle and major findings. *Minerals Engineering,* 79**,** 306-314.

ZUO, W., SHI, F., VAN DER WIELEN, K. P. & WEH, A. 2015b. Ore particle breakage behaviour in a pilot scale high voltage pulse machine. *Minerals Engineering,* 84**,** 64-73.

APPENDIX A - MINERALOGICAL DATA

The following appendix comprises results used in conducting reconciliation between XRF elemental assays and QEMScan or MLA calculated elemental assays as quality control for automated mineralogy results. It also presents additional data used to produce figures included in this thesis, and liberation grind calibration data.

A.1 MINERALOGY ASSAY RECONCILIATION

MZ XRF Assay								
Size	**UT1 150**	**T1 150**	**T2 150**	**T3 150**	**UT1 370**	**T1 425**	**T2 425**	**T3 425**
Element	Wt%	Wt%	Wt%	Wt%	Wt%	Wt%	Wt%	Wt%
Cu	0.42	0.40	0.42	0.40	0.40	0.41	0.40	0.40
Fe	4.30	4.50	4.30	4.60	4.60	4.50	4.30	4.40
S	2.60	2.80	2.60	2.90	2.80	2.80	2.60	2.50

Table A.1 MZ ore UT1, T1, T2 and T3 XRF chemical assay data.

MZ QEMScan Calculated Assay								
Size	**UT1 150**	**T1 150**	**T2 150**	**T3 150**	**UT1 370**	**T1 425**	**T2 425**	**T3 425**
Element	Wt%	Wt%	Wt%	Wt%	Wt%	Wt%	Wt%	Wt%
Cu	0.42	0.40	0.40	0.40	0.42	0.40	0.40	0.40
Fe	4.40	4.60	4.30	4.80	4.60	4.50	4.30	4.40
S	2.63	3.00	2.60	2.90	2.90	2.90	2.60	2.70

Table A.2 MZ ore UT1, T1, T2 and T3 QEMScan calculated assay data.

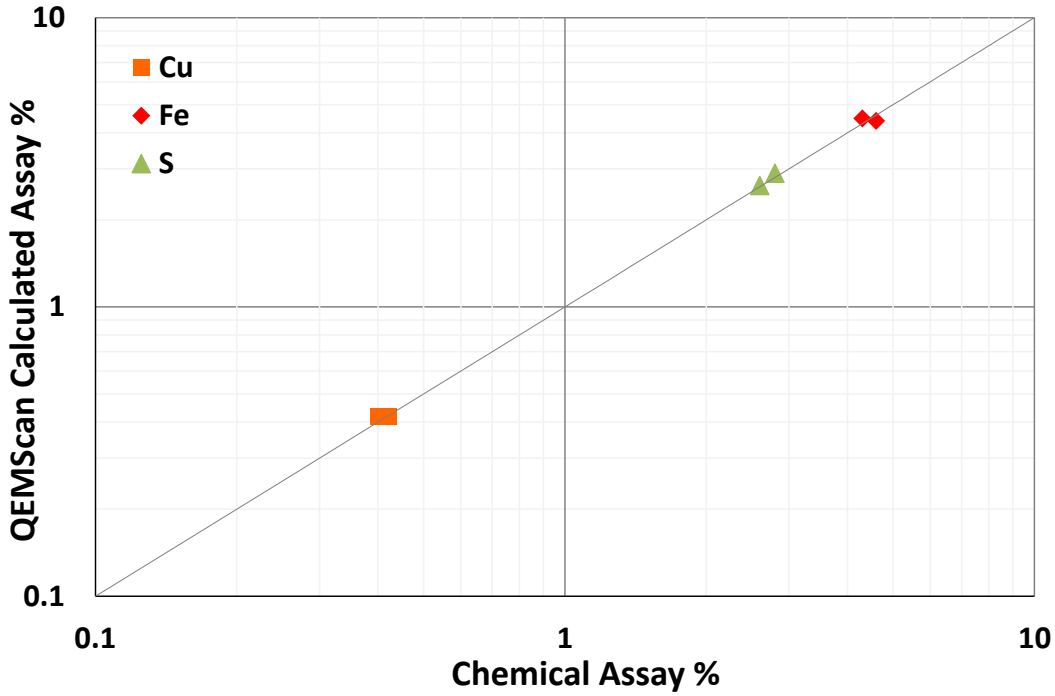


Figure A.1 MZ ore UT1 assay reconciliation.

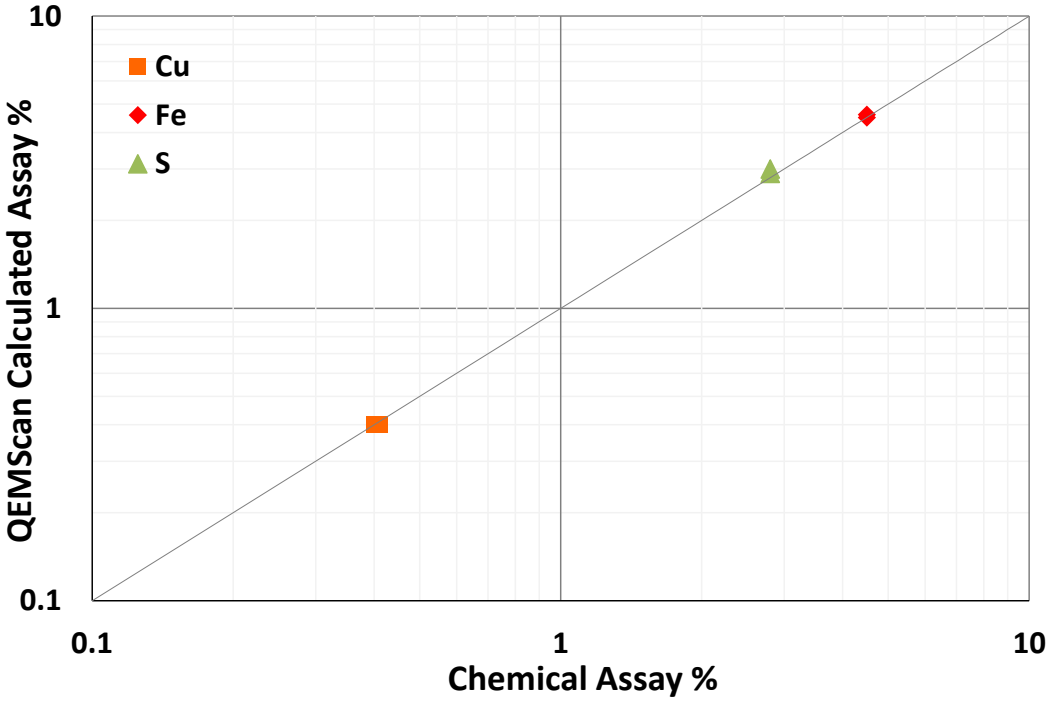


Figure A.2 MZ ore T1 assay reconciliation.

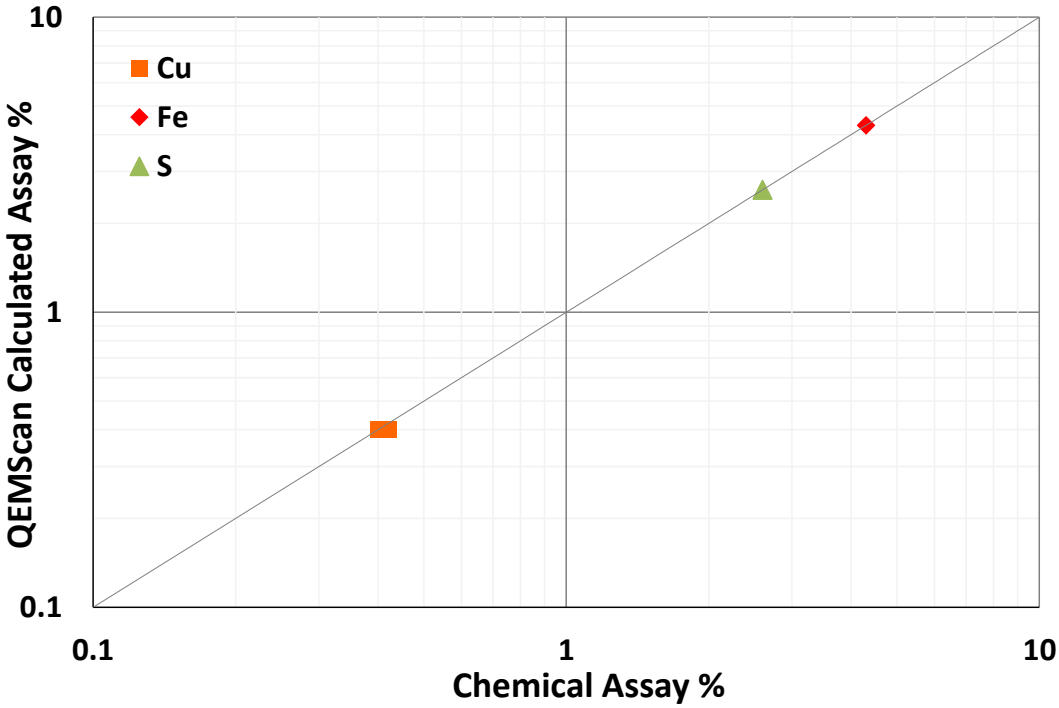


Figure A.3 MZ ore T2 assay reconciliation.

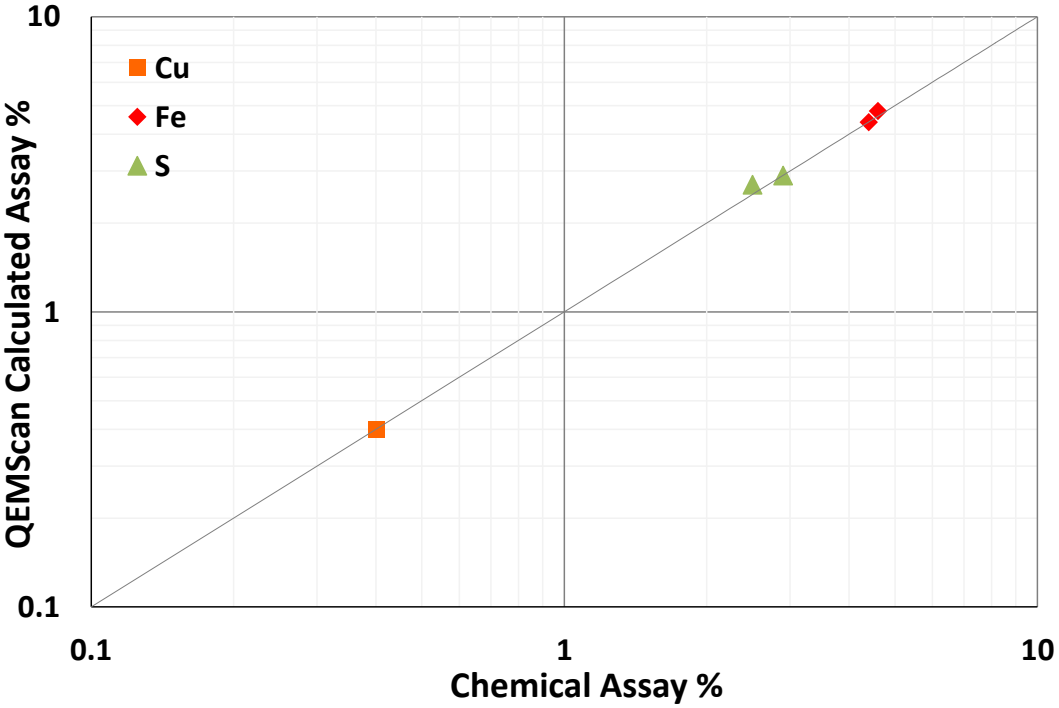


Figure A.4 MZ ore T3 assay reconciliation.

QZ XRF Assay								
Size	UT1 150	T1 150	T2 150	T3 150	UT1 370	T1 425	T2 425	T3 425
Element	Wt%	Wt%	Wt%	Wt%	Wt%	Wt%	Wt%	Wt%
Cu	0.67	0.70	0.70	0.60	0.60	0.70	0.70	0.70
Fe	1.30	1.20	1.20	1.20	1.60	1.20	1.30	1.20
S	1.00	0.80	0.80	0.80	0.90	0.80	0.90	0.80

Table A.3 QZ ore UT1, T1, T2 and T3 XRF chemical assay data.

QZ QEMScan Calculated Assay								
Size	UT1 150	T1 150	T2 150	T3 150	UT1 370	T1 425	T2 425	T3 425
Element	Wt%	Wt%	Wt%	Wt%	Wt%	Wt%	Wt%	Wt%
Cu	0.70	0.70	0.70	0.60	0.60	0.70	0.70	0.70
Fe	1.20	1.20	1.20	1.20	1.50	1.20	1.10	1.10
S	0.99	0.80	0.80	0.90	1.00	0.80	0.90	0.70

Table A.4 QZ ore UT1, T1, T2 and T3 QEMScan calculated assay data.

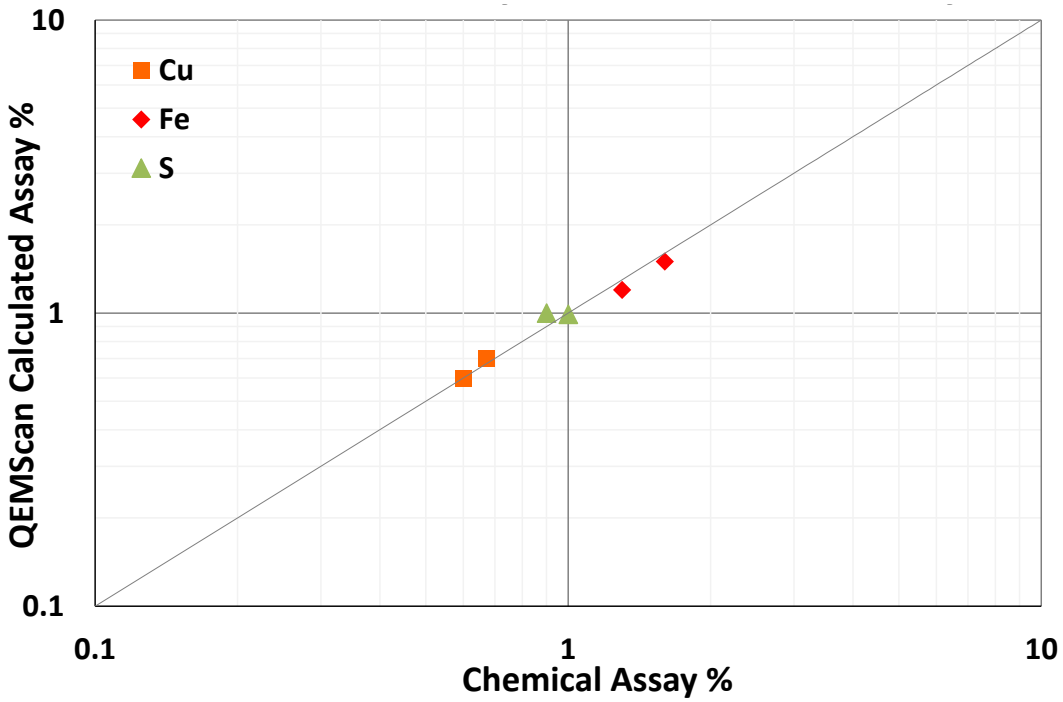


Figure A.5 QZ ore UT assay reconciliation.

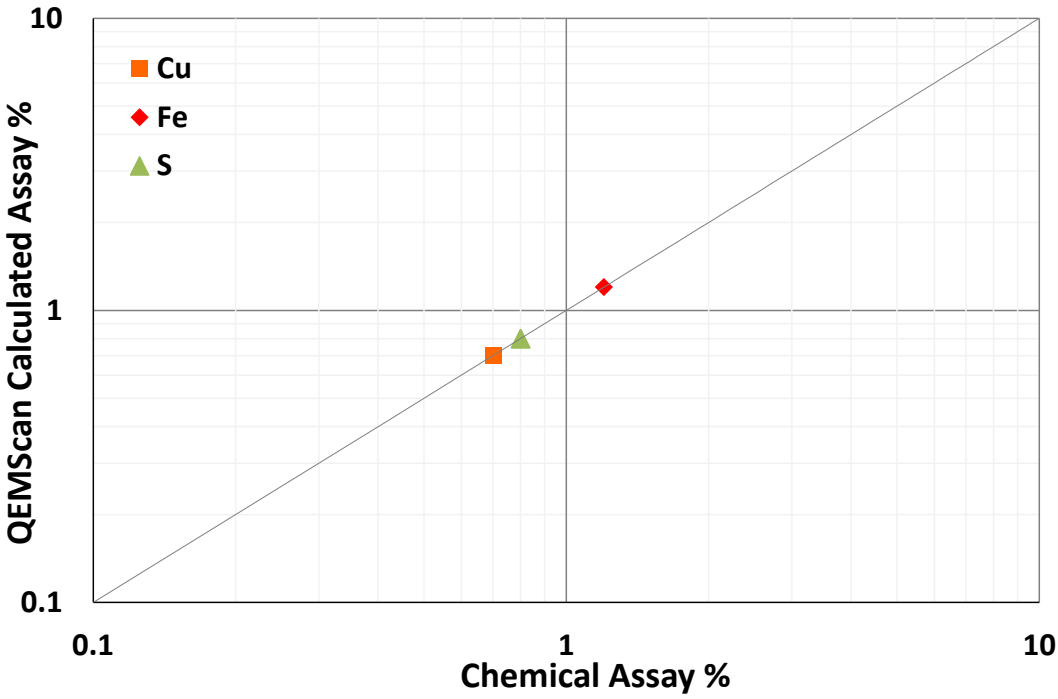


Figure A.6 QZ ore T1 assay reconciliation.

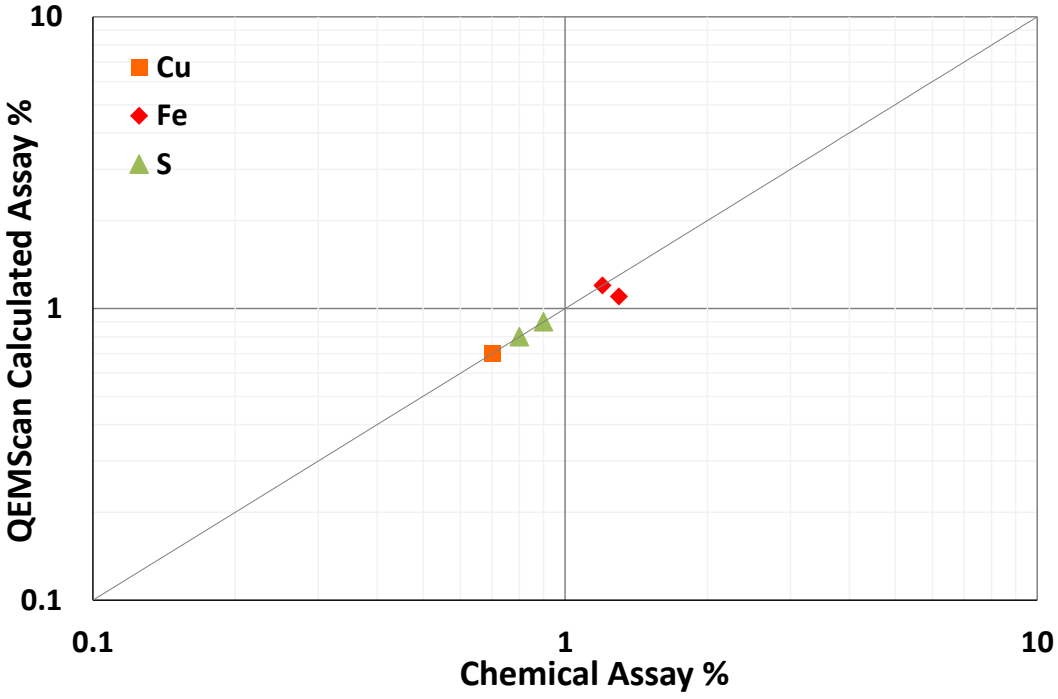


Figure A.7 QZ ore T2 assay reconciliation.

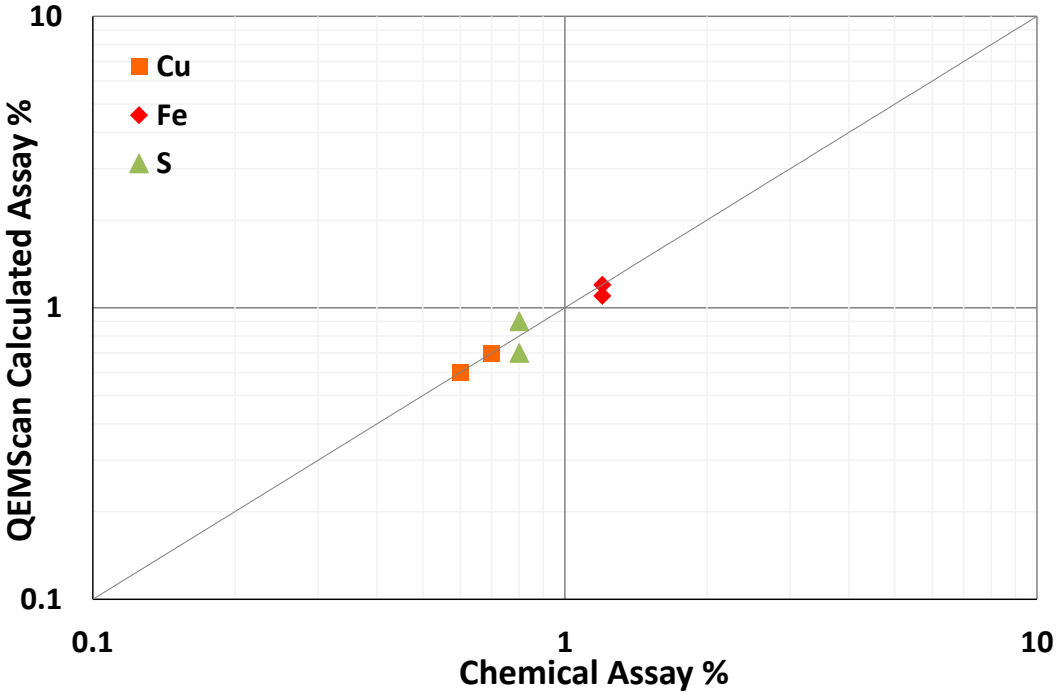


Figure A.8 QZ ore T3 assay reconciliation.

MZ UT2 XRF Assay (UoN)										
Size	+425	-425+300	-300+212	-212+150	-150+106	-106+75	-75+53	-53+38	-38	Combined
Mass	3.27	15.54	16.37	13.31	10.30	8.68	7.16	5.28	20.09	100.00
Element	Wt%	Wt%	Wt%	Wt%	Wt%	Wt%	Wt%	Wt%	Wt%	Wt%
Cu	0.20	0.22	0.23	0.30	0.36	0.53	0.71	0.70	0.59	0.41
Fe	3.45	3.57	3.81	4.31	4.57	4.51	4.33	3.77	3.86	4.01
S	1.54	1.88	3.36	3.14	3.42	3.35	2.94	2.27	1.38	2.56
Al	6.88	6.30	5.20	4.62	4.02	4.31	4.68	5.00	7.69	5.60
Ca	0.76	0.69	0.62	0.54	0.53	0.61	0.79	0.96	1.05	0.73
K	5.30	4.74	7.02	3.39	3.09	3.17	3.40	3.71	4.51	4.45
Mg	2.71	2.58	2.14	1.90	1.76	1.90	2.11	2.41	4.24	2.57
Si	30.68	31.73	33.09	33.79	34.35	33.98	33.24	32.41	28.53	32.16

Table A.5 MZ ore UT2 XRF chemical assay data.

MZ UT2 MLA Calculated Assay										
Size	+425	-425+300	-300+212	-212+150	-150+106	-106+75	-75+53	-53+38	-38	Combined
Mass	3.27	15.54	16.37	13.31	10.30	8.68	7.16	5.28	20.09	100.00
Element	Wt%	Wt%	Wt%	Wt%	Wt%	Wt%	Wt%	Wt%	Wt%	Wt%
Cu	0.26	0.25	0.32	0.35	0.40	0.63	0.75	0.75	0.58	0.45
Fe	3.73	3.88	4.30	5.19	5.02	4.88	4.17	3.21	3.71	4.27
S	2.28	2.67	2.78	3.42	3.55	3.41	3.26	1.98	1.38	2.68
Al	5.97	5.27	4.52	3.71	3.47	3.58	4.06	4.60	7.24	4.90
Ca	0.67	0.64	0.54	0.47	0.48	0.55	0.74	0.92	1.07	0.69
K	5.27	4.61	3.92	3.19	2.96	3.04	3.41	3.75	5.08	3.99
Mg	2.74	2.54	2.18	2.00	1.85	1.96	2.35	2.44	3.74	2.52
Si	30.24	31.58	32.72	33.53	34.19	33.89	33.27	33.05	27.02	31.73

Table A.6 MZ ore UT2 MLA calculated assay data.

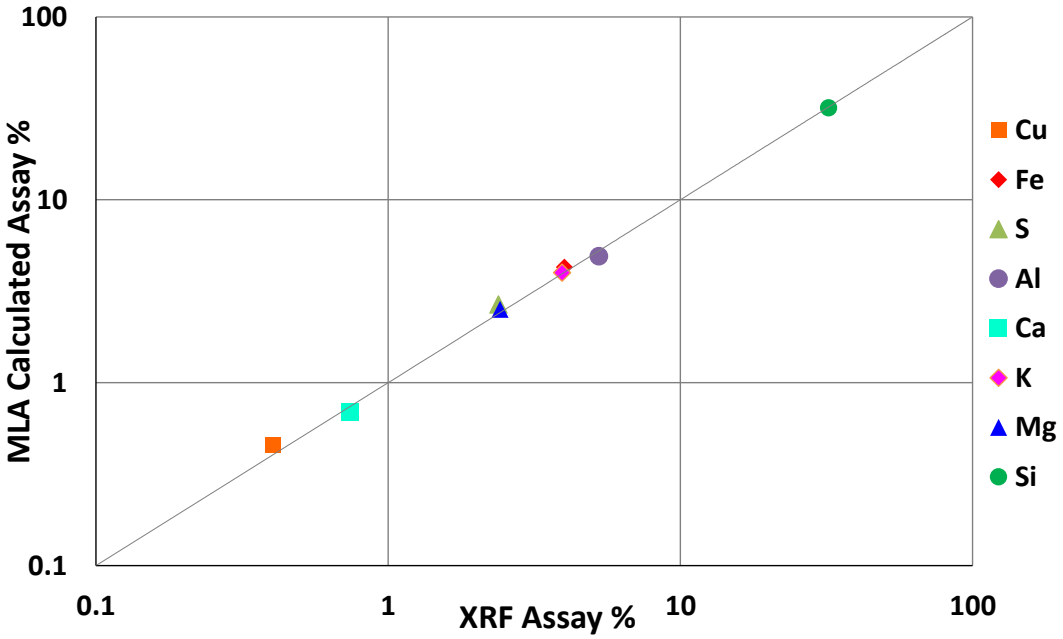


Figure A.9 MZ ore UT2 assay reconciliation.

MZ T4 XRF Assay (UoN)										
Size	+425	-425+300	-300+212	-212+150	-150+106	-106+75	-75+53	-53+38	-38	Combined
Mass	3.21	15.32	16.69	12.98	10.60	9.58	6.94	4.62	20.07	100.00
Element	Wt%	Wt%	Wt%	Wt%	Wt%	Wt%	Wt%	Wt%	Wt%	Wt%
Cu	0.19	0.22	0.22	0.30	0.34	0.54	0.68	0.68	0.53	0.39
Fe	3.46	3.57	3.77	4.23	4.39	4.50	4.31	3.73	3.81	3.96
S	1.58	1.88	2.34	3.22	3.26	3.38	2.88	2.19	1.31	2.37
Al	7.95	6.98	5.68	5.33	4.79	4.82	5.07	5.48	8.20	6.20
Ca	0.70	0.67	0.62	0.51	0.51	0.59	0.76	0.94	0.97	0.70
K	5.32	4.76	4.07	3.48	3.19	3.20	3.42	3.74	4.54	4.00
Mg	3.31	2.88	2.32	2.14	2.00	2.05	2.25	2.67	4.57	2.82
Si	30.52	31.76	33.14	33.83	34.47	33.90	33.22	32.74	28.44	32.17

Table A.7 MZ ore T4 XRF chemical assay data.

MZ T4 MLA Calculated Assay										
Size	+425	-425+300	-300+212	-212+150	-150+106	-106+75	-75+53	-53+38	-38	Combined
Mass	3.21	15.32	16.69	12.98	10.60	9.58	6.94	4.62	20.07	100.00
Element	Wt%	Wt%	Wt%	Wt%	Wt%	Wt%	Wt%	Wt%	Wt%	Wt%
Cu	0.18	0.21	0.25	0.30	0.40	0.65	0.70	0.83	0.48	0.41
Fe	2.67	2.78	4.06	4.60	4.77	4.67	4.01	3.64	3.68	3.91
S	1.14	1.60	3.24	3.45	3.77	3.80	3.13	2.57	1.20	2.60
Al	6.18	5.63	4.42	3.85	3.43	3.60	4.07	4.48	8.41	5.20
Ca	0.59	0.48	0.48	0.43	0.39	0.49	0.72	0.94	1.17	0.65
K	5.28	4.77	3.80	3.31	2.93	3.04	3.33	3.59	5.02	3.98
Mg	3.42	2.79	2.40	2.12	1.89	2.04	2.24	2.37	4.49	2.78
Si	31.22	32.47	33.31	33.91	34.63	34.08	33.60	32.96	26.79	32.09

Table A.8 MZ ore T4 MLA calculated assay data.

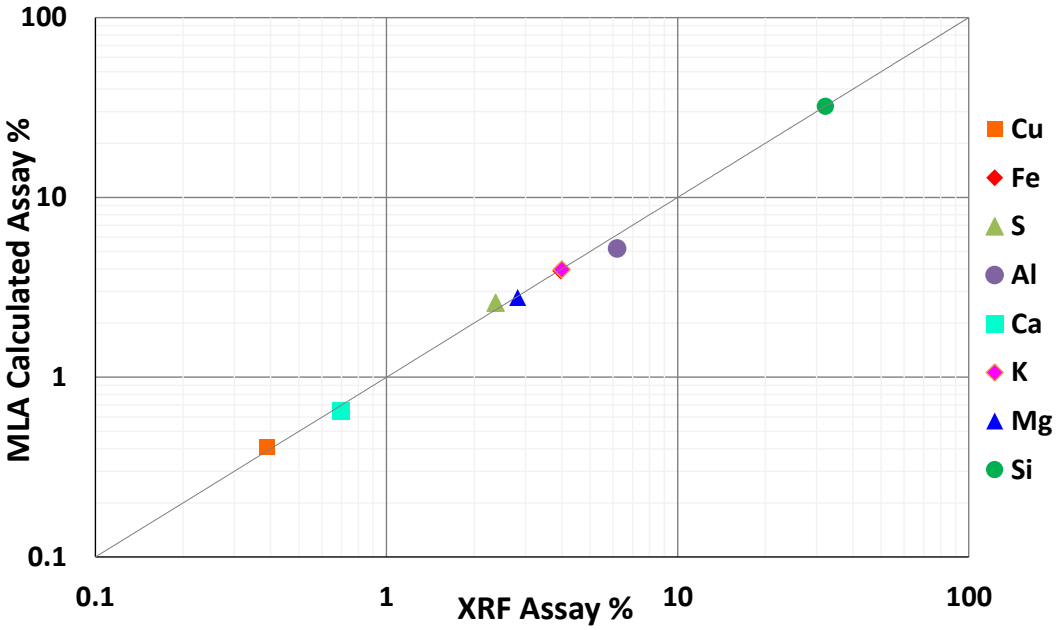


Figure A.10 MZ ore T4 assay reconciliation.

MZ T5 XRF Assay (UoN)										
Size	+425	-425+300	-300+212	-212+150	-150+106	-106+75	-75+53	-53+38	-38	Combined
Mass	3.15	15.55	16.50	12.96	10.20	8.76	7.55	4.64	20.69	100.00
Element	Wt%	Wt%	Wt%	Wt%	Wt%	Wt%	Wt%	Wt%	Wt%	Wt%
Cu	0.20	0.24	0.26	0.31	0.42	0.61	0.90	0.68	0.68	0.46
Fe	3.45	3.51	3.71	4.17	4.47	4.48	4.54	3.64	3.89	3.97
S	1.52	1.76	2.19	2.99	3.36	3.42	3.44	1.96	1.52	2.38
Al	6.22	5.43	4.67	4.25	3.98	3.87	3.86	5.02	7.17	5.10
Ca	0.74	0.74	0.67	0.58	0.56	0.66	0.87	1.02	1.12	0.78
K	5.48	4.99	4.26	3.58	3.26	3.28	3.43	3.94	4.62	4.13
Mg	2.31	2.19	1.91	1.76	1.71	1.73	1.74	2.52	3.81	2.31
Si	30.23	31.31	32.70	33.54	33.89	33.56	32.48	32.41	28.41	31.82

Table A.9 MZ ore T5 XRF chemical assay data.

MZ T5 MLA Calculated Assay										
Size	+425	-425+300	-300+212	-212+150	-150+106	-106+75	-75+53	-53+38	-38	Combined
Mass	3.15	15.55	16.50	12.96	10.20	8.76	7.55	4.64	20.69	100.00
Element	Wt%	Wt%	Wt%	Wt%	Wt%	Wt%	Wt%	Wt%	Wt%	Wt%
Cu	0.23	0.21	0.23	0.32	0.44	0.63	0.73	0.77	0.62	0.44
Fe	2.97	3.30	3.55	5.00	5.21	4.94	4.04	3.25	3.75	4.04
S	1.55	2.17	2.66	3.50	3.82	3.99	3.16	2.17	1.23	2.62
Al	6.17	5.54	4.73	4.01	3.70	3.68	4.22	4.77	7.45	5.12
Ca	0.71	0.74	0.48	0.44	0.43	0.52	0.75	0.89	1.12	0.69
K	5.40	4.75	4.09	3.43	3.13	3.12	3.52	3.88	5.19	4.13
Mg	2.41	2.30	2.47	2.06	1.96	1.94	2.29	2.52	4.20	2.63
Si	30.87	31.95	33.24	33.25	33.60	33.69	33.18	32.81	26.79	31.72

Table A.10 MZ ore T5 MLA calculated assay data.

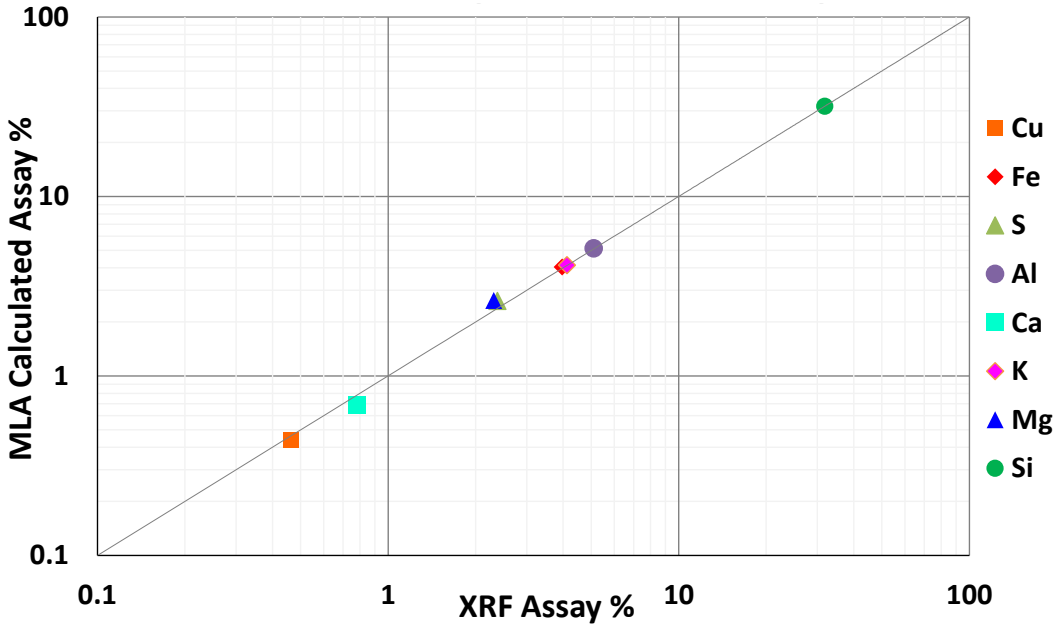


Figure A.11 MZ ore T5 assay reconciliation.

MZ T6 XRF Assay (UoN)										
Size	+425	-425+300	-300+212	-212+150	-150+106	-106+75	-75+53	-53+38	-38	Combined
Mass	3.13	15.01	16.53	13.03	10.42	9.74	6.96	4.56	20.62	100.00
Element	Wt%	Wt%	Wt%	Wt%	Wt%	Wt%	Wt%	Wt%	Wt%	Wt%
Cu	0.23	0.24	0.24	0.36	0.42	0.58	0.73	0.84	0.59	0.44
Fe	3.54	3.65	3.91	4.32	4.71	4.87	4.45	3.92	3.86	4.11
S	1.73	2.00	2.45	3.46	3.79	3.92	3.22	2.60	1.46	2.62
Al	8.13	6.98	5.74	5.47	4.46	4.04	5.10	5.03	8.26	6.12
Ca	0.67	0.63	0.57	0.50	0.49	0.56	0.73	0.95	0.93	0.67
K	5.47	4.90	4.16	3.62	3.24	3.16	3.48	3.74	4.61	4.08
Mg	3.49	2.84	2.23	2.15	1.74	1.65	2.16	2.45	4.63	2.74
Si	29.79	30.94	32.27	32.86	33.33	33.06	32.65	31.86	28.27	31.44

Table A.11 MZ ore T6 XRF chemical assay data.

MZ T6 MLA Calculated Assay										
Size	+425	-425+300	-300+212	-212+150	-150+106	-106+75	-75+53	-53+38	-38	Combined
Mass	3.13	15.01	16.53	13.03	10.42	9.74	6.96	4.56	20.62	100.00
Element	Wt%	Wt%	Wt%	Wt%	Wt%	Wt%	Wt%	Wt%	Wt%	Wt%
Cu	0.22	0.20	0.28	0.33	0.50	0.68	0.77	0.84	0.54	0.45
Fe	2.87	3.18	4.27	4.68	5.24	4.66	4.18	3.57	3.74	4.09
S	1.34	1.96	2.74	3.21	3.55	3.84	3.38	2.54	1.32	2.56
Al	6.19	5.56	4.73	3.99	3.50	3.65	4.11	5.04	8.45	5.31
Ca	0.61	0.60	0.50	0.44	0.42	0.52	0.70	0.98	1.07	0.66
K	5.40	4.79	4.10	3.43	2.98	3.07	3.43	3.69	5.13	4.09
Mg	3.49	2.95	2.46	2.09	1.87	1.92	2.27	2.37	4.30	2.77
Si	30.87	31.95	32.50	33.57	33.91	34.06	33.29	32.82	27.10	31.77

Table A.12 MZ ore T6 MLA calculated assay data.

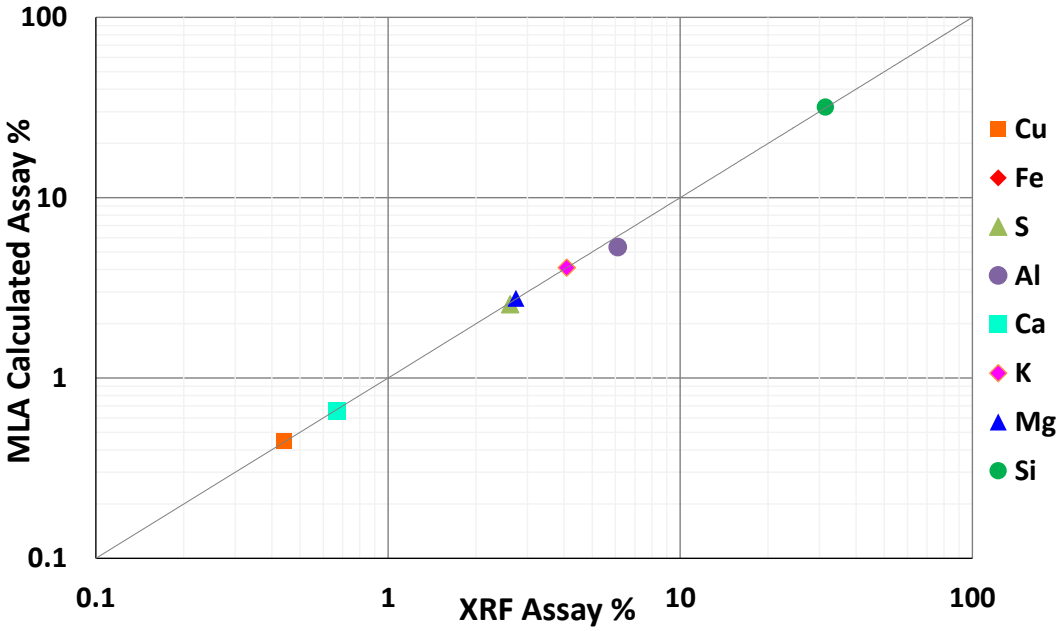


Figure A.12 MZ ore T6 assay reconciliation.

MZ T7 XRF Assay (UoN)										
Size	+425	-425+300	-300+212	-212+150	-150+106	-106+75	-75+53	-53+38	-38	Combined
Mass	3.54	15.78	16.17	12.63	10.25	9.58	7.18	4.84	20.01	100.00
Element	Wt%	Wt%	Wt%	Wt%	Wt%	Wt%	Wt%	Wt%	Wt%	Wt%
Cu	0.28	0.28	0.29	0.36	0.43	0.64	0.84	0.84	0.74	0.50
Fe	3.68	3.74	3.97	4.43	4.78	4.84	4.63	3.88	4.05	4.20
S	1.86	2.09	2.59	3.38	3.68	3.80	3.42	2.43	1.66	2.67
Al	7.20	6.80	5.71	5.15	4.42	4.18	4.99	5.54	7.95	5.98
Ca	0.78	0.71	0.63	0.56	0.54	0.62	0.80	1.01	1.09	0.75
K	5.16	4.67	4.06	3.49	3.16	3.16	3.39	3.71	4.43	3.95
Mg	3.07	2.89	2.37	2.06	1.83	1.78	2.21	2.84	4.62	2.79
Si	29.98	31.18	32.33	33.15	33.56	33.07	32.39	31.79	28.38	31.56

Table A.13 MZ ore T7 XRF chemical assay data.

MZ T7 MLA Calculated Assay										
Size	+425	-425+300	-300+212	-212+150	-150+106	-106+75	-75+53	-53+38	-38	Combined
Mass	3.54	15.78	16.17	12.63	10.25	9.58	7.18	4.84	20.01	100.00
Element	Wt%	Wt%	Wt%	Wt%	Wt%	Wt%	Wt%	Wt%	Wt%	Wt%
Cu	0.21	0.22	0.26	0.36	0.46	0.67	0.72	0.84	0.71	0.47
Fe	3.01	3.58	4.29	4.94	5.14	4.81	4.09	3.34	3.98	4.23
S	1.34	2.34	3.38	4.41	4.64	4.25	3.15	2.19	1.54	3.05
Al	7.12	6.74	5.32	3.97	4.01	4.11	4.80	5.50	8.08	5.71
Ca	0.79	0.68	0.57	0.47	0.48	0.57	0.70	1.05	1.05	0.70
K	5.21	4.63	3.92	3.43	3.09	3.08	3.47	3.65	5.09	4.04
Mg	3.52	2.99	2.56	2.15	2.03	2.09	2.41	2.48	4.48	2.88
Si	30.89	31.76	32.70	33.27	33.66	33.69	33.22	33.02	27.03	31.67

Table A.14 MZ ore T7 MLA calculated assay data.

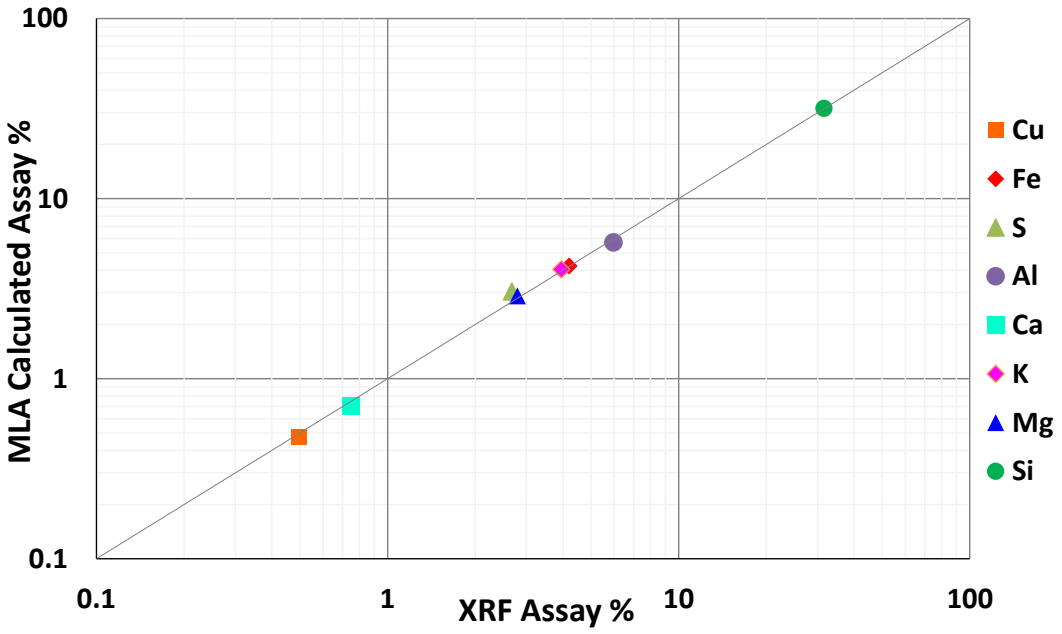


Figure A.13 MZ ore T7 assay reconciliation.

A.2 Coarse Ore Mineral Grain Size Distribution Data

MZ Coarse Ore Grain Size Distribution			
Seive Size (µm)	Cumulative Passing (wt%)		
	Copper Sulphides	Other Sulphides	Other Heaters
1700		100.00	
1400		97.58	
1200		97.06	
1000		95.95	
850	100.00	95.67	
710	97.44	95.12	
600	96.93	93.37	
500	96.21	91.37	100.00
425	94.53	86.02	98.82
355	92.12	81.42	98.82
300	87.22	74.10	98.82
250	81.73	65.50	97.71
212	74.83	55.50	96.56
180	67.96	46.20	95.99
150	58.56	37.11	93.63
125	48.98	28.53	92.21
106	40.30	21.65	90.84
90	32.84	16.66	88.22
75	25.11	12.57	83.79
63	19.36	9.29	78.82
53	14.47	6.74	71.53
45	10.76	4.73	60.72
38	8.22	3.46	51.50
32	6.15	2.49	43.69
27	4.54	1.81	35.30
22	3.31	1.24	26.10
19	2.58	0.90	20.75
16	1.91	0.65	15.42
13.5	1.38	0.45	11.24
11.4	0.98	0.31	7.50
9.6	0.70	0.20	5.18
8.1	0.46	0.12	3.54
6.8	0.28	0.06	2.23
5.7	0.12	0.02	1.22
4.8	0.04	0.01	0.44
4.1	0.00	0.00	0.00

Table A.15 MZ coarse ore mineral grain size distribution

QZ Coarse Ore Grain Size Distribution			
Seive Size (µm)	Cumulative Passing (wt%)		
	Copper Sulphides	Other Sulphides	Other Heaters
850	100.00		
710	99.07		
600	96.92	100.00	
500	94.75	98.27	
425	93.30	93.10	
355	89.78	89.49	
300	85.59	84.38	
250	78.27	77.60	100.00
212	69.86	67.84	97.33
180	59.87	58.55	97.33
150	50.28	45.86	97.33
125	41.27	35.34	97.33
106	34.04	27.23	95.61
90	27.57	20.23	92.82
75	22.11	14.67	90.48
63	18.07	10.74	86.36
53	13.08	7.66	77.15
45	9.16	5.11	59.76
38	7.33	3.85	49.80
32	5.80	2.78	40.78
27	4.67	1.96	31.85
22	3.53	1.28	23.51
19	2.84	0.96	17.62
16	2.18	0.68	11.92
13.5	1.67	0.52	7.73
11.4	1.23	0.36	4.87
9.6	0.90	0.25	3.10
8.1	0.66	0.17	1.91
6.8	0.43	0.09	1.17
5.7	0.24	0.04	0.55
4.8	0.09	0.01	0.20
4.1	0.00	0.00	0.00

Table A.16 QZ coarse ore mineral grain size distribution

QX Coarse Ore Grain Size Distribution			
Seive Size (µm)	Cumulative Passing (wt%)		
	Copper Sulphides	Other Sulphides	Other Heaters
1400		100.00	
1200		99.32	
1000		98.25	
850		97.43	
710		96.51	
600		95.57	
500		92.51	
425		88.70	
355	100.00	83.68	
300	98.17	76.80	
250	96.82	67.32	
212	95.19	57.88	
180	89.00	48.27	
150	82.81	37.97	
125	75.72	29.37	
106	69.76	22.32	
90	64.23	17.02	
75	55.97	12.16	
63	49.08	8.61	
53	42.61	6.12	100.00
45	36.39	4.39	93.61
38	28.68	3.20	87.12
32	19.84	1.91	66.81
27	15.77	1.35	54.26
22	12.26	0.85	39.33
19	9.82	0.60	27.82
16	7.72	0.40	19.64
13.5	5.88	0.27	13.52
11.4	4.40	0.19	8.74
9.6	3.35	0.12	5.86
8.1	2.46	0.09	3.94
6.8	1.67	0.05	2.46
5.7	1.07	0.03	1.34
4.8	0.63	0.02	0.91
4.1	0.42	0.01	0.66
3.4	0.11	0.00	0.07
2.9	0.00	0.00	0.00
2.4	0.00	0.00	0.00
2	0.00	0.00	0.00
1.75	0.00	0.00	0.00
1.45	0.00	0.00	0.00
1.2	0.00	0.00	0.00
1	0.00	0.00	0.00

Table A.17 QX coarse ore mineral grain size distribution

A.3 Mineral Abundance Data

MZ Ore Mineral Abundance (wt%)								
Sample	**UT**	**T1**	**T2**	**T3**	**UT**	**T1**	**T2**	**T3**
Grind Size P_{80}	**150**	**150**	**150**	**150**	**370**	**425**	**425**	**425**
Chalcopyrite	1.06	1.02	0.95	1.10	1.11	1.02	1.00	1.01
Bornite	0.02	0.03	0.04	0.04	0.02	0.04	0.04	0.03
Chalcocite/Covellite	0.00	0.04	0.01	0.01	0.00	0.02	0.02	0.03
Molybdenite	0.01	0.00	0.01	0.01	0.00	0.00	0.01	0.00
Pyrite	4.43	4.45	4.16	4.70	3.99	4.40	4.09	4.36
Other Sulphides	0.00	0.00	0.00	0.00	0.03	0.01	0.00	0.00
Iron Oxides	0.25	0.50	0.38	0.62	0.22	0.37	0.31	0.41
Quartz	35.80	37.60	40.30	38.70	35.00	38.40	37.90	39.00
Feldspar	32.80	29.30	29.90	28.40	32.30	28.90	30.40	28.60
Micas	22.60	20.70	18.70	19.90	23.80	20.40	20.30	19.80
Pyroxene/Amphibole	0.66	2.04	1.76	2.73	0.72	2.06	1.79	2.85
Andradite	0.08	0.75	0.82	0.85	0.07	0.84	0.91	0.91
Other Silicates	0.84	1.26	1.02	1.20	1.01	1.27	1.19	1.15
Calcite	0.21	0.37	0.51	0.43	0.20	0.49	0.48	0.47
Apatite	0.76	0.82	0.74	0.75	0.86	0.85	0.78	0.81
Other	0.49	1.04	0.66	0.62	0.71	0.86	0.82	0.57
Total	100	100	100	100	100	100	100	100

Table A.18 MZ Ore ungrouped mineral abundance.

MZ Ore Mineral Abundance (wt%)					
Sample	**UT2**	**T4**	**T5**	**T6**	**T7**
Grind Size P80	**290**	**290**	**290**	**290**	**290**
Chalcopyrite	1.05	1.08	1.02	0.99	1.10
Bornite	0.06	0.05	0.05	0.05	0.05
Chalcocite/Covellite	0.01	0.01	0.01	0.01	0.01
Molybdenite	0.02	0.01	0.01	0.01	0.01
Pyrite	4.41	4.28	4.41	4.45	4.32
Other Sulphides	0.03	0.02	0.02	0.02	0.01
Iron Oxides	0.22	0.24	0.41	0.32	0.19
Quartz	40.08	40.65	38.81	39.46	39.20
Feldspar	28.76	28.28	29.96	29.11	29.13
Micas	21.93	22.05	22.13	22.21	22.46
Pyroxene/Amphibole	0.97	0.84	0.68	0.90	1.10
Andradite	0.04	0.07	0.07	0.05	0.12
Other Silicates	0.77	0.80	0.76	0.78	0.81
Carbonates	0.35	0.25	0.28	0.24	0.25
Apatite	0.84	0.85	0.85	0.84	0.79
Other	0.45	0.53	0.52	0.55	0.45
Total	100	100	100	100	100

Table A.19 MZ Ore low dose microwave treatments ungrouped mineral abundance.

QZ Ore Mineral Abundance (wt%)								
Sample	**UT**	**T1**	**T2**	**T3**	**UT**	**T1**	**T2**	**T3**
Grind Size P_{80}	**150**	**150**	**150**	**150**	**370**	**425**	**425**	**425**
Chalcopyrite	0.99	1.04	1.01	0.96	1.01	1.20	1.06	1.04
Bornite	0.25	0.19	0.24	0.24	0.24	0.24	0.25	0.24
Chalcocite/Covellite	0.22	0.24	0.20	0.22	0.22	0.17	0.20	0.20
Molybdenite	0.01	0.02	0.01	0.01	0.01	0.01	0.02	0.01
Pyrite	0.68	0.59	0.65	0.69	0.74	0.64	0.63	0.67
Other Sulphides	0.00	0.01	0.00	0.01	0.00	0.01	0.00	0.01
Iron Oxides	0.26	0.35	0.37	0.34	0.19	0.22	0.17	0.17
Quartz	87.40	89.80	89.80	89.80	88.20	89.20	89.30	89.30
Feldspar	2.10	1.68	1.64	1.59	2.28	1.83	1.80	1.77
Micas	7.66	5.86	5.77	5.78	6.78	6.19	6.21	6.18
Pyroxene/Amphibole	0.01	0.02	0.10	0.02	0.02	0.02	0.02	0.02
Andradite	0.00	0.02	0.01	0.00	0.00	0.01	0.00	0.00
Other Silicates	0.04	0.03	0.04	0.03	0.04	0.03	0.03	0.03
Calcite	0.16	0.02	0.03	0.09	0.07	0.03	0.07	0.07
Apatite	0.11	0.06	0.06	0.07	0.06	0.07	0.07	0.07
Other	0.10	0.11	0.12	0.13	0.12	0.13	0.21	0.15
Total	100	100	100	100	100	100	100	100

Table A.20 QZ Ore ungrouped mineral abundance.

A.4 Mineral Liberation and Locking Data

MZ Ore Cu-Sulphide Liberation by Free Surface (Distribution of Mineral %)					
Sample	**Grind P_{80}**	**0%(Barren) -10%**	**10%-50%**	**50%-98%**	**98%-100%**
UT1	150	4.60	8.20	19.10	68.20
T1	150	5.00	5.70	10.70	78.50
T2	150	4.90	8.40	11.50	75.10
T3	150	3.00	5.60	11.50	79.90
UT1	370	13.90	14.70	14.00	57.40
T1	425	15.60	12.30	10.70	61.50
T2	425	13.70	12.60	12.43	61.27
T3	425	13.00	11.30	14.10	61.60
UT2	293	6.02	11.98	13.21	68.78
T4	292	5.70	12.40	13.05	69.08
T5	293	6.25	9.71	10.77	73.27
T6	290	5.99	11.59	11.87	70.55
T7	296	5.91	11.17	11.86	71.05

Table A.21 MZ Ore Cu-sulphide mineral liberation by free surface.

QZ Ore Cu-Sulphide Liberation by Free Surface (Distribution of Mineral %)					
Sample	**Grind P_{80}**	**0%(Barren) -10%**	**10%-50%**	**50%-98%**	**98%-100%**
UT1	150	2.50	4.20	23.50	69.90
T1	150	2.10	3.80	14.10	80.00
T2	150	2.40	4.30	17.10	76.20
T3	150	2.30	3.60	17.60	76.40
UT1	370	7.80	11.30	21.70	59.30
T1	425	9.40	8.90	15.50	66.20
T2	425	8.50	9.20	22.60	59.70
T3	425	10.90	8.20	15.20	65.80

Table A.22 QZ Ore Cu-sulphide mineral liberation by free surface.

MZ Ore Cu-Sulphide Liberation by Free Surface (5% Classes - Cumulative Distribution)					
Sample	**UT2**	**T4**	**T5**	**T6**	**T7**
0%	100.00	100.00	100.00	100.00	100.00
0-5%	98.64	98.61	98.53	98.74	98.71
5-10%	96.40	96.55	96.24	96.73	96.46
10-15%	93.96	94.17	93.74	94.00	94.07
15-20%	91.86	91.69	91.78	91.68	91.94
20-25%	89.86	90.04	90.05	89.96	90.54
25-30%	88.16	88.63	88.79	88.54	88.95
30-35%	86.72	86.76	87.29	87.18	87.38
35-40%	85.24	85.46	86.22	86.07	86.27
40-45%	84.07	84.28	85.53	85.09	85.32
45-50%	83.21	83.45	84.65	83.75	83.93
50- 55%	82.00	82.47	84.04	82.42	82.92
55-60%	80.69	81.24	83.22	81.58	81.77
60- 65%	79.54	79.98	82.13	80.33	80.90
65-70%	78.58	79.02	81.40	79.06	80.06
70-75%	77.22	77.61	80.63	77.84	79.23
75-80%	76.54	76.88	79.66	76.55	77.52
80-85%	75.45	75.85	78.77	75.50	76.65
85-90%	73.48	74.12	77.52	74.35	75.47
90-95%	71.96	72.84	76.14	73.00	73.86
95-100%	70.22	70.84	74.12	71.37	72.17
100%	68.10	68.97	72.62	70.16	70.62

Table A.23 MZ Ore Cu-sulphide mineral liberation by free surface in 5% liberation classes

MZ Ore				
Sample	**P_{80}**	**Cu-S:NSG Binary**	**Cu-S:Pyrite Binary**	**Multiphase**
UT	**150**	27.52	2.48	1.70
T1	**150**	17.80	2.90	0.70
T2	**150**	21.00	2.68	1.00
T3	**150**	16.30	2.50	1.40
UT	**370**	36.62	2.64	3.30
T1	**425**	31.00	3.70	3.90
T2	**425**	33.56	1.53	3.54
T3	**425**	31.80	2.00	4.40
UT2	**290**	22.25	2.40	2.42
T4	**290**	21.00	2.37	2.07
T5	**290**	18.30	2.59	1.94
T6	**290**	21.18	2.27	2.17
T7	**290**	21.27	2.38	2.22

Table A.24 MZ Ore Cu-sulphide mineral locking

MZ Ore					
Sample	**P_{80}**	**Cu-S:'Hard' NSG Binary**	**Cu-S:'Soft' NSG Binary**	**Cu-S:'Hard' NSG Multiphase**	**Cu-S:'Soft' NSG Multiphase**
UT2	**290**	8.52	6.01	5.08	3.98
T4	**290**	8.76	5.45	4.38	3.45
T5	**290**	7.08	4.63	3.97	3.60
T6	**290**	7.95	5.88	4.56	3.94
T7	**290**	7.92	5.77	4.68	4.03

Table A.25 MZ Ore Cu-sulphide mineral locking with Non-Sulphide Gangue

QZ Ore				
Sample	**P_{80}**	**Cu-S:NSG Binary**	**Cu-S:Pyrite Binary**	**Multiphase**
UT	**150**	23.90	2.04	3.22
T1	**150**	15.10	1.90	1.70
T2	**150**	18.00	3.70	1.30
T3	**150**	17.40	4.10	1.80
UT	**370**	32.03	4.41	4.40
T1	**425**	25.80	2.60	4.20
T2	**425**	31.30	2.90	4.40
T3	**425**	27.00	3.80	3.30

Table A.26 QZ Ore Cu-sulphide mineral locking

A.5 MZ Ore Grind Calibrations for Low Dose Treatments

MZ UT2	Calibration					Target
Time (min) / Mass (g)	0.0	2.0	4.0	8.0	16.0	5.7
3.35	10.10	0.00	0.00	0.00	0.00	
2.36	40.95	0.16	0.00	0.00	0.00	
1.70	106.73	1.95	0.00	0.00	0.00	
1.18	144.31	21.76	0.00	0.00	0.00	
0.850	109.98	78.58	1.47	0.00	0.00	0.05
0.600	113.88	146.13	35.26	0.00	0.00	0.79
0.425	94.37	134.87	145.32	0.72	0.00	31.57
0.300	70.76	109.31	159.14	39.17	0.00	154.21
0.212	54.89	91.04	125.79	164.30	4.38	162.51
0.150	47.69	78.22	103.36	172.97	72.82	132.11
0.106	38.53	63.09	83.10	129.23	183.45	102.25
0.075	34.95	55.56	73.02	108.09	177.42	86.10
0.053	26.90	44.09	55.78	79.28	130.50	71.03
0.038	21.72	34.74	42.87	61.64	89.92	52.44
-0.038	77.95	133.20	169.06	235.12	330.28	199.44
Total	993.71	992.70	994.17	990.52	988.78	992.50
Loss	*0.6%*	*0.7%*	*0.6%*	*0.9%*	*1.1%*	*0.8%*

Size (mm)	Cumulative % Passing					
3.35	98.98	100.00				
2.36	94.86	99.98				
1.70	84.12	99.79				
1.18	69.60	97.60	100.00			100.00
0.850	58.53	89.68	99.85			99.99
0.600	47.07	74.96	96.31	100.00		99.92
0.425	37.58	61.37	81.69	99.93		96.73
0.300	30.45	50.36	65.68	95.97	100.00	81.20
0.212	24.93	41.19	53.03	79.39	99.56	64.82
0.150	20.13	33.31	42.63	61.92	92.19	51.51
0.106	16.25	26.96	34.27	48.88	73.64	41.21
0.075	12.74	21.36	26.93	37.96	55.70	32.54
0.053	10.03	16.92	21.32	29.96	42.50	25.38
0.038	7.84	13.42	17.00	23.74	33.40	20.09
D_{xx}	% Passing					
95	2.388	1.063	0.583	0.294	0.172	0.410
80	1.543	0.681	0.411	0.215	0.120	0.293
50	0.661	0.296	0.193	0.110	0.065	0.143
20	0.148	0.068	0.048	<0.038	<0.038	<0.038
10	0.053	<0.038	<0.038	<0.038	<0.038	<0.038

Table A.27 MZ Ore UT2 target liberation grind calibration data

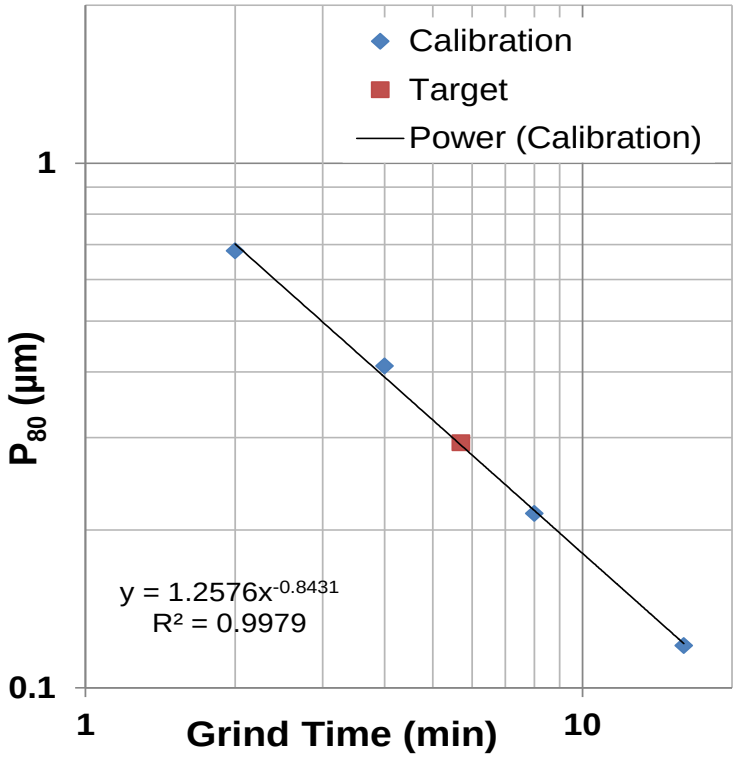


Figure A.14 MZ UT2 target grind calibration

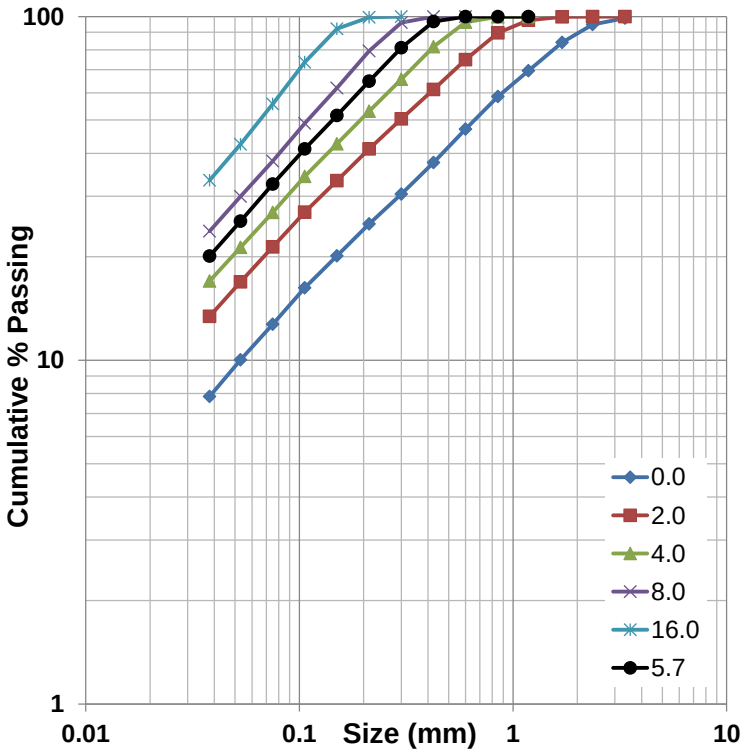


Figure A.15 MZ UT2 grind calibration particle size distributions.

MZ T4	Calibration					Target
Time (min) / Mass (g)	0.0	2.0	4.0	8.0	16.0	6.4
3.35	15.48	0.35	0.00	0.00	0.00	
2.36	54.13	1.05	0.00	0.00	0.00	
1.70	129.02	8.81	0.00	0.00	0.00	
1.18	164.71	52.86	0.32	0.00	0.00	
0.850	124.36	115.45	7.98	0.00	0.00	
0.600	113.84	150.92	88.03	0.08	0.00	0.71
0.425	79.55	120.39	159.97	2.26	0.00	31.21
0.300	55.81	94.90	137.37	70.88	1.28	152.20
0.212	44.10	78.14	109.04	157.59	5.59	165.80
0.150	39.41	69.42	92.09	148.28	67.22	128.94
0.106	32.89	57.86	76.89	145.52	218.03	105.26
0.075	30.86	50.45	67.01	99.27	163.87	95.22
0.053	25.12	40.91	52.71	71.82	117.60	68.91
0.038	18.49	30.26	40.96	62.39	95.56	45.87
-0.038	66.57	121.05	160.96	229.84	320.14	199.36
Total	994.34	992.82	993.33	987.92	989.29	993.48
Loss	*0.6%*	*0.7%*	*0.7%*	*1.2%*	*1.1%*	*0.7%*

Size (mm)	Cumulative % Passing					
3.35	98.44	99.96				
2.36	93.00	99.86				
1.70	80.02	98.97	100.00			
1.18	63.46	93.65	99.97			
0.850	50.95	82.02	99.16	100.00		100.00
0.600	39.50	66.82	90.30	99.99		99.93
0.425	31.50	54.69	74.20	99.76	100.00	96.79
0.300	25.89	45.13	60.37	92.59	99.87	81.47
0.212	21.46	37.26	49.39	76.64	99.31	64.78
0.150	17.49	30.27	40.12	61.63	92.51	51.80
0.106	14.18	24.44	32.38	46.90	70.47	41.20
0.075	11.08	19.36	25.63	36.85	53.91	31.62
0.053	8.55	15.24	20.33	29.58	42.02	24.68
0.038	6.69	12.19	16.20	23.26	32.36	20.07
D_{xx}	% Passing					
95	2.690	1.297	0.725	0.338	0.171	0.409
80	1.699	0.815	0.485	0.229	0.125	0.292
50	0.828	0.361	0.217	0.115	0.068	0.142
20	0.188	0.079	0.052	<0.038	<0.038	<0.038
10	0.065	<0.038	<0.038	<0.038	<0.038	<0.038

Table A.28 MZ Ore T4 target liberation grind calibration data

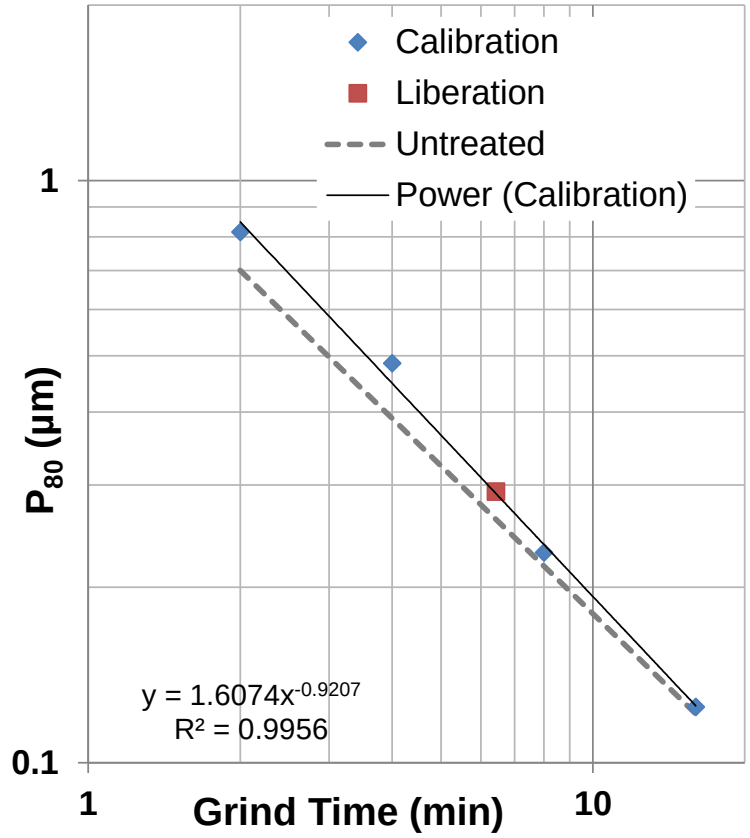


Figure A.16 MZ T4 target grind calibration

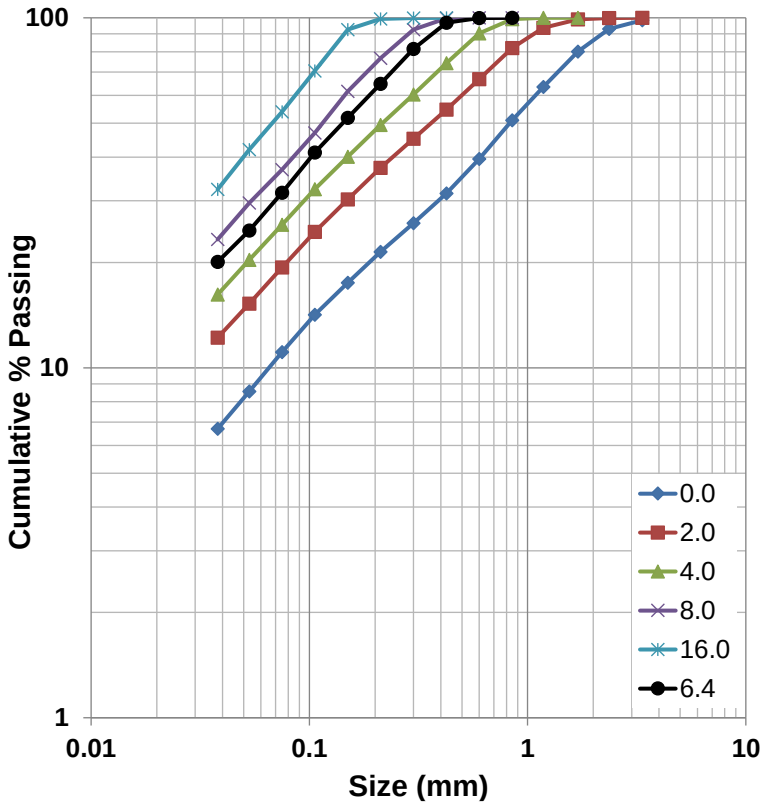


Figure A.17 MZ T4 grind calibration particle size distributions.

MZ T5	Calibration					Target
Time (min) / Mass (g)	0.0	2.0	4.0	8.0	16.0	6.2
3.35	10.48	0.10	0.00	0.00	0.00	
2.36	43.42	0.47	0.00	0.00	0.00	
1.70	114.36	4.06	0.00	0.00	0.00	
1.18	153.25	35.15	0.00	0.00	0.00	
0.850	119.37	101.15	4.57	0.00	0.00	0.09
0.600	118.97	154.01	70.47	0.00	0.00	0.65
0.425	90.99	130.59	163.95	2.03	0.00	30.50
0.300	64.64	102.88	145.23	62.10	0.00	154.26
0.212	48.90	83.82	112.37	176.16	5.35	163.67
0.150	42.96	70.72	93.65	161.19	59.45	128.62
0.106	35.43	57.91	76.49	118.68	209.44	101.17
0.075	32.30	53.71	66.43	100.81	164.96	86.93
0.053	26.21	41.27	52.57	74.37	117.76	74.92
0.038	20.71	32.53	41.26	58.35	91.64	46.02
-0.038	74.21	128.47	163.57	236.49	338.67	205.27
Total	996.20	996.84	990.55	990.18	987.29	992.10
Loss	*0.4%*	*0.3%*	*0.9%*	*1.0%*	*1.3%*	*0.8%*

Size (mm)	Cumulative % Passing					
3.35	98.95	99.99				
2.36	94.59	99.94				
1.70	83.11	99.54				
1.18	67.73	96.01	100.00			100.00
0.850	55.74	85.86	99.54			99.99
0.600	43.80	70.41	92.42	100.00		99.93
0.425	34.67	57.31	75.87	99.79		96.85
0.300	28.18	46.99	61.21	93.52	100.00	81.30
0.212	23.27	38.58	49.87	75.73	99.46	64.80
0.150	18.96	31.49	40.41	59.45	93.44	51.84
0.106	15.40	25.68	32.69	47.47	72.22	41.64
0.075	12.16	20.29	25.99	37.29	55.51	32.88
0.053	9.53	16.15	20.68	29.78	43.59	25.33
0.038	7.45	12.89	16.51	23.88	34.30	20.69
D_{xx}	% Passing					
95	2.441	1.144	0.683	0.326	0.164	0.409
80	1.588	0.751	0.466	0.232	0.122	0.293
50	0.726	0.335	0.213	0.115	0.065	0.142
20	0.164	0.073	0.050	<0.038	<0.038	<0.038
10	0.057	<0.038	<0.038	<0.038	<0.038	<0.038

Table A.29 MZ Ore T5 target liberation grind calibration data

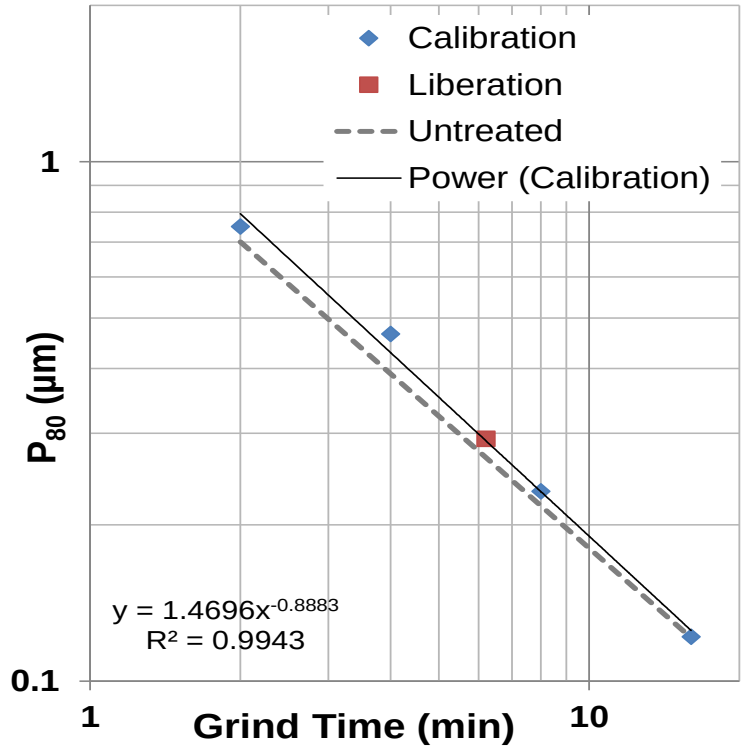


Figure A.18 MZ T5 target grind calibration

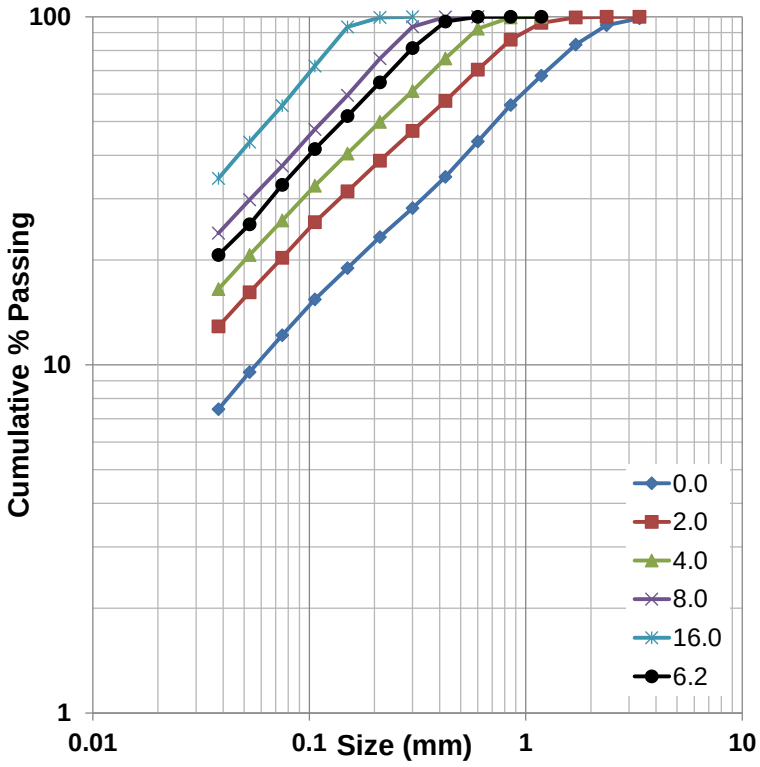


Figure A.19 MZ T5 grind calibration particle size distributions.

MZ T6	Calibration					Target
Time (min) / Mass (g)	0.0	2.0	4.0	8.0	16.0	7.2
3.35	62.15	4.10	0.00	0.00	0.00	
2.36	109.73	11.32	0.00	0.00	0.00	
1.70	133.08	40.99	0.00	0.00	0.00	
1.18	132.79	102.88	3.28	0.00	0.00	
0.850	93.74	115.12	32.35	0.00	0.00	
0.600	92.67	123.30	131.66	0.00	0.00	0.61
0.425	73.01	103.55	145.98	8.03	0.00	30.40
0.300	54.25	84.24	119.32	107.55	2.25	148.90
0.212	41.86	70.71	98.17	159.04	6.40	164.00
0.150	37.29	62.46	84.61	135.81	68.68	129.27
0.106	31.21	51.36	71.17	134.24	213.87	103.42
0.075	29.32	48.91	64.60	92.65	162.08	96.64
0.053	23.33	37.75	49.07	71.25	112.24	69.10
0.038	17.86	27.92	38.44	57.35	97.51	45.26
-0.038	60.94	109.77	153.77	225.21	319.88	204.60
Total	993.23	994.38	992.42	991.13	982.91	992.20
Loss	*0.7%*	*0.6%*	*0.8%*	*0.9%*	*1.7%*	*0.8%*

Size (mm)	Cumulative % Passing					
3.35	93.74	99.59				
2.36	82.69	98.45				
1.70	69.30	94.33	100.00			
1.18	55.93	83.98	99.67			
0.850	46.49	72.40	96.41			100.00
0.600	37.16	60.00	83.14	100.00		99.94
0.425	29.81	49.59	68.43	99.19	100.00	96.87
0.300	24.35	41.12	56.41	88.34	99.77	81.87
0.212	20.13	34.01	46.52	72.29	99.12	65.34
0.150	16.38	27.73	37.99	58.59	92.13	52.31
0.106	13.23	22.56	30.82	45.05	70.37	41.89
0.075	10.28	17.64	24.31	35.70	53.88	32.15
0.053	7.93	13.85	19.37	28.51	42.46	25.18
0.038	6.14	11.04	15.49	22.72	32.54	20.62
D_{xx}	% Passing					
95	>3.350	1.795	0.821	0.373	0.173	0.408
80	2.219	1.060	0.560	0.253	0.125	0.290
50	0.967	0.431	0.241	0.122	0.067	0.140
20	0.210	0.089	0.056	<0.038	<0.038	<0.038
10	0.072	<0.038	<0.038	<0.038	<0.038	<0.038

Table A.30 MZ Ore T6 target liberation grind calibration data

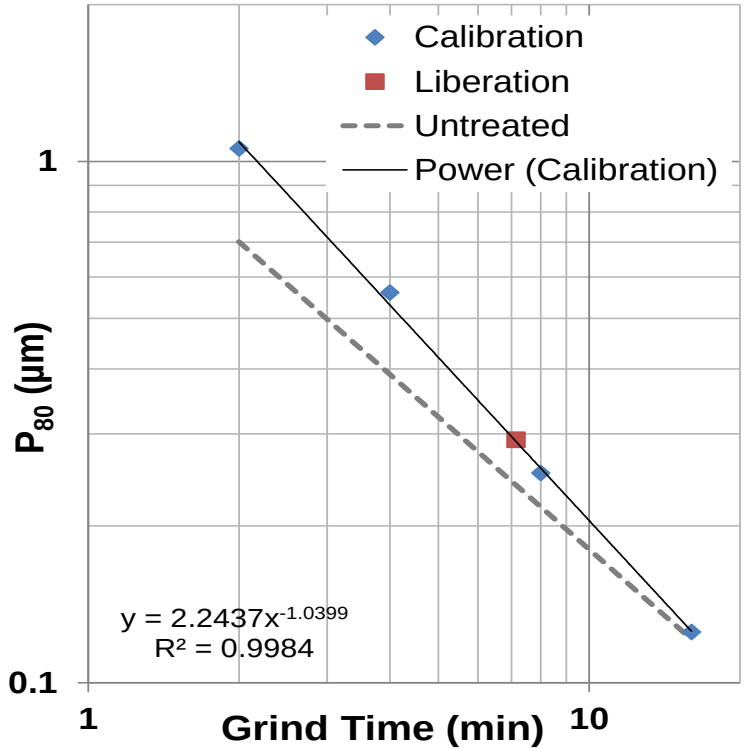


Figure A.20 MZ T6 target grind calibration

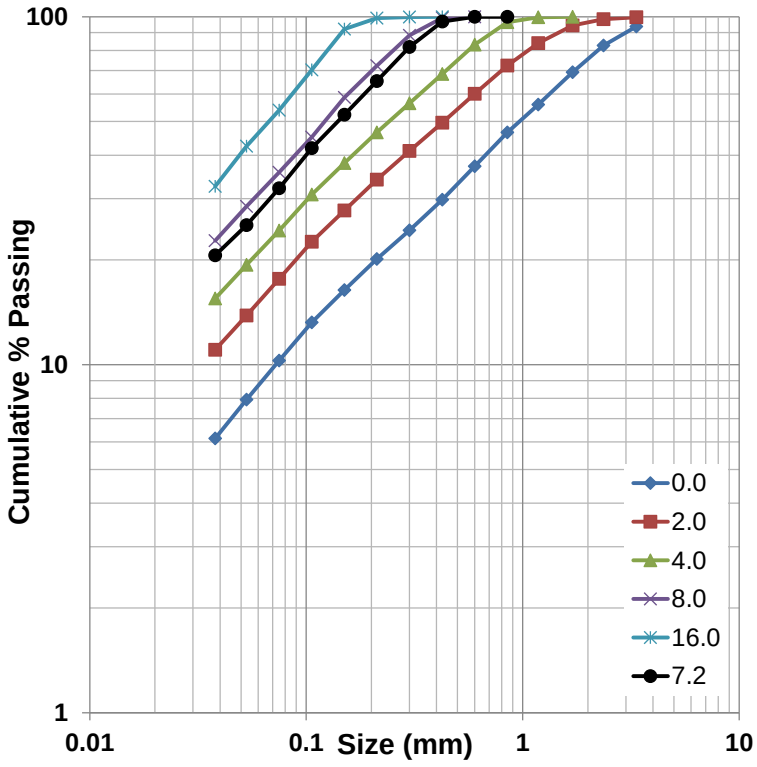


Figure A.21 MZ T6 grind calibration particle size distributions.

MZ T7	Calibration					Target
Time (min) / Mass (g)	0.0	2.0	4.0	8.0	16.0	6.4
3.35	15.03	0.06	0.00	0.00	0.00	
2.36	52.32	0.77	0.00	0.00	0.00	
1.70	120.62	8.03	0.00	0.00	0.00	
1.18	156.22	51.36	0.00	0.00	0.00	
0.850	122.61	113.94	7.37	0.00	0.00	
0.600	116.92	152.36	83.89	0.00	0.00	0.99
0.425	84.80	122.93	161.61	2.77	0.00	34.24
0.300	59.80	95.37	138.89	75.71	0.00	157.00
0.212	46.69	78.22	108.23	158.45	4.92	160.86
0.150	39.84	68.00	91.36	147.05	60.46	125.65
0.106	33.54	57.23	76.36	141.57	214.27	101.93
0.075	29.97	50.81	65.40	97.48	165.94	95.32
0.053	25.71	41.58	52.93	71.31	114.59	71.46
0.038	19.05	29.96	40.01	62.56	94.35	48.15
-0.038	68.59	125.10	165.71	234.64	336.26	199.05
Total	991.71	995.72	991.77	991.54	990.79	994.65
Loss	*0.8%*	*0.4%*	*0.8%*	*0.8%*	*0.9%*	*0.5%*

Size (mm)	Cumulative % Passing					
3.35	98.48	99.99				
2.36	93.21	99.92				
1.70	81.05	99.11				
1.18	65.29	93.95	100.00			
0.850	52.93	82.51	99.26			100.00
0.600	41.14	67.21	90.80	100.00		99.90
0.425	32.59	54.86	74.50	99.72		96.46
0.300	26.56	45.28	60.50	92.09	100.00	80.67
0.212	21.85	37.43	49.59	76.11	99.50	64.50
0.150	17.83	30.60	40.37	61.28	93.40	51.87
0.106	14.45	24.85	32.67	47.00	71.77	41.62
0.075	11.43	19.75	26.08	37.17	55.03	32.04
0.053	8.84	15.57	20.74	29.97	43.46	24.85
0.038	6.92	12.56	16.71	23.66	33.94	20.01
D_{xx}	% Passing					
95	2.664	1.273	0.716	0.344	0.165	0.413
80	1.663	0.807	0.481	0.232	0.122	0.296
50	0.786	0.359	0.215	0.115	0.065	0.142
20	0.182	0.076	0.050	<0.038	<0.038	<0.038
10	0.063	<0.038	<0.038	<0.038	<0.038	<0.038

Table A.31 MZ Ore T7 target liberation grind calibration data

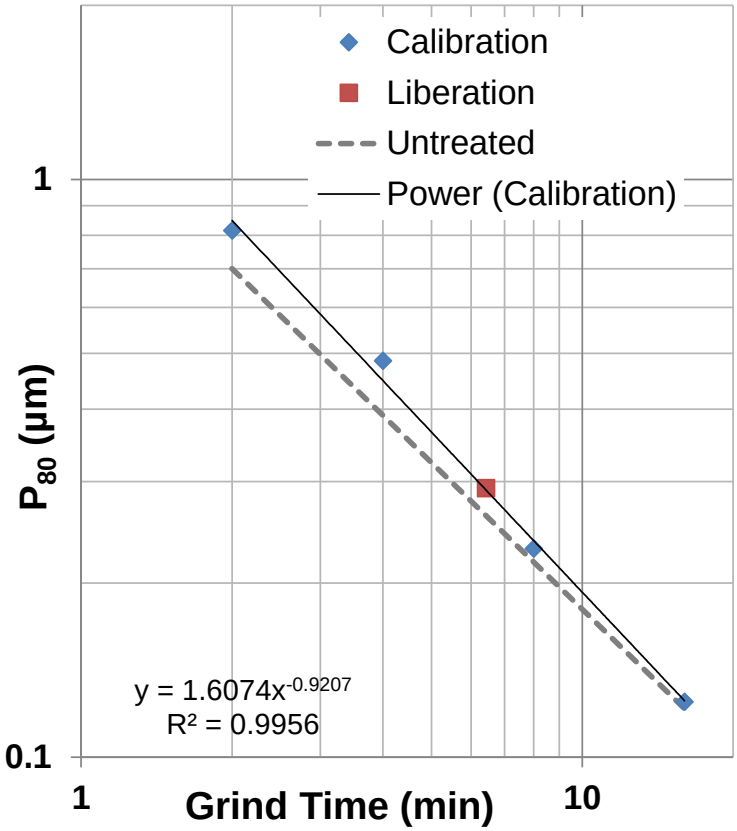


Figure A.22 MZ T7 target grind calibration

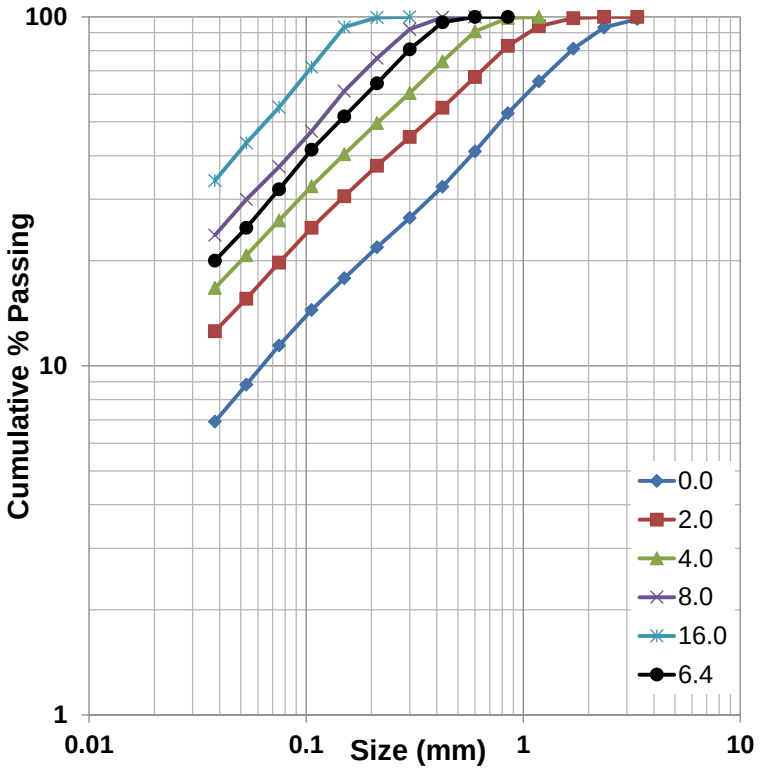


Figure A.23 MZ T7 grind calibration particle size distributions.

APPENDIX B – COMMINUTION TEST DATA

B.1 Ci Test Data

MZ UT1	Test				
Mass (gms)	1	2	3	Total	
Dry Wt Total	3387.70	3391.00	3344.40	10123.10	
+4.75	2997.80	2972.08	2936.93	8906.81	
-4.75	386.12	414.43	401.21	1201.76	
+3.35	98.34	106.34	96.97	301.65	
+1.70	107.74	116.00	113.66	337.40	
+1.18	39.72	42.18	41.09	122.99	
+0.600	41.23	45.78	42.76	129.77	
+0.300	30.19	29.92	31.00	91.11	
+0.150	24.08	23.78	23.61	71.47	
+0.106	11.65	11.62	11.54	34.81	
-0.106	32.78	38.77	39.65	111.20	
Ci Indices	1	2	3	Mean	Std Dev.
CRU	2.86	3.12	2.99	2.99	0.130
GRD	0.595	0.573	0.562	0.577	0.017
%-4.75mm	11.40	12.20	12.00	11.90	0.400

Figure B.1 MZ UT1 Ci test data

MZ T1	Test				
Mass (gms)	1	2	3	Total	
Dry Wt Total	3042.50	3014.00	3050.30	9106.80	
+4.75	2543.70	2518.80	2546.30	7608.80	
-4.75	490.00	489.70	498.60	1478.30	
+3.35	138.51	142.34	146.10	426.95	
+1.70	134.02	130.32	132.60	396.94	
+1.18	48.13	49.03	49.04	146.20	
+0.600	50.63	53.28	55.30	159.21	
+0.300	36.80	33.93	34.73	105.46	
+0.150	27.66	27.62	27.00	82.28	
+0.106	12.88	13.40	13.23	39.51	
-0.106	40.31	38.89	38.82	118.02	
Ci Indices	1	2	3	Mean	Std Dev.
CRU	3.01	3.10	3.16	3.09	0.080
GRD	0.598	0.603	0.609	0.603	0.006
%-4.75mm	16.10	16.20	16.30	16.20	0.100

Figure B.2 MZ T1 Ci test data

MZ T2	Test				
Mass (gms)	1	2	3	Total	
Dry Wt Total	3092.40			3092.40	
+4.75	2564.30			2564.30	
-4.75	568.00			568.00	
+3.35	174.23			174.23	
+1.70	144.42			144.42	
+1.18	49.14			49.14	
+0.600	60.68			60.68	
+0.300	36.50			36.50	
+0.150	28.73			28.73	
+0.106	14.20			14.20	
-0.106	58.19			58.19	
Ci Indices	1	2	3	Mean	Std Dev.
CRU	3.20			3.20	
GRD	0.529			0.529	
%-4.75mm	18.40			18.40	

Figure B.3 MZ T2 Ci test data

MZ T3	Test				
Mass (gms)	1	2	3	Total	
Dry Wt Total	2870.01	2877.21	2865.03	8612.25	
+4.75	2417.73	2391.41	2401.22	7210.36	
-4.75	454.09	486.24	454.78	1395.11	
+3.35	122.86	140.15	126.21	389.22	
+1.70	120.02	122.37	116.80	359.19	
+1.18	41.68	42.97	41.44	126.09	
+0.600	52.17	52.42	51.10	155.69	
+0.300	33.71	32.19	30.67	96.57	
+0.150	28.26	26.46	23.89	78.61	
+0.106	13.67	13.22	12.05	38.94	
-0.106	38.06	52.41	48.98	139.45	
Ci Indices	1	2	3	Mean	Std Dev.
CRU	2.83	3.03	3.14	3.00	0.160
GRD	0.590	0.519	0.527	0.545	0.039
%-4.75mm	15.80	16.90	15.90	16.20	0.600

Figure B.4 MZ T3 Ci test data

MZ UT2	Test				
Coarse Sieving (gms)	1	2	3	Total	
Total	5326.39	5333.59	5329.53	15989.51	
+26.50	50.13	46.05	63.02	159.20	
+19.00	132.93	176.05	118.18	427.16	
+13.20	1257.16	1256.57	1187.78	3701.51	
+9.50	1950.95	1845.42	2012.20	5808.57	
+6.70	746.38	785.04	733.67	2265.09	
+4.75	357.51	364.01	351.78	1073.30	
-4.75	821.91	820.99	856.26	2499.16	
Fine Sieving (gms)	1	2	3	Total	
Total	821.91	820.99	856.26	2499.16	
+3.35	161.11	181.15	190.95	533.21	
+2.36	139.99	129.20	140.01	409.20	
+1.70	100.94	99.95	106.99	307.88	
+1.18	71.55	76.18	74.63	222.36	
+0.850	50.92	49.51	51.31	151.74	
+0.600	44.55	45.15	44.04	133.74	
+0.425	32.26	34.92	31.82	99.00	
+0.300	31.45	30.22	30.85	92.52	
+0.212	24.80	28.85	24.38	78.03	
+0.150	24.03	27.64	23.49	75.16	
+0.106	28.36	23.48	28.31	80.15	
+0.075	23.43	25.18	23.08	71.69	
-0.075	87.54	67.98	85.36	240.88	
D_{xx}	% Passing			Mean	
90	17.34	17.54	17.23	17.37	
80	14.89	15.09	14.63	14.87	
50	11.05	11.00	10.99	11.02	
20	6.07	6.03	5.90	6.00	
10	2.44	2.50	2.41	2.45	
Ci Indices	1	2	3	Mean	Std Dev.
CRU	2.90	2.76	3.00	2.88	0.124
GRD	0.487	0.533	0.494	0.504	0.025
%-4.75mm	15.46	15.51	16.09	15.68	0.349

Figure B.5 MZ UT2 Ci test data

MZ T4	Test				
Coarse Sieving (gms)	1	2	3	Total	
Total	5103.55	5108.38	5114.30	15326.23	
+26.50	64.14	65.38	113.63	243.15	
+19.00	89.81	3.00	160.64	253.45	
+13.20	1505.64	1226.18	1194.80	3926.62	
+9.50	1661.20	1718.95	1754.46	5134.61	
+6.70	693.70	754.60	690.81	2139.11	
+4.75	318.77	337.06	351.30	1007.13	
-4.75	757.80	819.36	795.98	2373.14	
Fine Sieving (gms)	1	2	3	Total	
Total	757.80	819.36	795.98	2373.14	
+3.35	163.08	173.19	164.76	501.03	
+2.36	129.37	132.75	136.38	398.50	
+1.70	96.84	102.18	101.28	300.30	
+1.18	69.31	75.76	71.51	216.58	
+0.850	48.24	47.73	50.18	146.15	
+0.600	41.91	44.56	43.06	129.53	
+0.425	29.38	33.98	30.96	94.32	
+0.300	27.75	29.36	29.60	86.71	
+0.212	21.54	28.30	23.13	72.97	
+0.150	20.44	27.18	21.49	69.11	
+0.106	21.24	22.31	25.01	68.56	
+0.075	18.57	24.50	20.63	63.70	
-0.075	69.35	76.22	76.92	222.49	
D_{xx}	% Passing			Mean	
90	17.63	16.95	17.84	17.47	
80	15.67	14.62	15.36	15.22	
50	11.38	10.82	11.11	11.10	
20	6.34	5.71	5.96	6.00	
10	2.69	2.22	2.44	2.45	
Ci Indices	1	2	3	Mean	Std Dev.
CRU	3.20	2.86	3.09	3.04	0.178
GRD	0.530	0.515	0.513	0.519	0.009
%-4.75mm	14.88	16.64	15.73	15.74	0.877

Figure B.6 MZ T4 Ci test data

MZ T5	Test				
Coarse Sieving (gms)	1	2	3	Total	
Total	5157.38	5145.78	5126.21	15429.37	
+26.50	24.48	84.11	29.47	138.06	
+19.00	179.06	240.80	106.70	526.56	
+13.20	1236.18	1247.00	1103.81	3586.99	
+9.50	1795.79	1685.50	1943.80	5425.09	
+6.70	734.18	715.21	807.93	2257.32	
+4.75	371.40	371.24	317.55	1060.19	
-4.75	804.77	792.60	806.68	2404.05	
Fine Sieving (gms)	1	2	3	Total	
Total	804.77	792.60	806.68	2404.05	
+3.35	169.62	164.33	160.32	494.27	
+2.36	129.74	139.92	134.23	403.89	
+1.70	102.56	103.97	101.78	308.31	
+1.18	79.97	72.46	79.41	231.84	
+0.850	51.25	51.56	49.63	152.44	
+0.600	46.08	43.85	46.07	136.00	
+0.425	34.42	30.59	34.61	99.62	
+0.300	28.14	28.72	28.98	85.84	
+0.212	25.17	21.81	26.59	73.57	
+0.150	22.20	20.18	24.59	66.97	
+0.106	19.21	22.13	21.28	62.62	
+0.075	20.89	18.79	22.59	62.27	
-0.075	73.76	73.00	75.10	221.86	
D_{xx}	% Passing			Mean	
90	17.50	18.10	16.95	17.52	
80	15.08	15.69	14.29	15.02	
50	11.01	11.15	10.85	11.00	
20	5.94	5.99	6.08	6.00	
10	2.43	2.53	2.36	2.44	
Ci Indices	1	2	3	Mean	Std Dev.
CRU	3.17	3.34	3.02	3.17	0.157
GRD	0.537	0.533	0.528	0.532	0.004
%-4.75mm	15.64	15.43	15.77	15.61	0.170

Figure B.7 MZ T5 Ci test data

MZ T6	Test				
Coarse Sieving (gms)	1	2	3	Total	
Total	4505.38	4525.92	4514.22	13545.52	
+26.50	0.00	86.30	44.81	131.11	
+19.00	64.77	125.12	101.73	291.62	
+13.20	1050.85	1164.70	1186.56	3402.11	
+9.50	1662.40	1524.10	1509.00	4695.50	
+6.70	681.04	641.01	655.18	1977.23	
+4.75	300.73	296.26	291.34	888.33	
-4.75	737.75	674.73	718.80	2131.28	
Fine Sieving (gms)	1	2	3	Total	
Total	737.75	674.73	718.80	2131.28	
+3.35	164.99	145.07	151.98	462.04	
+2.36	124.42	112.57	123.13	360.12	
+1.70	90.30	84.98	89.54	264.82	
+1.18	64.77	64.43	64.48	193.68	
+0.850	46.21	41.56	45.81	133.58	
+0.600	39.22	37.39	39.41	116.02	
+0.425	27.97	29.02	27.91	84.90	
+0.300	27.32	24.09	27.10	78.51	
+0.212	21.80	22.24	20.55	64.59	
+0.150	20.75	20.24	19.21	60.20	
+0.106	22.12	17.17	21.84	61.13	
+0.075	18.53	17.79	17.82	54.14	
-0.075	68.40	56.59	68.61	193.60	
D_{xx}	% Passing			Mean	
90	16.81	17.78	17.49	17.36	
80	14.35	15.52	15.28	15.05	
50	10.82	11.22	11.08	11.04	
20	5.80	6.25	5.97	6.01	
10	2.37	2.65	2.42	2.48	
Ci Indices	1	2	3	Mean	Std Dev.
CRU	3.04	3.02	3.11	3.06	0.044
GRD	0.518	0.548	0.518	0.527	0.017
%-4.75mm	16.40	14.95	15.95	15.77	0.741

Figure B.8 MZ T6 Ci test data

MZ T7	Test				
Coarse Sieving (gms)	1	2	3	Total	
Total	5003.71	4968.67	4930.41	14902.79	
+26.50	46.50	49.21	67.25	162.96	
+19.00	219.90	131.78	115.55	467.23	
+13.20	1268.75	1131.46	1147.23	3547.44	
+9.50	1624.81	1767.15	1714.50	5106.46	
+6.70	709.31	720.72	737.38	2167.41	
+4.75	350.77	365.50	330.72	1046.99	
-4.75	770.95	766.42	791.00	2328.37	
Fine Sieving (gms)	1	2	3	Total	
Total	770.95	766.42	791.00	2328.37	
+3.35	163.10	147.91	173.28	484.29	
+2.36	129.34	136.75	124.95	391.04	
+1.70	96.40	100.41	101.07	297.88	
+1.18	74.06	71.33	75.80	221.19	
+0.850	46.66	50.48	47.88	145.02	
+0.600	42.31	43.57	43.07	128.95	
+0.425	32.67	30.47	33.05	96.19	
+0.300	26.63	28.76	27.87	83.26	
+0.212	24.66	22.08	25.49	72.23	
+0.150	22.23	20.71	23.50	66.44	
+0.106	19.19	22.87	20.12	62.18	
+0.075	20.24	18.65	21.52	60.41	
-0.075	71.68	71.24	71.73	214.65	
D_{xx}	% Passing			Mean	
90	17.91	17.35	17.40	17.55	
80	15.62	14.82	14.91	15.12	
50	11.15	10.93	10.92	11.00	
20	6.02	5.93	5.87	5.94	
10	2.51	2.44	2.35	2.43	
Ci Indices	1	2	3	Mean	Std Dev.
CRU	3.10	3.22	3.02	3.11	0.102
GRD	0.528	0.533	0.528	0.530	0.003
%-4.75mm	15.45	15.54	16.13	15.70	0.371

Figure B.9 MZ T7 Ci test data

QZ UT	Test				
Mass (gms)	1	2	3	Total	
Dry Wt Total	2966.50	2944.20	2983.30	8894.00	
+4.75	2626.61	2600.89	2602.86	7830.36	
-4.75	331.72	339.41	374.98	1046.11	
+3.35	86.16	85.46	103.75	275.37	
+1.70	94.54	96.43	107.65	298.62	
+1.18	27.93	28.70	31.65	88.28	
+0.600	32.30	31.20	34.02	97.52	
+0.300	21.07	21.97	22.44	65.48	
+0.150	19.21	21.41	20.62	61.24	
+0.106	11.99	13.27	12.81	38.07	
-0.106	37.92	38.99	41.13	118.04	
Ci Indices	1	2	3	Mean	Std Dev.
CRU	2.96	2.76	3.10	2.94	0.170
GRD	0.490	0.490	0.500	0.493	0.006
%-4.75mm	11.20	11.50	12.60	11.80	0.700

Figure B.10 QZ UT Ci test data

QZ T1	Test				
Mass (gms)	1	2	3	Total	
Dry Wt Total	2253.30	2258.30	2237.30	6748.90	
+4.75	1898.30	1889.20	1871.60	5659.10	
-4.75	349.00	364.40	360.60	1074.00	
+3.35	104.85	108.49	111.17	324.51	
+1.70	90.89	97.38	96.65	284.92	
+1.18	30.28	31.54	30.82	92.64	
+0.600	28.82	30.43	31.03	90.28	
+0.300	20.89	21.45	18.90	61.24	
+0.150	18.28	19.31	17.91	55.50	
+0.106	10.68	11.49	11.50	33.67	
-0.106	43.53	43.35	41.88	128.76	
Ci Indices	1	2	3	Mean	Std Dev.
CRU	3.01	3.05	3.28	3.11	0.150
GRD	0.470	0.470	0.460	0.467	0.006
%-4.75mm	15.50	16.10	16.10	15.90	0.400

Figure B.11 QZ T1 Ci test data

QZ T2	Test				
Mass (gms)	1	2	3	Total	
Dry Wt Total	2406.60	2403.90	2398.10	7208.60	
+4.75	2038.30	2022.20	2033.80	6094.30	
-4.75	363.60	379.90	388.30	1131.80	
+3.35	108.04	115.24	125.58	348.86	
+1.70	96.76	101.91	98.96	297.63	
+1.18	30.81	33.51	32.46	96.78	
+0.600	32.67	31.68	31.79	96.14	
+0.300	19.38	22.49	22.51	64.38	
+0.150	18.64	19.30	19.67	57.61	
+0.106	11.65	11.15	11.57	34.37	
-0.106	44.38	43.60	44.78	132.76	
Ci Indices	1	2	3	Mean	Std Dev.
CRU	3.23	3.16	3.04	3.14	0.100
GRD	0.460	0.480	0.470	0.47	0.010
%-4.75mm	15.10	15.80	16.20	15.70	0.500

Figure B.12 QZ T2 Ci test data

QZ T3	Test				
Mass (gms)	1	2	3	Total	
Dry Wt Total	2415.60	2449.40	2461.50	7326.50	
+4.75	2007.30	2059.70	2104.60	6171.60	
-4.75	402.70	379.90	355.50	1138.10	
+3.35	116.75	116.79	95.69	329.23	
+1.70	106.20	102.99	96.84	306.03	
+1.18	34.27	33.00	32.34	99.61	
+0.600	36.31	33.53	30.44	100.28	
+0.300	22.63	20.06	22.50	65.19	
+0.150	22.42	18.94	20.78	62.14	
+0.106	13.87	11.69	11.81	37.37	
-0.106	49.31	41.83	44.11	135.25	
Ci Indices	1	2	3	Mean	Std Dev.
CRU	3.00	3.34	2.90	3.08	0.230
GRD	0.460	0.490	0.470	0.473	0.015
%-4.75mm	16.70	15.50	14.40	15.50	1.100

Figure B.13 QZ T3 Ci test data

B.2 BBMWi Test Data

MZ		Test			Mean	Std Dev.	±95%CL
		1	2	3			
UT1	F_{80} (µm)	2176	2103	2141	2140	37	91
	P_{80} (µm)	156	156	155	156	0.6	1.4
	Gbp (g/rev)	2.005	2.023	2.057	2.028	0.026	0.07
	BBMWi (kWh/t)	13.80	13.78	13.49	13.69	0.17	0.43
T1	F_{80} (µm)	2109	2127	2100	2112	14	34
	P_{80} (µm)	156	157	157	157	0.6	1.4
	Gbp (g/rev)	2.262	2.273	2.318	2.284	0.030	0.07
	BBMWi (kWh/t)	12.57	12.55	12.38	12.50	0.10	0.26
T2	F_{80} (µm)	2127	2119	2158	2135	21	51
	P_{80} (µm)	157	157	158	157	0.6	1.4
	Gbp (g/rev)	2.228	2.154	2.161	2.181	0.041	0.10
	BBMWi (kWh/t)	12.76	13.13	13.11	13.00	0.21	0.51
T3	F_{80} (µm)	2151	2133	2118	2134	17	41
	P_{80} (µm)	158	157	159	158	1.0	2.5
	Gbp (g/rev)	2.226	2.264	2.274	2.255	0.025	0.06
	BBMWi (kWh/t)	12.80	12.59	12.67	12.69	0.11	0.27
UT2	F_{80} (µm)	1526			1526		
	P_{80} (µm)	165			165		
	Gbp (g/rev)	2.570			2.570		
	BBMWi (kWh/t)	12.67			12.67		
T4	F_{80} (µm)	1526			1526		
	P_{80} (µm)	168			168		
	Gbp (g/rev)	2.680			2.680		
	BBMWi (kWh/t)	12.36			12.36		
T5	F_{80} (µm)	1526			1526		
	P_{80} (µm)	167			167		
	Gbp (g/rev)	2.580			2.580		
	BBMWi (kWh/t)	12.74			12.74		
T6	F_{80} (µm)	1526			1526		
	P_{80} (µm)	167			167		
	Gbp (g/rev)	2.640			2.640		
	BBMWi (kWh/t)	12.46			12.46		
T7	F_{80} (µm)	1526			1526		
	P_{80} (µm)	166			166		
	Gbp (g/rev)	2.570			2.570		
	BBMWi (kWh/t)	12.65			12.65		

Table B.1 MZ Ore BBMWi test data summary

QZ		Test			Mean	Std Dev.	±95%CL
		1	2	3			
UT	F_{80} (µm)	2079	2051	2053	2061	16	39
	P_{80} (µm)	161	161	162	161	0.6	1.4
	Gbp (g/rev)	3.301	3.496	3.383	3.393	0.098	0.24
	BBMWi (kWh/t)	9.45	9.04	9.32	9.27	0.21	0.52
T1	F_{80} (µm)	2039	2035	2041	2038	3	8
	P_{80} (µm)	161	162	162	162	0.6	1.4
	Gbp (g/rev)	3.398	3.491	3.445	3.445	0.047	0.12
	BBMWi (kWh/t)	9.26	9.10	9.20	9.19	0.08	0.20
T2	F_{80} (µm)	2030	2077	2065	2057	24	61
	P_{80} (µm)	161	161	162	161	0.6	1.4
	Gbp (g/rev)	3.472	3.501	3.531	3.501	0.030	0.07
	BBMWi (kWh/t)	9.11	9.00	8.99	9.03	0.06	0.16
T3	F_{80} (µm)	2044	2048	2050	2047	3	8
	P_{80} (µm)	162	162	161	162	0.6	1.4
	Gbp (g/rev)	3.439	3.415	3.410	3.421	0.016	0.04
	BBMWi (kWh/t)	9.21	9.26	9.22	9.23	0.02	0.06

Table B.2 QZ Ore BBMWi test data summary

APPENDIX C – FRACTURE ANALYSIS DATA

C.1 FRACTURE LENGTH DISTRIBUTION DATA

MZ Ore			
Fracture Length (μm)	Cumulative Passing (wt%)		
	UT1	T1	T3
25000		100.00	100.00
19000	100.00	99.99	99.97
13200	99.98	99.97	99.94
11200	99.90	99.95	99.69
8000	99.87	99.85	99.39
6300	99.68	99.84	98.93
4750	99.48	99.52	98.25
3350	99.22	99.11	96.96
2360	98.43	98.45	93.86
1700	97.03	96.86	90.02
1180	95.02	94.45	84.34
850	89.85	88.92	73.07
600	83.02	81.77	59.63
425	70.99	68.04	40.07
300	55.15	49.33	23.70
212	34.78	27.14	10.29
180	23.12	13.31	5.00
150	12.05	4.15	2.00
125	4.21	0.03	0.50
106	1.30	0.01	0.00
90	0.00	0.00	0.00
75	0.00	0.00	0.00
63	0.00	0.00	0.00
53	0.00	0.00	0.00
45	0.00	0.00	0.00
38	0.00	0.00	0.00
20	0.00	0.00	0.00
1	0.00	0.00	0.00

Table C.1 MZ Ore fracture length distribution data

QZ Ore			
Fracture Length (μm)	Cumulative Passing (wt%)		
	UT	T1	T3
37500		100.00	
31500	100.00	99.98	100.00
25000	99.98	99.95	99.98
19000	99.95	99.92	99.92
13200	99.94	99.80	99.80
11200	99.71	99.45	99.54
8000	99.57	99.27	99.38
6300	98.88	98.63	98.76
4750	98.28	97.95	97.76
3350	97.33	96.84	96.19
2360	95.38	94.51	93.91
1700	92.33	90.63	89.86
1180	88.19	85.90	84.85
850	80.44	76.35	75.32
600	69.50	63.64	63.11
425	51.28	43.99	42.16
300	31.55	23.70	22.14
212	10.00	8.69	8.48
180	3.00	1.78	2.58
150	0.40	0.50	1.48
125	0.20	0.17	0.62
106	0.08	0.12	0.30
90	0.00	0.08	0.24
75	0.00	0.08	0.22
63	0.00	0.08	0.20
53	0.00	0.07	0.18
45	0.00	0.06	0.16
38	0.00	0.05	0.13
20	0.00	0.03	0.08
1	0.00	0.00	0.00

Table C.2 QZ Ore fracture length distribution data

QX Ore				
Fracture Length (μm)	Cumulative Passing (wt%)			
	UT	T1	T2	T3
31500		100.00		
25000	100.00	99.98	100.00	100.00
19000	99.99	99.96	99.98	99.97
13200	99.92	99.82	99.84	99.65
11200	99.81	99.49	99.56	99.68
8000	99.70	99.25	99.42	99.04
6300	99.46	98.48	98.85	99.41
4750	98.99	97.62	98.20	97.25
3350	98.13	96.20	97.00	95.24
2360	96.62	94.88	94.96	92.98
1700	93.89	92.70	91.48	90.14
1180	90.88	88.79	87.14	87.13
850	84.35	81.20	79.15	78.88
600	76.25	70.22	68.57	67.34
425	62.02	52.38	51.15	50.89
300	44.07	32.69	29.96	29.17
212	21.00	12.57	11.47	9.18
180	7.46	2.85	2.50	1.38
150	2.02	0.74	0.79	0.63
125	0.40	0.26	0.24	0.30
106	0.26	0.16	0.18	0.22
90	0.20	0.16	0.10	0.16
75	0.11	0.12	0.10	0.12
63	0.08	0.12	0.05	0.12
53	0.08	0.12	0.05	0.12
45	0.07	0.08	0.03	0.09
38	0.07	0.08	0.03	0.06
20	0.07	0.08	0.00	0.06
1	0.00	0.00	0.00	0.00

Table C.3 QX Ore fracture length distribution data

C.2 Fracture Length K-S Test Tables

MZ			
Length (μm)	UT vs T1	UT vs T3	T1 vs T3
37500	0.000	0.000	0.000
31500	0.000	0.000	0.000
25000	0.000	0.000	0.000
19000	0.000	0.000	0.000
13200	0.000	0.000	0.000
11200	0.000	0.002	0.003
8000	0.000	0.005	0.005
6300	0.002	0.008	0.009
4750	0.000	0.012	0.013
3350	0.001	0.023	0.022
2360	0.000	0.046	0.046
1700	0.002	0.070	0.068
1180	0.006	0.107	0.101
850	0.009	0.168	0.159
600	0.013	0.234	0.221
425	0.029	0.309	0.280
300	0.058	0.315	0.256
212	0.104	0.273	0.169
180	0.148	0.141	0.008
150	0.146	0.110	0.037
125	0.119	0.099	0.019
106	0.084	0.081	0.003
90	0.027	0.024	0.003
75	0.017	0.014	0.003
63	0.013	0.011	0.002
53	0.006	0.004	0.002
45	0.002	0.000	0.002
38	0.002	0.001	0.002
20	0.001	0.000	0.000
1	0.000	0.000	0.000

MZ			
Criteria	UT vs T1	UT vs T3	T1 vs T3
D	0.1484	0.3145	0.2797
D crit	0.0227	0.0222	0.0219
Significant (>95% confidence)	**Yes**	**Yes**	**Yes**
Significant (>99% confidence)	**Yes**	**Yes**	**Yes**

Table C.4: Calculated differences and K-S test results for MZ Ore

QZ			
Length (µm)	**UT vs T1**	**UT vs T3**	**T1 vs T3**
37500	0.000	0.000	0.000
31500	0.000	0.000	0.000
25000	0.000	0.000	0.000
19000	0.000	0.000	0.000
13200	0.001	0.001	0.000
11200	0.003	0.002	0.001
8000	0.003	0.002	0.001
6300	0.003	0.001	0.001
4750	0.003	0.005	0.002
3350	0.005	0.011	0.007
2360	0.009	0.015	0.006
1700	0.017	0.025	0.008
1180	0.023	0.033	0.011
850	0.041	0.051	0.010
600	0.059	0.064	0.005
425	0.073	0.091	0.018
300	0.078	0.094	0.016
212	0.043	0.045	0.002
180	0.011	0.003	0.008
150	0.006	0.004	0.010
125	0.004	0.001	0.005
106	0.002	0.000	0.002
90	0.002	0.000	0.002
75	0.002	0.000	0.001
63	0.002	0.000	0.001
53	0.002	0.000	0.001
45	0.001	0.000	0.001
38	0.001	0.000	0.001
20	0.001	0.000	0.001
1	0.000	0.000	0.000

QZ			
Criteria	**UT vs T1**	**UT vs T3**	**T1 vs T3**
D	0.0785	0.0941	0.0183
D crit	0.0245	0.0257	0.0259
Significant (>95% confidence)	**Yes**	**Yes**	**No**
Significant (>99% confidence)	**Yes**	**Yes**	**No**

Table C.5: Calculated differences and K-S test results for QZ Ore

QX						
Length (µm)	**UT vs T1**	**UT vs T3**	**UT vs E2**	**T1 vs T3**	**T1 vs E2**	**T3 vs E2**
37500	0.000	0.000	0.000	0.000	0.000	0.000
31500	0.000	0.000	0.000	0.000	0.000	0.000
25000	0.000	0.000	0.000	0.000	0.000	0.000
19000	0.000	0.000	0.000	0.000	0.000	0.000
13200	0.001	0.001	0.000	0.000	0.001	0.000
11200	0.003	0.003	0.002	0.001	0.002	0.001
8000	0.005	0.003	0.003	0.002	0.002	0.000
6300	0.010	0.006	0.004	0.004	0.006	0.002
4750	0.014	0.008	0.017	0.006	0.004	0.010
3350	0.019	0.011	0.029	0.008	0.010	0.018
2360	0.017	0.017	0.036	0.001	0.019	0.020
1700	0.012	0.024	0.038	0.012	0.026	0.013
1180	0.021	0.037	0.038	0.017	0.017	0.000
850	0.031	0.052	0.055	0.021	0.023	0.003
600	0.060	0.077	0.089	0.017	0.029	0.012
425	0.096	0.109	0.111	0.012	0.015	0.003
300	0.114	0.141	0.149	0.027	0.035	0.008
212	0.120	0.131	0.154	0.011	0.034	0.023
180	0.046	0.050	0.061	0.003	0.015	0.011
150	0.013	0.012	0.014	0.001	0.001	0.002
125	0.001	0.002	0.001	0.000	0.000	0.001
106	0.001	0.001	0.000	0.000	0.001	0.000
90	0.000	0.001	0.000	0.001	0.000	0.001
75	0.001	0.000	0.000	0.001	0.001	0.000
63	0.000	0.000	0.000	0.001	0.000	0.001
53	0.000	0.000	0.000	0.001	0.000	0.001
45	0.000	0.000	0.000	0.000	0.000	0.001
38	0.000	0.000	0.000	0.000	0.000	0.000
20	0.000	0.001	0.000	0.001	0.000	0.001
1	0.000	0.000	0.000	0.000	0.000	0.000

QX						
Criteria	**UT vs T1**	**UT vs T2**	**UT vs T3**	**T1 vs T2**	**T1 vs T3**	**T2 vs T3**
D	0.1201	0.1411	0.1540	0.0273	0.0352	0.0229
D crit	0.0252	0.0237	0.0202	0.0260	0.0228	0.0211
Significant (>95% confidence)	**Yes**	**Yes**	**Yes**	**Yes**	**Yes**	**Yes**
Significant (>99% confidence)	**Yes**	**Yes**	**Yes**	**No**	**Yes**	**No**

Table C.6: Calculated differences and K-S test results for QX Ore

Confidence	a	D value
99%	0.01	1.63
95%	0.05	1.36

Table C.7: Values from K-S table used in calculating D crit for >95% and >99% confidence levels

n \ α	0.01	0.05	0.1	0.15	0.2
1	0.995	0.975	0.950	0.925	0.900
2	0.929	0.842	0.776	0.726	0.684
3	0.828	0.708	0.642	0.597	0.565
4	0.733	0.624	0.564	0.525	0.494
5	0.669	0.565	0.510	0.474	0.446
6	0.618	0.521	0.470	0.436	0.410
7	0.577	0.486	0.438	0.405	0.381
8	0.543	0.457	0.411	0.381	0.358
9	0.514	0.432	0.388	0.360	0.339
10	0.490	0.410	0.368	0.342	0.322
11	0.468	0.391	0.352	0.326	0.307
12	0.450	0.375	0.338	0.313	0.295
13	0.433	0.361	0.325	0.302	0.284
14	0.418	0.349	0.314	0.292	0.274
15	0.404	0.338	0.304	0.283	0.266
16	0.392	0.328	0.295	0.274	0.258
17	0.381	0.318	0.286	0.266	0.250
18	0.371	0.309	0.278	0.259	0.244
19	0.363	0.301	0.272	0.252	0.237
20	0.356	0.294	0.264	0.246	0.231
25	0.320	0.270	0.240	0.220	0.210
30	0.290	0.240	0.220	0.200	0.190
35	0.270	0.230	0.210	0.190	0.180
40	0.250	0.210	0.190	0.180	0.170
45	0.240	0.200	0.180	0.170	0.160
50	0.230	0.190	0.170	0.160	0.150
OVER 50	$\frac{1.63}{\sqrt{n}}$	$\frac{1.36}{\sqrt{n}}$	$\frac{1.22}{\sqrt{n}}$	$\frac{1.14}{\sqrt{n}}$	$\frac{1.07}{\sqrt{n}}$

Table C.8 K-S table of critical values for D_n